Title
DNA Dynamics: From Picoseconds to Milliseconds

Author
Selvin, Paul R.

Publication Date
1990-10-01

Lawrence Berkeley Laboratory
UNIVERSITY OF CALIFORNIA

CHEMICAL BIODYNAMICS DIVISION

DNA Dynamics: From Picoseconds to Milliseconds

P.R. Selvin
(Ph.D. Thesis)

November 1990

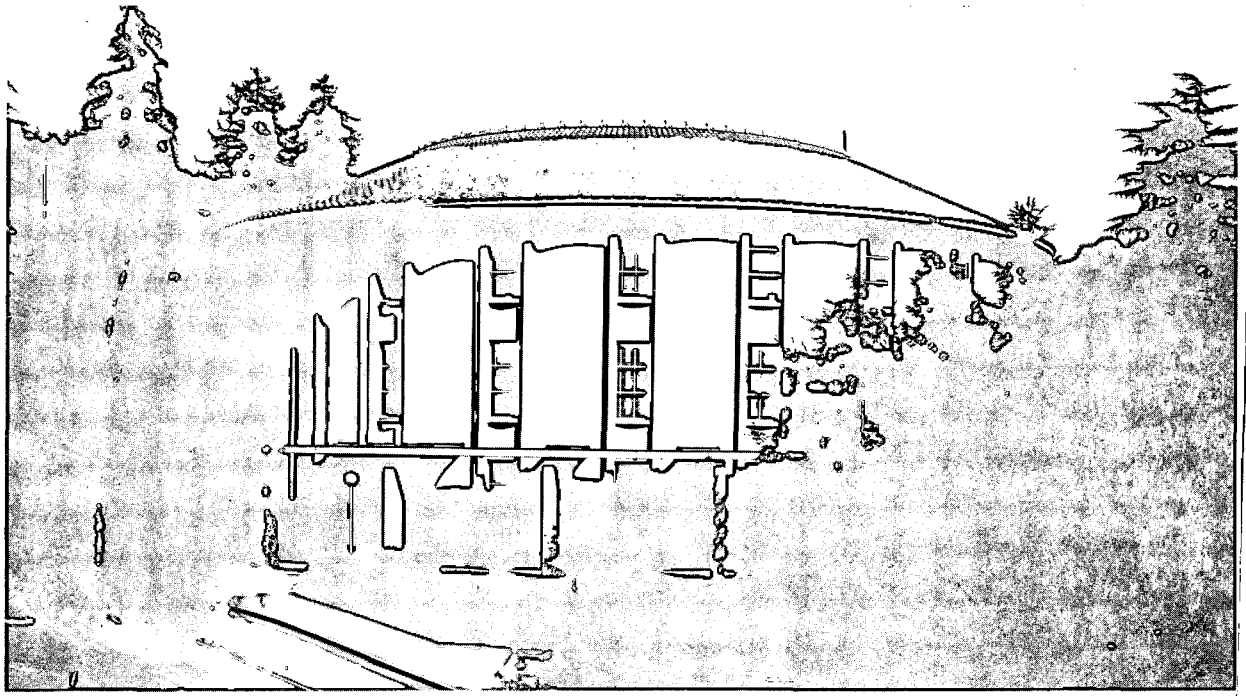

Prepared for the U.S. Department of Energy under Contract Number DE-AC03-76SF00098

DISCLAIMER

DNA Dynamics: From Picoseconds to Milliseconds

Paul Ronald Selvin

Ph.D. Thesis

November, 1990

Lawrence Berkeley Laboratory

University of California

Berkeley, California 94720

This work was supported by the Director, Office of Energy Research, Office of Biological Environmental Research General Life Sciences, Structural Biology Division of the U. S. Department of Energy under Contract No. DE-AC03-76SF00098.

DNA Dynamics: From Picoseconds to Milliseconds

Paul R. Selvin

Abstract

Bending and twisting of the DNA helix ocurrs during essential steps in genome organization and expression. Measuring these motions, which range from picoseconds to hours and angstroms to microns, provides insight into DNA structure, its local environment and the mechanism of gene expression. How DNA dynamics depend on important biological parameters, including DNA topology, solute, solvent and protein interactions, is the focus of this thesis. Time-domain optical techniques are the primary tools used — mostly fluorescence because of its exquisite sensitivity and time resolution — although we have also begun development of a new electron paramagnetic double-resonance technique. In total, these techniques allow measurements to be made from picoseconds up to approximately ten milliseconds, both *in vivo* and *in vitro*.

We first measure the bending and torsional flexibility of "naked" DNA and find that it undergoes rapid twisting motions that are well explained by theoretical models, as well as longer bending motions that are rather simple in form, but for which no quantitative theory yet exists. This forms a "baseline" for all further measurements.

DNA under torsional stress induced by supercoiling — both over and under-winding — is next examined. The bending constant of DNA does not change with supercoiling, whereas the torsional constant steadily increases as the DNA becomes more negatively supercoiled. The results can be explained by modelling DNA as a harmonic oscillator in bending and twisting, with an additional cubic perturbation to the twisting potential of 15% average magnitude.

Prelimary results indicate that polyamines make the DNA more flexible, primarily through sequence independent, charge neutralization of the DNA-phosphate backbone.

DNA complexed with protein in chromatin is found to be relatively free to move when only constrained by the lowest order of chromatin — the 10nm fiber — but greatly constrained by the higher order structure of chromatin — the 30nm fiber and aggregation of these fibers.

Lastly, motions of DNA in agarose gels with wavelength less than the gel pore size are relatively unhindered, whereas those larger than the pore size are damped out.

Approved by

Prof. Erwin Hahn
Department of Physics,
Univerisity of California, Berkeley

Acknowledgments

Some people have it lucky. They're surrounded by cheerful and intelligent friends, family and colleagues; they get to indulge their intellectual curiosity, all at the expense of the taxpayer. I'm one of those lucky people.

(This work was supported by the NIH, Grant GM41911; the DOE Office of Energy Research, Office of Health and Environmental Research, Contract DE AC03-76SF00098; and 3-year NSF Graduate Fellowship.)

This thesis is first dedicated to all those who aren't so fortunate. Maybe, just maybe, the work in these pages will someday help them. Maybe, someday, the resources of the world will be distributed in a more rational, equitable fashion.

All of my good luck has come through the people around me. My brother Eric, through his sometimes bitter experience in graduate school, taught me to find an advisor who is a *menche*. I found two of them. First, my official advisor, Mel Klein, is truly a scholar and a gentleman. He let me make my own mistakes, but was never critical when I made them — over and over again. Second, my unofficial advisor, John Hearst, taught me that a scientist need not be a nerd. There is life outside of the lab — and I fully partook. Travelling to Central America with my buddy and fellow graduate student, Nathan Hunt, and learning to write for the lay-public, were just two of the joys I experienced out of the lab and in graduate school. John also taught me much about DNA.

Nathan (affectionately known as Nathan-baby) taught me much about patience. Never have I met so mellow and nice a guy. During our two years of working on EPR together, he was the calming influence that kept me from taking it all too seriously. He's smart too.

Many discussions with him — both technical and political — advanced my work and play enormously.

Dan Axelrod (he never uses a middle initial — too formal) who was Mel's student in the early 1970s, directed me towards fluorescence in my undergraduate days and continued to collaborate in my graduate work. Dan is also a friend, mentor and politically-astute guy.

Bethe Scalletar appears on all of my published papers in graduate school. She's a work-horse and fun to work with. Dave Cook, whom I only occasionally agreed with in friendly arguments, is a biologist without whom I could not have done the supercoiling work. Don't vote Republican Dave! It's amazing how quickly he picked up physics, especially compared to how fast I picked up biology. It's a collaboration, intellectually and socially, I hope to continue.

Then there is "the group" who I've gone through seven years of graduate school with and who has made my life — whether backpacking naked in the mountains, working in the lab, or playing in Berkeley — a joy. It's been amusing to notice our hairlines recede over the years (only the guys). Marc and Karina, Robert (and later Eve), Marc, Nathan, Cathy, Eric and Gayle. You guys are the greatest!

My parents, M&M, emotionally supported me throughout. Most of all, they kindly overlooked the fact that their Jewish son became the wrong kind of doctor. My brother Larry kept me informed of what matters most: who won Wimbledon when.

Finally, there is my new-found family. Kathy put up with me through the last two years of graduate school — even through quals and the terror of my first published article (in the *Nation*). I suspect she will be around long after we've all forgotten what's in this thesis. And there will always be room in our bed, and in our hearts, for Chaos and Koala the cats.

DNA Dynamics: From Picoseconds to Milliseconds

Paul R. Selvin

Table of Contents

List of Figures and Tables*

* Tables are preceded by a T, e.g. T4-1. Figures are simply labelled with the relevant number.

Chapter Four: Isolated DNA

Chapter 5: Chromatin

Chapter 6: DNA in Agarose Gels

Chapter 7 : EPR

Chapter One

DNA Dynamics Overview

(Motivation, Background and Measurement)

Motivational Model

There are two reasons to study DNA dynamics: because the motions of DNA have important biological significance in their own right, and because they give insight into the structure and local environment of DNA. DNA dynamics spans 14 orders of magnitude in time -- from picoseconds to hours. The dynamics include both bending and twisting modes, as well as translational motion, and are a sensitive function of many biological parameters, including (but not limited to) DNA topology; solute, solvent and protein interactions; and stage in cell cycle.

Perhaps the most well known example of DNA dynamics occurs during cell division, a process observed by most high school students with access to a microscope or who have taken biology. This motion occurs over a time scale of several minutes to several hours, and if interupted, will kill the cell. A less trivial example, and one more directly related to the research performed here, is the relative motion of RNA polymerase and DNA which may occur during transcription. RNA polymerase, the enzyme which catalyzes the formation of RNA using the DNA as a template, is thought to maintain a constant orientation with respect to the DNA during transcription. Presumably the active site of the polymerase must always face the DNA. Since the DNA is a helix, this means that either the DNA or the polymerase must rotate (twist) as the enzyme travels down the DNA. The motion is analogous to a nut on a bolt, where the polymerase is the nut, and

DNA the bolt. Since the rate of transcription is approximately 50 base pairs/second, this motion occurs on the order of tens of milliseconds, with local, conformation fluctuations of both the DNA and protein occurring on a faster time scale.

Several dynamic scenarios can be envisioned, in particular, either the nut is free to rotate, or the bolt is free to rotate, or both can rotate (as viewed in the lab frame). Of course which of these scenarios is correct will be a function of the relative frictional drag of each component, including the effect of any anchors which may prevent rotation. Whether it is the RNA polymerase or the DNA that twists (again, as observed in the lab frame) has, at least, conceptual implications for gene regulation. In particular, supercoiling generated from transcription (see fig. 1) could act as a negative feedback, preventing further transcription or transcription of neighboring genes.

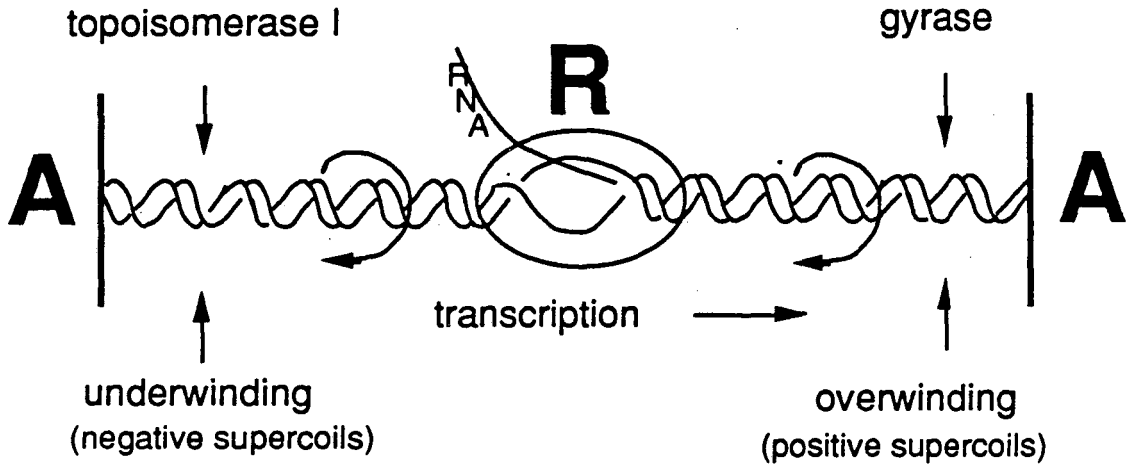

FIGURE 1-1: The transcription complex: The RNA polymerase proceeds down the DNA, producing RNA complementary to the DNA template. The DNA may become supercoiled if: the DNA is anchored (points A); if the polymerase does not rotate; if no "slippage" occurs between the polymerase; and if the rate of supercoil generation is faster than enzymes topoisomerase I and gyrase (also called topoisomerase II) can removed them. The polymerase, in this case, may topologically isolate the two domains, preventing the oppositely handed supercoils from annihilating one another.

The simplest and perhaps most intuitively obvious scenario is where the polymerase ("the nut") is free to rotate. Transcription then proceeds without any supercoiling of the DNA. The situation may not be so simple however. As the nascient RNA strand grows in length the drag on the polymerase-RNA complex will increase. This is particularly true if ribosomes (which make protein using RNA as a template in a process called translation) bind to the RNA. The size of the polymerase-RNA complex can grow quite large: the polymerase, has a molecular weight of about 500,000 daltons (the approximate size for E.Coli and for many eurcharyotes), the RNA is about 300,000 daltons for a 1000 base-pair gene, and each ribosome is about 50,000 daltons, with tens or even hundreds of ribosomes (in prokaryotes) possibly bound to the RNA. Furthermore, this structure is likely extended in space (i.e., not compact), meaning that it will have a large moment of inertia and be difficult to rotate. On the other hand, the DNA may also be very large — a molecular weight of many millions — although the structure may be relatively compact and may contain swivel points that allow for rotation. (The enzyme topoisomerase I, which removes negative supercoils, may create swivel points (Liu and Wang, 1987 and ref. therin). Experimentally, which has greater frictional drag has not yet been measured.

If the DNA is relatively free to rotate but the polymerase is not, then transcription may generate supercoiling *if* the DNA is fixed at some endpoints, for example, by periodic attachment to the nuclear membrane (Paulson and Laemmli, 1977) or nuclear scaffold (Ogden et al., 1988) and the supercoils are generated faster than topo I or gyrase can remove them. The region in front of the polymerase will be overwound (positively supercoiled) and the region behind the polymerase will be underwound (negatively supercoiled). The supercoils will not annihilate each other if the polymerase does not rotate (due to frictional drag) and no "slippage" occurs at the binding site, thereby topologically isolating the two regions. Distinct topological regions where supercoils of

opposite polarity can be formed without annihilating each other can also be formed by a circular DNA with simultaneous transcription of oppositely oriented complexes — in effect, the topology and complexes form topological anchors (Wu et al., 1988). The generation of supercoils, however, no matter what form of anchor, may impede further transcription because of the energy needed to continue over- and under-winding the DNA.

Which of these scenarios is correct? Or is some middle ground, where both the RNA and the DNA rotate slowly, perhaps generating supercoils inefficiently, the correct scenario? The answer, so far, is not yet known, although intriguing work by Lui, Wang and coworkers indicate that motion of the transcription complex along the DNA can induce supercoils both *in vivo* and *in vitro*, albeit inefficiently, if either gyrase (which removes positive supercoils in procharyotes) or topo I is inhibited (Liu and Wang, 1987; Wu et. al., 1988, Tsao et al, 1989).

To understand the biochemist's approach to transcriptional dynamics, it is worthwhile to briefly describe the approach taken by Liu and co-workers, where they have used supercoiling as a measure of transcriptional dynamics. Liu and co-workers inserted a modified plasmid pBR322 into a bacteria with active topoisiomerase I but Novobiocin-inhibited gyrase (Wu et al., 1988). The plasmid is circular and constructed to have to opposing promoters. If the second scenario is correct, in which polymerase does not rotate during transcription, supercoils should be generated when the two genes are transcribed simultaneously. With enough RNA polymerase, simultaneous transcription is expected to occur and the inhibition of gyrase means that the positive supercoils will not be eliminated, whereas topoI activity will eliminate negative supercoils. Consequently, the entire plasmid should have a net number of positive super-turns (or, in other words, a net positive superhelicity) after transcription. If the RNA polymerase is completely

stationary and no slippage occurs, then one superturn should be generated for each 10 base pairs of the DNA that is transcribed.

Experimentally, the extent of supercoiling of the DNA was measured on a two-dimensional agarose gel and then compared to the amount of RNA generated. (Supercoiled DNA moves faster than relaxed DNA in an agarose gel when an electric field is applied. This is because a supercoiled piece of DNA is more compact than a relaxed piece, and therefore has a smaller cross-section for interacting with the agarose matrix, which results in less drag and more speed.)

They found that positive supercoils were indeed generated, although quite inefficiently (Wu, 1988). That is, the drag on the polymerase was sufficient to generate some supercoils, but much less than the one superturn per 10 base pairs that would be expected if the polymerase was immobilized. To be specific, after a half hour of transcription the superhelical density increased to approximately +0.03, meaning 3 positive turns were added for every 100 turns normally present in the relaxed DNA. Since the pBR322 is normally at ≈-0.06, the net increase is 9 turns per 100turns initially present. For a molecule the size of pBR322, ≈4300 base pairs, that's an additional 39 turns. If superturns were generated with 100% efficiency, 9000 superturns would be generated! (A transcription rate of 50bp/sec = 5turns/sec, acting for 30minutes corresponds to 9000 superturns.) 9000 superturns, is, of course, ridiculous since the DNA helix could not possibly withstand such distortion, but the number does show that, while superturns are generated, they are done so quite inefficiently.

Liu and co-workers' experiments, however intriguing, is hardly the definitive answer to the questions of transcription dynamics. Their technique strictly looks at supercoiling, an indirect and apparently inefficient gauge of the dynamics. Furthermore, their system relies on using circular plasmids with opposing genes, a rather artificial and limiting

situation. Clearly, a more direct technique, namely a spectroscopic technique, that looks at motion directly would be desireable.

There are a number of steps which must be taken before the dynamics (and energetics) of the transcription complex, as measured by spectroscopy, can be adequately understood. Before measuring the relative motion of RNA polymerase and DNA, a first step is to measure the motion of the DNA in the absense of any enzymes. This will determine both the "baseline" DNA motion, as well as the bending and twisting rigidities of the DNA. A second step is to measure the properties of supercoiled DNA. A third step is to measure the dynamics of chromatin, since this is the physiological form of DNA. Once these "background" motions have been measured, the next, more difficult step of measuring the assembly's dynamics can be made and properly interpreted.

It should be noted that many of these "controls" are of inherent interest themselves, aside from the dynamics of the transcription complex. For example, measuring DNA rigidity is important because the stiffness of DNA strongly influences the binding of many proteins which regulate gene expression. When cro repressor binds to its complementary DNA recognition site, to pick one case, the protein forces the DNA to bend with a radius of curvature of 140 base pairs (Anderson 1981, Ohlendorf 1982). Experiments have shown that changing the rigidity of the DNA affects the binding constant of the protein. (The rigidity was changed by altering the base pair composition of sequences *surrounding* the protein footprint; hence the decrease in binding affinity is not due to a loss of base pair recognition by the protein.) A similar result was found for a number of other DNA-binding proteins (Gartenberg, 1988, and ref. therein.). Other proteins simultaneously bind to two separated sites on the DNA, requiring the proper twist of the helix to orient the major (or minor) groove towards the protein.

More generally, dynamic measurements give insight into static, structural properties. If DNA is modelled as a spring, then the spring constant — whether torsional or bending — as well as the damping constant can be measured by looking at the spectrum of motions. Anharmonic terms in the potential can also be detected. These parameters, in turn, give information about higher order structure, like superhelicity or chromatin organization. If the torsional constant is a function of superhelicity, for example, then by measuring the torsional constant (by watching twisting motions), it is possible to determine the superhelical state of the DNA (see Chpt 4). Information about the local environment of the DNA can also be garnered. For example, by comparing DNA motion in a solvent of known viscosity with DNA motion *in vitro,* the cell viscosity can be approximated.

Background: DNA Dynamics

Hopefully the previous discussion has convinced the reader that the study of DNA dynamics is a worthwhile field of endeavor in which much biologically useful information can be found. Not surprisingly, many studies have already been done. These are discussed in detail in each of the relevant chapters, but a brief overview will be presented here.

It is well known that DNA can be described as a semi-flexible polymer (Harris and Hearst, 1966; Hearst and Harris, 1966a,b, 1967; Hearst and Reese, 1980; and for a review, see Bloomfield, Crothers and Tinoco). Both the bending and twisting rigidities can be characterized by stiffness parameters. The persistence length of DNA, the distance over which the polymer "persists" in a given direction, characterizes the bending rigidity: for B-form DNA, it has been measured with several techniques to be approximately 550Å, or 140 base pairs (Bloomfield). The torsional constant describes the twisting

rigidity and has been found to be $\approx 2 \times 10^{-19}$ erg-cm (Wahl, 1970; Millar, 1980; Thomas, 1980). In the 100 nanosecond-and-shorter time scale, twisting motions dominate the depolarization seen in fluorescence-detected experiments of DNA. Theories have been developed which adequately describe this motion (Barkley, 1979, Allison, 1979). At longer time scales, twisting is essentially complete, and bending causes further depolarization/reorientation. A full theoretical description has not yet been made for these motions.

The physical parameters describing DNA vary with both DNA structure and environmental conditions. A-T rich regions of DNA, for example, are more flexible than G-C rich regions. (Dissolved) salt screens the negative charges of the phosphate backbone of DNA; with electrostatic repulsion minimized, the DNA becomes more flexible. Topological considerations, such as torsional stress caused by supercoiling of the DNA, can change the torsional rigidity. Millar et al. have found that the plasmid pBR322, for example, is roughly 40% stiffer in its native, negatively supercoiled state, than in its relaxed state (Millar,1980). In chapter 4 we present results, extending the work of Millar, to a series of both negatively and positively topoisomers of DNA.

Interactions with solute molecules are also important. Polyamines, for example, bind in the major groove of B-form DNA (Feuerstein,1988). By creating a "bridge" across the phosphate backbone of the major groove, the polyamines stiffen the DNA. This bridge, however, also shortens the major groove, displacing DNA-bound water molecules which stabilize the B-form of DNA; consequently, polyamines also induce a B to Z transition. Polyamines have also been implicated in cell cycle regulation, possibly through their ability to condense chromatin. (In patients with brain tumors, a case where cell cycle regulation has obviously failed, polyamines levels are found to be high — in fact polyamine levels are one test for diagnosing the presence of a brain tumor (Basu,

1989). In chapter 4 we examine the sequence dependent effects of spermidine binding on the torsional rigidity of DNA.

DNA- protein interaction is perhaps the most important class of interaction affecting DNA flexibility. DNA *in vivo*, is, of course, complexed with proteins to form chromatin. Nucleosomes found in eucharyotic organisms are tightly coiled DNA wrapped around a protein (histone) octamer. In the nucleosome core, the DNA is forced to bend one and three-fourths turns in only 140bp (less than a persistent length). It is intriguing, though as yet, unsubstantiated, to postulate that the placement of nucleosomes is a function of DNA stiffness, which in turn, is determined by base pair sequence, local salt concentration and solute interaction. In chapter 5 we show, using the polarized Fluorescence After Photobleaching (pFRAP) technique, that DNA in condensed chromatin is substantially more rigid than naked DNA (Selvin, 1990).

General Principles of Time-Resolved Spectroscopy

We now examine the general concepts of time-resolved spectroscopy. In particular, the time resolution, memory time and sensitivity of various techniques are examined and motivation is presented for the particular techniques used to study DNA dynamics in this thesis.

Essentially all (time-resolved) spectroscopic techniques that measure rotational motion work in the following simple way: The sample is initially perturbed from thermal equilibrium and the relaxation back to equilibrium is then monitored.

In the simplest case, the relaxation is due only to rotation, in which case, the relaxation time is the rotational time. An example is electric birefringence. Consider a DNA sample in water: at equilibrium, the DNA molecules point in all different directions, i.e., the sample is random and isotropic. If the DNA is then exposed to a pulse of electric field (by, e.g., placing the sample between the plates of a capacitor and discharging the capacitor rapidly) the DNA will experience a torque because it has an induced electric dipole moment, and if the field is strong enough, significant alignment will occur. Immediately after the pulse, however, the DNA will start to reorient (due to thermal motion) and eventually return to its random state which is thermal equilibrium. Information about the DNA can be inferred from the recovery time. A small piece of DNA, for example, will rapidly reorient; a large piece will take longer. For the same size piece of DNA, a stiffer piece will take longer to relax than a more flexible piece.

Unfortunately, the situation is usually not so simple. There are are often relaxation pathways that are independent of rotation. That is, even if the sample does not reorient, the system can evolve towards isotropicity. For example, if a bunch of stationary, randomly oriented fluorophores are excited with a pulse of plane polarized light, an anisotropic distribution of excited fluorophores will be produced: those molecules aligned with the plane of polarization will be excited; those aligned perpendicular will not. After the pulse, even in the absence of motion, the anisotropy will disappear in time as the excited molecules return to the ground state. This time is of course just the fluorescent lifetime. If instead of being stationary, the molecules are allowed to tumble, the anisotropy will also disappear due to the random motion.

Fortunately, in most cases, the two relaxation pathways can be independently measured, thereby isolating the rotation-dependent pathways. For example, the fluorescent lifetime can be measured by placing an analyzer (polarizer) in front of the detector, oriented at the magic angle (54.7 degrees) with respect to the plane of

polarization of the excitation light. With an analyzer at the magic angle, the fluorescent intensity striking the detector is independent of rotation of the fluorophore. Or the analyzer can be place alternatively in the parallel and perpendicular positions with respect to the incoming plane of polarization. By taking a ratio of the fluorescent intensities in the two positions and normalizing by the total intensity, the rotational time can be isolated.

For spectroscopy, there are three relevant time parameters: the pulse duration, the characteristic rotational time(s), and the characteristic time for relaxation via non-rotational processes. The later process can be called the "memory time" since it tells how quickly the system forgets about the initial pulse that disturbed the system from equilbrium. The memory time determines how long the technique can look — once the system has forgotten its initial anisotropy, no more information can be gamered.

The pulse duration determines the time resolution of the experiment. In general, the pulse width is the best possible time resolution, although, in some cases, deconvolution can improve the time resolution to approximately a tenth of the pulse width. The characteristic rotational time(s) is of course what's of interest.

In addition to the time characteristics of spectroscopic technique, the sensitivity — i.e., how few molecules can be detected — is also important. This is especially true when using biological samples, which are commonly available in limited quantities. The overriding principle is that dark background experiments are more sensitive than light-background experiments. A single photon can be detected in a dark background, but in a light-background experiment, the photon of interest will be lost amid the Poisson noise and other sources of fluctuations arising from a background. While integration of the background decreases Poisson noise, it does so frustratingly slowly — with the square root of time — and even then, may leave you with coherent noise remaining in the background, the signal of interest lost forever!

In addition, optical experiments are many thousands to many millions (even billions!) of times more sensitive than techniques which rely on comparatively long wavelength radiation (radio waves to microwaves), such as magnetic resonance. The higher energy involved in optical experiments confer a number of advantages. Whereas optical experiments involve the absorption or emission of photons many times the energy of thermal photons, this is not true for the longer-wavelength experiments. Consequently, the signal photons in the latter experiments are swimming in a pool of thermal photons (i.e., a big background). Furthermore, the sensitivity of long-wavelength experiments is decreased by a Boltzman factor that is close to one. This decreases the effective absorption cross section. In an EPR experiment at 10GHz, for example, the transition being probed is much less than k_bT at room temperature ($\approx$ 1/40 electron volt) and only one in a thousand of the molecules that could absorb (at zero kelvin, e.g.) actually do absorb. A final advantage of optical experiments is that single photon detectors are available. Visible photons have enough energy to ionize an electron from a semiconductor — the photoelectric effect. This tiny current can then be amplified and detected, which is just how a photomultiplier tube works. The state of the art photon-counting detectors can now detect photons of $\approx$28μm wavelength, although commercial instruments are limited to a micron or less (Brent Wurfel, private communication).

In many of these respects, fluorescence spectroscopy is nearly ideal. Our experiments have both excellent time resolution and exquisite sensitivity: they photon count with a dark background. The reason, of course, to use non-optical techniques is that they are capable of providing completely new and different information from optical experiments. EPR, for example is sensitive to paramagnetic ions and spin labels: NMR to the spin of a nucleus....

Let us now apply these general considerations to the spectroscopic techniques used here. The fluorescence experiments are the most sensitive, the absorption experiments

next (an optical experiment but with light background) and the EPR last. The fluorescence depolarization experiments have the fastest time resolution — picoseconds — but also the shortest memory time. The absorption experiment has approximately a thousand times worse time resolution, but a thousand times longer memory time. The pFRAP has yet worse time resolution, but even longer memory time. In time, the EPR falls between the absorption and pFRAP experiments. The interest in the EPR technique, however, is not primarily its time resolution (although that is part of its attraction) but its great sensitivity to small angular displacements. The relevent spectroscopic and biological time regimes are summarized in Fig. 1-2.

DNA dynamics: Measurement and Time Scales

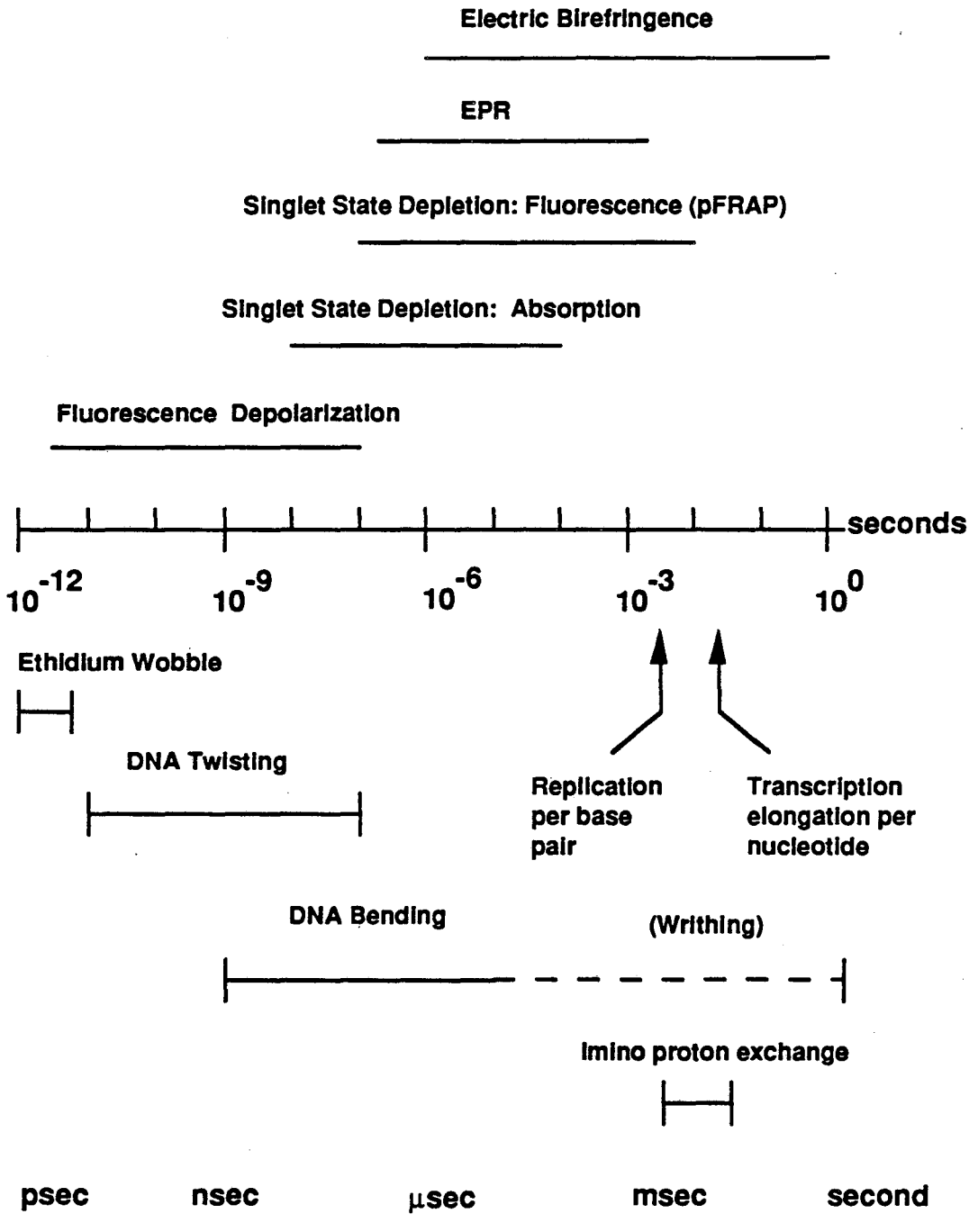

FIGURE 1-2: A combination of techniques allow probing of DNA dynamics from picoseconds to milliseconds, a time scale during which much biological activity takes place.

References

Allison, A.A., J. Shibata, J. Wilcoxon, and J.M. Schurr (1979) Torsion Dynamics and Depolarization of Fluorescence of LInear Macromolecules. I. Theory and Application to DNA. *J. Chem. Phys.* 41: 35-59.

Anderson, W., D. Ohlendorf, Y. Takeda, B. Mathews (1981) Structure of the cro repressor from bacteriophage Lambda and its interaction with DNA, *Nature,* 290: 754.

Barkley, M.D. and B. Zimm (1979) Theory of Twisting and Bending of Chain Macromolecules: an Analysis of the Fluorescence Depolarization of DNA *J. Chem. Phys.* 70: 2991-3007.

Basu, H., B. Feuerstein, D. Deen, W. Lubich, R. Bergeron, K. Samejima, L. Marton (1989) Correlations Between The Effects of Polyamine Analogs on DNA Conformation and Cell Growth, *Cancer Research.*

Bloomfield, V., D. Crothers, I. Tinoco, Jr. ,Physical Chemistry of Nucleic Acids.

Gartenberg, M., and D. Crothers (1988) DNA Sequence Determinants of CAP-induced Bending and Protein Binding Affinity, *Nature,* 333: 824.

Feuerstein, B., H. Basu, L. Marton (1988) Theoretical and Experimental Characterization of Polyamine/DNA Interactions, *Progress in Polyamine Research,* 517.

Harris, R.A. and J.E. Hearst (1966) On Polymer Dynamics, *J. Chem. Phys., 44 (7),* 2596-2602.

Hearst, J.E. and R.A. Harris (1966a) On Polymer Dynamics II, *J. Chem. Phys., 45(8),* 3106-3113.

Hearst, J.E. and R.A. Harris (1966b) A New Model for Polymer Dynamics, *J. of Polymer Science: Part C, 15,* 331-333.

Hearst, J.E. and R.A. Harris (1967) On Polymer Dynamics III, *J. Chem. Phys., 46(1),* 398.

Hearst, J.E. and D.A. Reese (1980) Sedimentation of Wormlike Coils. II. *J. Chem. Phys., 73,* 3007.

Liu, L.F. and J.C. Wang (1987) Supercoiling of the DNA Template During Transcription. *Proc. Natl. Acad. Sci. USA.* 84: 7024-7027.

Liu, L. F. (1989) DNA Topoisomerase Poisons as Antitumor Drugs. *Ann. Rev. Biochem* 58: 351 .

Millar, D., R. Robbins, A. Zewail (1980) Direct Observation of the Torsional Dynamics of DNA and RNA by Picoseconds Spectroscopy, *PNAS USA,* 77: 5593.

Ogden, G.B., M.J. Pratt and M. Schaechter (1988) The Replicative Origin of the *E. coli* Chromosome Binds to Cell Membranes Only When Hemimethylated. *Cell* 54: 127-135.

Ohlendorf, D., W. Anderson, R. Fisher, Y. Takeda, B. Mathews (1982) The Molecular Basis of DNA-Protein Recognition Inferred from the Structure of Cro Repressor, Nature, 298: 718.

Paulson, J.R. and U.K. Laemmli (1977) The sturcture of Histone-Depleted Metaphase Chromosomes. *Cell* 12: 817-828.

Selvin, P.R, B.A. Scalettar, J.P. Langmore, D. Axelrod, M.P. Klein and J.E. Hearst (1990) A Polarized Photobleaching Study of Chromatin Reorientation in Intact Nuclei. *J. Mol. Biol.* 214: 911-922.

Thomas, J., A. Allison, C. Appellof and J. Schurr (1980) Torsional Dynamics and Depolarization of Linear Macromolecules. II. Fluorescence Polarization Anisotropy Measurements on a Clean Viral ϕ29 DNA, *Biophysical Chemistry,* 12: 177.

Tsao, Y.-P., H.-Y. Wu and L.F. Liu (1989) Transcription-Driven Supercoiling of DNA: Direct Biochemical Evidence from *In Vitro* Studies. *Cell* 56: 111-118.

Wahl, Ph., J. Paoletti and J. Le Pecq (1970) Decay of Fluorescence Emission Anisotropy of the Ethidium Bromide DNA Complex — Evidence for Internal Motion in DNA, *PNAS USA* 65: 417.

Wu, H.-Y., S. Shyy, J.C. Wand and L.F. Liu (1988) Transcription Generates Positively and Negatively Supercoiled Domains in the Template. *Cell* 53: 433-440.

Chapter Two

Spectroscopy I

Time Correlated Single Photon Counting:

Measuring the rapid twisting motions of DNA requires a technique that has excellent time resolution. Time Correlated Single Photon Counting (TCPC) has picosecond resolution, a memory time of approximately one hundred nanoseconds (depending on the particular fluorophore used), and the sensitivity to measure relatively small amounts of sample.

TCPC is a modification of a standard fluorescence depolarization (FD) experiment (O'Connor and Phillips, 1984; Lackowicz, 1983). In a fluorescence depolarization experiment, a polarized laser pulse excites a fluorescently labelled sample, and the fluorescence is then collected, typically at right angles from the excitation beam, after passing through an analyzer. The analyzer is placed alternately parallel and perpendicular to the plane of polarization of the exciting pulse (see Figure 2-1).

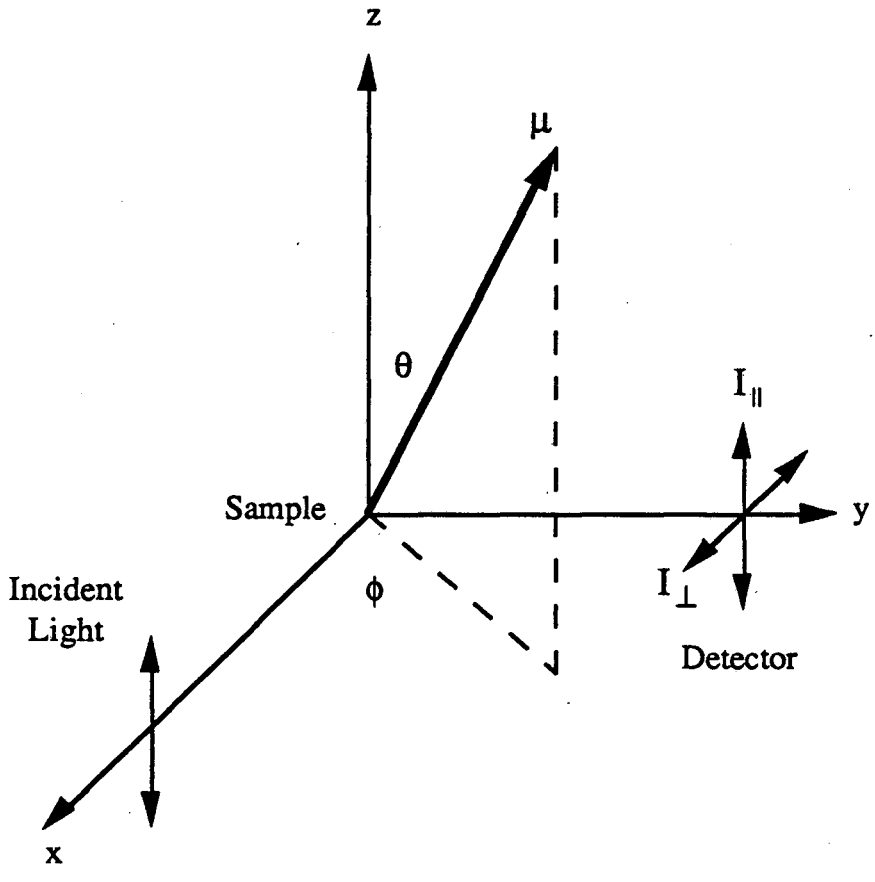

FIGURE 2-1: Coordinate system used to discuss fluorescence depolarization experiment. In the diagram, one fluorophore is shown with absorption and emission dipole parallel, along μ. (Adopted from Cantor and Schimmel, p. 456, 1980.)

As previously noted, the time evolution of the collected fluorescence is a convolution of the fluorescence lifetime decay and intensity changes due to rotational motion. Taking the ratio of the parallel and perpendicular modes eliminates the fluorescence lifetime decay from the data: the decay of the ratio is only a function of reorientational motion. Various ratios can be formed, the most common ones being the Polarization (P) and the Anisotropy (A).

$$P(t) = [I_{\parallel}(t) - I_{\perp}(t)] / [I_{\parallel}(t) + I_{\perp}(t)]$$

$$A(t) = [I_{\parallel}(t) - I_{\perp}(t)] / [I_{\parallel}(t) + 2I_{\perp}(t)]$$

For a spherical molecule undergoing diffussion, the anisotropy takes a particularly simple form:

$$A(t) = (2/5)e^{-t/\tau_c}[(3\cos^2\xi - 1)/2] \qquad \tau_c = 1/6D_{rot}$$

where ξ is the angle between the absorption and emission dipole moments of the dye, τ_c is the rotational correlation time and D_{rot} is the rotational diffussion constant. τ_c is approximately linear with molecular weight and a useful order of magnitude figure is that τ_c is about 1nsec for every 2400 daltons for a spherical protein. Commonly $\xi \approx 0$, in which case the expression reduces further: $A(t) = (2/5)e^{-t/\tau_c}$. (It trivially follows that a such a system has an initial anisotropy of 0.4, which, in the presence of motion, decays towards zero.)

The TCPC experiment is conceptually identical to a fluorescence depolarization experiment; experimentally, however, only one fluorescent photon per laser pulse is collected. (Actually, fewer than one photon/pulse — typically 0.02 photons/pulse — is collected on average to prevent accidental collection of two photons.) The time between the laser pulse and the arrival of the single photon is measured, and after many, many pulses, a histogram of the number of photons per time interval is produced. Formally, the resulting histogram is equivalent to the FD experimental results, where many photons are counted with each laser pulse. The advantage of TCPC is that excellent time resolution can be achieved (a few picoseconds) and the system is relatively immune from systematic noise; the disadvantage is that since many photons are "thrown away" data collection takes longer. The excellent time resolution and noise immunity in TCPCS comes about because it is only necessary to measure *when* an event occurred (the photon hitting the

detector), not the exact shape of the event (the pulse profile) as is the case in an FD experiment. Experimentally, the time resolution is achieved by using a stable time to amplitude converter. The time to amplitude converter consists of a voltage ramp which is started with the laser flash and stopped when the (first) fluorescent photon arrives. A multichannel pulse height analyzer makes a histogram as the experiment is repeated over and over again. (A technical note: the voltage ramp can be run in "reverse mode,", i.e., started with the fluorescent photon and stopped with a delayed laser pulse. Because there are fewer fluorescent photons than laser pulses — on average about 0.02 fluorescent photons/pulse — running in reverse mode prevents the ramp from starting unless there is actually a fluorescent photon present, i.e., a signal. This minimizes reset time of the electronics, allowing faster repetition of the experiment. Reverse mode was used in all TCPC experiments in this thesis.)

The particular system used here is a modified version of a TCPC spectrometer in the Laboratory of Chemical Biodynamics owned by Professor Ken Sauer. A new pumped-dye laser system was installed, including a light intensity monitoring circuit. The optical train, most notably the collection optics was reconfigured to give greater collection efficiency. Finally, the photon counting electronics was used with little modification, although they were set to minimized dead time. The machine as used here is shown in the following diagram (Figure 2-2) and discussed in some detail below.

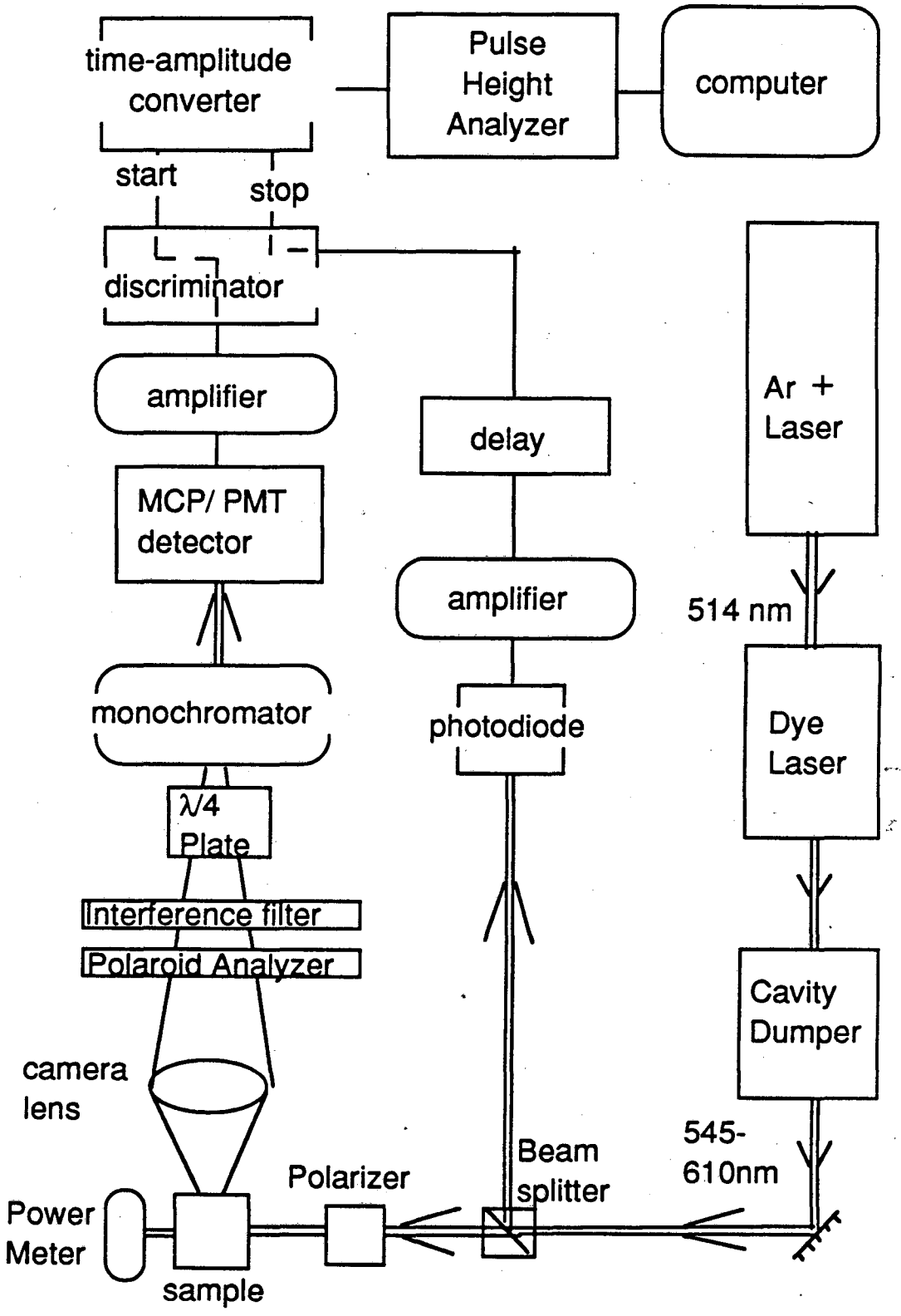

Figure 2-2: TCPC Schematic

The pump laser is a mode-locked argon ion laser (Spectra Physics 2040-15) operated at 514nm, a repetition rate of 82Mhz, and an output pulse width of approximately 100psec fwhm. Typical average (CW) output power is 1-1.4watts, which synchronously pumps a cavity-dumped dye laser (Spectra Physics 3500 with R6G mirrors but Rhodamine R110 dye, using Spectra Physics cavity-dumper driver 451). The output pulses are at 550nm and typically 4.5 picoseconds wide as detected by a Spectra Physics autocorrelator. AveragePulse shape is also monitored with an Antel Optronics AR-S3 fast photodiode (25psec rise time) and Tektronix 7603 sampling scope. The cavity dumper decreases the repetition rate from 82MHz to a selectable level — for our experiments it is always set to 4Mhz. The output power is 20-30mW. After attenuation by ≥1% neutral density filter and passing through a crystal polarizer, these pulses were used to excite the sample.

The fluorescence from the sample was collected by a high-numerical aperture lense (more on this later), passed through a polaroid analyzer, and focussed onto a red-sensitive microchannel plate photomultiplier tube (Hamamatsu MCP-PMT # R2809U-11).

The output of the MCP-PMT was amplified by a Hewlett Packard 8447F amplifier with a bandwidth of 1.3GHz and then sent to a Tennelec TC454 constant fraction discriminator. The discriminator has an upper and lower threshold. The lower threshold minimizes dark counts due to thermionic emission from the MCP-PMT by ensuring that only pulses of sufficient height get through. The upper threshold selects against large spikes, either caused by random voltage surges or from two photons simultaneously striking the detector. The discriminated pulse then starts the time to amplitude converter (Ortec 457). A portion of the laser pulse, detected by a home-built fast photodiode and delayed in time (Ortec 425 Delays and coax cable), then stops the converter. A Tracor Northern Econ II Series NS-710 pulse height analyzer creates a histogram. The data are then sent to a VAX-11-785 computer for data storage and manipulation. Laser intensity fluctuations were normalized by integrating the light intensity over the course of each

parallel and perpendicular run.

Technical Considerations in Fluorescence Depolarization

The goal of a TCPC fluorimeter is to collect data of high signal to noise with excellent time resolution. The parameters governing these two factors will be discussed in some detail. Many of the considerations are relevant to other time-resolved, fluorescence-based techniques.

Temporal Characteristics: Resolution and Memory Time:

There are two critical parameters that contribute to the time resolution: the excitation pulse width and the response time of the detection circuitry. In general, with today's technology, laser pulse widths of a few picosecond or less are easily (commercially) obtainable. Response times of photon counting detectors, however, are on the order of tens of picoseconds, with timing electronics commonly adding another tens of picoseconds jitter. It is therefore critical to use a fast detector and associated electroncs.

Traditionally photomultiplier tubes (PMT) have been used (operated in the photon counting mode), but more recently, the development of microchannel plates, placed in front of a photomultiplier tube, has become standard practice. (The MCP-PMT is available as one unit.) The MCP-PMT gives significantly faster time response than using a pmt alone and reduces troublesome "afterglow" ringing (see Hamamtsu technical bulletins, Chang et. al. (1985) and Leskovar, 1989,1988,1985). While the fastest PMTs (e.g. the Amperex XPQ-2020, or RCA C31034) have a rise time of 1-2nsec and time resolution of 250-310nsec, MCP-PMTs have a rise time of 240-400psec (check) and transit time spread (t.t.s.) of 50-100psec. The fastest MCP-PMT currently on the market is the Hamamtsu R2809, used in the experiments here, has a rise time of 0.24nsec, and a t.t.s. of 55psec (Hamamatsu technical bulletins #T-112, #ET-03/Oct 87 and product

bulletin PB-154/Sept 86). The time resolution of the detector is approximately equal to the t.t.s.

A glance at the innards of the MCP-PMT will explain why the t.t.s. limits the time resolution (Figure 2-3).

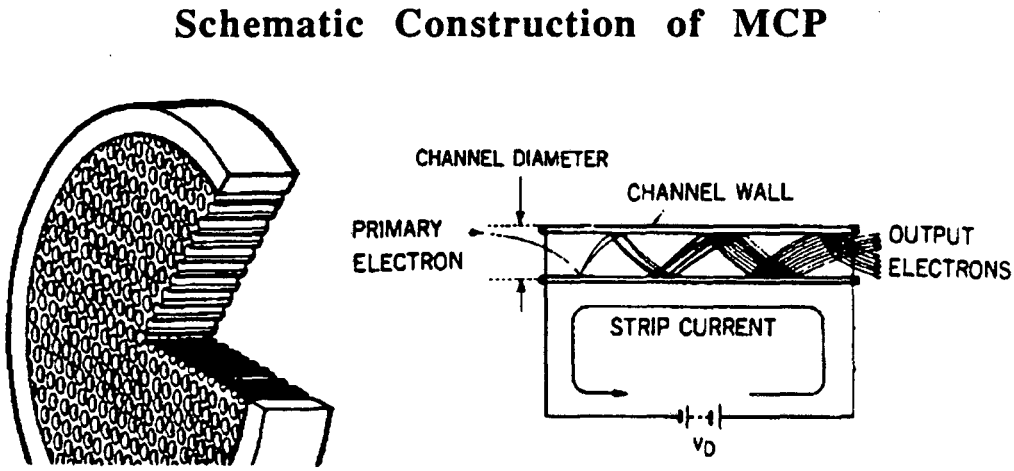

FIGURE 2-3: A photon hits the MCP (left), creating a photoelectron (also called primary electron) which then is amplified. The electrons from the MCP then hit the photocathode of the PMT and are amplified through a number of hi-voltage dynodes, until they are finally collected at the anode of the PMT.

When a photon hits the microchannel plate a photoelectron is ejected. This miniscule current is then amplified by the microchannel plate and a series of dynodes. The result is a cascade of electrons which finally hits the anode. The time between the photon hitting the cathode and the arrival of the electrons at the anode is the transit time. As long as the transit time is a constant, it is just a delay and does not limit time resolution. All of the electrons, however, do not arrive at the anode at the same time — there is a spread in time, which is called, appropriately enough, the transit time spread.

The inherent time resolution comes from the transit time spread. If two photons strike the cathode less than a t.t.s. time apart, the resulting electron cascade from each photon will overlap and it will appear as one large, broad pulse at the anode. Since in TCPC, we only look at the time of arrival of the pulse, and not its amplitude, the two photons cannot be resolved. Consequently, the t.t.s. is the limit of time resolution.

The t.t.s is caused by electrons that either have different initial velocities or follow a different path, and consequently take different amounts of time to reach the anode. In general placing the photocathode close to the first dynode and decreasing the number of dynodes will decrease the t.t.s. because any possible path length differences are minimized. In addition, using a microchannel plate at the front end of a photomultiplier tube greatly decreases the t.t.s.. The plate consists of thousands of capillary tubes (typically 12μm in diameter, with some newer versions at 6μm) coated with semiconducting material. A voltage gradient is placed along the tube length. As the electron is accelerated down the gradient, it hits the tube walls, releasing several secondary electrons, which in turn, hit the walls, releasing more electrons.... Because the capillary tube is so fine, the electron path is confined, thereby minizing t.t.s.

If one wants to push things, then the time resolution can be increased to a fraction of the t.t.s. (typically a tenth) via deconvolution. For deconvolution to work, the t.t.s. shape must be known accurately and the signal decay curve must have a simple functional dependence. Although deconvolution is commonly done, it is better to avoid if possible by going to a faster detector. Obviously, when you've bought the fastest, most expensive detector there is, and still need better time resolution, deconvolution is your only choice.

The memory time of the system is primarily determined by the fluorescent lifetime of the dye. After excitation, the fluorescence dies away until, eventually, the signal is buried in the noise. For ethidium bromide, the dye used in all our TCPC experiments, the

lifetime when bound to DNA is 22nsecs. Experimentally, it is realistic to look out to approximately a 100nsec (≈5 lifetimes). Obviously, the better the signal to noise, the longer it is possible to look for.

Obtaining High Signal to Noise

To obtain data of high quality, it is necessary to first decrease — ideally eliminate — all sources of coherent noise. Beyond this, it is advantageous to collect as many fluorescent photons as rapidly as possible. The two ways to do this are to increase the number of photons by turning up the excitation light, and collecting the emitted photons efficiently with high numerical aperture optics.

There are, however, limits to both methods. Most obviously, increasing the light increases the probability of light-induced damage to the DNA. (When the ethidium bromide becomes excited it can react with the oxygen to form singlet oxygen, which can then nick the DNA.) TCPC, because it is a single photon counting technique, generally uses very low light levels and sample damage is rarely a problem.

The maximum photons per second that can be counted is ultimately limited by the restriction that only one fluorescent photon per excitation pulse can be collected without distorting the data. If two photons strike the detector, only the earlier one will be processed. This results in a histogram skewed towards early times.

In practice, the count rate is limited by the deadtime of the instrument. After a photon is detected, there is a certain amount of time during which the instrument is "dead," i.e., if a second photon comes along during this time it will not be processed. In our system the 13μsec deadtime of the pulse height analyzer is the limiting factor. The fraction of photons missed, in the limit where the deadtime (d) is much less than the average time between photons (t_{av}) is just d/t_{av}. A more exact expression can be calculated using Poisson

statistics, as follows.

We can define in the usual fashion the probability, P(n), as the probability of n photons arriving in some interval of time when the average number of photons in that interval is λ,

$$P(n) = \frac{\lambda^n e^{-\lambda}}{n!}$$

Here λ is the average number of counts in the deadtime.

The pertinent question is: given that one photon arrived (at, say t=0) what is the probability of one or more photons arriving in the next d seconds, where d is the deadtime of the instrument?

The number of photons missed is

$$\sum_{n=1}^{\infty} nP(n) = \frac{\lambda^n e^{-\lambda}}{n!}$$

and the fraction of photons missed is:

$$\frac{\text{\# missed}}{\text{total \# photons}} = \frac{\sum_{n=1}^{\infty} nP(n)}{1 + \sum_{n=1}^{\infty} nP(n)}$$

The result is simply:

$$\text{Fraction Missed} = \lambda / (1+\lambda).$$

The fraction missed as a function of average count rate is plotted in Fig. 2-4 for the experimental deadtime of 13 μsec.

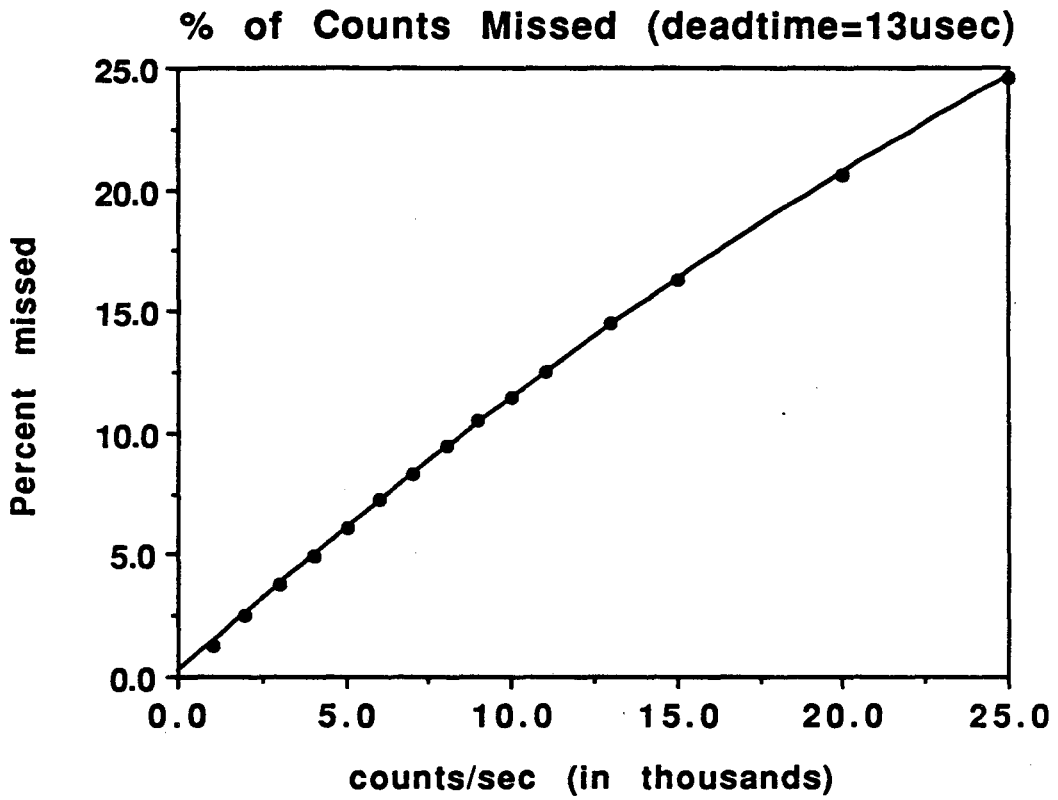

FIGURE 2-4: Fraction of photons missed due to deadtime: percent missed is [100 $\lambda/(1+\lambda)$] where λ is the average counts per second detected multiplied by the deadtime. As the fraction increases, the anisotropy is skewed to anomalously low values.

Experimentally, we limit the count rate to less than (5,000) counts per sec in the parallel. (For typical DNA samples, the counts in the perpendicular mode are roughly half that in the parallel mode.) This means in the parallel mode 6% is missed, and in the perpendicular mode, 3% is missed. Consequently, the anisotropy is skewed towards lower values by approximately 3% (6%-3% in the numerator). We correct for this relatively small effect in the data analysis.

Collection Optics: Effect of High Numerical Aperture Optics

Whatever the excitation light level chosen, it makes sense to collect as high a fraction

of the fluorescent photons as possible. The simplest way to do this is to place a high numerical aperture (or equivalently, low f-number) lense near the sample. The angle of collection is directly proportion to the numerical aperture of the lense.

$$\text{N.A.} = n_o \sin\theta \qquad f\# = \frac{1}{2}\text{N.A.} = \frac{\text{lense diameter}}{\text{focal length}}$$

where n_o is the index of refraction of the medium (for our system the medium was always air, so $n_o \approx 1$, θ is the maximum half angle subtended by the lense (objective) as viewed from the sample, and f# is the f-number.

The solid angle, or collection efficiency is proportional to the square of the numerical aperture. Obviously the larger the N.A. the higher the fraction of light that is collected. Numerical apertures of single lense's go up to about 0.5, and microscope objectives can have N.A.s greater than 1.

There is, however, a limit to the maximum N.A. that can be used for polarization studies. As the numerical aperture gets larger, the lense can "see around" the sample, blurring the distinction between the parallel and perpendicular modes. As the modes get blurred, the measured anisotropy decreases. The exact analytic expressions have been worked out by Axelrod (1979). They are:

$$I_{||} = K_a J_1 + K_b J_2 + K_c J_3$$

$$I_{\perp} = K_a J_1 + K_c J_2 + K_b J_3$$

where the K_i's are only a function of the collection optics, and the J_i's are only a function of the sample:

$$K_a = \frac{1}{3}(2 - 3\alpha + \alpha^3)$$

$$K_b = \frac{1}{12}(1 - 3\alpha + 3\alpha^2 - \alpha^3)$$

$$K_c = \frac{1}{4}(5 - 3\alpha - \alpha^2 - \alpha^3)$$

where $\alpha = \cos\theta$ and

$$J_1 = J_2 = \frac{1}{15}(\sin^2\beta + 1)$$

$$J_3 = \frac{1}{15}(3 - 2\sin^2\beta)$$

where β is the angle between absorption and emission dipole moments of the fluorophore. For a random, isotropic and immobile sample with $\beta = 0$, the anisotropy as a function of numerical aperture is plotted in figure 5.

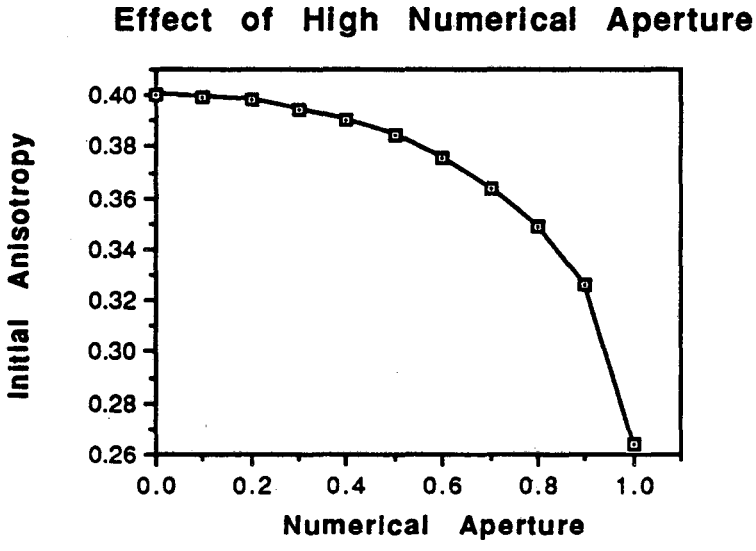

FIGURE 2-5: As the numerical aperture of the collection optics increases, the measured anisotropy decreases because the lense can "see around" the sample, blurring the distrinction between parallel and perpendicular.

Polarization Bias of Detection System

The dynamics information is found in the ratio of the fluorescence intensities in the parallel and perpendicular data. If the detection system has a polarization preference which remains uncorrected, the anisotropy function will be skewed. Note that the skewing is not just an offset, but alters the shape of the anisotropy decay function: at early times, when the anisotropy is large, any polarization preference will have a large effect, and at later times, when the anisotropy is small, the effect will be small. The torsional constant extracted from curve fitting will therefore be in error. The corrected anisotropy function is:

$$A(t) = [gI_{\parallel}(t) - I_{\perp}(t)] / [gI_{\parallel}(t) + 2I_{\perp}(t)]$$

where the g-value is the measured ratio of $I_{\perp}$ and $I_{\parallel}$ when it is known that $I_{\perp} = I_{\parallel}$ (i.e. the true anistropy value is one). A control sample with a ratio of one is made by taking a rapidly tumbling fluorophore and looking at the fluorescence after the molecule has tumbled completely: $I_{\perp}$ and $I_{\parallel}$ should then be equal.

First we attempted to make the g-value as close to one as possible by placing a quarter-wave plate in front of the detector. This reduced the g-value from 1/3.5 (heavily weighted against perpendicular photons) to approximately 0.93.

To measure the g-value, we used two different controls. First we used free ethidium bromide (*not* in the presence DNA), which has a tumbling time of approximately 100psec and a fluorescence spectrum similar to that of intercalated ethidium. The post-excitation fluorescence at times greater than approximately a nanosecond was then added in each polarization mode, and the ratio of the sum set equal to the g-value. The second control was similar, except that we used ethidium intercalated into a 20 base pair oligomer. The fluorescence spectrum was now identical to the samples of interest (longer pieces of DNA

with intercalated ethidium). This insures that the correct g-value will be determined, even if the g-value of the detector is wavelength dependent. Tumbling reduces the anisotropy to zero after 30nsec; consequently we used only points longer than this value. Furthermore, at this time only the intercalated ethidium contributes to the signal (there was considerable free dye in the oligo-dye solution, but the free dye, with a 2.5nsec lifetime, decays much more rapidly than the intercalated dye, with a lifetime of ≈23nsec). Consequently the fluorescence emission is identical to the samples of interest, completely eliminating any wavelength-dependent artifacts. The measured g-value was consistently 0.93, plus or minus 1%, even from day to day (so long as the quarter-wave plate was not moved).

Source (Laser Intensity) fluctuations:

Laser light intensity fluctuations, if not minimized or controlled, can render a ratio measurement meaningless. If the laser is brighter during one mode than the other, the measured ratio will be in error. The argon ion laser is specified to have a power stability of a few percent over days, theoretically sufficient for our purposes. Nevertheless, to minimize the effects of long term drift, we alternated data collection between parallel and perpendicular modes once every five minutes.

Even so, problems occured. We found that if we cavity dumped the argon-ion laser directly (no dye laser), the light intensity was indeed stable to within a few percent, but that if the beam was then passed through an external polarizer, the intensity after the polarizer typically varied by 10% over a few minutes. Presumably this is because the polarization of the beam was varying due to instabilities in the cavity dumper. While the reason for this was not clear, it could be corrected for by normalizing all results to the integrated laser intensity illuminating the sample (i.e., after the polarizer).

The integrating light-monitoring circuit was simple. A Spectra-Physics power meter was placed immediately after the sample. The analog output of the meter was digitized

with a voltage to frequency converter (based on Analog Devices V to F converter) and counted with an Ortec 778 Photon counter.

Elimination of Scattered Light

The two primary sources of scattered light are Raleigh scattering at the incident light frequency, and Raman scattering at some longer wavelength. For water, the Raman shift is $\approx 3450 cm^{-1}$, so for excitation at 550nm, the Raman emission is at $\approx$ 680nm ($1/\lambda_{Raman} = 1/\lambda_{exc} - 1/\Delta\lambda_{vib}$). Both sources of scattered light are prompt (meaning essentially no delay between excitation and emission) and highly polarized. Consequently, if they are not eliminated or corrected for, they will contribute a large source of error in the initial bins of the anisotropy, skewing the results towards higher anisotropy. Both can be eliminated by using a monochrometer in the detection circuitry, but this generally eliminates much of the signal light (fluorescence) as well. Although we had a monochrometer in our collection optics, all slits were removed and the wavelength was set to zero so that the monochromter was effectively just as a set of mirrors. (The monochrometer could not be removed because of the needs of other spectrometer users.)

Most commonly a high pass filter is used to eliminate the scattered laser light, and the Raman scattering is electronically subtracted from of the data. (A blank water sample is used to determine the Raman intensity.) Instead, we used a bandpass interference filter (Model #613DF68) from Omega Optical (Brattleboro Vt.), thereby eliminating both Raleigh and Raman scattering, as well as any phosphorescence which is common with the colored glass hi-passed filters. The 50% transmittance bandpass was centered at 613nm with $\pm$ 34nm, with O.D. $\geq$ 6 at 550nm and and O.D. $\geq$ 4 at 680nm.

Finally, after all these effects are controlled for or eliminated, data of very high signal to noise without systematic artifacts can be acquired. Fig. 2-6 is parallel, perpendicular and anisotropy data from a sample of Lambda DNA dissolved in water with 75mM KCl,

at room temperature. The quality of data is typical of all measurements made with the TCPC system.

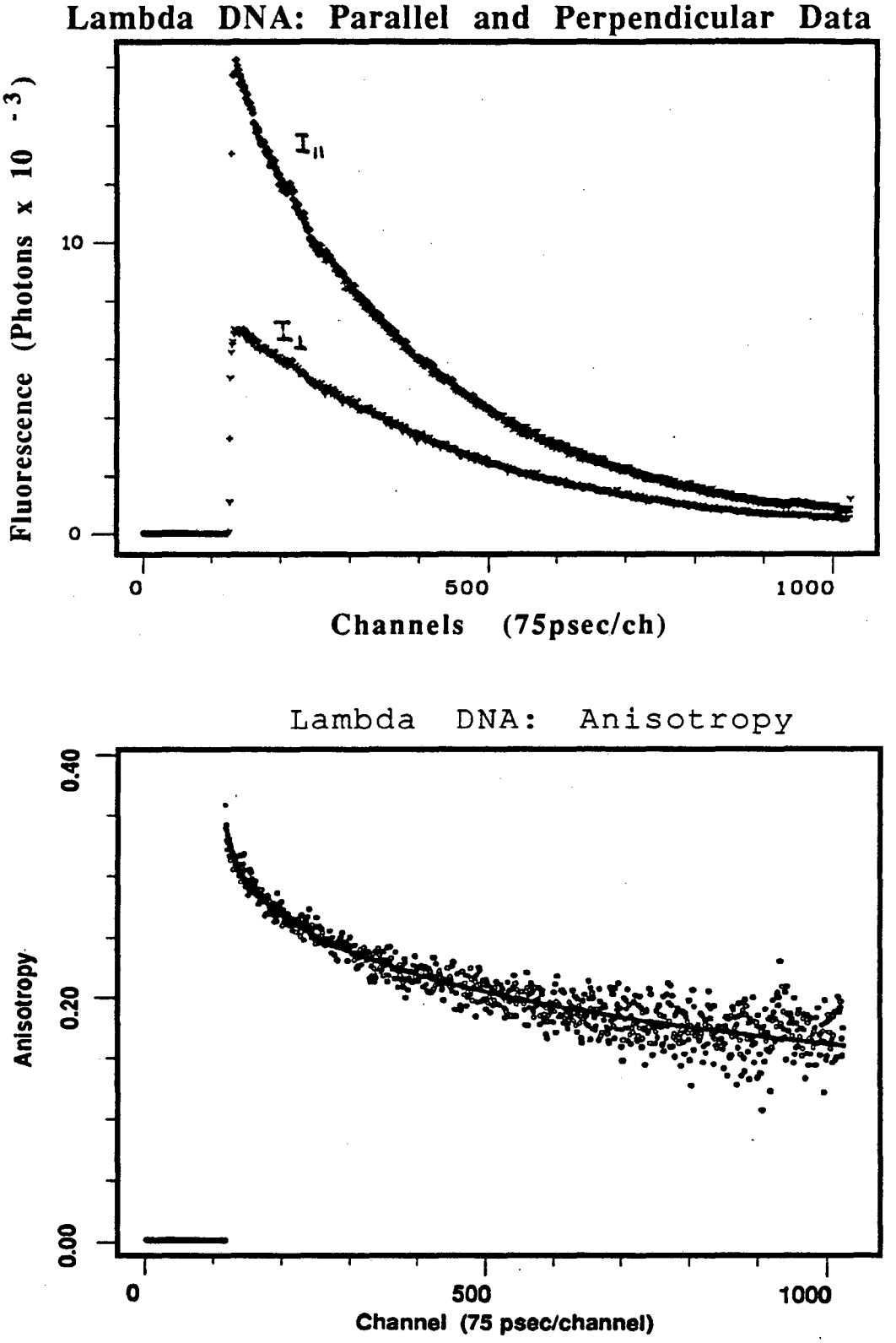

FIGURE 2-6: Representative TCPC data. Lambda DNA in 75mM KCl, room

temperature.

References

Axelrod, D. (1979) Carbocyanine Dye Orientation in Red Cell Membrane Studied by Microscopic Fluorescence Polarization, *Biophys. J. 26,* 557-574.

Cantor and Schimmel, Biophysical Chemistry, Part II, 1980, p. 456.

Chang, M.C., Courtney, S.H., Cross, A.J., Gulotty, R.J., Petrich, J.W., and Fleming, G.R. (1985) Time Correlated Single Photon Counting with Microchannel Plate Detectors. *Analytical Instrumentation,* 14(3&4), p. 433-464.

Hamamatsu technical bulletins #T-112, #ET-03 (Oct 1987) Application of MCP-PMTs to Time Correlated Single Photon Counting and Related Procedures.

Hamamatsu Product bulletin PB-154 (Sept 86) High Speed MCP-PMT R2809U

Lackowicz, J.R. (1983) *Principles of Fluorescence Spectroscopy.* Plenum Press, New York)

Leskovar, B. (May 1989) Recent Advanced in Detectors for Single-Photon Counting, LBL Report 26321

Leskovar, B. and Shimizu, T.T. (August 1985) Time Resolution Performance Studies of Hamamatsu R1564U Microchannel Plate Photomultiplier, LBL Report 20869.

Leskovar, B. (March 1985) Nanosecond Fluorescence Spectroscopy, LBL Report 19291.

Leskovar, B. (January 1985) The Afterpulse Time Spectra of High-Speed Photon

Detectors, LBL Report 18909.

O'Connor, D.V. and Phillips, D. *Time-correlated Single Photon Counting.* Academic Press, Orlando Fla.

Chapter Three

Spectroscopy II
Time-Resolved Ground State Depletion:
Absorption and Fluorescence Measurements

Abstract

Although TCPC offers excellent time resolution and sensitivity, its memory time is rather limited. While the time regime from 0 - 100 nanoseconds is appropriate for measuring DNA twisting and short wavelength bending, to measure the longer bending modes of DNA requires techniques with longer memory times. Here we use two techniques that rely on the long-lived triplet state. For technical reasons, both techniques measure the depletion of the ground state, rather than measuring the triplet state directly. The first relies on a decrease in absorption, and the second relies on a decrease in fluorescence, upon ground state depletion. The first we called transient absorption (TA), the second polarized Fluorescence Recovery After Photobleaching (pFRAP). By taking ratios of parallel and perpendicular modes, similar to those used in fluorescence depolarization experiments, reorientational motion can be measured with a time resolution of a few nanoseconds, extending out to a few milliseconds.

Some Background Chemistry

Fluorescent lifetimes tend to be short, on the order of 1-100 nanoseconds, because the fluorescence arises from an allowed transition: excited singlet state $\Rightarrow$ singlet ground state. On the other hand, the transition: excited triplet state $\Rightarrow$ singlet ground state is forbidden, making the triplet state long lived. For many DNA dyes, the triplet lifetime is

many microseconds to tens or even hundreds of milliseconds at room temperature. Consequently, by accessing the triplet lifetime, instead of the fluorescence lifetime, the memory time can be increased by up to a thousand fold.

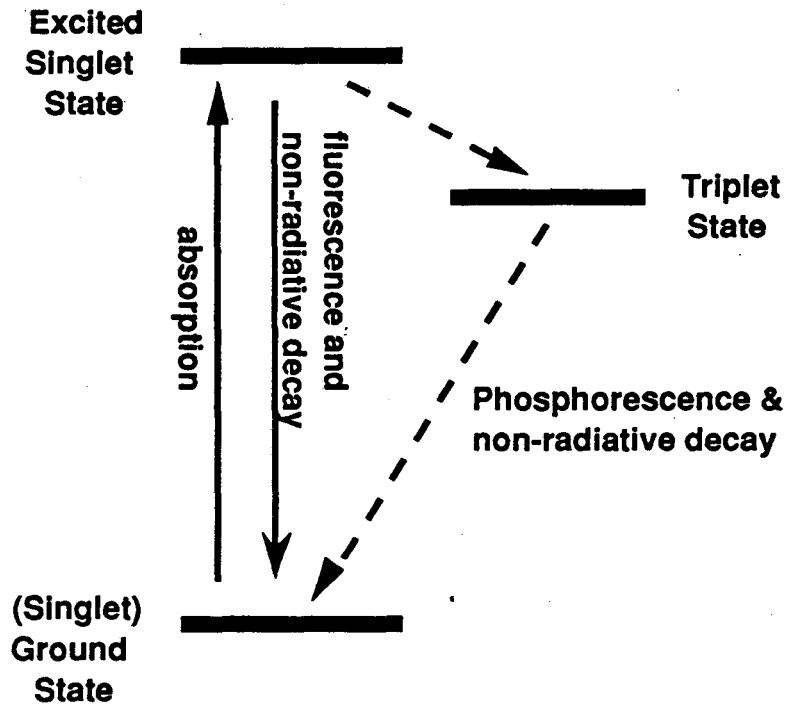

FIGURE 3-1: Photophysics: Techniques that monitor the triplet state, either directly through phosphorescence or indirectly through ground-state depletion have much longer memory times than those that monitor the first excited singlet state (via fluorescence).

To access the triplet state, the molecules are exposed to a pulse of (laser) light. The light induces some of the molecules into the excited singlet state, most of which decay back down to the ground state. (A fluorescence experiment just measures the radiative decay of this excited singlet state to the ground state). A fraction of the excited molecules, however, undergo inter-system crossing into the triplet state. In general, this is an

unlikely occurrence since it is a semi-forbidden transition. Nevertheless, some dye molecules, like methylene blue, have a quantum efficiency as high as 0.5 for intersystem crossing.

Once in the triplet state, the molecules can decay back down to the ground state via phosphorescence or non-radiative decay. If the branching ratio for phosphorescence is not too small, the phosphorescence can then be monitored. In complete analogy with the fluorescence experiment, anisotropy information can be deduced by taking the ratio of the number of emitted phosphorescent photons in the parallel and perpendicular modes. These photons can easily be distinguished from the fluorescent photons by their longer wavelength, and of course, their much longer lifetime.

Unfortunately, there are few molecules that have a high quantum efficiency for phosphorescence, i.e., they mostly decay from the triplet state via heat. This severely limits the sensitivity of the technique except in a few cases. This is in contrast to fluorescence, where there are many dyes with a quantum efficiency for fluorescence near unity.

One way to get around this problem, yet still have the advantage of the long memory time of the triplet state, is to monitor the depletion of the ground state instead of the population of the triplet state. If a sufficient number of molecules "get stuck" in the triplet state, the ground state will become depleted. This depletion will last as long as the triplet lifetime; in effect, the ground state depletion is just the negative or inverse of the phosphorescence experiment. A ground state depletion experiment also has the benefit that all molecules trapped in the triplet state contribute to the signal (the depletion), not just the fraction that phosphoruses.

Ground State Depletion: Measuring Rotation

We have used two different ways to monitor the depletion of the ground state — TA and pFRAP. In both cases, a short, intense pulse of light causes depletion of the ground state. In the first case, the absorption of a weak probe beam is then monitored. The wavelength of the probe beam is chosen so that it induces transitions between the ground state and the first excited state. Immediately after the pulse, there is little absorption of the monitoring beam because of ground state depletion. As the ground state recovers, however, the absorption of the beam increases. The second method, pFRAP, also uses a probe beam, but this time, the beam is used to excite fluorescence, i.e., instead of monitoring the absorption of the probe beam, the fluorescence (from the excited singlet state) induced by the beam, is monitored. As the ground state becomes depleted, there are fewer molecules for the probe beam to excite, resulting in a decrease in fluorescence.

For measuring rotation of molecules, the lifetime of the triplet state is only of interest because it determines the memory time. In complete analogy with the fluorescence depolarization experiment (see Chapter 2), to measure rotation we take the ratio (or anisotropy function) of the parallel and perpendicular modes (Fig. 3-2). The ratio, R(t), is defined as the post-bleach signal minus the pre-bleach signal in the parallel mode, divided by the same quantity in the perpendicular mode.

$$R(t) = \Delta F_{\parallel}(t)/\Delta F_{\perp}(t)$$

where

$$\Delta F_{\parallel}(t) = F_o - F_{\parallel}(t) \qquad \Delta F_{\perp}(t) = F_o - F_{\perp}(t).$$

Fo is the pre-bleach signal with just the probe beam on, and $F_i(t)$ is the post-bleach signal in the relevant mode. For pFRAP, the signal is fluorescence; for TA, the signal is absorption.

Qualitatively, the faster the reorientation, the quicker the ratio approaches one. Reversible photobleaching (i.e., ground state recover) does not contribute to the ratio, except in the second order effect to reduce the bleach depth at all times, which decreases the signal to noise.

Instead of a simple ratio, the anisotropy can be formed, in analogy with fluorescence depolarization experiments. The choice of the ratio or the anisotropy function is purely a matter of personal taste. In general, we will use the anisotropy.

$$rb = [\Delta F_{\parallel}(t) - \Delta F_{\perp}(t)]/[\Delta F_{\parallel}(t) + 2\Delta F_{\perp}(t)]$$

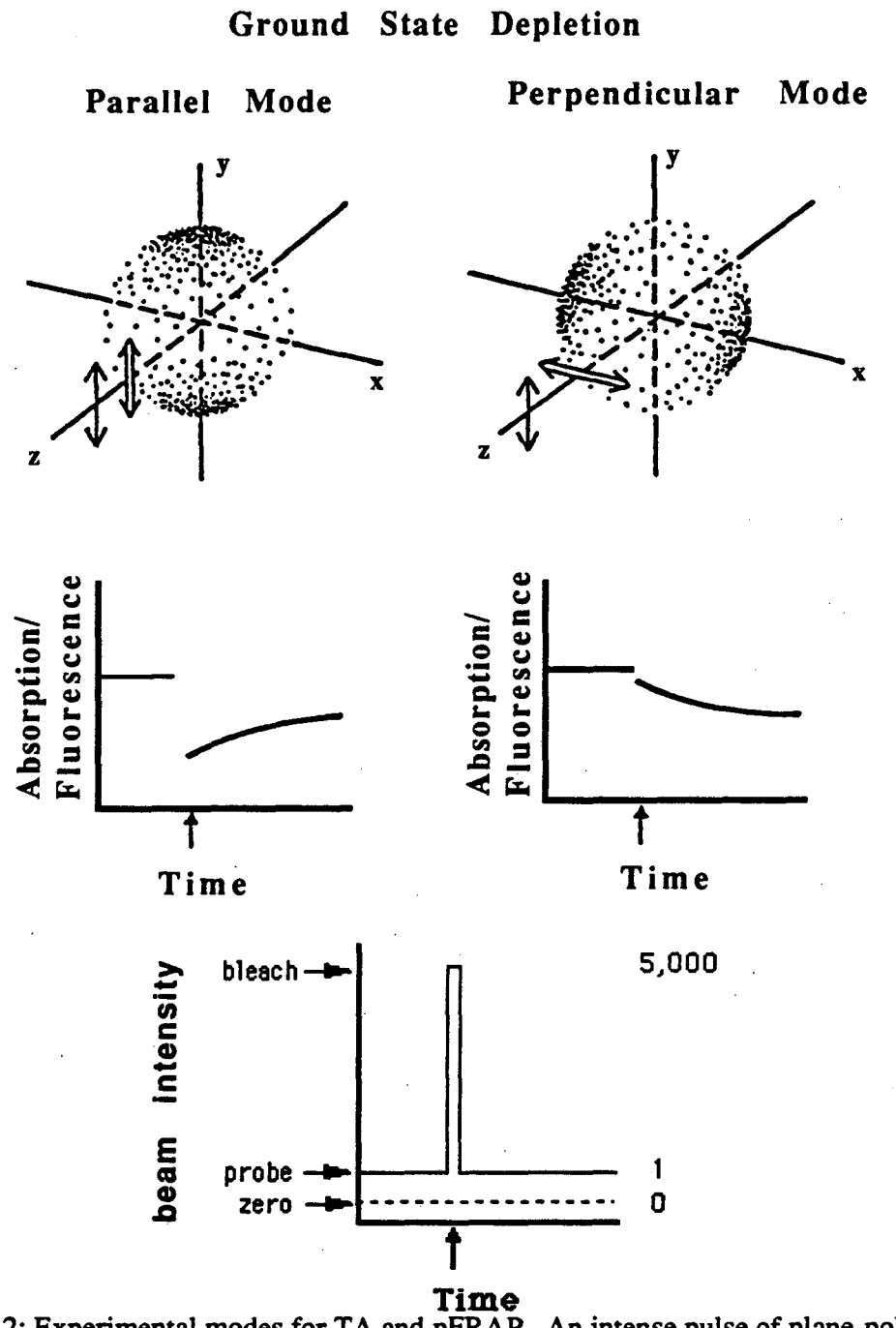

FIGURE 2: Experimental modes for TA and pFRAP. An intense pulse of plane-polarized light (double arrow) preferentially bleaches (i.e., excites into the triplet state or possibly made permanently non-absorbing) those dye molecules with absorption dipole moments parallel to the axis of bleach polarization. The observation beam (single arrow) then preferentially excites dye molecules that are oriented parallel or perpendicular to the bleach polarization. In the limit of very long recovery time (triplet lifetime), the rotational correlation time can be extracted from either curve. With finite photochemical recovery times, the rotational correlation time can be extracted from the ratio of the two modes.

Figure 3-2 is a schematic representation of the parallel and perpendicular mode pFRAP or TA experiments. The bleach beam (double arrow) first creates an anisotropic fluorophore distribution in the sample. The absorption or fluorescence induced by the probe beam (single arrow) is then used to follow the temporal evolution of this initial distribution. In a parallel mode experiment the probe beam initially sees a population of bleached dye and, thus, at t = O (immediately after the bleach) the signal is small. The post-bleach fluorescence then recovers with time as molecules rotate and the bleached dye thus becomes more uniformly distributed over angular space.

In a perpendicular mode experiment, on the other hand, the probe beam initially sees a population of unbleached dye and, thus, at t = O the signal is relatively large. Moreover, if reorientational motion alone leads to a return of an isotropic angular distribution of dye, the perpendicular mode fluorescence will decay with time.

In both the perpendicular and parallel modes, initially just the probe beam is on. The resulting signal level is F_0, the pre-bleach level. The beam intensity is then briefly raised 5-10,000 fold (typically for 5-10μsec in pFRAP, and ≤ 10nsec for TA), forming the bleach pulse. The beam intensity is then again, forming the post-bleach probe beam.

Figure 3-3 shows that experimental results for a TA control agrees well with the theoretical curves presented in Figure 3-2.

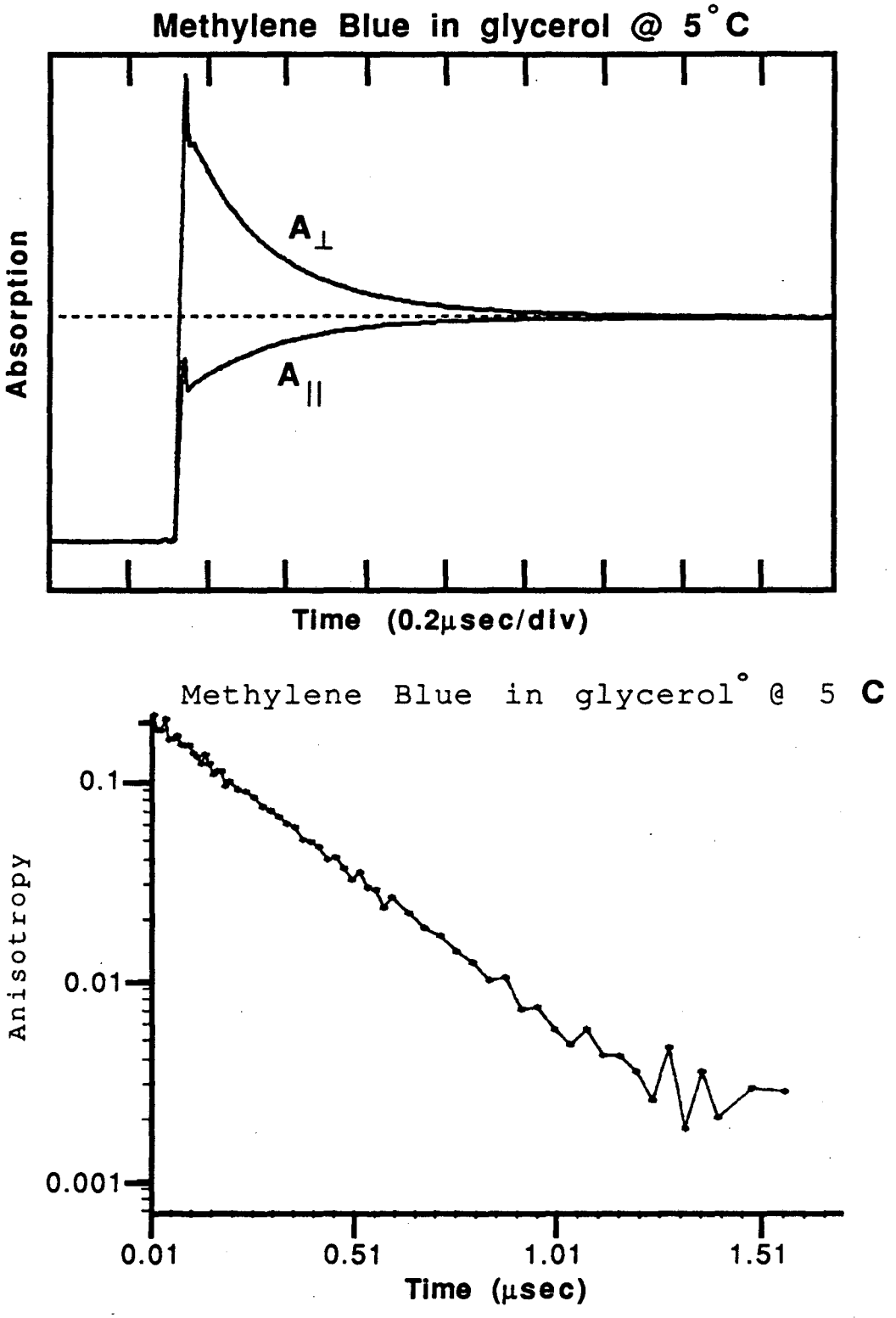

FIGURE 3-3: Experimental TA data (see text for details).

The experimental data in Fig. 3-3 is from a TA experiment on methylene blue, a small, roughly spherical dye, dissolved glycerol. The glycerol was chilled to 5 degrees Celsius to increase the viscosity of the solution and thereby increase the rotational correlation time. (In water, the tumbling time of a small molecule like MB is about 150psec, too short to measure with our TA setup.) Because the triplet lifetime of MB is about 7μsec, significantly longer than the rotational correlation time, the tumbling time can be extracted from either the parallel or perpendicular curves. Plotting the anisotropy function clearly shows that the MB tumbles with a single correlation time of approximately 300nsec, indicating that the molecule is roughly spherical and that the viscosity of the solution must be about 2000 centipoise.

The pFRAP technique has similarly been shown to provide an accurate measure of rotational relaxation rates in well-defined control samples of fluorescently labelled spherical beads (Velez and Axelrod (1988)). We tested the pFRAP system on two Ethidium Bromide-labelled DNA controls. First we looked at labelled oligomers which are expected to rapidly tumble. Indeed, we found that the (post-bleach) anisotropy was zero. Next we looked at DNA dried onto a quartz coverslip, where we would expect the anisotropy to be large and constant in time.

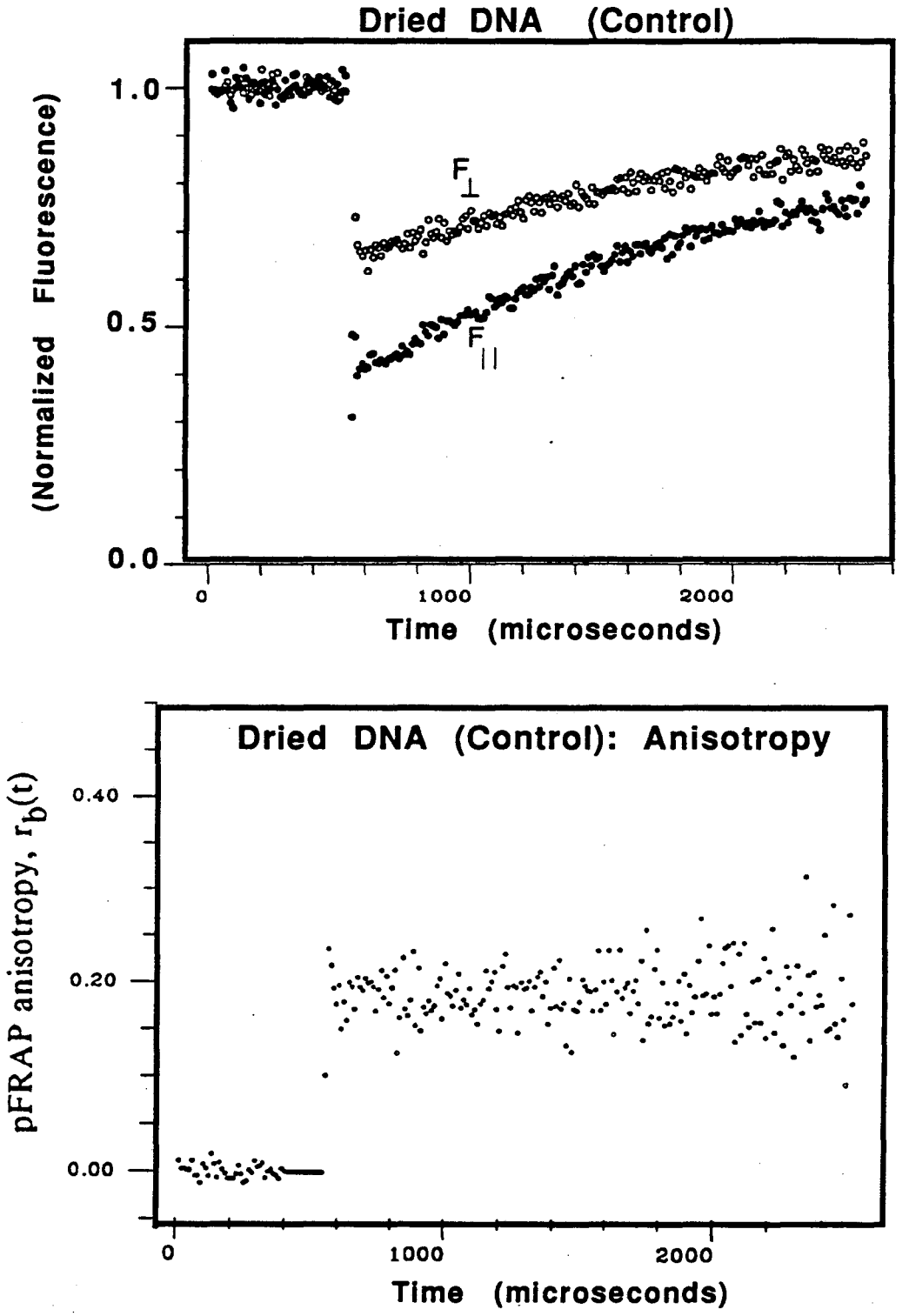

FIGURE 3-4: pFRAP experimental data for parallel, perpendicular and anisotropy of (deoxygenated) dried DNA, an immobilized control (see text for details).

From the pFRAP anisotropy curve it is clear that the sample anisotropy is flat, indicating a sample that is immobilized during the probe. The anisotropy, however, equals 0.20, significantly less than the theoretical maximum of 4/7 = 0.571 expected for a completely immobilized sample. (Note that the pFRAP anisotropy maximum of 4/7 is different than the fluorescence depolarization anisotropy maximum of 0.4. This is because of differences in the way they are defined, which will be explained in more detail in the latter section, "Comparison of pFRAP, FD and TA Ratios and Anisotropies".) This lower anisotropy indicates that the DNA, even though dried down on quartz, retains some fast, restricted motion, during the 10μsec-long bleach pulse. Looking at the pFRAP parallel and perpendicular data, it can be seen that post-bleach fluorescence in both graphs decay back to their pre-bleach level. This is because of the finite triplet lifetime. Indeed, the triplet lifetime can be extracted from either curve and is found to be 1.8msec. That the curve is single exponential, is suggestive that there is only one triplet state, rather than a series of states – triplet or other – that contribute to the ground state and decay back to the ground state with different lifetimes.

Comparison of pFRAP, FD and TA Ratios and Anisotropies

The anisotropy (and ratio) function used in the FD, pFRAP and TA experiments all have the same functional form, despite the fact that FD is a "pump-only" technique whereas pFRAP and TA are both "pump-probe" techniques.

$$r(t) = [\Delta F_{\parallel}(t) - \Delta F_{\perp}(t)]/[\Delta F_{\parallel}(t) + 2\Delta F_{\perp}(t)]$$

(One trivial difference: Since FD is a dark-background technique, the change in fluorescence is simply the fluorescence itself, and the Δ is unnecessary.)

That the anisotropies should be similar can be seen by the physical similarities in the techniques. In FD a pump pulse creates a cylindrically symmetric distribution of excited fluorophores, with the probability of excitation going approximately like the cosine squared of the angle between the absorption dipole moment and the laser polarization. These molecules then rotate and the rotation is monitored by observing how they sweep past an analyzer. As an excited fluorophore goes from nearly parallel to nearly perpendicular to the plane of polarization of the analyzer, for example, the detected fluorescence will decrease. In pFRAP and TA, a pump pulse creates a similar distribution of "excited" molecules – in this case bleached molecules – which give rise to the signal by rotating past the plane of polarization of the probe beam.

To be slightly more quantitative, the FD signal, S_{FD} is:

$$S_{FD} \alpha (\vec{\mu}_a \cdot \hat{z})^2 \ (\vec{\mu}_e \cdot \hat{p})^2$$

where $\vec{\mu}_a$ is the absorption dipole moment of the dye molecule, $\vec{\mu}_e$ is the emission dipole moment of the dye molecule, $\hat{z}$ is the polarization of the pump-pulse and $\hat{p}$ is the polarization of the analyzer. The first term is just the probability of excitation and the second term is the probability that the fluorescence from the excited molecule will make it through the analyzer. For the parallel mode, $\hat{p}$ is $\hat{z}$, and for the perpendicular mode, $\hat{p}$ is $\hat{y}$.

For TA the signal has the same form, except now the first term represents the probability of bleaching (in the limit of weak bleach) and the second term represents the probability of being excited by the probe beam. In the second term, $\hat{p}$ now represents the plane of polarization of the probe beam rather than the analyzer polarization – again, with either parallel or perpendicular modes – and the emission dipole moment, $\vec{\mu}_e$, must be replaced by the absorption dipole moment, $\vec{\mu}_a$. For most molecules – and all those used

in our experiments – the absorption and emission dipole moments are parallel so $\vec{\mu}_a = \vec{\mu}_e$. These are the only terms in TA since no analyzer is used.

$$S_{TA} \alpha (\vec{\mu}_a \cdot \hat{z})^2 (\vec{\mu}_a \cdot \hat{p})^2$$

Consequently, in the limit of weak bleach and absorption and emission dipole moments parallel, the anisotropy (or polarization ratio) in TA is the same as FD. Note that the correct term for the probability of a molecule being bleaching in TA (or pFRAP) is

$$P(\text{bleach})_{TA/pFRAP} \alpha 1 - \exp[-(\vec{\mu}_a \cdot \hat{z})^2]$$

which in the limit of weak bleach reduces to the above expression, $(\vec{\mu}_a \cdot \hat{z})^2$.

For our experimental pFRAP configuration, however, *the pFRAP anisotropy is not the same as the TA or FD anisotropy*, even in the limit of weak bleach and with absorption and emission dipoles parallel. We denote this difference by using the symbol $r_b(t)$ (the b stands for bleach) for the pFRAP anisotropy, whereas, the standard notation, r(t) is used for the FD and TA functions. The difference comes about because we use an analyzer in the pFRAP set up (see below, "pFRAP: Application to DNA and Experimental Details"). Therefore the pFRAP signal has not only the two terms present in the FD/TA anisotropy, but an additional term proportional to the probability of a fluorescent photon making it through the analyzer. Note that in pFRAP the analyzer is always placed parallel to the probe beam.

$$S_{pFRAP} \alpha (\vec{\mu}_a \cdot \hat{z})^2 (\vec{\mu}_a \cdot \hat{p})^2 (\vec{\mu}_e \cdot \hat{p})^2$$

Using an analyzer in the pFRAP set-up has two important *dis*advantages, namely, that the theories of DNA dynamics have all been made for the FD anisotropy function, and that it is difficult to directly compare the results of pFRAP with FD and TA. Nevertheless, the analyzer is useful because it eliminates any polarization dependence of the microscope of

detection system. Without it, results from one microscope to another could not be compared.

Given the above semi-quantitative relations, the individual anisotropies can be calculated (for FD, and by analogy, TA, see Cantor and Schimmel). In brief outline, the anisotropy for the pFRAP will be calculated below. The interested reader is referred to Velez (1988) for an excellent discussion and more details.

The intensity of fluorescence in the parallel mode is:

$$I_{\parallel}(t) = \int_{\substack{\text{all}\\ \text{angles}}} C(\Omega,t)\left(\vec{\mu}_a \cdot \hat{z}\right)^2 \left(\vec{\mu}_e \cdot \hat{z}\right)^2 \, d\Omega$$

where the first term is the concentration of unbleached fluorophores at time t and angle Ω due to an initial distribution $C(\Omega,0)$ created by a bleach pulse polarized along z; the second term is the probability of absorption of the z-polarized probe beam, the last term is the probability of an emitted fluorophore making it through the analyzer.

The intensity of fluorescence in the perpendicular mode is the same, except the concentration term is now due to a bleach polarized along y. It is mathematically more convenient, however, to keep the concentration term the same and rotate the probe and analyzer. Then

$$I_{\perp}(t) = \int_{\substack{\text{all}\\ \text{angles}}} C(\Omega,t)\left(\vec{\mu}_a \cdot \hat{y}\right)^2 \left(\vec{\mu}_e \cdot \hat{y}\right)^2 \, d\Omega$$

The terms that appear in the anisotropy are the change in intensity, $\Delta I_{\perp}(t)$ and $\Delta I_{\parallel}(t)$. These are simply $C(\Omega,t)$ replaced by $\Delta C(\Omega,t) \equiv 1 - C(\Omega,t)$. $\Delta C(\Omega,t)$ is determined by the diffusion equation with a loss term:

$$\frac{\partial \Delta C(\Omega,t)}{\partial t} = \left[\nabla \cdot \mathbf{D}_{rot} \cdot \nabla\right] \Delta C(\Omega,t) - k\Delta C(\Omega,t)$$

subject to the boundary condition that $\Delta C(\Omega,t=0) = \Delta C(\Omega,0)$, the initial distribution of bleached fluorophores. k is the inverse of the triplet lifetime (if there is more than one lifetime, the equation can be generalized — see Velez (1988)). $\mathbf{D}_{rot}$ is the diffusion tensor, which, for a spherical molecule reduces to a single number – the diffusion coefficient – and the diffusion equation reduces to the simpler form

$$\frac{\partial \Delta C(\Omega,t)}{\partial t} = D_{rot} \nabla^2 \Delta C(\Omega,t) - k\Delta C(\Omega,t)$$

The solution is simply:

$$\Delta C(\Omega,t) = \Delta C_0 e^{-kt} \cdot \Delta C'(\Omega,t)$$

where $\Delta C'(\Omega,t)$ satisfies the diffusion equation without the decay term and ΔC_0 is a constant proportional to the total amount of unbleached fluorophores initially. This is important because the Green's function for the ordinary diffusion equation is well known and from it, the concentration of unbleached fluorophores at any time and angle can be found given the initial distribution:

$$\Delta C'(\Omega,t) = \int_{\substack{\text{all} \\ \text{angles}}} \Delta C'(\Omega_0,0) G(\Omega,\Omega_0,t) d\Omega_0$$

The initial distribution is just

$$\Delta C'(\Omega_0,0) = 1 - \exp\left[-B(\vec{\mu}_{a_0} \cdot \hat{z})^2\right]$$

where B is a bleaching parameter related to the bleach intensity, duration, efficiency and absorption coefficient of the absorbing fluorophore. The Green's function assuming isotropic diffusion is:

$$G(\Omega,\Omega_0,t) = \sum_{n=0} \frac{2n+1}{2} P_n(\cos\Delta\theta)e^{-n(n+1)Dt}$$

where $\Delta\theta = \theta - \theta_0$ and $P_n(\cos\Delta\theta)$ is a Legendre polynomial. Upon integration over θ_0 only the n=0,2,4 terms survive. After some algebra, the results are:

$$\Delta I_{\perp}(t) = a - be^{-6Dt} - ce^{-20Dt}$$

$$\Delta I_{\parallel}(t) = a + 2be^{-6Dt} - \frac{8}{3}ce^{-20Dt}$$

where a,b, and c are rather complex functions of the bleach depth, wobble during the bleach, angle between absorption and emission dipole moments (Velez, 1988). The ratio is:

$$r_b(t) = \frac{3be^{-6Dt} + -\frac{5}{3}c\,e^{-20Dt}}{3a - \frac{14}{3}c\,e^{-20Dt}}$$

For small bleach depth and no wobble during the bleach, $r_b(0) = 4/7$. The ratio b/a Qualitatively, c/b indicates the amount of double exponential character in the individual recovery curves and in the ratio. c/b decreases as the bleach depth decreases. For the deepest bleaches reasonable without overheating due to excessive laser power, $c/b \leq 0.16$, indicating that the ratio is primarily single exponential. Indeed, for $\frac{c}{b} \to 0$, $r_b(t) \approx \frac{b}{a} e^{-6Dt}$. In this limit, the pFRAP anisotropy function behaves like the FD or TA functions, with a normalization factor of 4/7 instead of 0.4.

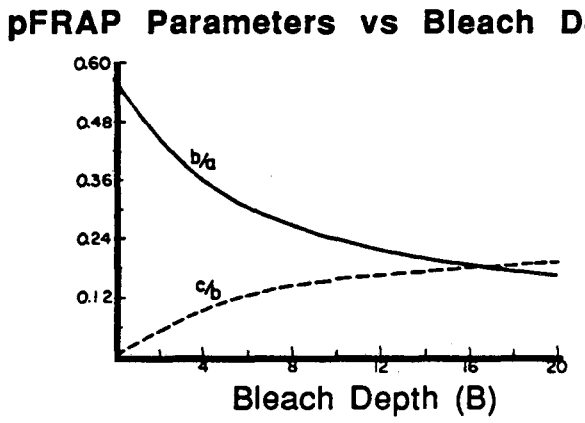

Figure 3-5: pFRAP constants, a,b,c, as a function of bleach depth. The highest practical bleach depth is $B \leq 10$ (from Velez and Axelrod, 1988).

Is the Long-lived State Really a Triplet State?

Both pFRAP and TA rely on a long-lived intermediate state which causes ground state depletion. To determine if this long-lived state is indeed a triplet state, we have examined the oxygen dependence of the photophysics. It is well known that triplet states are relaxed by dissolved oxygen; hence triplet lifetimes increase markedly in deoxygenated solutions (Cantor & Schimmel, 1980). Note that other bleaching processes can and do occur under certain experimental conditions. If enough bleach light impinges on the sample, two- photon effects can occur, leading to excited states other than the first excited triplet state. Chemical reactions can also occur between the excited molecule and dissolved oxygen or even with the solvent molecules. These chemical reactions, if they permanently alter the structure of the molecule, lead to irreversible photobleaching – the molecule never returns to the original ground state. Indeed, before the introduction of the microsecond polarized photobleaching technique it was generally assumed that photobleaching in FRAP was an irreversible reaction. Indeed, the theory of translational FRAP is based on such an assumption (Axelrod *et al.*, 1976).

Our results (figures 3-6 and 3-7), although not definitive, are consistent with a reversible photobleaching mechanism that involves the excited singlet state crossing into a triplet state and then falling back into the ground (singlet) state (see figure 1). As the oxygen concentration increases, the triplet lifetime decreases because paramagnetic oxygen provides a pathway for the semi-forbidden transition, triplet to singlet state.

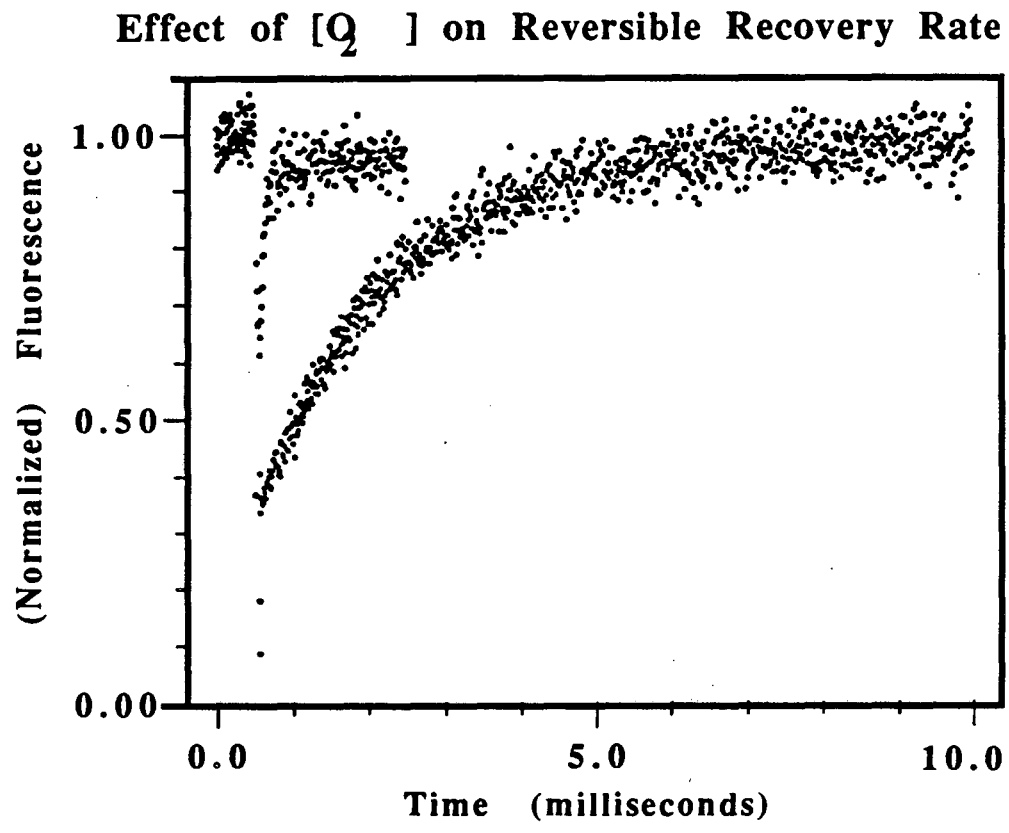

FIGURE 3-6: Photophysical recovery data obtained from a dilute solution of ethidium bromide-stained phage λ DNA. Only parallel mode curves, $F_{\parallel}(t)$, are shown, although $F_{\perp}(t)$, because the sample completely reorients during the bleach, is equivalent. An oxygen-saturated solution yielded the upper, more rapidly recovering data; a deoxygenated sample produced the lower, more slowly relaxing data. Data corresponding to atmospheric conditions are not shown. The photophysical recovery time is a sensitive function of the oxygen concentration in the sample. Specifically, the photophysical recovery time for the phage λ DNA in an oxygen-saturated solution is 70 μsec. If phage λ DNA is in equilibrium with the atmosphere the time constant is 140 μsec. Finally, upon deoxygenation, the recovery time increases to 1.8 msec. Note also that the depth of bleach is a monotonically decreasing function of O_2 concentration. We have also observed that the irreversible component, F_o-$F(\infty)$ of the pFRAP bleach is slightly larger in oxygenated samples. This latter result reaffirms the fairly well documented (Magde *et al.*, 1974) idea that oxygen is also involved in the molecular events that lead to irreversible bleaching.

Furthermore, in oxygen quenching of triplet states, the relaxation reaction often is diffusion controlled, and its rate then is expected to be a linear function of oxygen concentration (Berkoff *et al.*, 1986). Thus, if our model of the reversible photobleaching phenomenon is correct we would expect the pFRAP photophysical recovery time, the inverse of the reaction rate, to be a monotonically decreasing function of oxygen concentration. This is indeed what we have observed experimentally. However, since we currently have measured pFRAP relaxation times at only three oxygen concentrations, it is somewhat difficult unambiguously to test for a linear dependence of reaction rate on O_2 concentration.

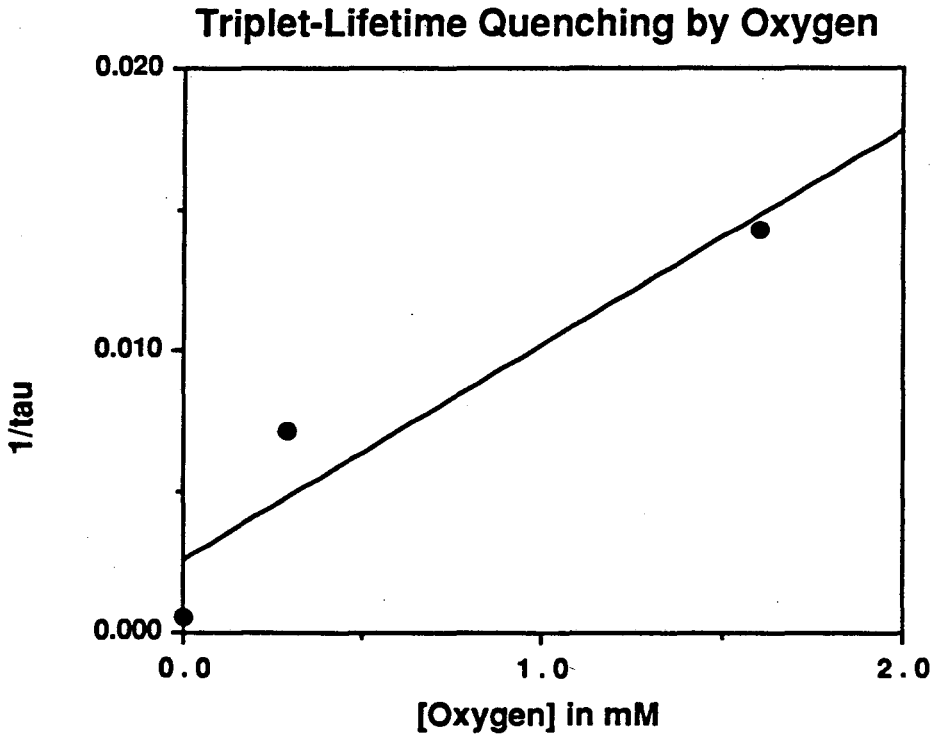

FIGURE 3-7: Relaxation rate (= inverse of triplet lifetime) vs Oxygen concentration. The graph is approximately linear, indicating triplet lifetime quenching via a diffusion controlled reaction with dissolved oxygen, although with only three points and a non-perfect fit (r^2 =0.895), a definitive conclusion cannot be reached. For water at room temperature and 1atm of pressure, the dissolved [O_2] is 0.29mM when the solution is in equilibrium with air and 1.6mM when oxygen-saturated. The best fit line is 1/ tau = $(2.53 + 7.62[O_2])\cdot 10^{-3}$ with a linear regression fit of $r^2 = 0.895$.

The dependence of the (reversible) bleach depth on oxygen concentration also supports the triplet hypothesis. If the scheme that we have outlined is correct, the reversible component of pFRAP is due to depletion of the singlet state by intersystem crossing to the triplet state and, therefore, a pFRAP experiment which relies primarily on reversible bleaching is essentially equivalent to a singlet state depletion experiment (Johnson & Garland, 1982; Yoshida & Barisas, 1986). In singlet state depletion experiments it is found that the depth of bleach increases in deoxygenated solutions (Johnson & Garland, 1982; Yoshida & Barisas, 1986). Since the reversible pFRAP bleach depth also exhibits this sort of oxygen dependence (see Fig. 6), we again find consistency between the triplet scheme and our experimental observations.

It is helpful to compare the photophysical behavior of the putative triplet state seen in our pFRAP experiments to that of a putative ethidium triplet detected previously (Atherton & Beaumont, 1986 and 1987). We first note that the deoxygenated triplet lifetime found here (2 msec) agrees well with the literature value. Moreover, both Atherton and Beaumont's data, and our data, indicate that ethidium bromide has an atypically long triplet lifetime in oxygenated samples; for example, Atherton and Beaumont find that the apparent rate constant for oxygen quenching of the ethidium triplet is two orders of magnitude smaller than typical rate constants for oxygen quenching of triplet states in homogeneous solution. Their speculation that intercalation of ethidium might serve to protect the triplet from interaction with O_2 seems reasonable.

A quantum efficiency for the intersystem crossing, ϕ, of ethidium bromide determined from our data can also be compared with a crude estimate ($\phi \approx 1\%$) made by Atherton and Beaumont. We can calculate ϕ if it is assumed that the bleach is due solely to crossover into the triplet state. In this case ϕ equals the bleach depth, B_D, divided by the number of photons absorbed per molecule during the bleaching pulse. A relatively straightforward application of Beer's law then shows that

$$\phi = 6x10^{20} B_D hc\pi\omega_0^2/[2.3\epsilon\lambda P_0 t].$$

Here P_0 is the laser power, h is Planck's constant, c is the speed of light, λ is the wavelength of the laser light, t is the bleach duration, ϵ is the molar extinction coefficient of ethidium (in units of $cm^{-1}\ M^{-1}$), ω_0 is the beam spot size (in cm) and $6x10^{20}$ is a conversion factor. Note that ϕ is independent of dye concentration and path length. We find $\phi \approx 0.1\%$; the difference in the two values for ϕ probably stems from the approximate nature of both the Atherton and Beaumont calculation and the one presented here.

Triplet and Ground State Depletion Sensitivity

The above controls (figures 3 and 4) show that the ground-state depletion techniques – TA and pFRAP – can yield information about rotational motion in the sub-microsecond to millisecond time regime, significantly longer than fluorescence lifetime-based techniques. Furthermore, figures 5 and 6 indicate that the long memory time of the ground state depletion experiments are due to an intermediate triplet state, although other oxygen-dependent states (e.g. reaction of an excited singlet or triplet state with molecular oxygen to form a non-fluorescent species) may contribute to ground state depletion as well.

The downside of the triplet techniques – whether phosphorescence or ground-state depletion – is that they do not have as good sensitivity as the standard fluorescence technique (Jovin, 1981). A semi-quantitative comparison between the sensitivity of phosphorescence and fluorescence can be made. For every molecule that is excited, there is a certain probability that it will emit a fluorescent photon, or that it will emit a phosphorescent photon. The relative sensitivity of the techniques is the ratio of these two probabilities. The probability of emission for a fluorescent photon is simply the quantum efficiency for fluorescence, Φ_f, and the probability of emission of a phosphorescent photon is simply the probability of the molecule crossing over into the triplet state (=

quantum efficiency for intersystem crossing, Φ_c) times the probability that it will then emit a photon (= quantum efficiency for phosphorescence, Φ_p)

$$\frac{\text{fluorescence sensitivity}}{\text{phosphorescence sensitivity}} \approx \frac{\Phi_f}{\Phi_c \Phi_p}$$

$$\frac{\text{fluorescence sensitivity}}{\text{ground state depletion sensitivity}} \approx \frac{\Phi_f}{\Phi_c}$$

For fluorescent dyes, $\Phi_f \approx 1$; Φ_c ranges from a high of 0.5 for methylene blue to $\approx 10^{-3}$ for ethidium bromide; Φ_p ranges from 0.01 for eosin in glycerol (Austin, 1979; Eads, 1984) to essentially zero for many dyes. In general, both phosphorescence and ground state depletion experiments are tens, to thousands, of times less sensitive than fluorescence. Among the two triplet techniques, ground state depletion experiments are more sensitive than phosphorescence experiments when Φ_p is small; for Φ_p near unity, phosphorescence is more sensitive because it is a dark background experiment (in contrast to the ground state depletion experiment).

The above calculation however, underestimates the sensitivity of triplet-based experiments somewhat. The sensitivity of a phosphorescence, or of a ground state depletion experiment, can be increased by using a (temporally) long excitation pulse — on the order of, or longer than, the fluorescent lifetime. Although time resolution is sacrificed, a long pulse causes multiple excitations, which increases the likelihood that a molecule will end up in the triplet state. In the case of ethidium bromide, for example, which has a fluorescent lifetime of 22nsec, a 10μsec pulse will excite a molecule approximately 500 times. With a 0.1% probability for intersystem crossing, approximately half the molecules will go into the triplet state by the end of the pulse. (With a triplet lifetime of approximately a millisecond, only a small fraction of the

molecules relax back to the ground state during the pulse.) Consequently, a detectable ground state depletion, measured via absorption or fluorescence, will result. (The phosphorescence of ethidium bromide has not been measured.)

In fact, as Johnson and Garland point out, and our data demonstrate, if enough laser power is available to do the requisite "bleaching", a small intersystem efficiency is actually advantageous in a FRAP-type fluorescence experiment (Johnson & Garland, 1982). Because enough power is available in the bleach pulse, a sizeable fraction of the molecules can be forced into the triplet state, despite the small intersystem crossing probability. The small intersystem crossing efficiency, however, means the probe beam can be fairly intense without causing bleaching and the signal will therefore be large. We note finally, in this context, that the very high light intensities used to do bleaching in pFRAP; the intensities are not far removed from the regime in which two photon events could conceivably take place. The actual bleaching process, may therefore be more complicated than the simple triplet scheme presented above

Both ground state depletion experiments — measured via absorption or fluorescence — have the disadvantage that they are light-background experiments. As the depletion goes away and the system returns to equilibrium, the light hitting the detector increases, either because less light is absorbed (TA) or fluorescence increases (pFRAP). As previously discussed, the light background reduces the sensitivity of the technique. This is particularly true for the absorption experiment, where the background is very bright. In fact, the background is so bright for this experiment that fluctuations of the probe beam intensity due to laser instabilities are a greater source of noise than the Poisson noise. Cancelling out the laser fluctuations is discussed below, in the technical details section of TA.

pFRAP: Application to DNA & Experimental Details

Fluorescence Recovery After Photobleaching (FRAP) has been used for a number of years to measure translational motion — commonly translational diffusion (Axelrod, 1976). The recently modified FRAP technique we use, *polarized* FRAP, is capable of measuring rotational motion (Velez, 1988). We have shown that the technique has adequate sensitivity for DNA dynamic measurements, both *in vitro* and *in vivo,* with a time resolution of a few microseconds and a memory time of a few milliseconds (Scalettar, Selvin et al., 1988,90; Selvin, Scalettar, et al., 1990).

For our experiments, we used the pFRAP apparatus of Physics Prof. Daniel Axelrod of the University of Michigan, Ann Arbor. As an undergraduate senior, I worked in his lab, developing pFRAP for application to DNA.

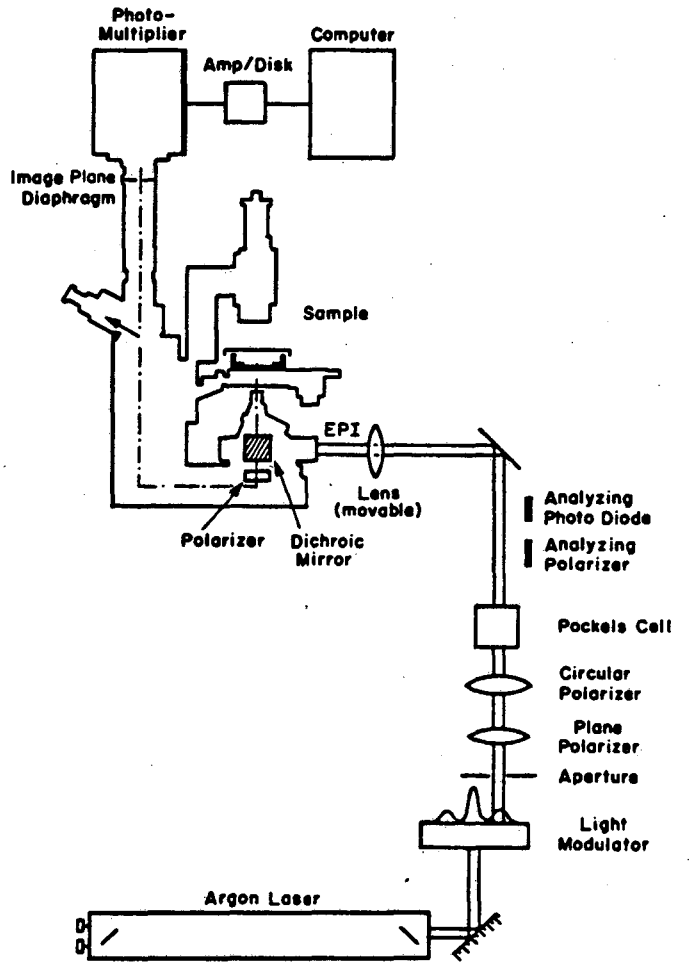

FIGURE 3-8: Schematic of pFRAP Apparatus (details in text).

The Argon-ion laser (Coherent 15W) is operated at 514nm in the CW mode. The bleach pulse and probe beams are formed by the acousto-optic modulator. To form the bleach pulse, an electrical signal is sent to the AOM, setting up a standing wave in the crystal which diffracts approximately half of the light into the first order spot. A pin hole placed after the AOM passes only this first order diffracted spot. With the particular AOM

used, pulses as short as 1μsec can be formed. After passing through a few polarizers, a pockels cell rotates the plane of polarization of the light, either into the vertical (parallel mode) or the horizontal (perpendicular). After proper attenuation the light is then focussed onto the sample, typically to a few microns spot size, using epi-illumination optics. Those fluorophores orientated parallel, or nearly parallel, to the light's polarization will be bleached during the pulse.

The bleach pulse is terminated by greatly reducing the standing wave in the AOM crystal. The AOM, however, is not completely turned off — a low level standing wave is maintained to produce a weak, CW probe beam. During the probe, the Pockels cell voltage is set so that the probe polarization is always vertical.

The CW probe beam induces fluorescence in the sample, without appreciable bleaching. The fluorescence is collected by a microscope objective, filtered to remove scattered light, sent through an analyzer, and detected by a PMT. (The presence of the analyzer is important in understanding the differences between the anisotropy function used in pFRAP and that used in FD and TA — see "Comparison of Anisotropy functions" section.) The same considerations concerning numerical aperture that were discussed in the fluorescence depolarization experiment apply to pFRAP as well.

To acquire sufficient signal to noise, signal averaging is done by repeating the experiment ten times a second. In between each bleach-probe experiment, the sample is minutely translated via a computer controlled stepper motor mounted on the microscope stage to prevent over-bleaching due to several pulses. To minimize the effects of laser light fluctuations, the bleach pulse polarization is altered from parallel to perpendicular after every experiment. Minimizing the effect of laser light fluctuations is important because the signal of interest is a ratio of two intensities — the parallel and perpendicular modes — which is affected by source fluctuations. As previously discussed, this ratio,

analogous to fluorescence depolarization experiments, eliminates non-reorientational effects (e.g. ground state recovery due to the finite triplet lifetime) on the signal.

The time resolution of pFRAP is presently limited by the available power of the CW laser. Given the 10W maximum power output of the laser at 514nm, a pulse shorter than a few microseconds would not have sufficient energy to cause significant bleaching. In the future, this problem can be solved by using a pulsed dye laser, pumped by a nitrogen laser. 100μjoule, 300psec pulses are achievable, which is sufficient energy for bleaching in a much reduced period of time. At this point the time resolution will likely be limited by the enormous burst of fluorescence during the bleach pulse which will saturate the detection system for at least a few fluorescent lifetimes — probably between 100-500nseconds.

The dyes used in all pFRAP DNA experiments were either ethidium monoazide (Scalettar and Selvin, 1988) or more often ethidium bromide (Etbr). Ethidium monoazide is a derivative of Etbr capable of covalently binding to DNA, thereby eliminating any on/off kinetics. Since the off rate of Etbr from DNA is slow, approximately 40msec, on/off rates were generally not a problem and ethidium monoazide was primarily used as an experimental control to confirm that on/off kinetics were not affecting the results. Etbr is generally preferable to Ethidium monoazide because the latter is somewhat less fluorescent and causes greater distortion of the DNA helix (Graves, 1977; Garland, 1980, Firth, 1983)

pFRAP Technical Details

There are a number of factors which can cause distortion of the pFRAP data. Most obviously, the Pockels cell voltage must be carefully set to produce a high degree of linear polarization. If not, perpendicular and parallel will be mixed and the anisotropy will be erroneously low. We tested the degree of polarization of both the bleach and probe beams

by sending each beam through an analyzer, oriented either parallel or perpendicular to the intended polarization. The intensity getting through the analyzer in the two modes was compared. A 40:1 intensity ratio was achievable.

Overbleaching, will also cause the anisotropy to decrease. As discussed in the Anisotropy Comparison section, the pFRAP anisotropy ratio will decrease from a theoretically maximum value of 4/7 in the limit of weak bleach down to ≈ 0.24 for the strongest bleach experimentally reasonable. In the limit of extremely strong bleach, all orientations are bleached and the anisotropy is zero. We limit the depth of bleach to $\leq$ 40% (i.e., the post-bleach fluorescence immediately following the pulse in the parallel mode is $\geq$60% of the pre-bleach fluorescence).

Because of the relatively long bleaching time in pFRAP, motion of the fluorophore generally occurs during the bleach ("wobble"). In fact, for naked DNA essentially all twisting is complete and all that remains is bending motions. Consequently, the initial ratio will be less 4/7. Indeed, even for a sample of DNA dried on a coverslip, the anisotropy was 0.2. Velez et al. has incorporated the effect of wobble in their analysis of the pFRAP ratio.

Temperature rise:

Finally, it is important that the absorbed laser light does not produce a significant temperature increase. A temperature increase will speed the rate of diffusional processes and can also cause thermal lensing, an effect where a temperature gradient causes a spatial-dependent change in the index of refraction, in effect, forming a lense. This can affect the apparent rate of reversible recovery if the lense causes more (or less) light to be collected. We have shown that an upperbound for the bleach-induced temperature rise is (Scalettar, Selvin et al., 1988):

$$T(0,t) = \frac{2.3\varepsilon\, CP}{2\pi\kappa c_p \rho} \ln\left(1 + \frac{8\kappa t}{\omega_0^2}\right)$$

where T(0,t) is the temperature increase at r=0, the center of the laser beam (which is the point of maximum light intensity); P is the power of the laser beam which has a Gaussian profile with beam waist ω_0; ε and C are the absorption coefficient and concentration, respectively, of the dye; and finally, κ, c_p and ρ are the thermal diffusivity, the specific heat, and the density of the solution, respectively.

Experimentally, the relevant numbers are: $P \approx 2$ Watts, the amount of 514.5nm laser light diffracted into the first order spot during a bleach; the beam waist is typically $\approx 3\mu m$; the extinction coefficient and concentration for ethidium, the dye used, are $\approx 5 \times 10^3$ cm^{-1} M^{-1} and $\approx 1\mu m$, respectively, and the sample thickness is $\approx 150\mu m$. The thermal parameters of the solution are taken to be those of water. We find that the temperature increase is 0.8°C. This calculation indicates that the samples are not heated excessively by the pFRAP bleach pulse.

Because of the complexity of calculating the maximal temperature rise in a three-dimensional absorbing sample illuminated with light having a diverging Gaussian intensity profile, we have made two approximations in the calculation, both of which lead to an *overestimate* of the temperature increase. First, the divergence of the beam is neglected. Second, we compute the temperature rise by assuming it is the product of the initial rate of temperature increase multiplied by the length of the bleach pulse. Since the initial rate of temperature increase is larger than the average rate, this leads to an overestimation.

The details of the derivation leading to the above equation can be found in the literature (Scalettar, Selvin, et.al, 1988; Axelrod, 1977); consequently, only the conceptual outline will be presented here.

The temperature distribution is governed by the inhomogeneous diffusion equation

$$-\frac{\partial T}{\partial t} + \kappa \nabla^2 T(\mathbf{r}, t) = \frac{A(\mathbf{r}, t)}{c_p \rho}$$

$A(\mathbf{r},t)$ is the power per unit volume deposited by the laser beam at point $\mathbf{r}$ at time. If the heat source has a nondiverging Gaussian intensity profile then $A(\mathbf{r},t) = (4.6\varepsilon CP/\pi\omega_0^2)$ $\exp(-2r^2/\omega_0^2)$. Here r is the standard radial cylindrical distance of point $\mathbf{r}$ from the position of maximal light intensity.

We compute the temperature profile by integrating the three-dimensional free space Green's function over the inhomogeneous term, $A(\mathbf{r},t)$. The Green's function is

$$G(\mathbf{r} - \mathbf{r}', t - t') = \frac{1}{[4\pi\kappa(t-t')]^{3/2}} \exp\left[\frac{-(\mathbf{r} - \mathbf{r}')^2}{4\pi\kappa(t-t')}\right] \qquad t > t'$$

$$G(\mathbf{r} - \mathbf{r}', t - t') = 0 \qquad t < t'$$

Hence the solution of the inhomogeneous diffusion equation is:

$$T(0,t) = \int_0^t dt' \int d\mathbf{r}'\, G(0-\mathbf{r}', t-t') \frac{A(\mathbf{r}',t')}{c_p \rho}$$

If we substitute in our particular choice of $A(\mathbf{r},t)$, set $B \equiv 4.6\varepsilon CP/\pi\omega_0^2 c_p \rho$, and make the change of variable $\beta = (t-t')^{-1/2}$, it follows that:

$$T(0,t) = \frac{4\pi B}{[4\pi\kappa]^{3/2}} \int_{t^{-1/2}}^{\infty} d\beta \int_{-\infty}^{\infty} dz' \int_{0}^{\infty} dr' r' \exp\left[-r'^2\left(\frac{\beta^2}{4\kappa} + \frac{2}{\omega_0{}^2}\right)\right] \exp\left(\frac{-z'^2\beta^2}{4\kappa}\right)$$

We are interested in the bleach-induced temperature rise, ΔT, at the position of maximal beam intensity (r=0). The approximate relationship $\Delta T = dT/dt\ \Delta t$ where dT/dt is the rate of temperature increase at t=0, r=0 and Δt is the length of the bleach. Note that this overestimates the temperature increase since the initial rate of temperature increase (dT/dt at t=0) is larger than the average rate over the length of the bleach. The derivative of the temperature with respect to time may be determined from the chain rule. It then follows that:

$$\frac{dT}{dt} = \frac{4\pi B}{[4\pi\kappa]^{3/2}} \int_{-\infty}^{\infty} dz' \int_{0}^{\infty} dr' r' \exp\left[-r'^2\left(\frac{1}{4\kappa t} + \frac{2}{\omega_0{}^2}\right)\right] \exp\left(\frac{-z'^2}{4\kappa t}\right)$$

Evaluation of the integral over r' yields:

$$\frac{dT}{dt} = \pi B(4\pi\kappa t)^{-3/2} \int_{-\infty}^{\infty} dz' \left(\frac{1}{4\kappa t} + \frac{2}{\omega_0{}^2}\right)^{-1} \exp\left(\frac{-z'^2}{4\kappa t}\right)$$

Finally, if the integral over z' is computed, then:

$$\frac{dT}{dt} = \frac{2B}{1 + \frac{8\kappa t}{\omega_0{}^2}}$$

An upperbound for the bleach-induced temperature rise is therefore

$$\Delta T = 2B\Delta t = \frac{9.2\varepsilon CP}{\pi\omega_0^2 c_p \rho}\Delta t$$

which is just the short time limit of the more precise equation for T(0,t), shown above:

$$T(0,t) = \frac{2.3\varepsilon CP}{2\pi\kappa c_p \rho}\ln\left(1 + \frac{8\kappa t}{\omega_0^2}\right)$$

Ground State Depletion Measured by Absorption

While pFRAP has a long memory time as well as good sensitivity, its μsec time resolution is fairly poor, precluding measurements of short to medium wavelength DNA bending motions. Consequently, a technique with better time resolution while retaining a long memory time is desirable. Ground state depletion measured by absorption is such a technique. It's memory time is long, determined by the triplet state lifetime, and at least theoretically, the technique can have very fast time resolution since absorption occurs on the order of a femtoseconds. (Intersystem crossing occurs typically on the ten picosecond scale, although once the molecule is in the excited singlet state, it contributes to ground state depletion; consequently the time resolution can be less than 10psec.) Practically, the time resolution is limited by digitizing rates of transient digitizers and signal averagers, and by the pulse width of hi-energy lasers. Here the time resolution is limited by the 10nsec/pt digitizing rate of the LeCroy 9400 digitizing oscilliscope used for data collection and averaging. The memory time is approximately 40μsec, determined by the triplet state of Methylene Blue, the dye used here, which has a triplet lifetime of 13μsec. The one major drawback of the technique is it's relative insensitivity, since it is, after all, an absorption-based technique.

The experimental apparatus is shown below.

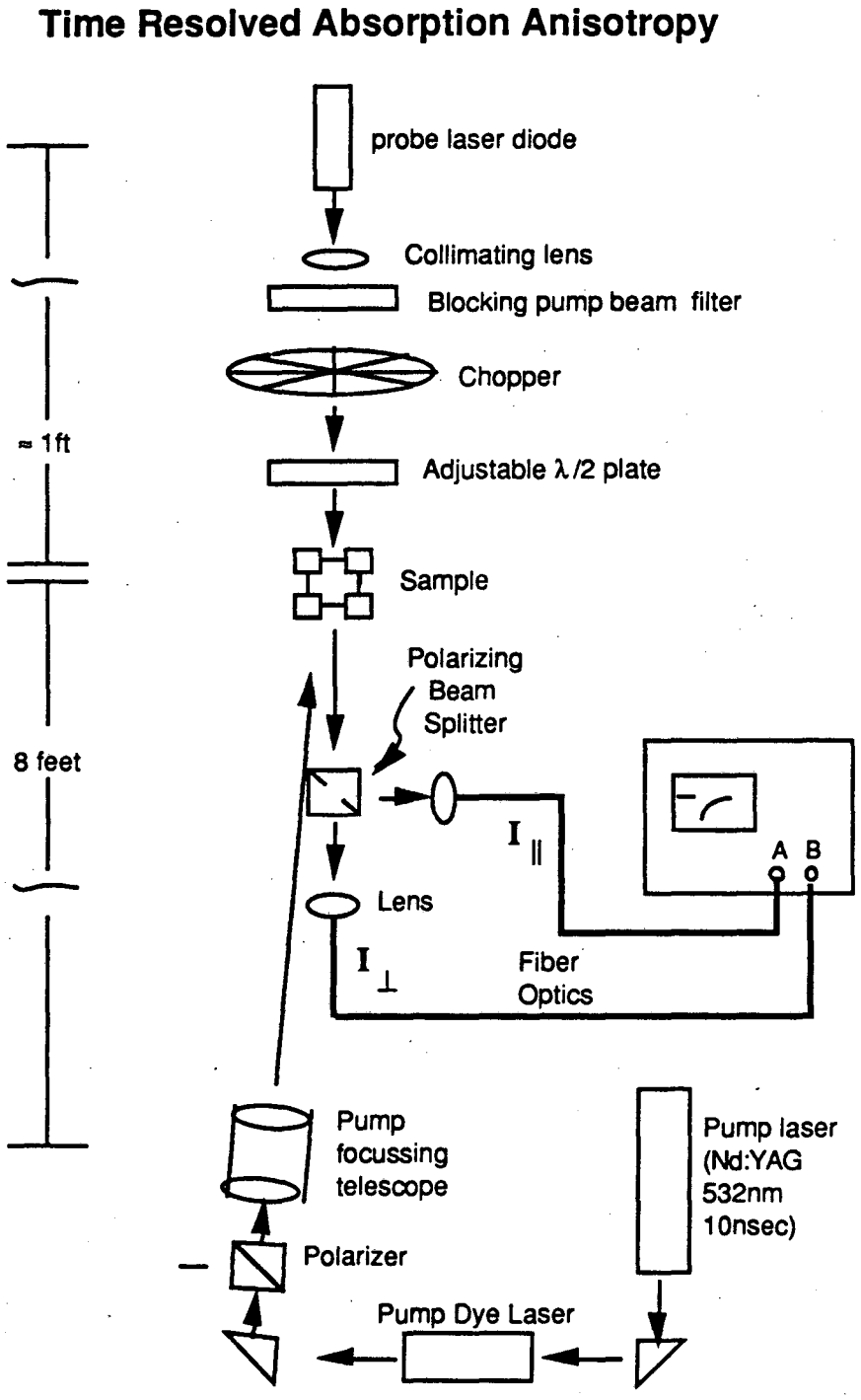

FIGURE 3-9: Schematic of Time resolved anisotropy measured by absorption (or Transient Absorption, TA). Details in text.

The bleaching pulse is formed by a dye laser pumped by a doubled Nd:YAG laser. The output of the rhodamine dye laser is approximately 700nm, which corresponds to the absorption band of methylene blue, the DNA dye used here. (Methylene blue is convenient for this experiment because it has such a high probability for intersystem crossing, ≈ 0.5). The beam is vertically polarized.

The c.w. probe beam is derived from a diode laser with output at 705nm. The wavelength of the probe beam is chosen close to the pump pulse wavelength to ensure that the same transition is being pumped and monitored. Having a slightly different probe beam wavelength, however, is convenient because a colored glass filter can be used to prevent the pump beam from hitting the diode laser, while having the probe and pump beams nearly parallel. Indeed, the relatively long distance between the pump laser and the sample is so that the pump and probe beams are nearly parallel. A diode laser is used, rather than a helium-neon laser, for example, because the diode lasers have significantly smaller intensity fluctuations.

Before reaching the sample, the probe beam is chopped and sent through an adjustable half-wave plate. The chopper simply prevents the probe beam from impinging on the sample when data is not being taken, thereby reducing any (unwanted) bleaching effects from the probe beam. (The pump laser fires only ten times a second, or once every 100msec, and the ground state depletion last for less than a millisecond; consequently, >99% of the time there is no sense to having the probe beam on.) The adjustable half-wave plate rotates the plane of polarization of the probe beam to 45 degrees from the vertical, so that the beam's vertical and horizontal intensity components are equal. Simultaneous parallel (vertical) and perpendicular (horizontal) measurements are then made. The horizontal and vertical absorption components are isolated by a polarizing beamsplitter. Each component is then focussed down into a fiber optic cable and

(simultaneously) sent to the A and B channels of a LeCroy digitizing oscilloscope and signal averager. The anisotropy function is then just (A-B)/(A+2B).

Note that the simultaneous detection is very important for reducing the impact of laser intensity fluctuations. After signal averaging, typically for a few minutes, the A and B channels of the scope are subtracted from each other. The laser intensity fluctuations cancel out almost completely (the common mode rejection of the scope is about 90 dB) in the numerator. Of course they do not cancel out in the denominator, but here the fluctuations are not as significant because they are a small part of the sum (except after a long time when the amount of ground state depletion is very small), whereas they are always a significant fraction of the difference — the numerator.

The TA results in figure 3-3 shows that data of high quality can be collected and is in good agreement with well established theoretical rotational relaxation rates. Similarly high quality data on DNA is presented in Chapter 4 (Figures 4-1B and 4-2).

References

Austin, R.H., Chan, S.S. and Jovin, T.M. (1979) Rotational Diffusion of Cell Surface Components by Time-resolved Phosphorescence Anisotropy. *Proc. Natl. Acad. Sci. 76(11),* 5650-5654.

Axelrod, D., Koppel, D.E., Schlessinger, J.S., Elson, E, and Webb, W.W. (1976) Mobility Measurement by Analysis of Fluorescence Photobleaching Recovery Kinetics. *Biophys.* J. 16, 1055-1069.

Axelrod, D. (1977) Cell Surface Heating in Fluorescence Photobleaching Recovery Experiments. *Biophys. J. 18,* 129-137.

Axelrod, D. (1979) Carbocyanine Dye Orientation in Red Cell Membrane Studied by Microscopic Fluorescence Polarization, *Biophys. J. 26,* 557-574.

Cantor C. and Schimmel, P. Biophysical Chemistry, part II, 1980 455-462.

Eads, T.M., Thomas, D.D., and Austin, R.H. (1984) Microsecond Rotational Motions of Eosin-labeled Myosin Measured by Time-resolved Anisotropy of Absorption and Phosphorescence. *J. Mol. Biol., 179,* 55-81.

Firth, W.J. III., Watkins, C.L., Graves D.E. and Yielding, L.W. (1983) Synthesis and Characterization of Ethidium Analogs: Emphasis on Amino and Azido Substituents. *J. Heterocyclic Chem. 20,* 759.

Garland, F., Graves, D.E., Yielding, L.W. and Cheung, H.C. (1980) Comparative studies of the Binding of Ethidium Bromide and its Photoreactive Analogues to Nuclei Acids by Fluorescence and Rapid Kinetics. *Biochem.,* 19, 3221.

Graves, D.E., Yielding, L.W., Watkins, C.L. and Yielding, K.L. (1977) Synthesis, Separation and Characterization of the Monoazide and Diazide analogs of Ethidium Bromide. *Bioch. Biophys. Acta* 479, 98.

Johnson, P., & Garland, P.B. (1982) Fluorescent Triplet Probes for Measuring the Rotational Diffusion of Membrane Proteins *Biochem. J. 203,* 313-321.

Jovin, T.M., Bartholdi, M., Vaz W.L., Austin. R.H. (1981) *Ann. New York Acad. Sci., 366,* 176-196.

Magde, D., Elson, E.L., & Webb, W.W. (1974) Fluorescence Correlation Spectroscopy. II. An Experimental Realization. *Biopolymers 13,* 29-61.

Scalettar, B.A., Selvin, P.R., Axelrod, D., Hearst, J.E., & Klein, M.P. (1988) A Fluorescence Photobleaching Study of the Microsecond Reorientational Motions of DNA. *Biophys. J. 53,* 215-226.

Scalettar, B.A., Selvin, P.R., Axelrod, D., Klein, M.P. & Hearst, J.E. (1990) A Polarized Photobleaching Study of DNA Reorientation in Agarose Gels. *Biochemistry 29,* 4790-4798.

Selvin, P.R., Scalettar, B.A., Langmore, J.P., Axelrod, D., Klein, M.P.& Hearst, J.E., (1990) A Polarized Photobleaching Study of Chromatin Reorientation in Intact Nuclei. *J. Mol. Biol.* 214(4), 911-922.

Velez, M., & Axelrod, D. (1988) Polarized Fluorescence Photobleaching Recovery for Measuring Rotational Diffusion in Solutions and Membranes. *Biophys. J. 53,* 575-591.

Yoshida, T.M., & Barisas, B.G. (1986) Protein Rotational Motion in Solution Measured by Polarized Fluorescence Depletion. *Biophys. J. 50,* 41-53.

Chapter Four

Dynamics of Isolated DNA

Including the Effects of Supercoiling, Base Pair Composition and Polyamine Interaction

Abstract

We have used Time Correlated Single Photon Counting of intercalated Ethidium Bromide to measure the torsional constant of isolated DNA, including the effects of supercoiling, both positive and negative, base pair sequence, salt concentration, and spermine. All data fit well to the theory of Barkely and Zimm. The torsional constant is found to be $\approx 2.0 \times 10^{-19}$ erg-cm for relaxed, native DNA at physiological salt concentration. The DNA becomes torsionally more rigid as the salt concentration decreases or as the DNA becomes more negatively supercoiled. Alternating homopolymers of G-C were found to be considerably stiffer than those composed of A-T. Spermine binding made both homopolymers more flexible, and in the same proportion, indicating that spermine interaction is primarily electrostatic, neutralizing negative phosphate charges, and is not sequence specific. For supercoiled DNA, at physiological salt concentration, the torsional constant monotonically increases from 1.76×10^{-19} erg-cm for the most positively supercoiled DNA ($\sigma = +0.042$) to 2.28×10^{-19} erg-cm for the most negatively supercoiled DNA ($\sigma = -0.123$). These results indicate that the positively supercoiled DNA is signficantly more flexible torsionally than negatively supercoiled DNA and that the DNA behaves as a non-linear torsional oscillator under superhelical stress. The magnitude of the anharmonic term in the Hamiltonian is approximately 15% at the rms twist deviation. Transient absorption studies indicate a simple, single-exponential

anisotropy decay due to bending and suggest that the bending constant does not vary with superhelicity.

DNA Dynamics from Picoseconds to Microseconds

Many studies have been made on the dynamics of isolated DNA. Our results for phage Lambda DNA, shown in Fig. 4-1a and 4-1b, present the dynamics from approximately 10 picoseconds to 40 microseconds. In Fig. 4-1a TCPC was used to measure the dynamics from 0 - 75 nanoseconds with a time resolution of 75 picoseconds. Our TCPC results closely agree with the work of others (Wahl, 1970; Millar, 1980, 1982; Thomas, 1980,1983). The ground state depletion experiments (measured via absorption) extend the measurement to longer times, covering the 0-40microsecond scale, with 10 nanosecond resolution. The TCPC experiment was repeated for a number of different DNA samples, including homopolymers of dA-dT and dG-dC, and pBR322 in linear, closed-circular relaxed and supercoiled conformations. All data displayed similar qualitative shapes, although the decay constant (DNA torsional rigidity) varied, in a manner that will be discussed in this chapter. The TA experiment was also repeated using a large (≈50,000bp) plasmid, pSM1, either relaxed or supercoiled. These preliminary results indicate that the fast motions — primarily twisting — are affected by the supercoiling, but the longer motions — primarily bending motions — are unchanged (see Supercoiling section).

The dynamics of isolated DNA, as shown in Fig. 4-1, can be summarized rather succinctly: The DNA undergoes rapid twisting on a time scale less than 100 nanoseconds. Most of the depolarization of an intercalated fluorophore in this time regime (or of any "arrow" placed roughly perpendicular to the helix axis on the DNA) is due to twisting motion, although a rigorous fit to the data requires some fast bending motion to be included as well. The Barkley-Zimm theory (1979) fits the fluorescence data in this time

regime extremely well (see below), yielding a torsional constant for naturally occuring DNA, C = 2.0-2.3 x 10^{-19} erg-cm (depending on whether pBR322, phage λ or Calf-thymus DNA is used. Also the torsional constants for synthetic homopolymers of DNA can vary over a considerable range — see Sequence Dependence section of this chapter). The anisotropy, which starts at ≈0.36, decreases to approximately 0.16 by 75nsec and decays to a good approximation as $\exp[-(t/C)^{1/2}]$, where t is time and C is the torsional constant . A similar theory by Allison and Schurr (1979) also fits the data well, with the same functional time dependence.

After 75-100nsec, depolarization due to twisting is essentially complete, with further depolarization due to bending motions. The longer bending motions, as the ground-state depletion data presented in Fig. 4-1b show, can be characterized rather simply, although a rigorous theoretical treatment does not yet exist. The polarization decay is nearly a single exponential, with a time constant of 13usec, which is the tumbling time of a rigid rod of 1000A. This distance is just the statistical length, or twice the persistence length of DNA. An approximately ten microsecond reorientational relaxation has also been detected in light scattering and dichroism experiments and has been atrributed to end-over-end tumbling of a persistence length segments of long DNAs (Schmitz and Schurr, 1973; Ding et al., 1972).

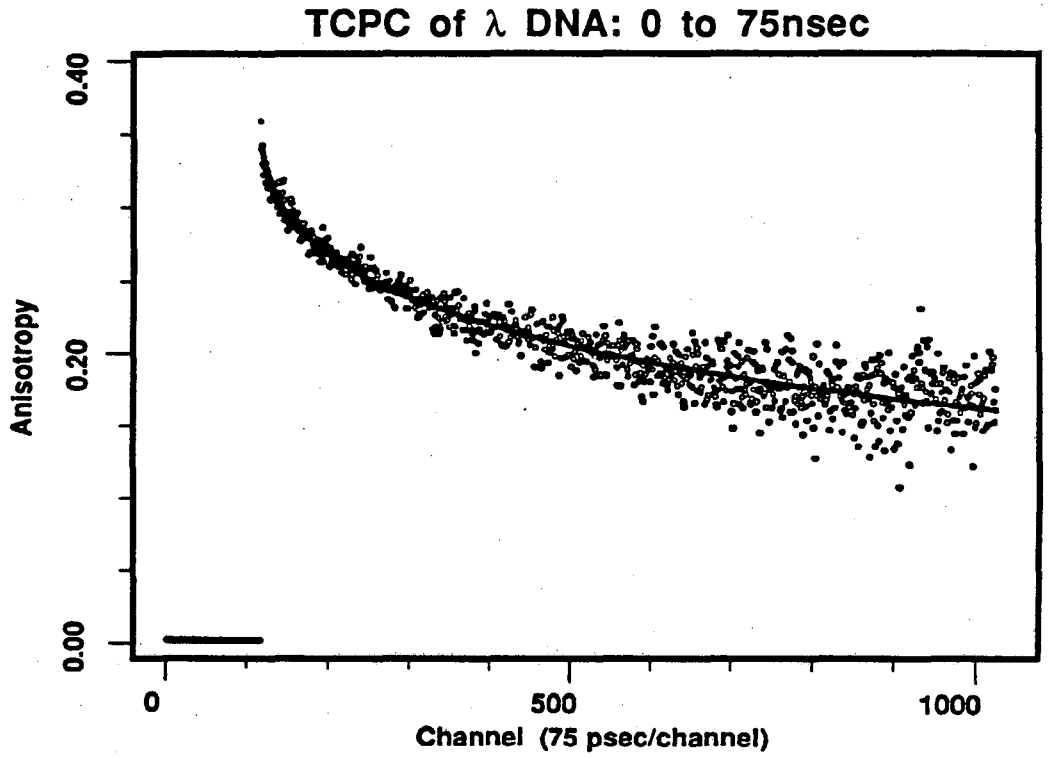

FIGURE 4-1A: Time Correlated Single Photon Counting of phage Lambda DNA labelled 1:150 Ethidium Bromide: base pairs, and dissolved in 75 mM KCl, 25 mM Tris, pH 8.0, 0.5 mM EDTA. The solid line is the best fit curve based on the Barkeley-Zimm model with two free parameters, the initial anisotropy and the torsional constant.

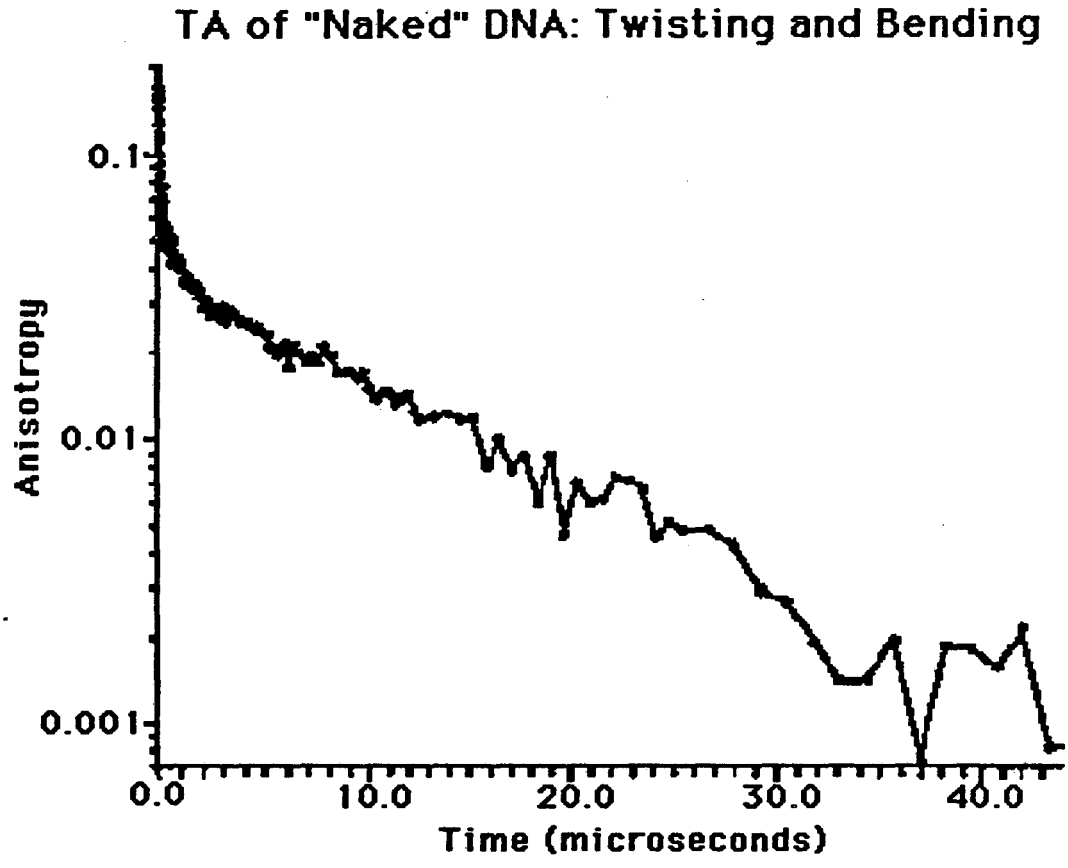

FIGURE 4-1B: Transient Absorption of phage λ DNA labelled 1:100 Methylene Blu Pairs in BRL (Bethesda Research Lab) buffer. The very fast depolarization in the first ≈ 10 points (100nsec) is due primarily to twisting. The single exponential decay (with 13μsec decay time) from a few μseconds to 40 μsec is primarily due to bending of statistical length segments of DNA.

Experimentally, for both graphs, the DNA concentration was kept sufficiently low to avoid interactions between DNA molecules: for TCPC, the DNA concentration was 200μg/ml; for TA the DNA concentration was 300μg/ml. Lambda DNA was obtained from Bethesda Research Laboratory and was used "as is" for the TA experiment (Tris-EDTA (TE) buffer) and placed in the 0.5x Spectroscopy buffer (1x SB = 150 mM KCl, 50 mM Tris, pH 8.0, 1 mM EDTA) for the TCPC experiment. The spectroscopy for both

the TA and TCPC was done as described in chapters three and four. Intercalated ethidium bromide was used as the reporter molecule in the TCPC experiment. A fluorescence depolarization experiment taken at the magic angle and fitted to two exponentials show that the 99.9% of the dye is intercalated. (The data were deconvoluted with the instrument response function and fitted using SIM.EXE, a fortran program available at the Calvin lab. Also the time constant of the two exponentials was left free: the fact that they did indeed fit the established free and bound fluorescent lifetime of ethidium bromide — 1.6 and 23nsec, respectively, gives extra confidence in the results. The quality of the fits were determined by standard reduced χ^2 fits (O'Connor and Phillips, 1984).

The TCPC and TA spectroscopy were done as described in Chapters 2 and 3. For TCPC, the anisotropy was fit to the function:

$$r(t) = \frac{gL_fI_{\parallel} - I_{\perp}}{gL_fI_{\parallel} + 2I_{\perp}}$$

where g accounts for the polarization sensitivity of the detection system and L_f is the integrated laser light intensity in the perpendicular mode divided by the intensity in the parallel mode. L_f accounts for any fluctuation in integrated excitation light intensity in the perpendicular or parallel modes. $I_{\parallel}$ and $I_{\perp}$ are the fluorescence in the parallel and perpendicular modes, respectively, *corrected* for the missed photons due to instrumetent dead time (see chapter 3). The uncorrected $I_{\parallel}$ was kept below 5,000 cps to keep the correction small.

For the TA experiment, methylene blue was used as the reporter molecule. Like EtBr, it is an intercalator and has a similar binding equilibrium constant — consequently, essentially all of the MB is expected to be bound. MB was chosen because of the ease of depleting its ground state due to its high intersystem crossing efficiency into the triplet state. The data were fit to the standard anisotropy function. Because the parallel and

perpendicular data was taken simultaneously, no "L_f" correction is required and the angle of polarization of the pump pulse is adjusted prior to the start of the experiment to offset any g-factor.

The individual parallel and perpendicular curves for the TCPC anisotropy in Fig. 4-1a are shown in figure 7 of chapter 2. The individual curves for the TA anisotropy in Fig. 4-1b is shown in Fig. 4-2 below.

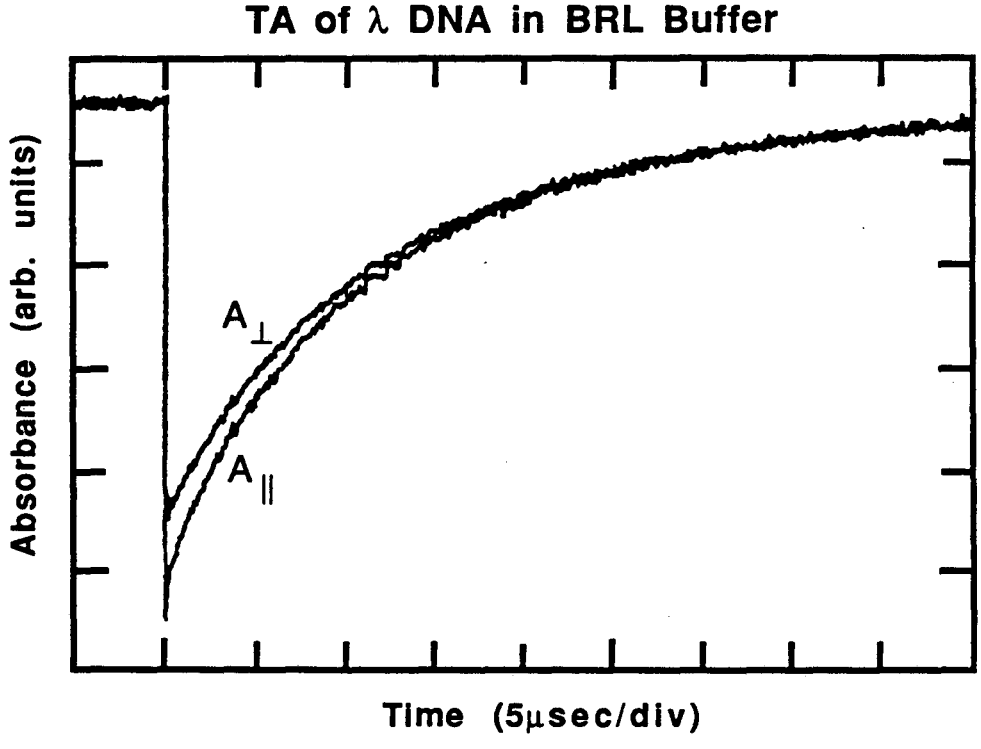

FIGURE 4-2: Transient Absorption data on Lambda DNA in TE buffer. The associated anisotropy is shown in Figure 4-1b. Note that in the actual experiment, $-A_{\parallel}$ and $-A_{\perp}$ are collected because of the presence of an inverting amplifier. These have been multiplied by -1 for presentation here.

The torsional constant is obtained by fitting the TCPC data with a theory of DNA twisting developed by Barkley and Zimm (1979). The theory models DNA as a uniform, elastic rod which behaves according to classical elasticity and hydrodynamic theories. Allison and Schurr (1979) have also developed a theory of DNA twisting which treats

DNA as a series of beads connected by harmonic torsional springs subject to the hydrodynamic drag of the connected beads (Allison and Schurr, 1979). Although the physical assumptions differ, these models yield identical mathematical descriptions of the torsional motions of the DNA helix over the time range of interest for TCPC. Because it is slightly simpler, we use the Barkley-Zimm model. The reader is referred to the paper of Millar et al., for an excellent synopsis of the theory, from which much of this discussion is taken.

Theory of Barkley-Zimm

Treating DNA as a uniform elastic rod in a viscous medium, Barkley-Zimm calculate the fluorescence depolarization anisotropy function of a DNA-intercalated dye. The time evolution of the anisotropy function is determined primarily by short wavelength twisting, and to second order, to short wavelength bending modes. It is these modes that will lead to significant angular displacement of the fluorophore on the time scale of a fluorescence depolarization experiment (≈100nsec). For example, the tumbling time of a rigid rod of one persistence length — 190 base pairs — about its transverse (short) axis (analogous to bending) is ≈5 msec, too long to contribute significantly to the anisotropy decay. The correlation time about its helical (long) axis is about 100 nsec; consequently twisting motions of ≥ one persistence length wavelength will not significantly contribute to the depolarization (although clearly a twisting mode of one persistence length will contribute significantly more than the bending mode of the same wavelength). Furthermore, they argue that the contribution to depolarization by either of these tumbling modes will be even smaller when the segment is part of a high molecular weight DNA (such as that used in the experiments described in this chapter).

In addition, Barkley-Zimm assume that bending and twisting are uncoupled. This will be approximately true if the angular displacements due to bending are sufficiently small, as is expected to be the case from the above order-of-magnitude calculations.

To begin their analysis, Barkley and Zimm derive the dynamical equations for bending and torsion of an elastic rod for arbitrary initial amplitude of the normal modes using results from classical hydrodynamic and elasticity theories. These general diffusion equations are then adapted to the initial distribution of dipoles in the fluorescence depolarization experiment. The final result for the time-dependent anisotropy, which incorporates both bending and torsion, is:

$$r(t) = r_o \frac{[A_1(\varepsilon)\, e^{-\Delta} + A_2(\varepsilon)[\frac{5}{8} + \frac{3}{8}e^{-\Delta}]e^{-\Gamma} + A_3(\varepsilon)e^{-\Delta}e^{-\Gamma/4}]}{[A_4(\varepsilon) + A_5(\varepsilon)e^{-\Delta}]}$$

where r_0 is the initial anisotropy (a theoretical maximum of 0.4), $\Gamma(t)$ and $\Delta(t)$ are the torsion and bending decay functions, respectively, and the $A_j(\varepsilon)$ are simple trigonometric functions of ε, the angle between the transition dipole of the intercalated dye and the helix axis.

$$A_1(\varepsilon) = \frac{1}{4}(1 - 3\cos^2\varepsilon)^2$$
$$A_2(\varepsilon) = \frac{3}{4}\sin^4\varepsilon$$
$$A_3(\varepsilon) = 3\sin^2\varepsilon\cos^2\varepsilon$$
$$A_4(\varepsilon) = \frac{3}{4}(1 + \cos^2\varepsilon)$$
$$A_5(\varepsilon) = \frac{1}{4}(1 - 3\cos^2\varepsilon)$$

Γ and Δ are superpositions of relaxations due to all torsional and bending normal modes, respectively. For a rod of length 2L,

$$\Gamma(t) = 4D_1 t + \left(\frac{4k_B T}{CL}\right) \sum_{k=1}^{\infty} \frac{1 - \exp(-t/\tau_k)}{\lambda_k^2}$$

$$\Delta(t) = 4D_2 t + \left(\frac{4k_B T}{EIL}\right) \sum_{k=1}^{\infty} \frac{1 - \exp(-t/\tau_k')}{\kappa_k^2}$$

The torsional and bending modes have time constants τ_k and τ_k', respectively, and wavenumbers $\lambda_k = k\pi/L$, $\kappa_k = (2k+1)\pi/4L$, respectively. There is also a term corresponding to rotation of the entire rod about its long axis (with diffusion coefficient D_1) and a similary term for bending, corresponding to rotation of the entire rod about its transverse axis with diffusion coefficient D_2. These large scale tumbling terms, as discussed above, have a negligible effect on the anisotropy decay. C and EI are the torsional and bending rigidity, respectively, of the rod. (EI is the product of E, the Young's modulus and I, the moment of inertia and is directly related to the commonly used persistence length P, through the relation $EI=k_B TP$, where k_B is Boltzman's constant.)

The relaxation times can be related to the relevant force constants by the relations:

$$\tau_k = \frac{\rho}{C\lambda_k^2} \qquad \tau_k' = \frac{\rho_k}{EI\kappa_k^2}$$

where ρ and ρ_k are the frictional coefficient per unit length for twisting and bending, respectively. For twisting ρ is independent of length **true??*, whereas for bending, it is a function of k. With η as the solvent viscosity,

$$\rho = 4\pi\eta b^2 \qquad \rho_k = \frac{4\pi\eta}{\kappa_k^2 f(b\kappa_k)}$$

in which f(z) is the sum of modified Bessel functions:

$$f(z) = K_0(z) + \frac{z}{2}K_1(z)$$

and b is the radius of the DNA helix. For consistency with previous fluorescence depolarization work, we use b=13.4 Angstroms, the value used by Millar et al.. This is the hydrodynamics radius of B-form DNA assuming one layer of hydration. There is currently some disagreement over what radius to use in analyzing fluorescence depolarization experiments, which accounts for some of the difference in torsional constants found by Schurr and co-workers and other (Wu et al. , 1987). In any event, when the value for b is agreed upon, all results can be easily scaled appropriately.

The above analysis is predicated on a uniform elastic rod model. At what point does this assumption break down? Clearly for very short wavelength motions, the detailed structural features and inhomogeneity will be significant. Barkley-Zimm estimate that modes longer than two turns of the helix (70 Å) will be insensitive to non-uniformities, which have corresponding relaxation time of ≈ 100psec. Therefore experimental observations longer than this should be consistent with the theoretical assumption. In our experiments we collect data with a temporal bin size of 75-100psecs.

At sufficiently short times the discrete sum can be approximated by an integral; at long times the exponentials vanish and the infinite sum can be done directly, leading to the approximate results:

$$\Gamma(t) \approx At^{1/2} \qquad t \leq \tau_1$$

$$\approx 4D_1 t + 2k_B\frac{TL}{3C} \qquad t >> \tau_1$$

in which

$$A = 2k_BT/\pi b\eta^{1/2}\, C^{1/2}$$

and

$$\Delta(t) \approx B(t)\, t^{1/4} \qquad t \leq \tau_1'$$

$$\approx 4D_2t + 0.4853k_BTL/EI \qquad t >> \tau_1'$$

and B(t) is the slowly varying function of time

$$B(t) = (3.466k_BT/\pi^{5/4}\eta^{1/4}EI^{3/4})\, f(z_{max})^{1/4}$$

in which f(z) is the sum of modified Bessel functions:

$$f(z) = K_0(z) + \frac{z}{2}K_1(z)$$

and z_{max} is determined by iteration from the equation

$$z_{max}(t) \approx b\, [\, 5.024\pi\eta\, /\, tEI\, f(z_{max})\,]^{1/4}.$$

The equation for r(t) given at the beginning, and the short-time approximations for Γ and Δ are the most useful expressions of this section and are the relevant expressions for TCPC. Note that the anisotropy due to twisting decays as the square root of time and for bending decays as the fourth-root of time. Bending therefore has a weaker dependence on time and for this reason alone will contribute less to the anisotropy decay. For both twisting and bending there is a linear dependence on absolute temperature, but because measurements are restricted to a relatively narrow temperature range (from approximately 273°K to 300 or 310°K), this is not a sensitive dependence. For twisting, the anisotropy decay is inversely proportional to the square root of the solvent viscosity (a parameter that can be varied by three orders of magnitude) and to the torsional constant. The relatively

weak dependence of the anisotropy on the torsional constant makes experimental accuracy crucial — the anisotropy decay curves are very similar, for example, for two molecules with torsional constant that differ by 10%.

Barkley and Zimm evaluate the relative contributions of twisting and bending to the anisotropy decay by calculating $r_{(t= 100nsec)}$ for two extreme cases. First, twisting of the helix is entirely suppressed ($\Gamma(t) = 0$) in which case $r = 0.379$, very close to the rigid limit of 0.4. Bending therefore contributes little to the anisotropy decay. Second, bending is entirely suppressed, ($\Delta(t) = 0$), in which case $r_{(100nsec)} = 0.209$, not far from the $r \approx 0.16$ @ 75-100nsec value commonly observed (Millar et al., 1980; Millar et al., 1982; Thomas et al., 1980; Thomas and Schurr, 1983; Wu et al., 1988). Twisting, is therefore the primary cause of the anisotropy decay.

The expression for r(t) can be further simplified if it is assumed that the depolarization of the intercalated dye is due solely to torsional motion, then

$$r(t) = r_0\{\frac{1}{4}(3\cos^2\varepsilon - 1) + \frac{3}{4}e^{-\Gamma}\sin^4\varepsilon + 3e^{-\Gamma/4}\sin^2\varepsilon\cos^2\varepsilon$$

and finally, if we assume that the dipole moment of the intercalated dye molecule is perpendicular to the DNA long axis, then $\varepsilon = \pi/2$ and the anisotropy reduces to a particularly simple form:

$$r(t) = r_0\{\frac{1}{4} + \frac{3}{4}e^{-\Gamma}\}$$

Both of these later assumptions are approximations: ε is in fact close to 70 degrees, and while Millar and Zewail have found that data can be fit well to the expression for r(t) assuming no bending, the torsional constant found from the curve fitting differs by roughly a factor of two from the result derived when bending motions (and more accurate

value of ε) are included. In calculating the torsional constants presented in this thesis, we use the full expression for r(t), including the bending terms and $\varepsilon = 70°$.

Comparison of Torsion Constant for Linear DNA with the Work of Others.

The torsion constant of DNA has been measured by a number of different investigators. Two different techniques have been used: dynamics spectroscopic techniques of DNA (usually with intercalated ethidium bromide) similar or identical to the TCPC experiments performed here (Wahl, 1970; Millar, 1980,1982; Thomas and Schurr, 1983; Shibata, 1984; Wu, 1988; Fujimoto and Schurr, 1990) and the static ligation method, a completely different technique that relies on the probability of ring closure of short ($\leq$ 500 bp) DNAs being a function of the torsional constant (Shore and Baldwin, 1983a; Shore and Baldwin, 1983b; Horowitz and Wang, 1984). The two techniques give similar, though somewhat different results. The torsional constant calculated from fluorescence experiments tend to be somewhat lower, although systematic uncertainties in each technique make it unclear whether the difference is significant.

The static ligation method involves taking a series of DNA pieces that vary in length by one base pair, say from 300 to 310bp. For each length of DNA there is some probability that the ends will come together, and if placed in the presence of the enzyme ligase, will form a covalently closed circular molecule. Cyclization probability is measured by determining the ratio of rates for cyclization vs. oligomerization at the early times in a ligation reaction. If the length of DNA is exactly a multiple of 10.45bases, then no net twisting will be required to form the closed circular molecule. If however, the DNA is one or two or three... bases longer or shorter than this multiple, some twisting will be required. These molecules will be slightly higher in energy and the probability of them forming will be less. (The probability goes like $\exp(-\Delta G/kT)$, where ΔG is the free energy of the closed circular molecule, with ΔG clearly a function of the torsional

constant.) Conversely, by knowing the probability of formation as a function of length of DNA, the torsional constant can be derived. Because the lengths of DNA vary by only a few base pairs (10 at most) it is assumed that the energy of bending is the same for all the molecules.

The fluorescence and the ligation methods are fundamentally different, although they portend to measure the same quantity — the torsional constant. The fluorescence measurement is based on measuring the *dynamics* of DNA (or more precisely, of an intercalated dye in DNA) due to thermal fluctuations. These fluctuation occur in the subnanosecond to 100nanosecond time scale. In contrast, the ligation method is a static, or equilibrium value measurement that takes place over many minutes. It also involved a *net* change in twist, as opposed to localized fluctuations. For this reason it is not clear that the two measurements should in fact yield the same value for the torsional constant. It is well known, for example, that the elastic property of polymers can depend on the time scale or range of motion. This can be due to non-linearities, or can even be present in linear systems via a resonance phenomenon. On resonance, for example, a very little force creates a large response. Since the force constant is the ratio of applied force to displacement the measured force constant is small. Off resonance, a larger force is required for the same response and the measured force constant is thus larger.

Our results based on TCPC measurements are consistent with the fluorescence work of others. Assuming a persistence length of 510 Å (Millar et al., 1982) (which means the flexural rigidity $EI \equiv k_B TP = 2.15 \times 10^{-19}$ erg·cm (Barkley and Zimm, 1979)) we calculate the torsional constant of linear pBR322 DNA in 150 mM KCl to be $C = 1.90 \pm 0.06 \times 10^{-19}$ erg·cm. Millar et al. (1982) measured $C = 1.95 \pm 0.18 \times 10^{-19}$ erg·cm for supercoiled pBR322 of unspecified superhelix density and $1.43 \pm 0.11 \times 10^{-19}$ erg·cm for calf thymus DNA, both in 150 mM NaCl, 100 mM Tris·Cl, pH 7.7. The calf thymus results however, are difficult to interpret because the DNA was commercially obtained

and used without purification, and consequently likely had significant amount of bound proteins. Schurr and collaborators have made a number of measurements but in general ignore the contribution of bending to the anisotropy decay (Fujimoto and Schurr, 1990; Shibata et al., 1984; Taylor and Hagerman, 1990; Thomas et al., 1980; Thomas and Schurr, 1983; Wu et al., 1988). Assuming all the depolarization is due to twisting they get $C = 1.3$ to 1.4×10^{-19} erg·cm. When they do correct for bending, they report a value of $C = 1.9 \times 10^{-19}$ erg·cm, in excellent agreement with out results.

A different dynamics spectroscopic technique, linear and saturation transfer EPR, has also been used to measure the torsional constant of DNA (Robinson, 1980; Hurley, 1982). Based on a theory which neglects bending and which requires computer simulations of CW-EPR spectra, they report a values of $C = 1.2$ and 1.5×10^{-19} erg·cm.

Three groups have used the static ligation method to measure the torsional constant of DNA (Shore and Baldwin, 1983a,b; Horowitz and Wang, 1984; Taylor and Hagerman, 1990). Based on classical thermodynamics anlaysis, Shore and Baldwin estimated that $C = 2.4 \times 10^{-19}$ erg·cm, Horowitz and Wang in a similar experiment, find $C = 3.0 \times 10^{-19}$ erg·cm, and Taylor and Hagerman, using a different DNA sequence and Monte-Carlo simulations of their data get 2.0×10^{-19}erg·cm.

A number of workers have reanalyzed the data of Shore and Baldwin using Monte Carlo simulations. The torsional constant extracted from these simulations range from 2.3 to 3.8×10^{-19} erg·cm (Frank-Kamenetskii, 1985; Levene and Crothers (1986); Hagerman and Ramadevi, 1990; Shimada and Yamakawa, 1984; Klenin, 1990), although the highest value obtained by Levene and Crothers, has come under criticism because of their assumption of ring-closure (Hagerman, 1990). Levene and Crothers assume the molecule is closed if the end-to-end distance is less than 20% of the persistence length. For the 250bp DNA molecule used by Shore and Baldwin, assuming a persistence length of

500Å, this corresponds to 12% of the contour length, a rather lax definition of ring closure. Under this definition even relatively stiff molecules can cyclicize easily, leading to an overestimte of C. Excluding the Levene and Crothers, the range of torsional constants measured via the static ligation technique varies from 2.0 to 3.1x 10^{-19} erg·cm.

That the results from the dynamics and static techniques are so similar implies that DNA is not very non-linear and there is not a large resonance phenonenon. A large resonance would not be expected because small molecules in solution are always overdamped, which spoils any resonator Q. That there is some difference between the techniques implies that DNA is may not be completely linear. In a non-linear system, the frequency of oscillation is a function of displacement. In the ligation experiment there is a net twist of the molecule, whereas in the TCPC (of linear DNA) there is no net twist, only local, thermal fluctuations. For a DNA molecule a few thousand base pairs long — the length used in TCPC experiments —the net twist due to these thermal fluctuations is very small, on the order of a turn or less (see discussion of twist and topoisomers, below).

It is also possible that the difference (or even similarity!) between the results from each technique merely reflect different systematic errors. Perhaps the biggest uncertainty in the dynamics fluorescence data is the contribution that bending makes to the depolarization. In the absence of any truly satisfactory theory of DNA bending, the absolute value of the torsional constant measured via fluorescence depolarization should not be overinterpreted. Fujimoto and Schurr (1990), for example, calculate an upper bound for the torsional constant of $C = 2.55 \times 10^{-19}$ erg·cm when they use the maximal contribution of bending to depolarization. This value lies in the range of the ligation method. They argue, for example, that the usual persistence length should not be used to calculate the effect of bending on fluorescence depolarization, but instead a "dynamic" persistence length should be used. Their best estimate for this dynamic persistence length is 1,500Å, approximately three times longer than the usual persistence length (Fujimoto and Schurr, 1990). Using this larger value, the torsional constants calculated from fluorescence depolarization are in good agreement with the static ligation method (Taylor and Hagerman, 1990).

The static ligation method also suffers from problems and assumptions. The particular DNA sequence used by Shore and Baldwin, the data most widely used in subsequent analysis, may contain special bending sequences which would increase the probability of ring closure (Hagerman et al., 1990). The Monte-Carlo simulations based on the data are just simulations (despite the propensity of computer programmers to call the computer "experiments"!) and require a multiparameter fit, including the pitch, helical repeat and torsional constant. An over or under-estimate of one of these parameters may compensate for an under- or over-estimate of another and still yield a good fit to the data. Furthermore, an arbitrary cutoff point must be assumed as to how close the ends of the DNA molecule must come to each other before the molecule in these simulations are classified as "closed". Perhaps most critically, the Monte-Carlo simulations assume that

twist and writhe can vary independently (Levene and Crothers, 1986; Vologodskii 1979; Klenin, 1990), an assumption which is clearly not true. (The sum of the Twist and Writhe must equal the Linking Number, a fixed topological quantity — see Supercoiling discussion). It is therefore not surprising that Monte Carlo simulations of even the same data set (that of Shore and Baldwin) yield values that vary by 70% (33% if the Levene and Crothers data is excluded).

Comparison of TA Bending Data to the Work of Others:

There are few techniques capable of measuring DNA dynamics in the microsecond to millisecond time regime. Our results, presented in Fig. 4-1B are consistent with the light scattering work of Schmitz and Schurr and the dichroism work of Ding et al., who found a single exponential 10μsec decay which they attributed to bending of statistical length segments of DNA (Schmitz and Schurr, 1973; Ding et al., 1972). Unfortunately, there is, as yet, no quantitative theory of DNA bending with which to compare the TA results. It is hoped that these experimental results will help stimulate work on such a theory.

Significance of Torsional Constant: Base-Pair Fluctuations, Twist Persistence Length and Topoisomer Conformation.

Just as the persistance length of DNA is a measure of how stiff in a bending sense DNA is, the torsional constant similarly determines how stiff the DNA is torsionally. Indeed, we can define a rotational persistence length as the number of base pairs it takes for a base pair to "forget" the twist of another, N base pairs away.

First we calculate the mean square angular deviation of a single base pair. A one dimensional harmonic oscillator — the model of a base pair that can twist — has two degrees of freedom (both the potential and kinetic energy are proportional to the square of

their conjugate variables). Consequently, when in contact with a thermal bath, its average energy will be k_BT, which must equal $\frac{C}{h}\langle(\Delta\phi)^2\rangle/2$, where $<\Delta\phi>^2$ is the rms angular deviation and C/h is the torsional constant per base pair. With $C \approx 2.2 \times 10^{-19}$ erg-cm for relaxed DNA and h=3.4 Angstroms, the distance between base pairs:

$$\langle(\Delta\phi)^2\rangle = \frac{2hk_BT}{C} \approx 5°$$

Note that this is a fairly large angular deviation. For relaxed DNA, with 10.45 bp/turn the average angle between base pairs is 34.5°. The rms fluctuation about this mean is ± 5 °, or about 15%.

We can now calculate the "rotational persistence length" of DNA. (The expression is put in quotes because I have never seen this term, nor this direct comparison between bending and twisting, used in the literature.) We can define the rotational persistence length as that distance for which the angular standard deviation is ± 180°. At this distance, one base pair has essentially "forgotten" the orientation of another a persistence length away. The problem is equivalent to a random walk calculation. Treating the changes in net twist as an *unbiased* random walk will be true if the associated changes in net writhe do not cause significant changes in bending (see topoisomer discussion later this chapter). If they do, then the walk will be biased, i.e., the walk will be on an energetically sloped surface. Since changes in large net writhe can be accomplished with minimal changes in bend, the model of an unbiased walk is reasonable. (Extra turns put into a plectonemically wrapped DNA — DNA wrapped on a cylinder — where the cylinder radius is small and the pitch is large, will give large changes in writhe with little additional bending.)

The walk is N steps long, where N is the number of base pairs, and the step length is 5°. The net angular distance travelled is therefore $\pm(\sqrt{N})5°$. *The rotational persistence*

length, as defined above, is therefore 1296bp. Note that this is almost 10 times as long as the bending persistence length. In this sense then, *the DNA is considerably stiffer in twist than in bend*. Or to put it another way, the DNA resists changes in twist considerably more than changes in bend.

The above calculation is also directly applicable to the average change in net twist of a molecule with N base pairs. The standard deviation in twist is then:

$$\sigma(\text{twist}) = \langle(\Delta Tw)^2\rangle^{1/2} = (\text{angular distance/bp})(\text{number bp})^{1/2}/(360°/\text{twist})$$

A molecule 1296bp long will have a standard deviation of 0.5, i.e., fluctuate in net twist by $\pm$0.5turns, or one turn total. For pBR322, a 4363 bp long molecule, the flucutation in twist is $\pm$0.92turns. This is particular important for an understanding of the conformations of topoisomers — closed circular DNA molecules with different amounts of net twist initially put into them (see Topoisomer separation discussion toward the latter part of the Supercoiling section, below).

Measuring Changes in Torsional and Bending Constants

Sensitivity of TCPC to Changes in Torsional Constant

An important control in attempting to measure any possible changes in torsional constant due either to sequence dependence, superhelical stress, polyamine interactions etc. is to determine how small a change is detectable using the TCPC technique. As mentioned in the Barkley-Zimm theory section, varying the viscosity has the same effect on the anisotropy decay curve as changing the torsional constant. Furthermore, the viscosity can be increased approximately a thousand-fold or as little as a few percent by adding sucrose to the solution. We used DNA solutions containing from 0 to 24% sucrose, corresponding to viscosities from 1.0 centipoise to 2.45 centipoise (Table 4-1). The sucrose concentration could be measured extremely accurately — to four significant

figures — using a Bausch and Lomb refractometer. The viscosity as a function of sucrose concentration (and temperature) is extensively tabulated in the CRC Handbook of Chemistry and Physics.

It is assumed that the sucrose does not itself affect the torsional constant, most likely a very good assumption because sucrose is a small molecule without any particular affinity for DNA, making the on/off kinetics fast, so on average, the DNA sees overwhelmingly water molecules, which are present at 55M compared to $\approx$ 0.75M for the highest sucrose concentration.

TABLE 4-1: Data for sucrose viscosity titration of λ DNA in 75 mM KCl, 50 mM Tris·Cl, pH 8.0

η_{rel} [a]	$\sqrt{1/\eta_{rel}}$	A [b]
1.000	1.000	4.818
1.000	1.000	4.775
1.000	1.000	4.802
1.140	0.936	4.436
1.245	0.896	4.323
1.382	0.851	3.989
1.509	0.814	3.906
1.763	0.753	3.612
2.454	0.638	3.125

[a] Relative viscosity calculated from refractive index reading and corrected for temperature using a linear interpolation of data from CRC Handbook of Chem. and Physics, 65th ed. and CRC Handbook of Biochem, 2nd ed.

[b] Fit Parameter $A = \frac{2k_BT}{\pi b\sqrt{\eta C}}$ with symbols as defined in the text.

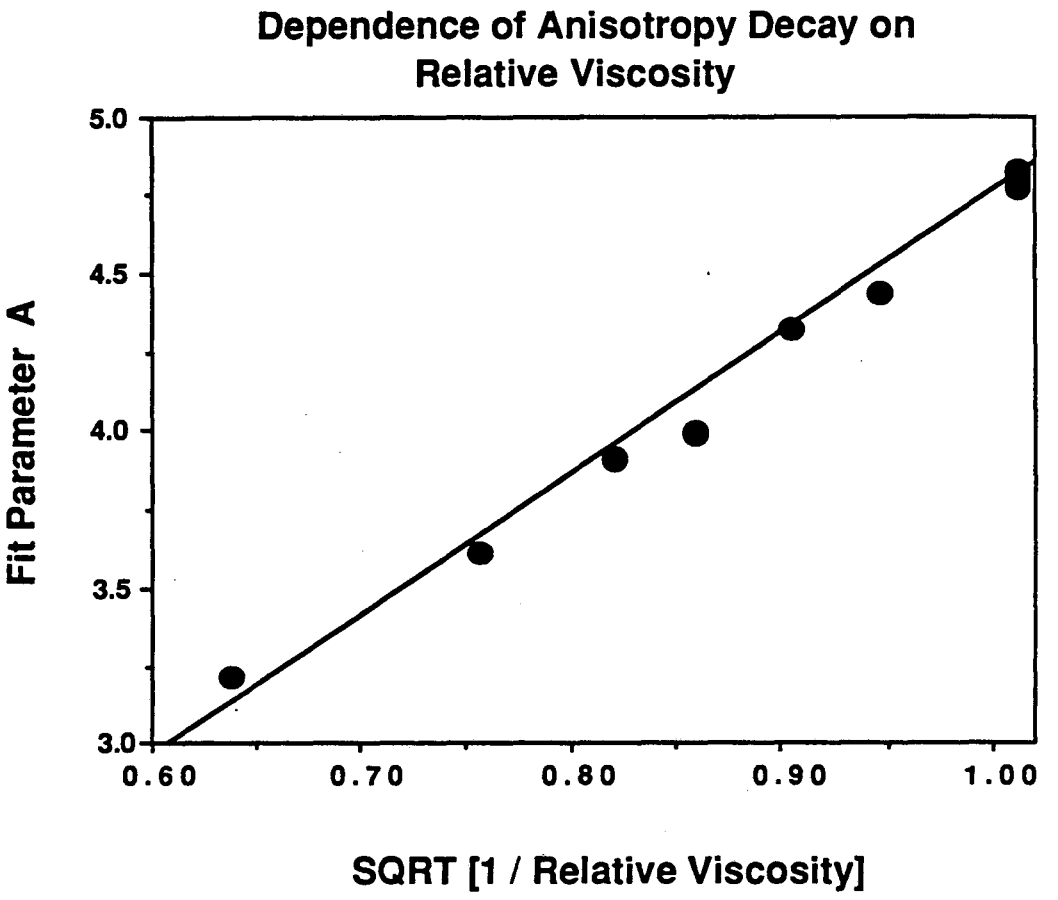

FIGURE 4-3: Plot of the data from Table 4-1 The data are in excellent agreement with the theory and demonstrates a sensitivity of the FPA measurements to changes in η_{rel} and therfore the torsional constant, C, of 10% or less.

Figure 4-4 show representative curves for λ DNA in 0% and 24% Sucrose and their Barkely-Zimm best fit curves. Figure 4-5 show the best fits on one graph for easy comparison.

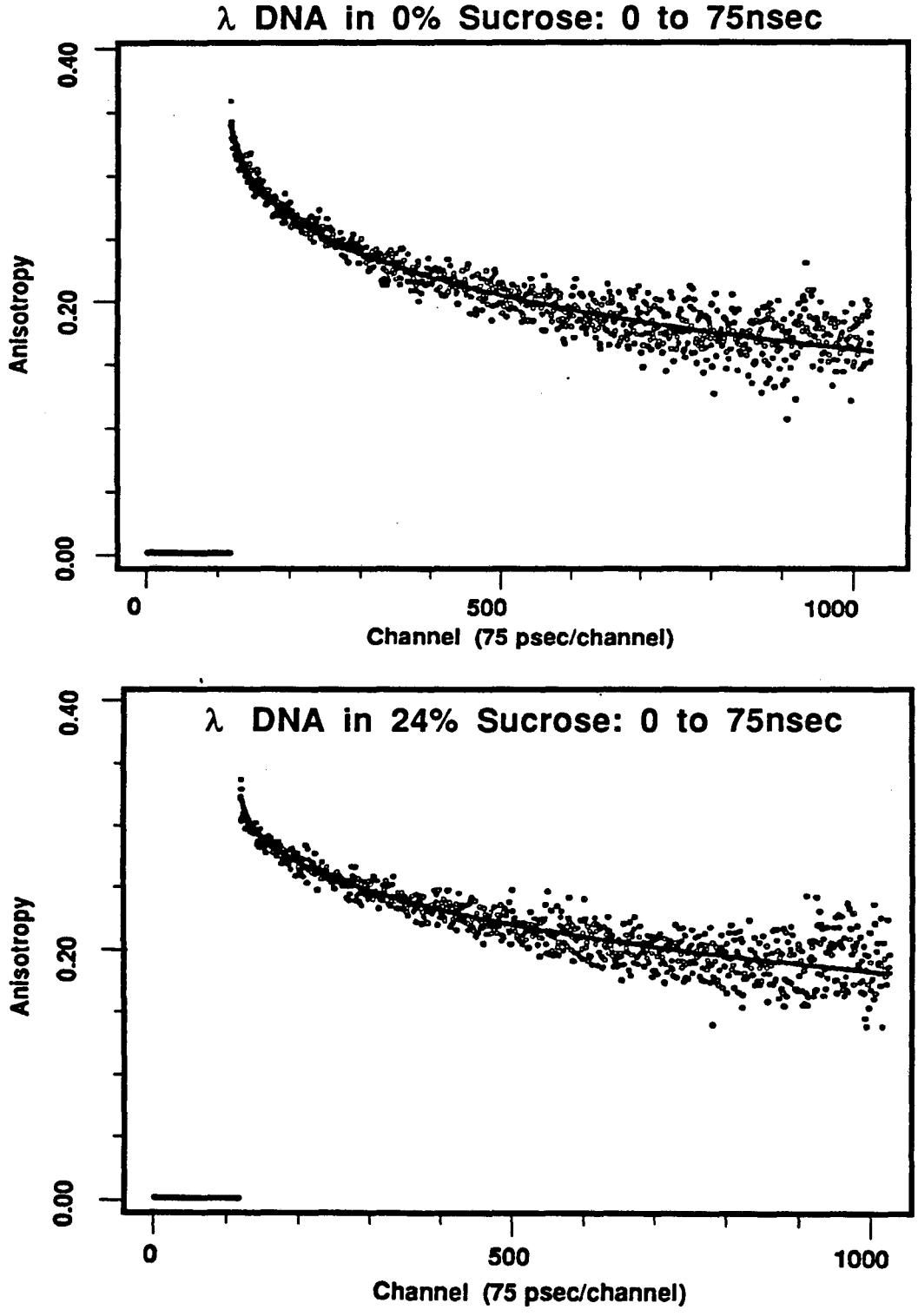

FIGURE 4-4: Anisotropy Curves for Lambda DNA in 0% and 24% Sucrose.

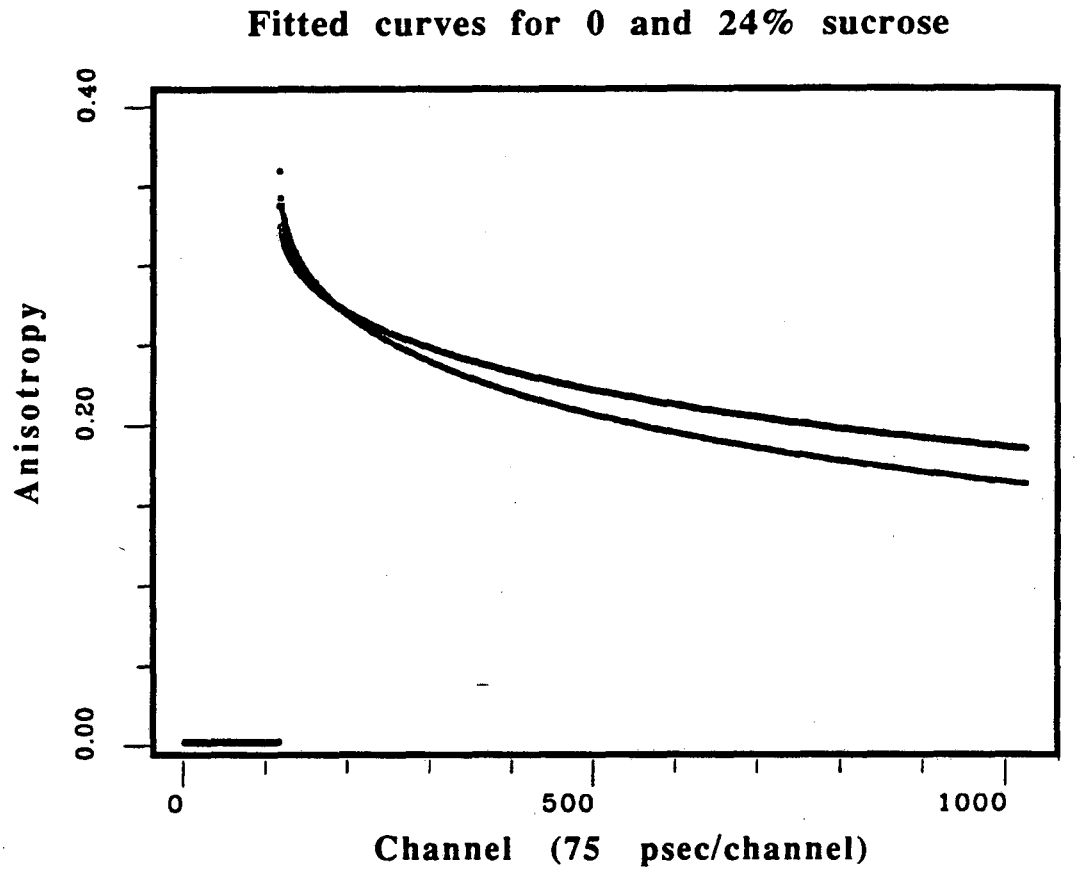

FIGURE 4-5: Best fit Anisotropy fits of data in Fig. 4-4, based on Barkely-Zimm model.

From figures 4-4 and 4-5 it is clear that the decay curves for 0% and 24% can indeed be separated, although the differences are not large. The viscosity data, however, gives us confidence that torsional constants differing by 10% can readily be distinguished. The initial anisotropy for both curves is less than 0.4, the maximum theoretically possible. This is due either to some fast (<75psec) wobble of the dye or because the absorption and emission dipole moments of ethidium bromide are not quite parallel. We found that the initial anisotropy did not seem to have any systematic dependence on the viscosity. This would tend to indicate that there is some dye wobble which is independent of viscosity, most likely because the intercalated dye is shielded from the solvent. Tentative evidence that the aborption and emission dipoles are parallel come from the work of Magde et al.,

who found an initial anisotropy of 0.4 for DNA-intercalated ethidium bromide using a streak camera detector, which has <100psec time resolution (Magde, 1983). Their results, however, are suspect because they used hi-pass (colored glass) filters in their detection circuitry which does not eliminate Raman scattering. Even a small amount of such scattering, which is highly polarized, will give anomalously large anisotropy measurements. Furthermore, they did not deconvolute their data and the 0.4 initial anisotropy they claim to get is clearly during the pulse width. The cause of the less than 0.4 initial anisotropy is therefore still an open question.

Salt Dependence of Torsional Constant

Presumably a good deal of the torsional rigidity of DNA is due to the repulsion of the negatively charged phosphate molecules from one another in the DNA backbone. If the helix is forced to increase or decrease the average angle between phosphates, presumably the distance between these negative charges decreases and the energy of the molecule increases. To determine whether ionic interactions play a role in torsional rigidity, the anisotropy decay was measured for linearized pBR322 as a function of ionic strength at three values ranging from 5 mM to 325 mM (Table 4-2). As the salt concentration increases, one would expect the charges to be screened more (equivalent to saying the dielectric constant of the solution increases) and the torsional rigidity to decrease. This is indeed what we have found (Table 4.2). This observation is similar to experiments which demonstrate that DNA bends more easily with increasing salt concentration.

Torsion Constant of Linear pBR322 as a Function of Ionic Strength

μ (mM)[a]	C x 10^{19} (erg·cm)[b]	N[c]
5	2.14 ± 0.04	3
175	1.91 ± 0.06	6
325	1.60	1

[a] Ionic strength.
[b] Torsion constant.
[c] Number of measurements.

TABLE 4-2: The torsional rigidity of DNA decreases as charge-charge repulsion within the phosphate backbone is screened by dissolved salt. The TCPC spectroscopy is as described in Chapter 2 and the Supercoiled DNA section of this chapter.

Sequence Dependence of Torsional Constant and Effect of Polyamines

Abstract

We performed fluorescence anistropy depolarization measurements on alternating AT and GC homopolymers of DNA in order to examine the dependence of DNA torsional rigidity on sequence. We then added spermine, a polyamine, to a concentration of 1spermine:5bp, to see whether spermine stiffens the DNA and if so, whether the effect is sequence dependent. Unfortunately, our results must be considered preliminary because time limitations on the TCPC instrument prevented the measurements from being repeated. They are however, suggestive of trends: that G-C sequences are torsionally

more rigid than A-T sequences and that spermine makes both A-T and G-C sequences more flexible, and in the same proportion. Based on spermine stiffening as a function of salt concentration and using a simple model, we conclude that spermine stiffens DNA through simple electrostatic charge neutralization.

Introduction

Millar et al. (1982) and Ashikawa et al. (1984) have found that dG-dC homopolymers are considerably stiffer than the A-T homopolymers, although Fujimoto and Schurr (1990) claim that the results are invalid because these groups used commercially available, unfractionated synthetic DNAs which likely contained short fragments that would invalidate the data analysis used based on the Barkley-Zimm theory. Fujimoto and Schurr measured a series of DNAs varying in G-C content from 34% to 100% and found only small differences in the torsional constant (Fujimoto et al., 1990). Their attempt to measure 100% AT sequence failed because of the presence of additional species besides intercalated and free dye, implying multiple modes of binding, which mades data analysis impossible unless the orientations of the dipoles of each mode are known. In addition, they point out the possibility of altered structures, such as cruciforms or branched structures with 100% AT sequences.

A further complication is that Hogan and Austin have found that the DNA bending constant is a function of sequence (see Hogan et.al, 1982, and subsequent papers). We either have the choice of using the measured bending constants in the the Barkey-Zimm theory or alternatively, of assuming the bending constant is infinite. This latter choice gives a lower bound of the torsional constant, and as pointed out by Fujimoto and Schurr (1990), faithfully monitors any change in the torsional constant. We choice the latter, although at some future point, if the experiments can be repeated, we plan on analyzing the data both ways.

Materials and Methods

We used homopolymers of approximately 150bp in length (about a persistence length) at a concentration of 100μM in bp, 1μM EtBr, dissolved in 1mM Cacodylate buffer with either 5mM NaCl or 50mM NaCl. We then added a 5mM stock solution of spermine to the DNA samples to the maximum possible concentration without aggregation or precipitation. At 5mM NaCl, this was 1spermine to 5bp; at 50mM NaCl, this was 1spermine:2.5bp. The maximum concentration was chosen simply to see if there is any effect of spermine.

Results

		Torsional Constant in erg-cm x 10^{-19}	
		5mM NaCl	**50mM NaCl**
No spermine	**dA-dT**	0.91 (0.348)	0.80 (0.352)
	dG-dC	1.49 (0.334)	1.38 (0.347)
With spermine	**dA-dT**	0.768 (0.356)	0.75 (0.352)
	dG-dC	1.327 (0.346)	1.35 (0.343)

TABLE 4-3: Torsional constant in erg-cm x 10^{-19} and initial anisotropy (in parenthesis) for alternating homopolymers of dA-dT and dG-dC, at 5mM and 50mM NaCl concentration, with and without spermine. At low salt, spermine was added to 1spermine:5bp; at high salt to 1:2.5.

Data taken at the magic angle did not indicate the presence of any additional species besides free and bound dye , and the bound dye accounted for >99% of the fluorescent photons, as determined by a two exponential, deconvoluted fit to the anisotropy data.

Discussion

The percent change in torsional constant upon the addition of spermine can be calculated from Table 4-3 and is presented in Table 4-4

Percent Change in Torsional Constant:
No Spermine ⇒ Spermine

	5mM NaCl	50mM NaCl
poly dG-dC	-11.6%	-1.7%
poly dA-dT	-16.7%	-7.0%

TABLE 4-4: Percent change in DNA torsional constant upon addition of either 1 spermine per 5 base pairs (at low salt) or 1 spermine per 2.5 base pairs (at high salt).

The percent change going from low salt to high salt, in the presence or absence of spermine can also be calculated, as shown in Table 4-5

Percent Change in Torsional Constant: Low Salt ⇒ High Salt

	w/o Spermine	with Spermine
poly dG-dC	-8.0%	-1.9%
poly dA-dT	-12.1%	-2.4%

TABLE 4-5: is the percent change in DNA torsional constant upon going from 5mM NaCl to 50mM NaCl, with or without Spermine.

The data can be interpreted with a simple model: the torsional constant of DNA is a function of intrinsic bond angles which resist change, assumed to be independent of ionic strength, and an electrostatic component which is affected by the ionic strength. A major part of the electrostatic component is expected to be the charge-charge repulsion of the phosphate backbone. Shielding these charges makes the DNA more flexible (see previous section on the effect of salt on linear pBR322 DNA). We denote the ionic-independent, bond contribution to the torsional constant by C_o, and the electrostatic, ionic dependent part by C_{el}.

Without doing any calculations, the fact that spermine causes a decrease in the torsional constant of both poly dA-dT and poly dG-dC immediately implies that the primary influence of spermine, which is a trivalent cation, is to neutralize the negative charge of the phosphate backbone. Spermine, which is an extended molecule, might also be expected to stiffen the DNA by binding like a third strand. Evidently, this effect, if present, is outweighed by the charge neutralization. The fact that spermine has a lesser effect — if any at all — at high salt concentration is no surprise: the binding constant of spermine at 50mM NaCl concentration is greatly reduced compared to that at 5mM.

Does spermine act in a sequence specific fashion, e.g. binding more tightly to poly dA-dT or to poly dG-dC, and therefore have a larger effect on one than the other? The fact that the torsional constant for poly dA-dT decreases by 16.7% whereas poly dG-dC only decreases by 11.6% says that spermine does have a proportionately larger effect on poly dA-dT than on poly dG-dC. One cannot conclude from this, however, that spermine is interacting sequence specifically. In both cases spermine may simply be shielding phosphate charges, which may have a larger effect on the overall torsional constant of poly dA-dT, than poly dG-dC. Indeed, this is entirely reasonable. The electrostatic component of the two homopolymers are likely the same — in both cases C_{el} arises largely from phosphate repulsion. However, C_o is likely larger for poly dG-dC which has

an extra hydrogen bond for base pairing. Consequently, C_{el} may be a larger fraction of the total torsional constant for poly dA-dT than for poly dG-dC. An equal reduction in C_{el}, due to charge screening by spermine (or by salt effects) will have a proportionally bigger effect on the torsional constant of poly dA-dT than on poly dG-dC.

It would be desireable to verify that C_{el} is indeed (approximately) the same for poly dA-dT and poly dG-dC. This can be done by measuring the torsional constant for each homopolymer at high and at low salt concentrations. At high salt concentration, all charge is screened, the effect of C_{el} is therefore zero, and the measured torsional constant simply equals C_o. At low salt, the measured torsional constant is the sum of C_o and C_{el}. The difference in measured torsional constants at high and low salt is therefore just C_{el}. This can be done for each homopolymer.

Unfortunately, the high (50mM) and low salt (5mM) data are neither sufficiently high to eliminate the effect of C_{el} and therefore isolate C_o, nor sufficiently low to ensure that C_{el} is not partially screened. Nevertheless, an approximate value for C_{el} can be calculated by comparing the torsional constants at 5 and 50mM salt (no spermine). This will tend to underestimate the magnitude of C_{el}, although the relative comparison of C_{el} for poly dA-dT and poly dG-dC should be not too bad. We find $C_{el:G\text{-}C}$ to be 0.115 and $C_{el:A\text{-}T}$ to be 0.104×10^{-19} erg-cm, a difference of only 10%. By comparison, the difference between C_{total} is 48% (The difference, 1.49 - 0.91, divided by the average, 1.2). Given the limitations of the experiment and the simplistic nature of the model, the assumption that C_{el} is the same is reasonable.

At a spermine concentration of 1 spermine to 2.5 base pairs, over half of the phosphate charges should be neutralized. (Recall that spermine is trivalent). This would be expected to greatly reduce C_{el}. (Note that the shielding is probably non-linear, and most likely, shielding half the phosphates will result in a proportionally greater decrease in

repulsion. If half the charges are neutralized, then the average distance between charges is doubled, and assuming a distance dependence of repulsion of greater than 1/r, the repulsion is more than halved.) The data at least semi-quantitatively support this hypothesis. Without spermine, adding salt significantly decreases the torsional constant for both poly dA-dT (-12%) and poly dG-dC (-8%), as would be expected due to charge screening. (Again, poly dA-dT is affected more.) But in the presence of spermine, the change is insignificant (-1.9% for poly dG-dC and -2.4% for poly dA-dT), which would be expected if the charge repulsion has already been neutralized.

If we assume the effect of C_{el} goes to zero upon addition of spermine at low salt, and using the admittedly small values of Cel calculated above, then the fractional decrease in torsional constant $C_{el}/C_{total} = C_{el}/(C_o + C_{el})$ for poly dA-dT is 11.4% and 7.7% for poly dG-dC. These figures are considerably lower than the measured decrease in C_{total} of 16.7% for dA-dT and 11.6% for dG-dC. This is no surprise, however, since we knew we were underestimating C_{el} for both homopolymers. The salient feature is that *the effect of spermine, assuming its only effect is to screen charge, is indeed larger for poly dA-dT than for poly dG-dC*. The relative magnitude of the effect, as predicted by this simple model, is even correct. The model predicts that the torsional constant of poly dA-dT will decrease by 1.48 times more than poly dG-dC (11.4% divided by 7.7%). Experimentally, the decrease is 1.44 times (16.7% divided by 11.6%).

Consequently, we conclude that the effect of spermine is primarily to screen the phosphate charges of both poly dA-dT and poly dG-dC, and that sequence specific interactions need not be invoked to explain the data. As stated previously, for these conclusions to be made firm, the data presented here need to be repeated and, in addition, measurements of the torsional constants of both homopolymers at higher and lower salt concentrations need to be made.

Supercoiled DNA

Supercoiling is the coiling of the DNA helix, in particular, over- or underwinding the helix. In the relaxed state, the B-form DNA helix has 10.45bp/turn. So for a DNA molecule of length 1045bp, for example, one strand of the DNA backbone wraps around the other 100 times, and its linking number is then defined to be 100. Overwinding the DNA helix is called positively supercoiling and underwinding is called negatively supercoiled.

Although the purpose of supercoiling is not well understood, phenomenologically, we know that is is important. Bacterial DNA is on average negatively supercoiled, typically at a superhelical density of -0.06 (meaning 6 turns are taken out for every 100turns of the relaxed DNA molecule) and evolution has generated enzymes known as topoisomerases to control the level of supercoiling. Without these enzymes, organisms die or are severely weakened. Bacterial mutants deleted for topoisomerase I, for example, are weakened, and acquire compensatory mutations to survive (DiNardo, 1982). Furthermore, supercoiling likely affects gene regulation. Many chemotherapeutic agents for the treatment of cancer, for example, where gene regulation has obviously broken down, target topoisomerases (Liu,1987). Supercoiling, at least, *in vitro,* occurs during transcription, a process which may inhibit further transcription and suppress neighboring genes because of the energy required to add supercoils (Liu, 1987; Wu, 1988).

Supercoiling also plays a role in organizing the genome. DNA is supercoiled when wrapped into nucleosomes in eucharyotes and in similar structures in procharyotes and chromosomes have been found to have domains of supercoiling (Sinden, 1981). John Hearst (private communication) has suggested that supercoiling may be important for minimizing the occurance of knots which can prevent DNA strands from separating, a necessary step in mitosis. (Knots are not fatal because organisms have developed

enzymes which can eliminate them (Liu (1980) but it still seems reasonable that minimizing the number of knots is advantageous.)

A physicist's model for supercoiling is a simple rope, with its ends tied together, forming a closed loop. The relaxed form is a floppy, roughly circular structure. Now cut the rope, twist one end and glue the ends back together. The rope is now supercoiled. By definition, the relaxed rope had a linking number of zero; now it has a linking number equal to the number of turns put in, not necessary integral. The linking number is a topological property — no matter what shape the rope takes or how the rope is bent or twisted, so long as it is not cut, its linking number is fixed. Note that the conformation of the supercoiled rope will in general be different than the relaxed rope, most likely forming some sort of figure 8 shape. If the linking number of the rope is further increased, it will further wrap on itself. This wrapping is, roughly speaking, called writhe and is approximately equal to the number of times the rope crosses itself.

Topologists have studied the linking number, twist and writhe of space curves. A particularly simple and elegant result is found:

$$Lk = Tw + Wr$$

That is, Linking Number equals Twist plus Writhe. It is actually easiest to understand twist in terms of a discrete model, instead of a continuous space curve. Since DNA is best modelled as a discrete chain of base pairs, this suffices.

Tw may be defined as the sum of the twist angles around the entire DNA chain

$$Tw \equiv \frac{1}{2\pi} \sum_{i=1}^{N} \phi_i$$

where ϕ_i is the azimuthal twist angle in radians between base pairs i and $i + 1$ (α is sometimes used interchangeably with ϕ), and N is the number of base pairs. The average twist angle is simply given by $\langle\phi\rangle = 2\pi$ Tw/N. For relaxed DNA it is 34.5°.

The writhe is a less intuitively obvious quantity. It is the number of time the space curve (or DNA) crosses itself, integrated over all projections.

We can define the writhe of a continuous curve as:

$$Wr = \frac{1}{4\pi}\int_{r_1}\cdot\int_{r_2}\frac{(d\vec{r}_1\times d\vec{r}_2)\hat{r}_{12}}{|\vec{r}_{12}|^2}$$

where $\vec{r}_1$ and $\vec{r}_2$ are tangents along the curve at arbitrary points one and two, and $\vec{r}_{12}$ is the vector connecting them (Vologodskii, 1979). Notice that if the two tangents lie in the same plane, i.e., are parallel to one another, the contribution to the writhe is zero. For a molecule like DNA, made up of discrete base pairs (or disks, in our model), the integral becomes a sum, the tangent vectors are replaced by bond vectors, $\vec{b}_i$ connecting the center of disk i and (i+1) and $\vec{r}_{12}$ becomes $\vec{r}_{ij}$ the vector connecting bonds i and j, and $\hat{t}_i$ is the unit vector, $\hat{t}_i \equiv \vec{b}_i / |\vec{b}_i|$ (Wu, 1988; Levene, 1986; Vologodskii, 1979). The writhe density (equivalent to the integrand in the above surface integral) is then:

$$w_i = \frac{|\vec{b}_i|^2}{4\pi}\sum_{j\neq i}\frac{(\hat{t}_i\times\hat{r}_{ij})\ \hat{t}_i}{|\vec{r}_j - \vec{r}_i|^2}$$

and the writhe is:

$$Wr = \sum_{i=1}^{N} w_i$$

At finite temperature, there will be fluctuations in writhe, just as there are in twist. However, the sum of twist and writhe — the linking number — is a fixed topological constant which does not fluctuate .

The linking number distributes itself between twisting and writhing. How much the DNA twists vs bends will be a function of the respective torsional and bending constants, subject to excluded-volume constraints. (In the limit of large writhe, excluded volume becomes important. The DNA cannot further wrap on itself because the strands start hitting each other — image a tightly coiled rope.) In the limit of infinite bending constant and finite twisting constant, all of the supercoiling will go into twist and the conformation of the relaxed and supercoiled rope will be the same. In the limit of infinite torsional constant but finite bending constant, the molecule will become highly kinked (large writhe) in order to avoid twisting. The ratio of the bending and twisting force constants determine the rope's global, three-dimensional conformation as well as its local twist.

Because the DNA is a right-handed helix, not simply a rope, the direction of twist initially put in is relevant, corresponding to under- or over-winding. Negative supercoiling involves taking turns out of the DNA duplex (underwinding) and positive supercoiling involves putting turns into the helix (overwinding). Also, unlike the simple rope model, the linking number of a relaxed molecule is not zero, but equal to the number of crossing of the phosphate backbone around each other. This is denoted by Lk_o. For our 1045bp piece of relaxed DNA, the linking number is 100. Lk_o will be an integer only if the length of DNA is a multiple of 10.45bp (although the least strained closed molecule will be a length of DNA that is a multiple of 10.45bp). Unlike the rope however, the

additional linking number due to supercoiling must be integral. This is because of the structure of DNA, where the 3' and 5' ends of the backbone must be bound (Fig **).

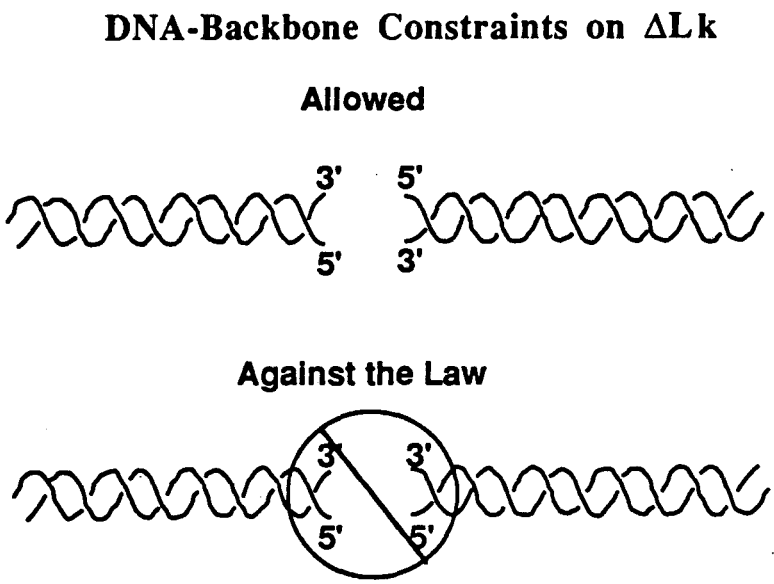

FIGURE 4-6: The structure of the DNA helix backbone requires that the 3' end bind to the 5' end, which forces any change in linking number to be integral. The bottom diagram would result in a half-integral linking number, and any other configuration would not have the ends of the helix backbone touching.

Also unlike the rope, the DNA is made of discrete units — base pairs — that make the relationship between the bending and force constants of DNA unclear — perhaps even unrelated if they are determined by different chemical bonds. Whereas, in a rope made of a continous deformable material, the relationship between bending and twisting constants is fixed by the Poisson's ratio for a given material. ($C = EI(1+\sigma)$, where C and EI are the torsional and bending rigidities and σ is Poisson's ratio.)

These difference have led Schurr and others to model DNA in a slightly more complicated fashion than a simple rope — as a series of "tuna fish" cans, which represent

the base pairs, coupled together via two Hookian springs, one sensitive to only twisting motion and the other only to bending motions.

Tuna-Fish Can Model of DNA

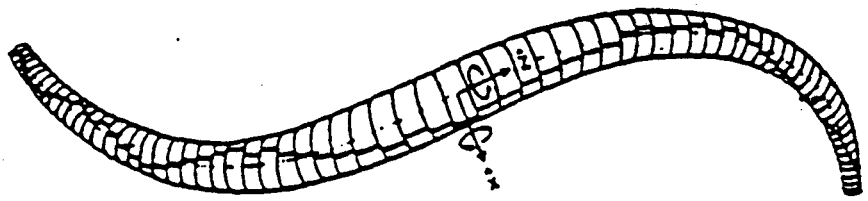

FIGURE 4-7: The DNA is modelled as a series of disks connected by hookian springs, both torsional and bending.

What we are interested in measuring is whether the DNA bending and twisting potentials are truly harmonic, i.e., how good of an approximation it is to model the DNA as a series of Hookian springs. This measurement goes beyond Schurr's particular model however. Essentially all models of DNA treat DNA as ideal springs and the potential energy curves for DNA are fundamental parameters. Spectroscopically, we can determine these force constants (or potentials) by looking at the dynamics of an intercalated fluorophore, which, as we have seen from the Barkley-Zimm theory, is sensitive to the twisting, and to a lesser extent, to the bending constants. If the DNA is harmonic, these constants should be independent of displacement, either bending or twisting. If however, there is an anharmonic term, then the force constants and dynamics will change.

We have therefore prepared a series of topoisomers of DNA with different linking numbers. The average displacement in both twist and bending will be different for these molecules. TCPC is used to measure the torsional constant as a function of superhelicity; TA, which is capable of looking at long times, after all twisting is completed, is used to

measure the bending constants. We have looked at a very large range of superhelical density, from -0.123 to +0.04, and in particular, have made the first measurement of the torsional constant of positively supercoiled DNA. We have also made preliminary TA measurements on the bending constant as a function of superhelicity. The TCPC results will be presented first.

DNA Preparation:

DNA samples were prepared by David Cook, a graduate student in John Hearst's lab and Dr. Ning Pon, emeritus professor. Topoisomers of negatively supercoiled plasmid pBR322 were prepared according to the method of Keller (Singleton, 1982; Keller, 1975). 60μg of supercoiled plasmid (approximately 10-20% nicked starting material) was combined with 2.85, 8.71, 11.7 or 14.8 mM ethidium bromide (EtBr; Sigma; recrystalized in EtOH) in 1.5 ml of buffer containing 50mM Tris·Cl, pH 7.6, 50mM KCl, 10mM $MgCl_2$, 0.5 mM DTT, 0.1 mM EDTA, and 30mg/ml acetylated BSA. Topoisomerase I eliminates (negative) supercoils of the ethidium-stained DNA by nicking and resealing. EtBr, however, overwinds the DNA, so upon removal of the EtBr after TopoI treatment, the molecules are underwound, or negatively supercoiled, the extent determined by the amount of bound dye during TopoI treatment. A relaxed sample (no EtBr) was prepared in a similar buffer without $MgCl_2$ but containing 150 mM KCl. This buffer is identical to that used for fluorescence anisotropy measurements. This sample served as a reference, defining Lk_o under ionic conditions very similar to that *in vivo*. Excess calf thymus topoisomerase I (Bethesda Research Labs), 4 U/μg, was added to each reaction and incubated at 37°C for 4 hr. Samples were loaded into EtBr-CsCl density gradients (Sambrook, 1989) and spun to equilibrium in a VTi65 rotor (55,000 rpm for 18 hr at 18°C). The lower, supercoiled plasmid band was removed from the gradients with 18 ga needles, extracted repeatedly with 20xSSC-saturated isopropanol to remove traces of EtBr, and EtOH precipitated two times. After measuring the concentration of DNA by

absorption (A_{260}/A_{280} = 1.8 to 1.9), the samples were again precipitated with alcohol and resuspended to a final concentration of 400 μg/ml in TE buffer (10 mM Tris·Cl, pH 8.0, 1 mM EDTA). The final product was >95% intact form I plasmid.

Positively supercoiled pBR322 was prepared in vivo by treating strain AS19 (pBR322) with novobiocin, according to the protocol of Lockshon and Morris (Lockshon, 1983). AS19 is an E. coli B derivative which is particularly permeable to a wide range of small hydrophobic molecules (Sinden, 1980) including novobiocin. Novobiocin blocks the catalytic action of the enzyme DNA gyrase by binding efficiently to the ATPase site on the enzyme (Sugino, 1978). Cells were grown in a rich medium (LC (Sambrook, 1989) containing 50 mg/ml ampicillin to mid-log phase (OD600 = 0.4 to 0.5 as measured on a Bausch and Lomb Spectronic 21). Novobiocin (8 mg/ml in ddH20) was added to a final concentration of 80 mg/ml, and the cultures were incubated at 37°C on a gyratory shaker for another 30 min. Plasmid DNA was isolated according to the standard alkaline-SDS lysis protocol (Sambrook, 1989) and banded twice on EtBr-CsCl equilibrium density gradients. The final work-up procedures were carried out as for the negative topoisomers above.

Characterization of topoisomer distributions. The center of the linking number distribution for each sample was determined by the band counting method (Keller, 1975). DNA was run in 1.8% agarose gels in 0.5x TPE buffer (Sambrook, 1989) at 2 V/cm for 16 to 20 h. Chloroquine (Sigma) was added to the same final concentration in both the gel and the buffer to aid in the resolution of topoisomers, and buffer was recirculated during the run. The center of each linking number distribution was determined relative to the center of the relaxed distribution.

Samples for spectroscopy: Lambda DNA was prepared at a concentration of 300 μM in base pairs (200 μg/ml) in 0.5x Spectroscopy Buffer (1x SB = 150 mM KCl, 50

mM Tris, pH 8.0, 1 mM EDTA) with varying dilutions of a 60% sucrose stock (Sigma, grade1). Sucrose concentrations were measured both before and after FPA using a Bausch and Lomb refractometer. The relative viscosity, η_{rel}, was determined at the the experimental temperature, 23.5°, by a linear interpolation of the published values at 20° and 25°C. This approximation should not affect our interpretation of the data since, unlike the absolute viscosity, η_{rel} varies only weakly with temperature. Topoisomer samples were diluted to 300 μM in base pairs in 1x SB. Recrystalized EtBr, dissolved in 1xSB, was added to all samples to a final concentration of 2 μM.

Instrumentation and Data Analysis

The TCPC and TA spectroscopy were done as described in Chapters 3 and 4 and at the beginning of this chapter under the "Naked DNA" section.

Results

Initial characterization of samples (adopted from Dave Cook's thesis): Gel analysis of the topoisomer samples demonstrated that >95 % of the DNA was supercoiled, even after multiple precipitations and exposure to light during the TCPC experiment. Control gels indicate that irradiation with 10- to 100-fold more light than in a typical fluorescence experiment resulted in essentially no nicking of the DNA. Small amounts of observed nicking was probably due to handling of samples before and after irradiation.

The linking difference, ΔLk, of the various samples was determined by running the DNA in gels containing from 0 to 17.5 μg/ml chloroquine. Chloroquine intercalates between base pairs, unwinding the DNA. For negatively supercoiled DNA, at low levels of chloroquine binding, this unwinding increases the hydrodynamic radius of the molecule. Agarose gels are sensitive to this increase in size, and so covalently-closed, negatively supercoiled plasmids decrease in mobility upon addition of chloroquine at low

concentrations. At some point, depending on the initial underwinding of the DNA, the intercalator begins to overwind the DNA, and the plasmid runs faster in the gel. The population of molecules is positively supercoiled compared to a plasmid sample relaxed to equilibrium in the presence of the same concentration of chloroquine. Thus, titration of supercoiled DNA with an intercalator initially decreases the DNA mobility to a minimum and then increases mobility upon positive supercoiling.

Since the energy difference between negatively supercoiled topoisomers is small compared to kT, the equilibrium state contains a Boltzmann distribution of several linking numbers, reflected as several bands in an agarose gel (Depew and Wang, 1975; Pulleyblank et al., 1975). Positively supercoiled DNA, because of its method of preparation inside *E. coli.*, does not follow a Boltzmann distribution. It's distribution is governed by kinetics associated with inactivation of DNA gyrase with novobiocin. Although the distribution of positive topoisomers is broad, it does not overlap with any other sample on the gel.

Determining the superhelicity of negatively supercoiled samples is performed by measuring their linking deficit, ΔLk, compared to the relaxed sample. The linking deficit can be measured by simply counting bands in the ladders formed by the topoisomers starting from the center of the relaxed sample. Adjacent bands differ in Lk by -1 going from slower to faster mobility for the negatively supercoiled state. The number of bands between the primary relaxed topoisomer and a particular topoisomer of interest is equal to ΔLk. The number of steps to the strongest band in a lane is the average ΔLk of that sample. The specific linking difference, σ, is the linking deficit ΔLk normalized by the linking number Lk_o of the relaxed molecule: $\sigma = \Delta Lk/Lk_o$. Lk_o is estimated under standard physiological conditions to be N/10.5, where N is the total number of base pairs. All measurements of σ therefore relate to the set of conditions which define Lk_o.

A measurement of σ for the positively supercoiled sample gives only a lower bound estimate of the superhelicity. As the plasmid becomes overwound, it decreases in hydrodynamic radius. The positively supercoiled DNA migrates faster than relaxed or negatively supercoiled DNA under all conditions. The gel cannot resolve the individual topoisomers within this population. For the positively supercoiled sample, Lk increases by 1 for each band of increasing mobility in the gel. A lower bound of $\sigma \geq 0.042$ can be estimated by counting bands up to the point where the gel fails to resolve any further. At this point, $\Delta Lk = +17$, and the bulk of the topoisomer distribution is unresolved. The value of σ for this sample is significantly greater than that reported by Wu et al. (1988), who estimate $\sigma \geq 0.03$ for their samples prepared by a similar method.

TABLE 4.6: Fluorescence Lifetimes of Topoisomer Samples from data taken with analyzer set at 54.7°

Sample[a]	μ[b]	τ_b[c]	τ_f[d]	A[e]	χ^2_{red}[f]	Φb[g]
linear	175	23.4	1.9	0.94	1.27	0.995
+0.042	175	23.6	1.9	0.93	1.21	0.994
0.00	175	23.3	1.5	0.89	1.22	0.992
-0.025	175	23.4	1.1	0.90	1.27	0.994
-0.069	175	23.8	3.0	0.95	1.23	0.993
-0.096	175	23.5	1.1	0.91	1.29	0.996
-0.123	175	23.6	2.4	0.96	1.28	0.995
linear	5	23.5	2.3	0.96	1.18	0.996
+0.042	5	23.5	1.7	0.95	1.29	0.997
0.00	5	23.3	1.4	0.92	1.26	0.995
-0.025	5	23.5	1.1	0.91	1.34	0.996
-0.069	5	23.6	1.6	0.95	1.26	0.996
-0.123	5	23.6	2.1	0.94	1.29	0.994

[a] Superhelix density of sample.

[b] Ionic strength in mM.

[c] Fluorescence lifetime of intercalated ethidium in nsec.

[d] Fluorescence lifetime of free dye in nsec.

[e] Initial amplitude of bound fluorescence species at t = 0.

[f] Reduced chi-squared of two parameter fit to magic angle data.

[g] Fraction of fluorescence from bound species.

It is important that the vast majority of fluorescent photons collected be from DNA-intercalated EtBr. Free dye, or other bound species will seriously confuse the interpretation of results. That the magic angle data fits to two exponential so well indicates that only two species are present. Their lifetimes are in excellent agreement with the known lifetimes for intercalated and free Etbr. Table 4-6 shows that greater than 99% of the fluorescence arises from Etbr intercalated in DNA. At the concentration of dye and DNA used in these experiments (2 μM in dye and 300 μM in base pairs), about 5% of the ethidium is expected to be free in solution for linear DNA. The binding constant for linear or nicked circular DNA is $K_b = 6.4 \times 10^4\ M^{-1}$, and somewhat higher for negatively supercoiled DNA since intercalation relaxes some of the torsional strain of the underwound helix (Bauer and Vinograd, 1970). Since free ethidium has a 20-fold lower quantum yield for fluorescence than does bound ethidium (LePecq and Paoletti, 1967), and since at 552 nm, the absorbance cross section of free ethidium is reduced 3-fold compared to bound dye (Bresloff and Crothers, 1975), the total fluorescence yield from free dye is much lower than that from the bound species.

Although it has not yet been measured, the binding constant of EtBr to positively supercoiled DNA, is expected to be less than for linear or negatively supercoiled DNA. At the DNA concentration in these experiments, however, there is no detectable increase in free dye for the positively supercoiled samples, at either high or low salt conditions. This is an important conclusion for later interpretations of the anisotropy data, since the positively supercoiled DNA, most notably at low ionic strength, seems to have different dynamic behavior from relaxed or negatively supercoiled DNA. Figure 4-8 shows the excellent two exponential fit to the positively supercoiled DNA data, with the data shown above, in Tables 4-6 and 4-7.

A: Positively Supercoiled pBR322 in 5mM Tris, 1mM EDTA

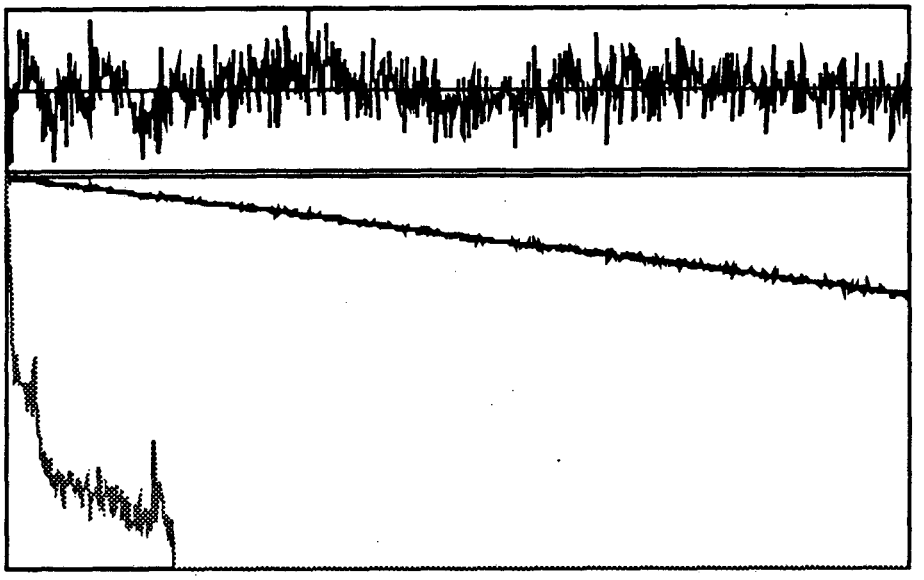

B: Positively Supercoiled pBR322 in 150mM KCl, 50mM Tris

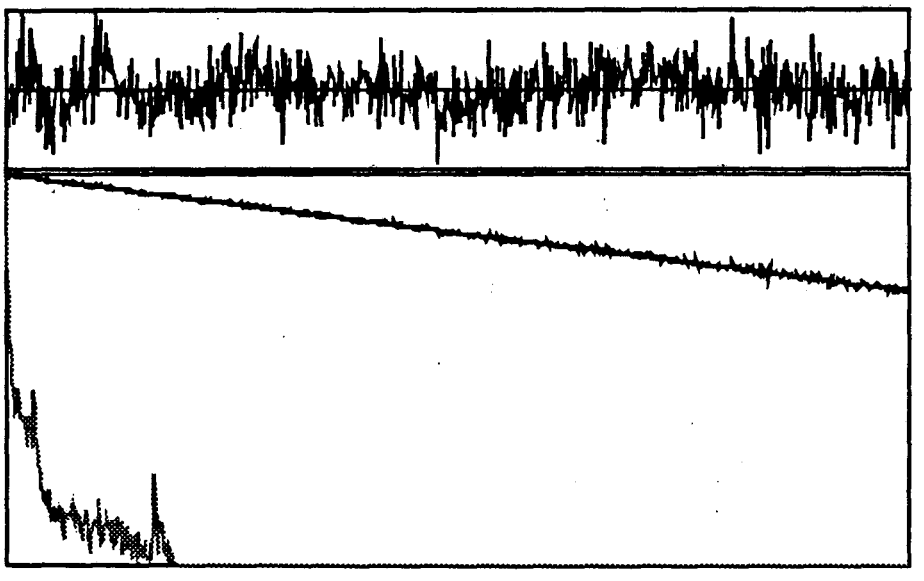

FIGURE 4-8: Magic Angle data for positively supercoiled DNA shows that essentially all of the fluorescence arises from a single species, intercalated Ethidium Bromide, under both high and low salt conditions. The y-axis is the logarithm of fluorescence, the x-axis is time, from 0 to 75psec. The upper panels are the residual to the fit. The middle curves are the fluorescence decay and best fit (they essentially superimpose). The lower curves are the instrument response functions (full-width, half-max of 60psec) taken at 14psec/ch. See table 4-6 for fitting parameters.

Torsional Constant as a Function of Superhelicity

We have now shown that essentially all of the fluorescent photons from the ethidium bromide supercoiled-DNA samples arise from the intercalated dye, and that TCPC is sensitive to changes in torsional constant. With these controls in hand, Figure 4-9 and tables 4-7 and 4-8 show the TCPC results for the torsional constant of DNA as a function of superhelicity. Figure 4-10 shows representative parallel, perpendicular and anisotropy curves.

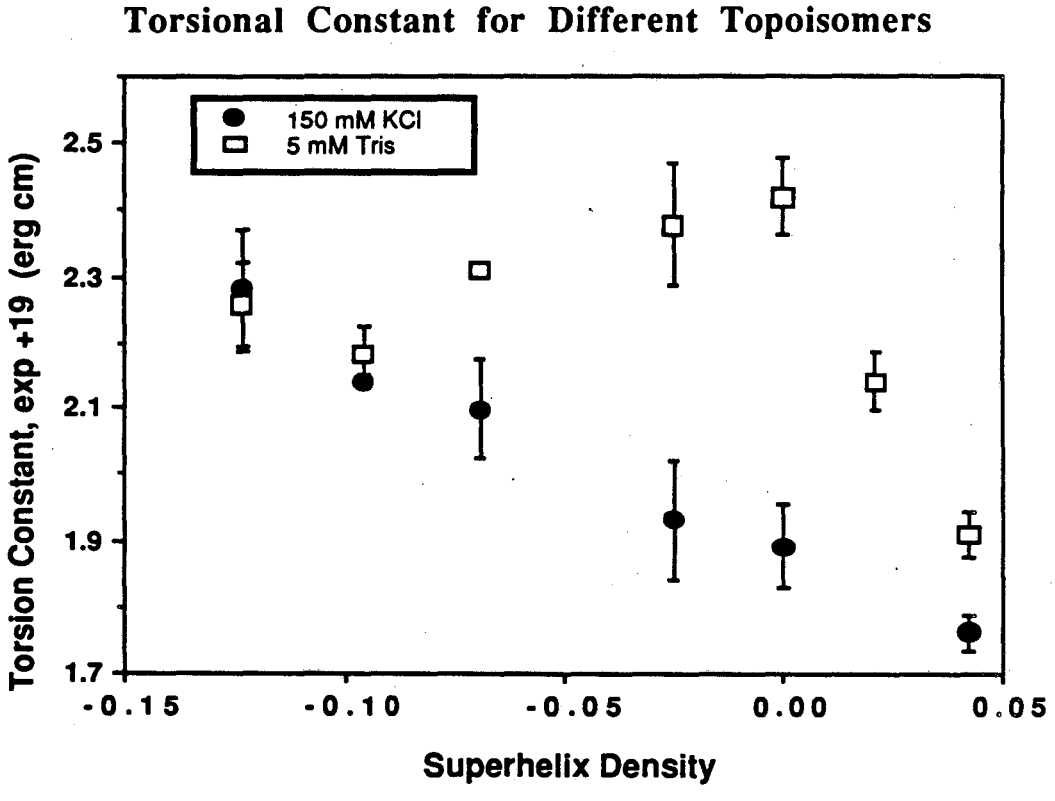

FIGURE 4-9: Torsion constants of topoisomer samples in 150 mM KCl and in 5 mM Tris, pH 8.0. Data is from Tables 4-7 and 4-8. Error bars represent the standard deviation for $N \geq 3$ or the spread between independent measurements for $N = 2$. Although the data at low salt is plotted as a function of the measured σ, the true value for σ under these solvent conditions is somewhat more negative. The difference $\Delta\sigma$ between various samples, however, is unaffected.

Table 4-7: Data Summary for TCPC Measurements in 150 mM KCl, 50 mM Tris·Cl, pH 8.0, 1 mM EDTA.

Sample[a]	r_0[b]	C[c]	χ^2_{red}[d]
+0.042a	0.3579	1.773	1.239
+0.042b	0.3554	1.778	1.225
+0.042c	0.3602	1.728	1.264
lineara	0.3463	1.963	1.226
linearb	0.3397	1.895	1.162
linearc	0.3503	1.952	1.232
lineard	0.3564	1.933	1.175
lineare	0.3514	1.876	1.153
linearf	0.3518	1.816	1.240
relaxa	0.3388	1.806	1.211
-0.025a	0.2476	2.021	1.274
-0.025b	0.3368	1.843	1.211
-0.069a	0.3535	2.175	1.302
-0.069b	0.3453	2.023	1.229
-0.096a	0.3446	2.130	1.233
-0.096b	0.3452	2.150	1.233
-0.123a	0.3381	2.353	1.245
-0.123b	0.3445	2.307	1.224
-0.123c	0.3380	2.175	1.245

[a] Superhelix density of sample.

[b] Initial anisotropy at t = 0.

[c] Torsion constant, x 10^{19} (erg·cm).

[d] Reduced chi-squared of fit to anisotropy decay.

Table 4-8: Data Summary for TCPC Measurements in 5 mM Tris·Cl, pH 8.0, 0.5 mM EDTA.

Sample[a]	r_0[b]	C[c]	χ^2_{red}[d]
+0.042a	0.3580	1.950	1.215
+0.042b	0.3526	1.882	1.151
+0.042c	0.3508	1.902	1.220
linearb	0.3535	2.152	1.186
linearc	0.3518	2.179	1.247
lineard	0.3390	2.092	1.155
relaxa	0.3528	2.479	1.196
relaxb	0.3489	2.362	1.245
-0.025a	0.3464	2.468	1.229
-0.025b	0.3425	2.287	1.034
-0.069a	0.3475	2.304	1.274
-0.069b	0.3478	2.316	1.275
-0.096a	0.3435	2.224	1.236
-0.096b	0.3446	2.142	1.136
-0.123a	0.3483	2.220	1.264
-0.123b	0.3424	2.323	1.180
-0.123c	0.3417	2.301	1.117
-0.123d	0.3371	2.190	1.236

[a] Superhelix density of sample.

[b] Initial anisotropy at t = 0.

[c] Torsion constant, x 10^{19} (erg·cm).

[d] Reduced chi-squared of fit to anisotropy decay.

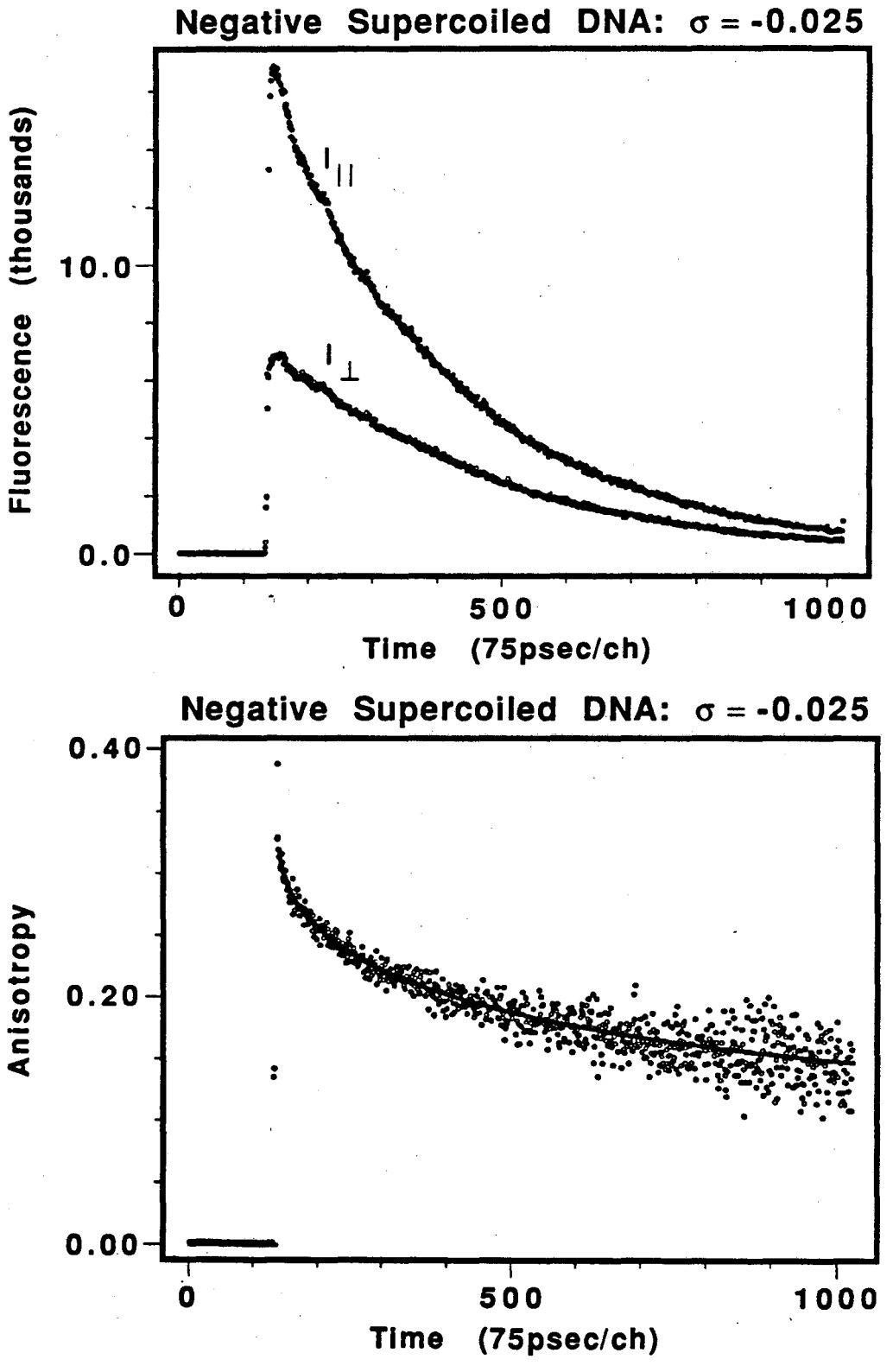

FIGURE 4-10: Representative data for supercoiled DNA. See table 4-7 and 4-8.

Transient Absorption of Supercoiled DNA

We are interested in measuring the bending constant of DNA as a function of superhelicity, in an analogous fashion to that which we did with the torsional constant. Because bending primarily occurs on longer time scale than twisting, we used TA to measure the microsecond dynamics of DNA, which is appropriate for bending times. The question of whether or not the bending constant changes is also critical in the interpretation of the TCPC results, because that data are fit assuming a constant bending term. In the extreme, the change in TCPC anisotropy decay with superhelicity could be fit assuming a variable bending constant and unchanged torsional constant. (This extreme scenario is not likely because the relative change in bending constant would have to be much larger than a similar change in torsional constant to account for the different anisotropy decays, but a change in both the bending and torsional constants is entirely feasible.)

We used pSM1, a large, ≈50,000bp plasmid, at a concentration of 300μg/ml with 1 methylene blue per 150 base pairs. The superhelical density was approximately -0.05. The results, presented below, indicate that the bending constant does not change with superhelicity.

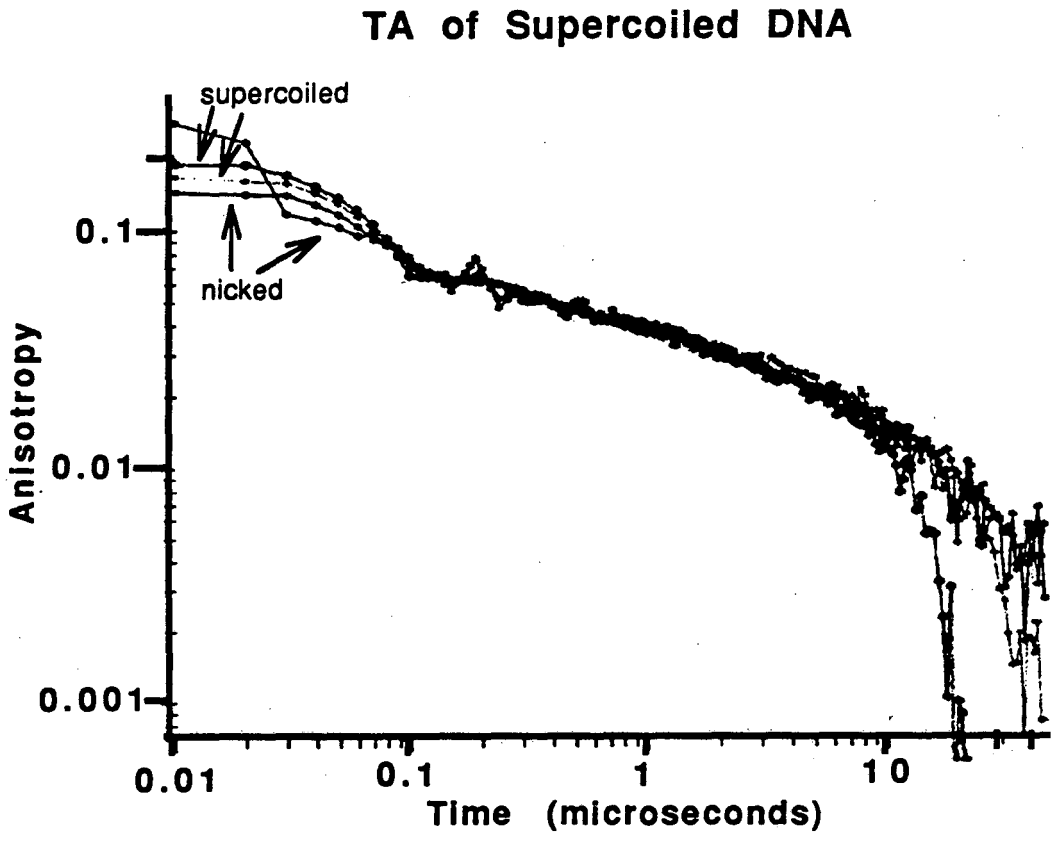

FIGURE 4-11: Transient absorption of methylene blue intercalated in pSM1 DNA, either nicked or supercoiled. Note at times longer than 100nsec, when twisting is completed and bending is the cause of anisotropy decay, all four curves are identical. At short times the curves suggest there may be a difference in anisotropy decay between supercoiled and nicked DNA, although the limited time resolution (10nsec/pt) makes it difficult to say definitively. The two nicked and two supercoiled curves are repeated measurements on the same sample. The anomalously high first two points for one of the nicked curves is due to accidentally placing the starting point (when the pulse ocurred) for the parallel curve in a different position than in the perpendicular curve in the data analysis. The original data was lost so the error could not easily be corrected.

Supercoiling Discussion

The results plotted in Fig. 4-9 and Tables 4-7, 4-8 show that the torsional constant is dependent on the superhelical density, based on the assumption, supported in Fig 4-11, that the bending constant does not change. Since each topoisomer has a different net twist (the relation between superhelical density and net twist will be discussed below) the torsional constant evidently is a function of net angular displacement, a characteristic of a non-linear spring.

A reasonable model for DNA twisting is a series of coupled torsional oscillators (each base is one disk), as discussed previously concerning the "tuna fish" can model (Fig. 4-7). Each topoisomer can be thought of as coupled torsional pendulums with different equilibrium angles. Consider, for example, just one disk connected by rubber strips to the floor and ceiling (the neighboring disks). The position where the rubber strips are untwisted correspond to the equilibrium configuration of relaxed DNA. If the rubber strip is unconnected and one twist put in and then resealed, there will be a new equilibrium angle. This corresponds to a topoisomer with some net linking number. In either case, the disk will oscillate about the equilibrium point, sitting in a harmonic potential if it is an ideal pendulum (Fig. 4-12), with an anharmonic term if non-ideal (Fig. 4-13).

Each topoisomer has an equilibrium twist angle (α_o, α_o'...) which is the minimum point on its potential energy curve. The difference in energy between these minima represent the energy required to form the topoisomer. The curvature of each of the potential surfaces will be the same if the DNA acts like an ideal spring. The potential energy curves shown in Fig. 4-13 is for the case of a cubic pertubation to the ideal, harmonic curves, and for m negative, corresponding to the case where it is easier to overwind (positive supercoiling) than underwind (negative supercoiling) the DNA.

What form is the anharmonic potential and how large is it? The simplest treatment is to assume that the potential is primarily harmonic and the non-harmonic term is a perturbation on this. We can later test this assumption by looking at the size of the perturbation and comparing it with the harmonic term. The simplest anharmonic term is a cubic. Note that adding a cubic term to the potential is equivalent to adding a squared term to the restoring force, which in turn, is equivalent to making the spring constant a linear function of displacement (or twist angle).

Twist Energy of an Ideal Torsional Pendulum

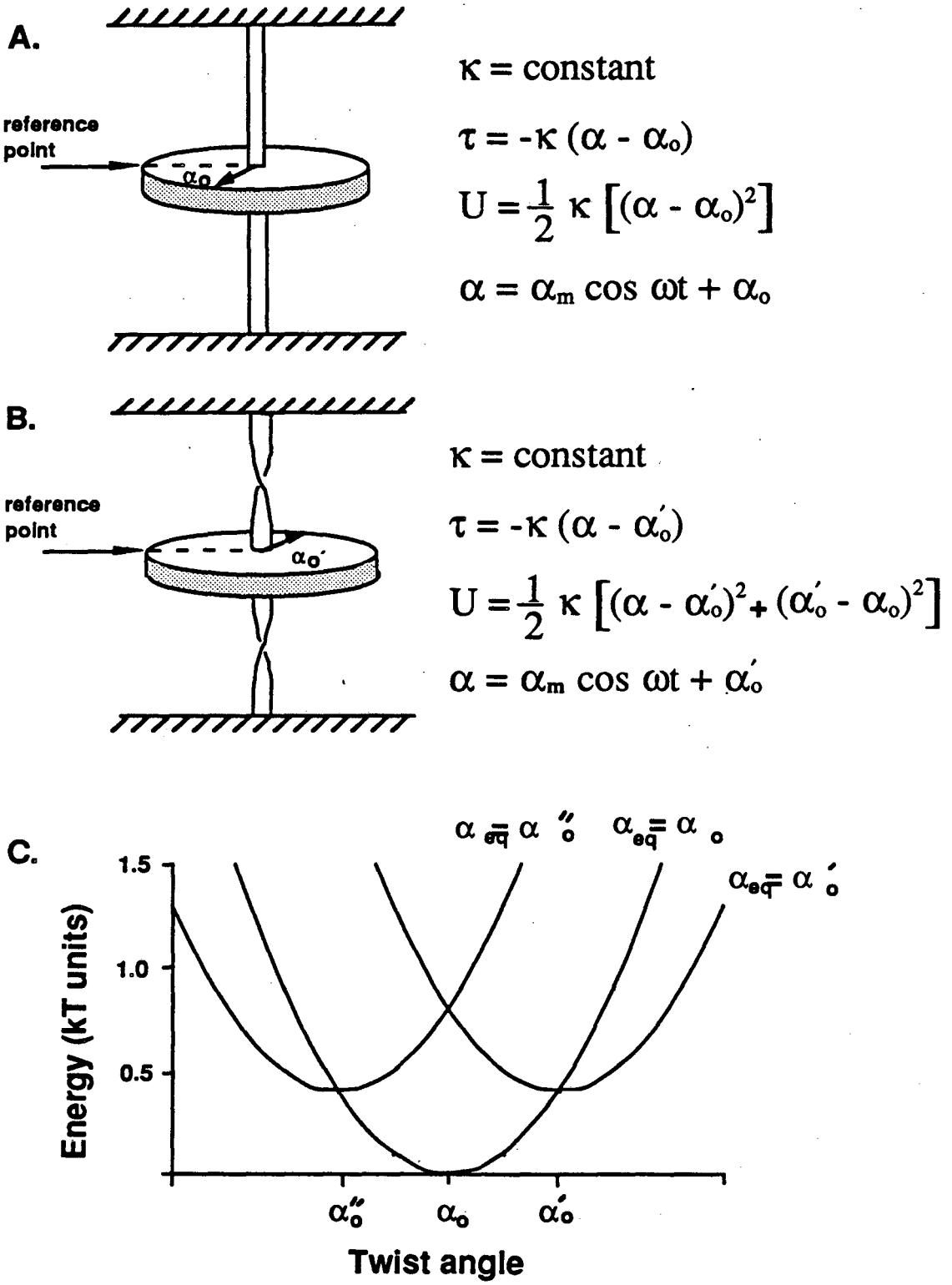

FIGURE 4-12: Energetics of an ideal pendulum.

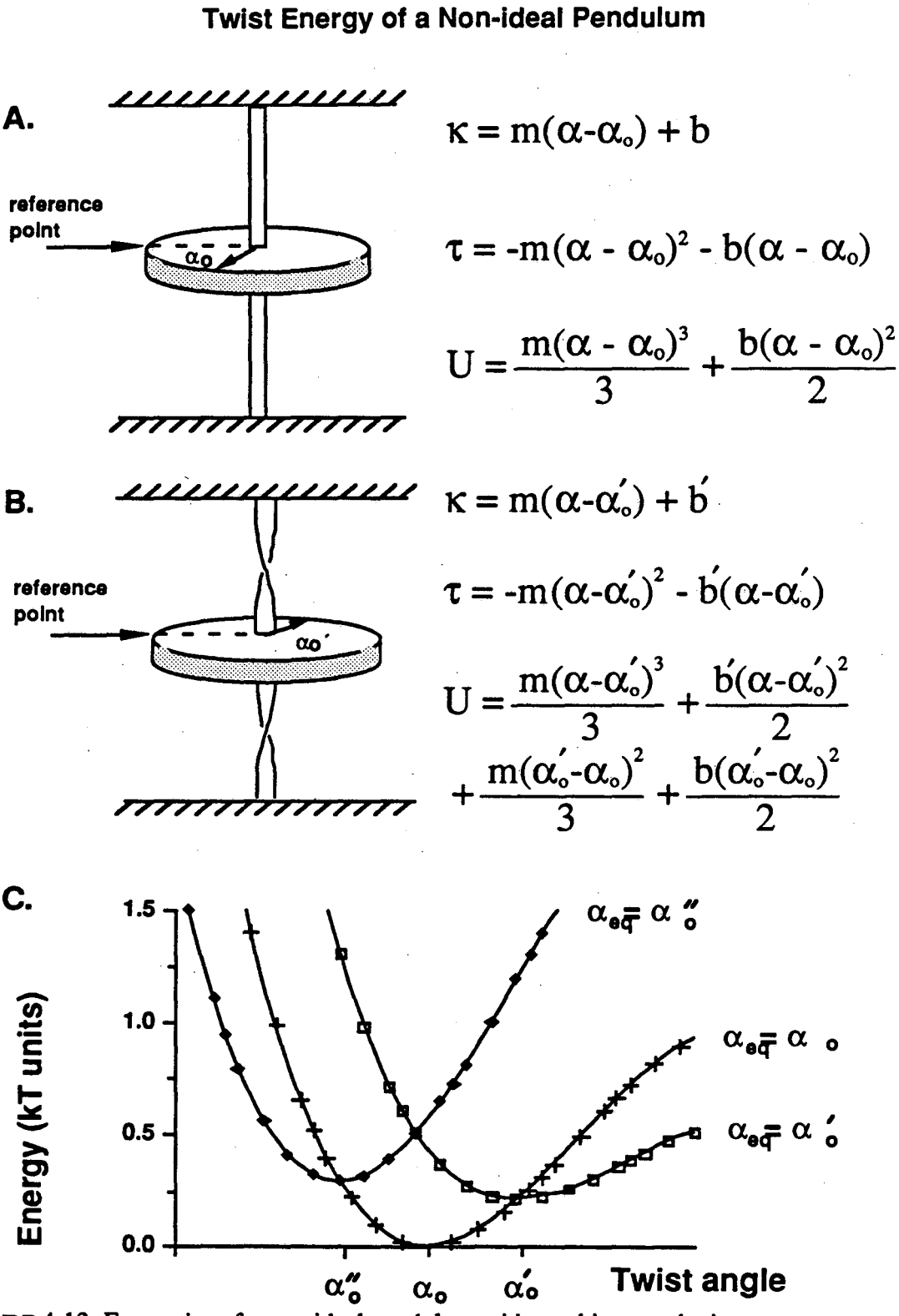

FIGURE 4-13: Energetics of a non-ideal pendulum with a cubic perturbation.

Experimentally, we measure the torsional constant and find that it is well approximated by a linear dependence on superhelical density (Fig. 4-9). Since the superhelical density, δ, equals $\Delta Lk / Lk_0$, this means that the torsional constant is linearly proportional to changes in linking number, ΔLk, as well. Experimentally, the best fit line of torsion constant/base pair vs ΔLk, from Fig. 4-9 is $C/h = m\Delta Lk + b$ where b= 135 and m = -218, both in units kT/base pair. m is the experimentally-determined slope of torsional constant vs linking number; b is the y-intercept, which is also the torsional constant in the absense of topological stress. Note that this approximation must break down at sufficiently positive superhelical density — the line would intersect and go below the x-axis, implying a zero or negative torsional constant.

If, in addition, the average twist angle between base pairs is linearly proportional the linking number, then the spring constant will be a linear function of twist angle and the cubic term in the potential will fit the experimental results well. For a series of coupled torsional pendula this linear relationship is certainly true since all of linking number goes into twist and the proportionality constant is simply $2\pi/N$ ($\Delta\phi_{eq} = 2\pi\Delta Lk/N$ radians). But it is less clear for DNA, because some of the linking number goes into writhe. We must therefore determine how linking number is distributed between twist and writhe.

Two groups have approached this problem, finding that there is indeed a linear relation between twist and linking number. Klenin et al., via Monte-Carlo simulations, have found that $\Delta Tw/\Delta Lk \approx 0.3$ (0.2-0.4) (Klenin, 1990; Vologodskii, personal communication). Boles et al., based on electron microscopy and topological methods have found that $\Delta Tw/\Delta Lk \approx 1/3.6 = 0.277$ (Boles, 1990).

The equilibrium twist angle of a molecule with linking deficit ΔLk is therefore given in radians by:

$$\langle\phi\rangle = \frac{F}{N} 2\pi \Delta Lk + 0.6013$$

where F is the partition factor, ≈0.3, equal to the fraction of ΔLk which ends up in Tw, and 0.6013radians is the equilibrium twist angle of relaxed DNA (34.45°) (Rhodes and Klug, 1980; Shore and Baldwin, 1983a; Wang, 1979).

The potential energy curve can now be written:

$$U = \frac{b}{2} (\phi - \phi_o)^2 + \frac{Fm}{3}(\phi - \phi_o)^3$$

as shown in Fig. 4-13 and Fig. 4-14. Alpha is the instantaneous angle between neighboring base pairs for the particular topoisomer and alpha(0) is the equilibrium angle between base pairs (all angles measured in radians).

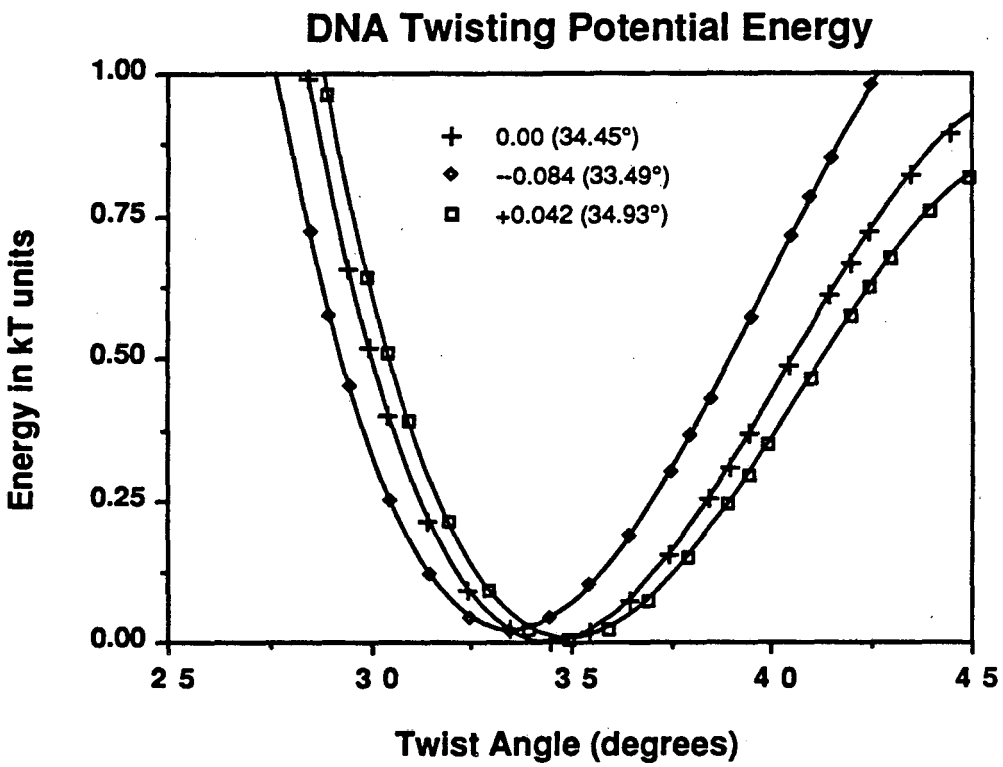

FIGURE 4-14: Plot of the potential energy surface for base pair twisting at superhelix densities of 0.00, -0.084 and +0.042, assuming that the twist is one-third the linking number (F = 0.33). This plot is based on an extrapolation of the linear relationship of the torsion constant vs. superhelix density data in Fig 4.9 to large deviations in twist angle. Such an extrapolation has clear limits since, at extreme positive deviations in twist angle, the torsion constant is predicted to go to zero. Note also that the equilibrium twist angle at a given superhelix density differs depending on the value of the Partition Factor F.

The magnitude of the anharmonicity can be estimated by determining the size of the cubic correction relative to the quadratic term in the potential energy expression when (ϕ - ϕ_o) is ± 5°, the rms deviation due to thermal energy. For F = 0.33, the correction term represents a change of ± 15% in the height of the potential energy surface for the relaxed topoisomer at U = 1/2 k_bT. Note that this is sufficiently small that the perturbation type expansion we have used is expected to be valid. Furthermore, an rms value is always

greater than the mean, and so most twist angles deviate on average by less than 5° from the equilibrium angle α_o., indicating that the correction term is actually somewhat smaller. Also, using the Barkely-Zimm model, a harmonic approximation, should still be reasonable with this size anharmonic term.

Comparison to Other Work

Two other groups have measured the torsional constant of DNA as a function of superhelicity, although none of the groups measured as wide a superhelical range or measured positively supercoiled DNA. Millar et al. (1982) suggested a possible change in torsional constant with superhelicity by showing that the torsional constant of linear calf thymus DNA differed from supercoiled pBR322. The superhelical density of the pBR322 was unspecified. Schurr and co-workers have published three papers on the subject (Wu 1988; Shibata 1984, Song, 1990). Initially they found no difference when they compared linear pBR322 and two negatively supercoiled pBR322 molecules, at σ = -0.048 and σ = -0.083 (Wu, 1988). They found the torsional constant for all three in 0.1M NaCl to be $2.3 \pm 0.2 \times 10^{-19}$ erg·cm (corrected for bending using their best estimate). More recently they have found that the torsional constant varies with superhelicity in the range σ = 0 to -0.05 (Song, 1990). They claim to see a structural transition at σ = -0.020 to a low torsion constant and then another one at σ = -0.035, bring the DNA back to a more normal state. A puzzling aspect of their experiment is a dramatic, time-dependent change in C over the course of several weeks for the same sample, the cause of which is unknown to them.

No other workers have measured the torsional constant of positively supercoiled DNA. Note that there has been recent interest in the properties of positively supercoiled DNA because it may affect the stability of Z DNA and may also be produced via transcription *in vivo* (Liu and Wang, 1987; Rahmouni and Wells, 1989).

Possible Problems in Interpretation — DNA Structural Transitions.

The data have all been interpreted using the Barkely-Zimm model for a uniform elastic rod. It is possible that structural changes due to superhelical stress are occuring which cause significant non-uniformities in the DNA structure. B to Z transitions, for example, are possible when the superhelicity becomes more negative than -0.08 (Vologodskii, personal communication). Also possible is local melting of the DNA helix with cruciform formation, a process that has been seen in the electron microscope for small DNA plasmids.

While B-Z transitions are possible, it is nevertheless likely that the ethidium is still reporting the torsional constant of B-form DNA. EtBr will not bind Z-DNA and the B-Z junctions would likely be few enough in number that just from random statistics, they would be more than 200bp away from the ethidium for a 4300bp plasmid like pBR322. The presence of stetches of Z-DNA would however, make it difficult to relate the superhelical density to the average twist angle per base pair. In other words, Fig. 4-9 (the torsional constant as a function of superhelical density) would still likely be valid, but the next step, of plotting torsional constant vs twist angle — and the analysis that follows from it — would not be valid. Finally we note that Schurr and co-workers have found a time dependence to their measurements which they propose is due to a metastable states in which the equilibrium constant between these and other states and is a sensitive function of environmental conditions (Song, 1990). We have not found such time dependence although if their results are correct, the interpretation of our results could be very difficult indeed.

Application of Torsional Constant Measurements to Topoisomer Separation via Gel Electrophoresis

We know that gel electrophoresis can separate DNA topoisomers (of 2-6kb length) that differ by only one linking number. Is this because the conformations of these

topoisomers are quite distinct, or is it that their conformations are very similar and its just that there are so many interactions between the DNA and the agarose gel that the gel is able to separate them? The hope, of course, is that a more thorough understanding of the phenomenon will lead to better abilities to separate topoisomers, either faster or using larger pieces, for example.

By knowing the torsional constant of DNA (here we neglect changes in torsional constants from supercoiling), from the earlier discussion we can calculate the fluctuation in net twist of a molecule. If the fluctuations in twist are large, then the fluctuations in writhe are also large, since they must add up to Lk, the linking number. For topoisomers that differ in linking number by only one, significant fluctuations in twist, and therefore writhe, mean that their conformations largely overlap.

Consider pBR322, a plasmid 4363bp long. The standard deviation in net twist is 0.92 turns (say 1 for simplicity). Note that this number is based on the same assumption of the previous net twist calculations — namely that the net twist can be treated as an unbiased random walk, which will be true if the associated changes in net writhe do cause the DNA to bend too much The fluctuation in writhe is therefore also ±1. For two topoisomers of pBR322 that differ by only one linking number, this means that their distribution of writhe largely overlap and therefore their conformations are largely the same. Fig. 4-15A, below, shows this graphically, assuming that all the change in linking number goes into writhe ($\Delta Lk = \Delta Wr = 1$). This is the most the two distributions could possibly be separated in writhe. In reality, all of the linking number is not taken up by writhe, so in fact, the distributions overlap even more. As previously noted, Vologodskii (1990) and Cozzarelli have both found that approximately 70% of linking number goes into writhe. This is shown in Fig. 4-15B. Finally, the distribution in twist, assuming 30% of linking number goes into twist, is shown in Fig. 4-15C. From the graphs it is clear that for topoisomers that differ by one linking number, the conformations are similar. It is

because the gel interacts so many times with the DNA topoisomers that it is able to resolve them. The fact that the gel stops being able to distinguish between topoisomers differing by one linking number for molecules greater than about 6kb is most likely due to other factors, most likely a size dependent DNA-agarose interaction. For example, these large molecules, no matter what their linking number might get caught in the gel.

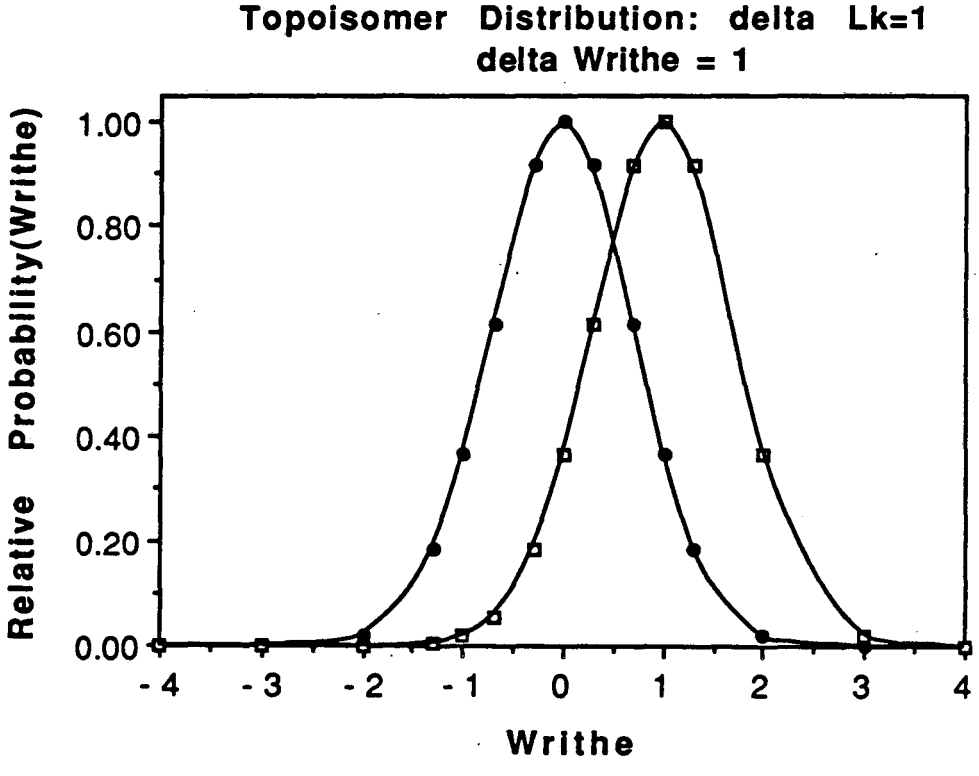

FIGURE 4-15A: Gaussian distribution in writhe of two topoisomers with ΔLk=1 and assuming all the difference in linking number goes into writhe.

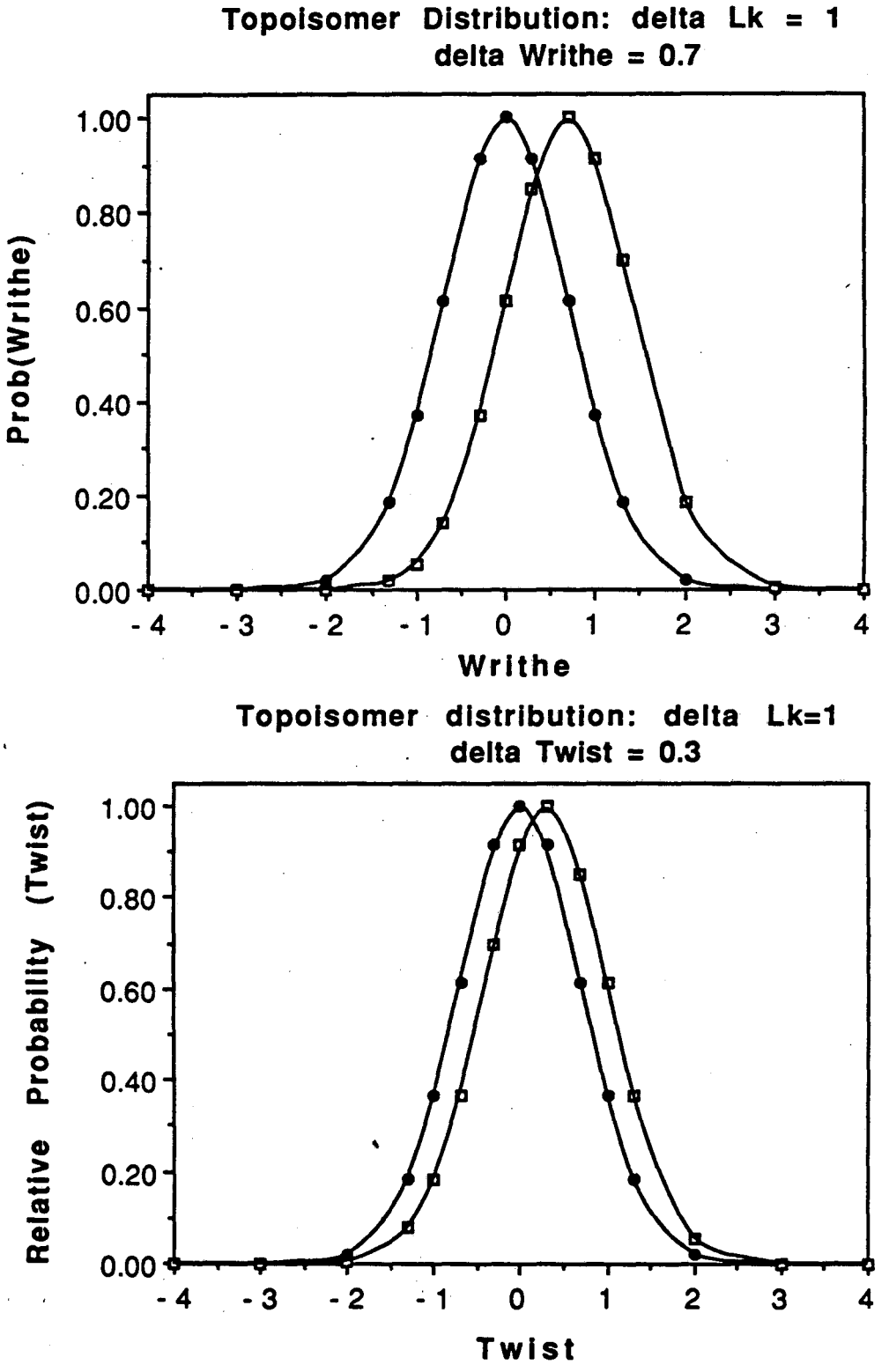

FIGURE 4-15 B &C: Gaussian distribution in writhe and twist for two topoisomers with ΔLk=1 and assuming that 70% of the difference in linking number goes into writhe.

Biological Effect of Anharmonic Term Due to Supercoiling

The anharmonic term of DNA twisting, while nonzero, is sufficiently small that it is probably does not have a signficant *direct* effect on biological processes. It may, however, play an indirect role. In particular, the asymmetry between positive and negatively supercoiled DNA may by significant. A number of DNA-binding proteins that attach to two different points on the DNA, for example, require that the DNA be supercoiled for binding to take place (Lobell and Scheif, 1990). Presumably two affects are simultaneously going on: one is that the supercoiling reduces the conformational (or writhe) phase space such that it is likely that the protein can find both sites, and that the supercoiling orients the DNA such that the proper base pairs face towards the protein. This orientation, however, may require twisting the DNA, an energetically uphill process, one which would be expected to reduce the binding constant. This process, however, may be easier than previously believed because of the relatively small torsional constant of positively supercoiled DNA. To orient the binding sites, the DNA can be either by under- or overwound. By overwinding the DNA, yielding positively supercoiled DNA, the binding sites can be brought into the correct phase with less cost in energy than if underwinding were required.

References

Allison, S.A. and Schurr, J.M. (1979) Torsion Dynamics and Depolarization of Fluorescence of Linear Macromolecules I. Theory and Applications to DNA. *J. Chem. Phys. 41,* 35-59.

Ashikawa, I., Kinosita, K and Ikegami, A (1984) *Biochim biophys. Acta, 789,* 87-93.

Barkley, M.D., & Zimm, B.H. (1979) Theory of Twisting and Bending of Chain Macromoleclues: Analysis of the Fluorescence Depolarization of DNA: J. *Chem. Phys. 70,* 2991-3007.

Bauer, W.R. and Vinograd, J. (1970) Interaction of Closed Circular DNA with Intercalative Dyes. II. The Free Energy of Superhelix Formation in SV40 DNA. *J. Mol. Biol., 47,* 419-435.

Bevington, Philip, R. (1969) Data Reduction and Error Analysis for the Physical Sciences. McGraw-Hill, USA.

Boles, T. C., White, J.H. and Cozzarelli, N.R. (1990) Structure of Plectonemically Supercoiled DNA. *J. Mol. Biol., 213,* 931-951.

Bresloff, J.L. and Crothers, D.M. (1975) DNA-Ethidium Reaction Kinetics: Demonstration of Direct Ligand Transfer between DNA Binding Sites. *J. Mol. Biol., 95,* 103-123.

Cook, David (1990) Ph.D. Thesis, University of California, Berkeley.

Depew, R.E. and Wang, J.C. (1975) Conformational Fluctuations of the DNA Helix. *Proc. Natl. Acad. Sci. USA, 72,* 4275-4279.

DiNardo, S., Voekel, K., Sternglanz R., Reynolds, A.E. and Wright, A. (1982) *Escherichia Coli* DNA Topoisomerase I Mutants have Compensatory Mutations in DNA gyrase genes. *Cell, 31,* 43-51.

Ding, D., Rill, R.L., & Van Holde, K.E. (1972) The Dichroism of DNA in Electric Fields. *Biopolymers 11,* 2109-2124.

Frank-Kamenetskii, M.D., Lukashin, A.V., Anshelvich, V.V. and Vologodskii, A.V. (1985) Torsional and Bending Rigidity of the Double Helix from data on Small DNA Rings. *J. Biomol. Struct. and Dynamics, 2,* 1005-1012.

Fujimoto, B.S. and Schurr, J.M. (1990) Dependence of the Torsional Rigidity of DNA on Base Composition. *Nature, 344,* 175-178.

Hagerman, P.J., and Ramadevi, V.A. (1990) Application of the Method of Phage T4 DNA ligase-catalyzed Ring-Closure to the Study of DNA Structure. I. Computational Analysis. *J. Mol. Biol., 212,* 351-362.

Hogan, M., Wang, J., Austin, R.H., Monitto, C.L.and Hershkowitz, S. (1982) Molecular Motion of DNA as Measured by Triplet Anisotropy Decay. *Proc. Natl. Acad. Sci, USA, 79,* 3518-3522.

Horowitz, D.S. and Wang, J.C. (1984) Torsional Rigidity of DNA and Length Dependence of the Free Energy of DNA Supercoiling. *J. Mol. Biol., 173,* 75-91.

Hurley, I., Osei-Gyimah, P., Archer, S. Scholes, C.P. and Lerman, L.S. (1982) Torsional Motion and Elasticity of the Deoxyribonucleic Acid Double Helix and Its Nucleosomal Complexes. *Biochemistry, 21,* 4999-5009.

Keller, W. (1975) Determination of the Number of Superhelical Turns in Simian Virus 40 DNA by Gel Electrophoresis: *Proc. Natl. Acad. Sci., USA. 72,* 4876-4880.

Klenin, K.V., Vologodskii, A.V., Anshelevich, V.V., Dykhne, A.M., and Frank-Kamenetskii, M.D.(1990) Computer Simulation of DNA Supercoiling. *J. Mol. Biol.* (in press)

LePecq, J.B. and Paoletti, C. (1967) A Fluorescent Complex between Ethidium Bromide and Nucleic Acids. *J.Mol. Biol, 27,* 87-106.

Levene, S.D. and Crothers, D.M. (1986) Topological Distributions and the Torsional Rigidity of DNA: a Monte Carlo Study of DNA circles. *J. Mol. Biol. 189,* 73-83.

Liu, L.F. and Liu, C.C. (1980) Type II DNA topoisomerases: Enzymes that can Unknot a Topologically knotted DNA Molecule via a Reversible Double-Strand Break. *Cell, 19,* 697-707.

Liu, L.F. and Wang, J.C. (1987) Supercoiling of the DNA Template during Transcription. *Proc. Natl. Acad. Sci., USA. 84,* 7024-7027.

Lobell, R.B. and Schleif, R.F. (1990) DNA Looping and Unlooping by AraC Protein. *Science, 250,* 528-532.

Lockshon, D. and Morris, D.R. (1983) Positively Supercoiled Plasmid DNA is Produced by Treatment of *Escherichia coli* with DNA gyrase inhibitors. *Nucleic Acids Res., 11,* 2999-3017.

Magde, D., Zappala, M., Knox, W.H. and Nordlund, T.M. (1983) Picosecond Fluorescence Anisotropy Decay in the Ethidium/DNA Complex. *J. Phys. Chem., 87,* 3286-3288.

Millar, D.P., Robbins, R.J., and Zewail, A.H. (1980) Direct Observation of the Torsional Dynamics of DNA and RNA by Picosecond Spectroscopy. *Proc. Natl. Acad. Sci., USA. 77,* 5593-5597.

Millar, D.P., Robbins, R.J., and Zewail, A.H. (1982), Torsion and Bending of Nucleic Acids Studied by Subnanosecond Time-Resolved Fluorescence Depolarization of Intercalated Dyes. *J. Chem. Phys. 76(4),* 2080-2094.

O'Connor, D. and Phillips, D. (1984) Time Correlated Single Photon Counting, London, Academic Press.

Pulleyblank, E.E., Shure, M. Tang, D., Vinograd, J. and Vosberg, H.P (1975). Action of nicking-closing Enzyme on Supercoiled and Nonsupercoiled Closed Circular DNA: Formation of a Boltzmann Distribution of Topological Isomers. *Proc. Natl. Acad. Sci. USA, 72,* 4280-4284.

Rahmouni, A. R. and Wells, R.D. (1989) Stabilizatin of Z-DNA *in vivo* by localized supercoiling. *Science, 246,* 358-363.

Rhodes, E. and Klug, A. (1980) Helical periodicity of DNA Determined by Enzyme Digestion. *Nature, 286,*

Robinson, B.H., Lerman, L.S., Bethe, A.H., Frisch, H.L., Dalton, L.R. and Auer, C. (1980) Analysis of Double-Helix Motions with Spin-labeled Probes: Binding Geometry and the Limit of Torsional Plasticity. *J. Mol. Biol, 139,* 19.

Sambrook, J., Frisch, E.F. and Maniatis, T. (1989) Molecular Cloning: A Laboratory Manual. Cold Spring Harbor, Cold Spring Harbor Laboratory Press.

Schmitz, K.S., & Schurr, J.M. (1973) Rotational Relaxation of Macromolecules Determined by Dynamic Light Scattering. II. Temperature Dependence for DNA. *Biopolymers 12,* 1543-1564.

Shibata, J.H., Wilcoxon, J., Schurr, J.M. and Knauf, V. (1984) Strctures and Dynamics of a Supercoiled DNA. *Biochemistry, 23,* 1188-1194.

Shimada, J. and Yamakawa, H. (1984) Ring-closure Probabilities for Twisted Wormlike Chains. Applications to DNA.

Shore, D. and Baldwin, R.L. (1983a) Energetics of DNA Twisting. I. Relation between Twist and Cyclicization Probability. *J. Mol. Biol., 170,* 957-981.

Shore, D. and Baldwin, R.L. (1983b) Energetics of DNA Twisting. II. Topoisomer Analysis. *J. Mol. Biol., 170,* 983-1007.

Sinden, R.R. Carlson, J.O. and Pettijohn, D.E. (1980) Torsional Tension in the DNA Double Helix measured with Trimethylpsoralen in Living *E. coli* Cells: Analogous Measurements in Insect and Human Cells. *Cell, 21,* 773-783.

Sinden, R.R. and Pettijohn, D.E. (1981) Chromosomes in Living *Escherichia coli* Cells are Segregated into Domains of Supercoiling. *Proc. Natl. Acad. Sci., USA. 78,* 224-228.

Singleton, C.K. and Wells, R.D. (1982) The Facile Generation of Covalently Closed, Circular DNAs with Defined Negative Superhelical Densities. *Anal. Biochem, 122,* 253-257.

Song, L., Fujimoto, B.S., Wu. P., Thomas, J.C., Shibata H.H., and Schurr, J.M. (1990) Evidence for Allosteric Transitions in Secondary Structure Induced by Superhelical Stress. *J. Mol. Biol., 214,* 307-326.

Sugino, A., Higgins, N.P., Brown P.O., Peebles, C.L. and Cozzarelli, N.R. (1978) Energy Coupling in DNA Gyrase and the Mechanism of Action of Novobiocin. *Proc. Natl. Acad. Sci. USA. 75,* 4838-4842.

Taylor, W.H. and Hagerman, P.J. (1990) Application of the Method of Phage T4 DNA ligase-catalyzed Ring-Closure to the Study of DNA Structure. II. NaCl-dependence of DNA Flexibility and Helical Repeat. *J. Mol. Biol., 212,* 363-376.

Thomas, J.C., Allison, S.A., Appellof, C.J. and Schurr, J.M. (1980) Torsion Dynamics and Depolarization of Fluorescence of Linear Macromolecules II. Fluorescence Polarization Anisotropy Measurements on a Clean Viral φ29 DNA *Biophys. Chem. 12,* 177-188.

Thomas J.C.,and Schurr, J.M. (1983) Fluorescence Depolarization and Temperature Dependence of the Torsion Elastic Constant of Linear φ29 Deoxyribonucleic Acid. *Biochem., 22,* 6194-6198.

Wahl, Ph., Paoletti, J. and LePecq, J.B. (1970) Decay of Fluorescence Emission Anisotropy of the Ethidium Bromide DNA complex. Evidence for internal motion in DNA. *Proc. Natl. Acad. Sci. USA., 65,* 417-421.

Wang, J.C. (1979) Helical Repeat of DNA in Solution. *Proc. Natl. Acad. Sci. USA, 76,* 200-203.

Wu, P., Fujimoto, B.S., Schurr, J.M. Time-Resolved Fluorescence Polarization Anisotropy of Short Restriction Fragments: The Friction Factor for Rotation of DNA About Its Symmetry Axis. *Biopolymers, 26,* 1463-1488.

Wu, H. Y., Shyy, S., Wang, J.C. and Liu, L.F. (1988). Transcription Generates Positively and Negatively Supercoiled Domains in the Template. *Cell, 53,* 433-440.

Wu, P., Song, L. Clendenning, J.B., Fujimoto, B.S., Benight, A.S., and Schurr, J.M. (1988) Interaction of Chloroquine with Linear and Supercoiled DNAs. Effect on the Torsional Dynamics, Rigidity and Twist Energy Parameter. *Biochemistry 27,* 8128-8144.

Volodoskii, A.V., Anshelevish, V.V., Lukashin, A.V. and Frank-Kamenetskii, M.D. (1979) Statistical Mechanics of Supercoils and the Torsional Stiffness of the DNA Double Helix. *Nature, 280,* 294-298.

Chapter Five

Chomatin

Abstract

Polarized fluorescence recovery after photobleaching (pFRAP) was used to monitor the micro- and millisecond reorientational dynamics of chromatin in mud-puppy nuclei as a function of salt concentration. Under conditions where 30nm chromatin fibers are intact and aggregated (physiological-level monovalent salt with divalent cations) the chromatin was immobile to the long-time limits of detection, approximately 40msec. Removal of the divalent cations to disperse the fibers led to a millisecond relaxation. Subsequent dilution of the monovalent salt, which is known to cause the 30nm fiber to decondense into a "beads-on-a-string" structure, caused a dramatic increase in flexibility. The data indicate that the structural and dynamic transitions occur gradually and that the high local concentrations of chromatin found under physiological conditions are a major determinant of chromatin dynamics (Selvin et al., 1990).

Introduction

As previously mentioned, the dynamics of DNA can be profoundly altered by local structure and environment. Chromatin — DNA and its associated proteins, namely histone and non-histone proteins — is the physiological state of DNA in all eucharyotic (nucleated) cells. The importance of the associated proteins, and their interaction with DNA, can be inferred from evolutionary data: the more highly conserved a protein structure is, the more critical its role is believed to be — almost any mutation is lethal. Histones are among the most highly conserved proteins known.

Histones play their important role by binding to DNA with extremely high affinity (k $\approx 10^{12}$), probably in a sequence specific manner. The histones help organize DNA into higher order structure, which is important for both the packaging of DNA, and the expression of genes on the DNA. The packaging of DNA is a monumental task: it requires arranging three billion base pairs, with a contour length of a meter, into a cell with a diameter approximately one-millionth as long. All this must be done in an orderly manner so that necessary enzymes can interact with the proper sequences, or sections of DNA.

The lowest order of chromatin structure is the "beads on a string" structure, composed of a repeating array of bead-like particles known as nucleosomes. Each nucleosome is composed of a "core," containing 146 base pairs wrapped one-and-three-quarters times around a histone octamer (H2A, H2B, H3, H3, H4), and a linker, containing between 20 and 100 base pairs of DNA, which is associated with yet another histone (H1) protein. The linker DNA interconnects each core particle. The next higher structure of chromatin is the 30nm fiber. The exact structure is not known, although its diameter is 30nm, (as the name implies), and its radial distribution and mass per unit length have recently been determined (Williams et al., 1986; Smith *et al.*, 1990). A number of structures have been proposed for the fiber, perhaps the simplest of which is a solenoid consisting of six nucleosomes per turn (see Figure 1, below) proposed by Finch and Klug (1976). (For reviews, see Butler, 1983; Felsenfeld and McGhee, 1986; Williams, 1986; Van Holde, 1989; Widom, 1989.) In yet higher order structure, the 30nm fibers are believed to fold into looped domains, although little evidence exists for this, or any other proposed larger scale organization of chromatin. At the highest order is the mitotic chromosome.

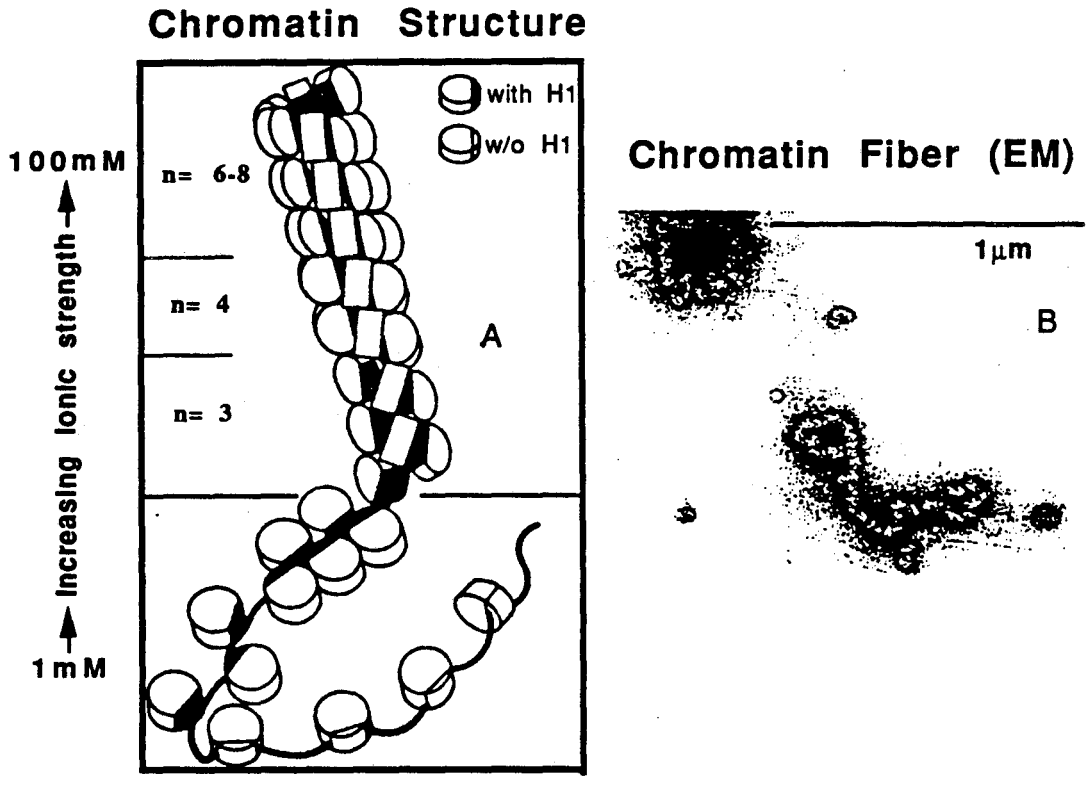

FIGURE 5-1: Model for 30nm chromatin organization as a function of salt concentration (A). At the lowest salt concentration, the beads-on-a-string structure is favored. As salt concentration increased, increasingly compact structures predominate, until at physiological levels, the 30nm chromatin fiber is favored. The solenoidal model of the 30nm fiber shown here has been advocated by Finch and Klug in 1976, although a number of other fiber structures have been proposed (see text). Electron micrograph of intact 30nm fiber (Langmore and Paulson, 1983).

These various levels of structure have profound effects on the expression of DNA. At one end is the metabolically inert mitotic chromosome which is packed very tightly. At the other end is actively transcribing and replicating chromatin in the beads-on-a-string structure. (although even this structure may be too closed for biological activity — the nucleosomes may have to transiently dissolve to allow contact between RNA polymerase and the core DNA during transcription.) In between is the 30nm fiber, which is believed to prevent transcription. Intuitively, open structures facilitate interaction of enzymes and reactants with the DNA, allowing expression of the genetic material.

What triggers the transition from a compact to open structure is largely unknown. Many studies, however, have shown that the conformation of chromatin becomes increasingly compact as the cation concentration of the surrounding solution increases (see e.g. Thoma et al., 1979; Suau et al., 1979; Widom, 1986). In a low salt solution, charge repulsion causes the chromatin to adopt the extended "beads-on-a-string" conformation. At higher cation concentration, the unfavorable electrostatic interactions are reduced, and the 30nm fiber is favored. The structural transitions are believed to be gradual.

Materials and Methods

(a) *Buffers*

Wash buffer consisted of 130 mM NaCl, 5.0 mM KCl, 2.0 mM $MgCl_2$, 10 mM Hepes (pH7.0), and 0.1 M sucrose. Synthetic sea water was prepared from a powder obtained from Instant Ocean (Eastlake, OH). Buffer A contained 60 mM KCl, 15 mM NaCl, 15 mM Pipes (pH 7.0), 0.5 mM spermine, 0.5 mM spermidine, 2.0 mM EDTA, 0.02% NaN_3. Buffer mMB consisted of 5 mM Pipes, 3 mM $MgCl_2$, 18 mM NaCl and 72 mM KCl; Buffer mEB consisted of mMB in which 3 mM EDTA replaced Mg^{2+}. Micrococcal nuclease digestion buffer contained 60 mM KCl, 15 mM NaCl, 15 mM Pipes

(pH 7.0), 0.5 mM $CaCl_2$, 0.25 mM $MgCl_2$, 0.1 mM PMSF (phenylmethylsulfonyl fluoride), and 0.2% NaN_3.

(b) *Isolation of Nuclei*

Necturus maculosus (mudpuppy) and *Strongylocentrotus purpuratus* (sea urchin) were obtained from Charles Sullivan (Nashville, TN) and Alacrity Marine Biological Supply (Redondo Beach, CA), respectively. Erythrocytes from *Necturus* were obtained by heart puncture; sea urchin embryos from *Strongylocentrotus purpuratus* were grown to 18 hours as described by Workman and Langmore (1985). All subsequent steps were performed at 4°C, all wash volumes were at least 10 times the volume of the pellet, and each centrifugation of the *Necturus* samples involved spinning at 60g for 6 minutes.

Necturus erythrocytes were washed two times in wash buffer to separate the cells from lymphocytes. The erythrocytes were then incubated for 1 hour on ice in wash buffer with 3 mM iodoacetate, and 0.2 mM PMSF to inhibit proteases. The cells were then lysed by washing three times in Buffer A with 0.1% digitonin, 1 mM iodoacetate, and 0.1 mM PMSF, and three times in Buffer A with 0.1% Non-idet P40, 1 mM iodoacetate, and 0.1 mM PMSF. At this point the cells had lysed and were free from cellular debris. Nuclei (at 1mg/ml DNA) were quickly frozen in 50% glycerol Buffer A by placing tubes into methanol cooled with dry ice. The nuclei were stored at -70°C. Before nuclei were used in a pFRAP experiment, they were washed three times in mMB and then stored at 4°C in mMB.

Sea urchin nuclei were isolated from 18 hour embryos as described by Workman and Langmore (1985). The published method was modified to keep the nuclei in buffer A, including storage in 50% glycerol at -70°C.

(c) Isolation of Chromatin Fibers

For the study of isolated chromatin fibers, nuclei (1mg in 1ml) were pelleted at 4°C and washed with mMB (this procedure removes multivalent cations) and then pelleted again and washed with micrococcal nuclease digestion buffer. Nuclei were then resuspended in 1 ml of micrococcal nuclease digestion buffer and incubated at 22°C for five minutes. Nuclei were digested for five minutes by adding 20 units of micrococcal nuclease (Worthington, Freehold, NJ). Digestion was stopped by increasing the EGTA and $MgCl_2$ to 5.0 mM and 1.0 mM, respectively. Nuclei were then gently pelleted and resuspended in 1 ml 0.2 mM EDTA (pH 7.0), 0.1 mM PMSF, 0.02% NaN_3 to solubilize the chromatin. Nuclei were allowed to lyse at 4°C for 45 minutes and were then spun for five minutes in an Eppendorf centrifuge to remove nuclear debris. Chromatin solutions were brought to physiological ionic strength by adding 1/10 volume of lOx mEB. This isolation procedure produces chromatin with the native amount of histone H1 (Williams and Langmore, submitted). The final concentration of the fibers in solution was ≈ 150 μg/ml.

Successful isolation of 30 nm fibers was confirmed by examining the digested fibers in an electron microscope by the method of Williams *et al.* (1986). The approximate molecular weight was determined by electrophoresis in 0.3% agarose. The mode of the molecular weight distribution of soluble chromatin was 55 kbp.; the weight average molecular weight was 45 kbp.

(d) *Deoxygenation of Samples*

After the nuclei and fibers were isolated, all sample manipulations were conducted in a nitrogen-saturated glove bag. Buffers were deoxygenated by bubbling nitrogen through them for approximately 15 minutes. Air tight sample chambers were constructed from 500 μl Eppendorf tubes that were slit (in the transverse direction) near the tip with a razor blade; the slit end was then glued to a silanized quartz coverslip with epoxy resin.

(e) *Preparation of Fluorescently Labeled Chromatin Samples*

Typically 0.1 mg of nuclei was placed into the Eppendorf holder. Ethidium bromide (Etbr) (2 μg/ml in H_20) (Sigma Chemicals, St. Louis, MO) was then added and assumed to bind stoichiometrically; labeling levels were kept lower than 1 Etbr bound per 1000 base pairs. At these low labeling levels energy transfer between ethidium molecules is negligible (Ashikawa *et al.*, 1983). The total sample volume was increased to 400 μl by adding mMB or mEB. We waited about 30 minutes for the nuclei to settle onto the quartz coverslip and for the ethidium to stain the chromatin. After this length of time, the fluorescence was confined to regions containing chromatin, and the nuclei essentially formed a continuous monolayer on the coverslip. Thus, as the microscope stage was translated (see Section g), the light remained focussed on nuclei. The data were not affected by the fact that the beam occassionally passed over an area with no nuclei because the fluorescence count rate then fell by 2 orders of magnitude.

(f) *Manipulation of Salt Concentration*

Salt concentrations were manipulated by serial dilution of the monovalent salt or chelation of magnesium with EDTA. Specifically, mMB was converted into mEB by adding enough EDTA to chelate the Mg^{2+} in the mMB and to raise the free EDTA concentration to 3 mM. The monovalent salt concentration was manipulated by removing an appropriate volume of buffer from the top of the sample and replacing it with an equal volume of a 5 mM Pipes, 3 mM EDTA solution. The sample was then gently pipeted and incubated 30 minutes before beginning the next experiment to ensure that the salt distribution in the solution was uniform. The binding constant of ethidium bromide is a function of salt concentration; however, our calculations (and the fact that the total fluorescence count rate did not vary as the salt concentration was changed) indicate that the number of Etbr molecules bound per nucleus did not change significantly during the

salt studies. The expected decrease in binding with increasing salt concentration would produce effects opposite to those reported here.

(g) *Description of Apparatus and pFRAP Experimental Methods*

The pFRAP apparatus used was very similar to that described previously (see Chapter 4 and Velez and Axelrod, 1988). After each round of bleach and probe, the stage was moved horizontally about one beam spot diameter (3μm) by a computer-controlled stepping motor. In this way it was possible to obtain data from about 10^5 areas without bleaching the same nucleus twice. A microscope was used to collect and focus light because effective bleaching can be achieved with focussed light and effective detection can be achieved with a high numerical aperture lense.

For all of the chromatin experiments we used a 10μsec bleaching pulse. The prebleach and postbleach fluorescence count rates were monitored for 50 and 200 time points (10 μsec/point), respectively. Typically the prebleach fluorescence signals yielded ≈100,000 counts/sec. About two hours of signal averaging was usually required to obtain a signal-to-noise ratio of about 20 to 1 .

Bleach depth was 25-40% to prevent an artificially low initial anisotropy (Velez and Axelrod, 1988). At such bleaching levels $r_b(t)$ is essentially bleach independent. The light source for both bleach and probe beams was a Coherent 15 watt argon-ion laser, tuned to 514.5nm line and attenuated with a 0.6 O.D. filter. Other light losses from optical components reduced the bleach intensity was approximately 100mW at the sample. Probe beam intensity was typically 5-10,000 less. We used a lOx glycerine immersion objective with a numerical aperture of 0.5 to focus the light onto the sample and collect fluorescence via epi-illumination. These experimental conditions lead to negligible light-associated temperature rises in our samples (Velez and Axelrod, 1988; Scalettar *el al.*, 1988).

(h) *Data Analysis*

Time constants and initial values of the anisotropy, $r_b(t)$, were determined by a two-parameter fitting of the raw data to a single decaying exponential function. Although there is no *a priori* reason for $r_b(t)$ to exhibit an exponential decay, it was found empirically that a single exponential fit the data quite well. The algorithm utilized by Curfit (Bevington, 1969) was adapted for use in our curvefitting program. All data points were used to determine the best-fit parameters, but the weighting attached to each time point was set by its statistical significance. When necessary, data were also adjusted for slight differences in the intensities of parallel and perpendicular polarized light.

Results

a) Diffusion of Chromatin in Mudpuppy Nuclei at Physiclogical Salt Concentration

The reorientational motion of native chromatin fibers in intact mudpuppy nuclei was measured in near physiological (mMB) salt. The polarized photobleaching data obtained from mudpuppy nuclei suspended in mMB are displayed in Fig. 2a.

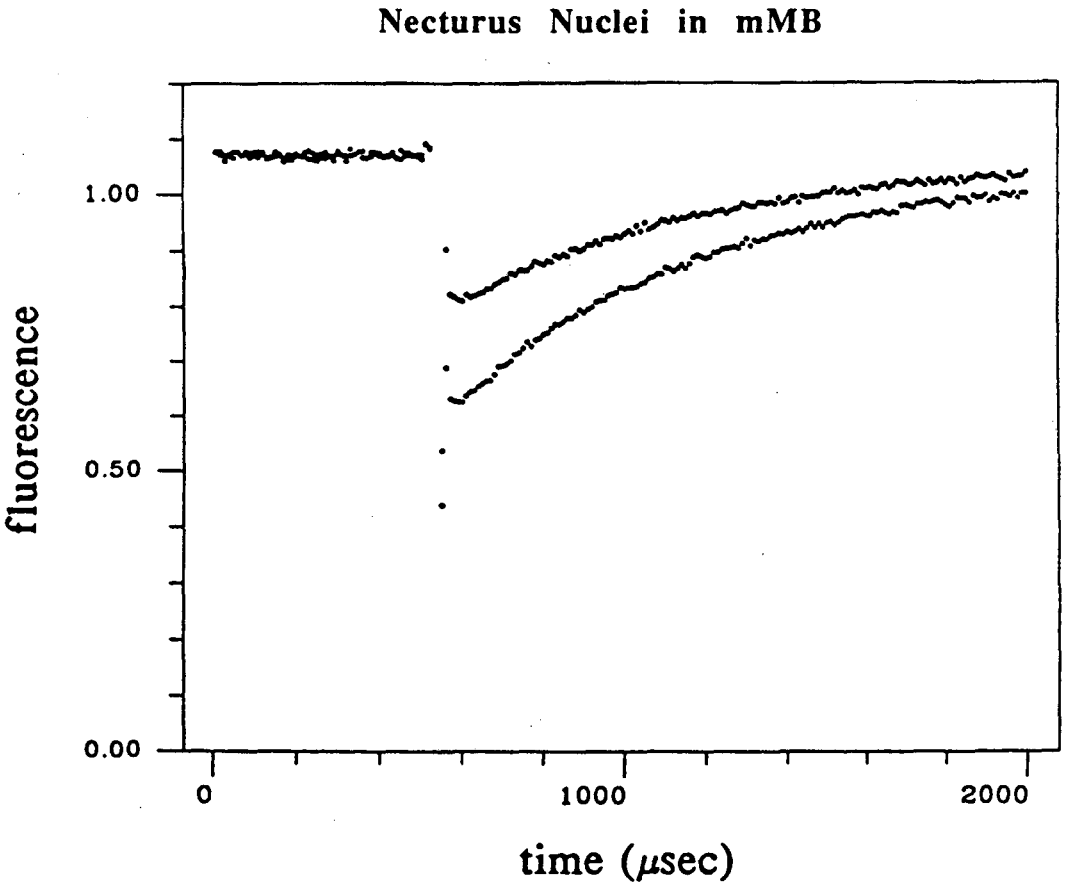

FIGURE 5-2a: Polarized photobleaching recovery curves, $F_{\parallel}(t)$ (lower) and $F_{\perp}(t)$ (upper) obtained from a sample of mudpuppy nuclei suspended in mMB. The associated anisotropy is shown in Fig. 2b. From the temporal behavior of the individual recovery curves it is not obvious that this aggregated chromatin sample is rotationally immobile; this fact becomes apparent only upon examination of the anisotropy function.

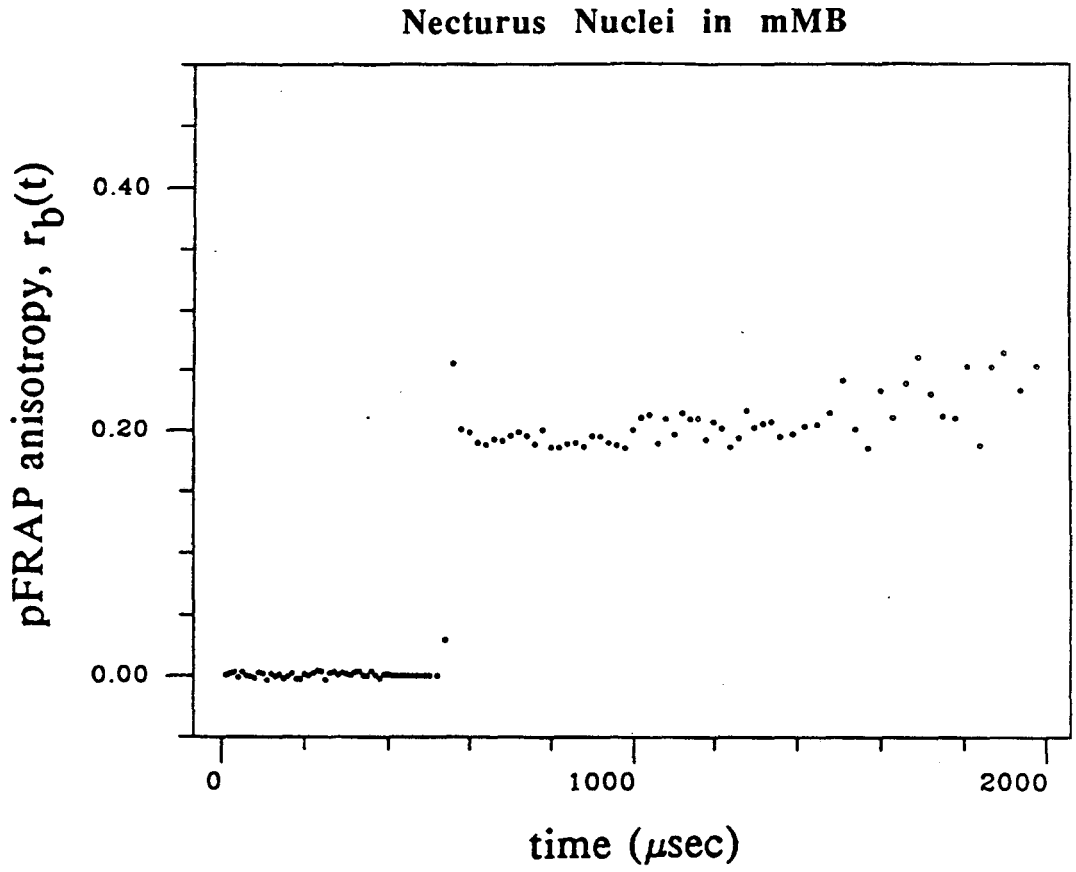

FIGURE 5-2b: Anisotropy function for mudpuppy nuclei suspended in mMB, constructed from data in Fig. 2a. Note that although the raw parallel and perpendicular curves (Fig. 2a) were collected at 10 μsec sample intervals (bins), the anisotropy functions in Figs. 2b, 3 and 6 were obtained by adding together neighboring bins (for the long time data points only); this procedure improves the signal-to-noise ratio at long times.

The substantial difference between the bleach depth in the parallel mode and in the perpendicular mode shows that this sample retains a substantial amount of anisotropy at the end of the 10 μsec bleaching pulse. It is also evident, upon comparing $F_{\parallel}(t)$ and $F_{\perp}(t)$, that the anisotropy is quite long-lived, *i.e.*, reorientation in this sample is slow. These statements can be made quantitative by calculating $r_b(t)$. It is then seen (see Fig. 5-2b) that the initial value of the anisotropy, 0.20, is positive and quite large. Moreover, $r_b(t)$ is basically flat for several milliseconds after bleaching. An estimated lower bound for the

time constant (40 ms) was obtained by assuming that there is less than a 5% decay of anisotropy in 2 milliseconds and that an exponential describes the temporal dependence of $r_b(t)$.

(b) *Diffusion and Compaction of Chromatin in Mudpuppy Nuclei as a Function of Salt Concentration*

The reorientational motion of native chromatin in mudpuppy nuclei was also followed as a function of salt concentration. pFRAP data were obtained from mudpuppy samples that contained no divalent cations and had monovalent salt concentrations of 90 mM (mEB), 69 mM, 54 mM, 45 mM, 36 mM, 22 mM and 11 mM. $F_{\|}(t)$, $F_{\perp}(t)$, and $r_b(t)$ are shown for mudpuppy in mEB in Fig. 3a and 3b.

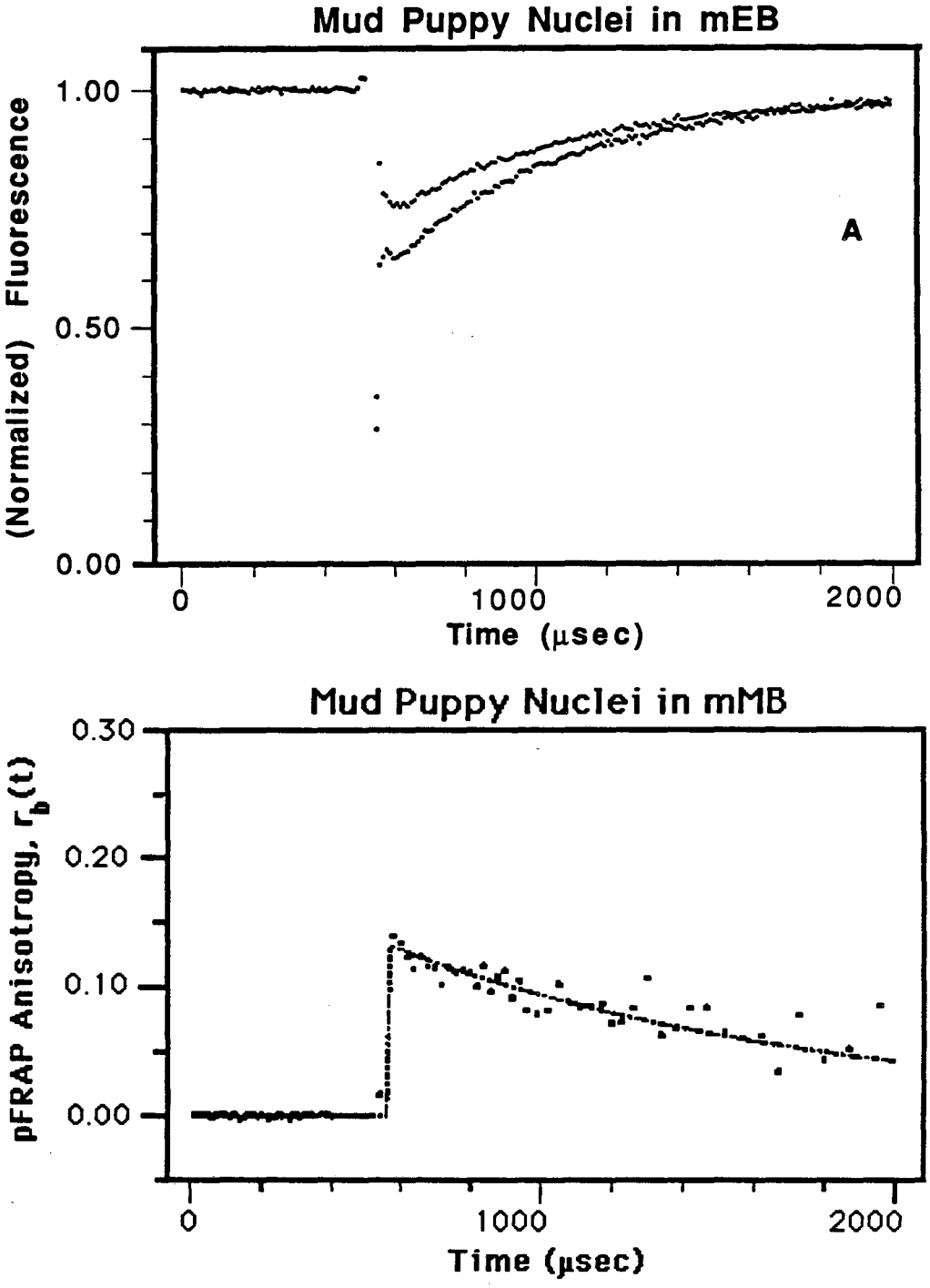

FIGURE 5-3: Individual recovery curves (3a) and anisotropy function (3b) obtained from mudpuppy nuclei suspended in mEB. Chelation of magnesium has converted an immobile sample (Fig. 2b) into a mobile one (Fig. 3b). The initial anisotropy also decreases upon removal of Mg^{2+}.

Figures 4 and 5 are summaries of the best fit initial anisotropies and time constants for all of the salt concentrations measured.

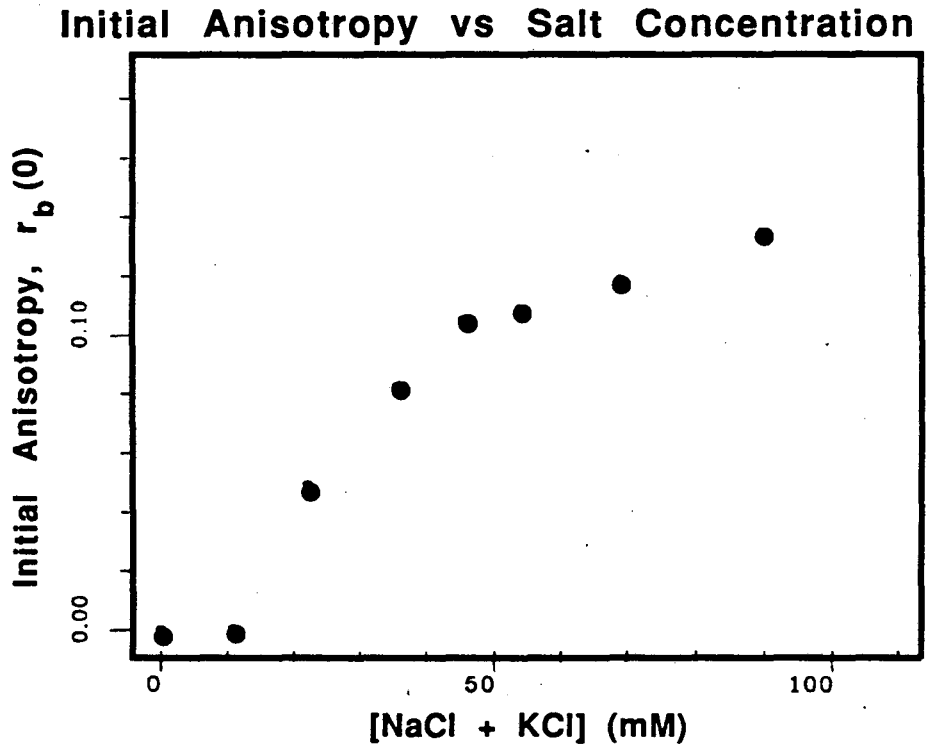

FIGURE 5-4: Best-fit initial anisotropies obtained from mudpuppy nuclei suspended in solutions of varying salt concentration. The anisotropy is plotted as a function of the NaCl+KCl concentration (mM). All buffers contained 5 mM Pipes (pH 7) and 3 mM EDTA, but they differed in their total NaCl+KCl concentration. The NaCl/KCl concentrations were: 72 mM KCl, 18 mM NaCl; 55 mM KCl, 14 mM NaCl; 43 mM KCl, 11 mM NaCl; 36 mM KCl, 9 mM NaCl; 29 mM KCl, 7 mM NaCl; 18 mM KCl, 4 mM NaCl; 9 mM KCl, 2 mM NaCl. The magnesium containing (mMB) solution gave the highest initial anisotropy, 0.19; this point is not plotted above.

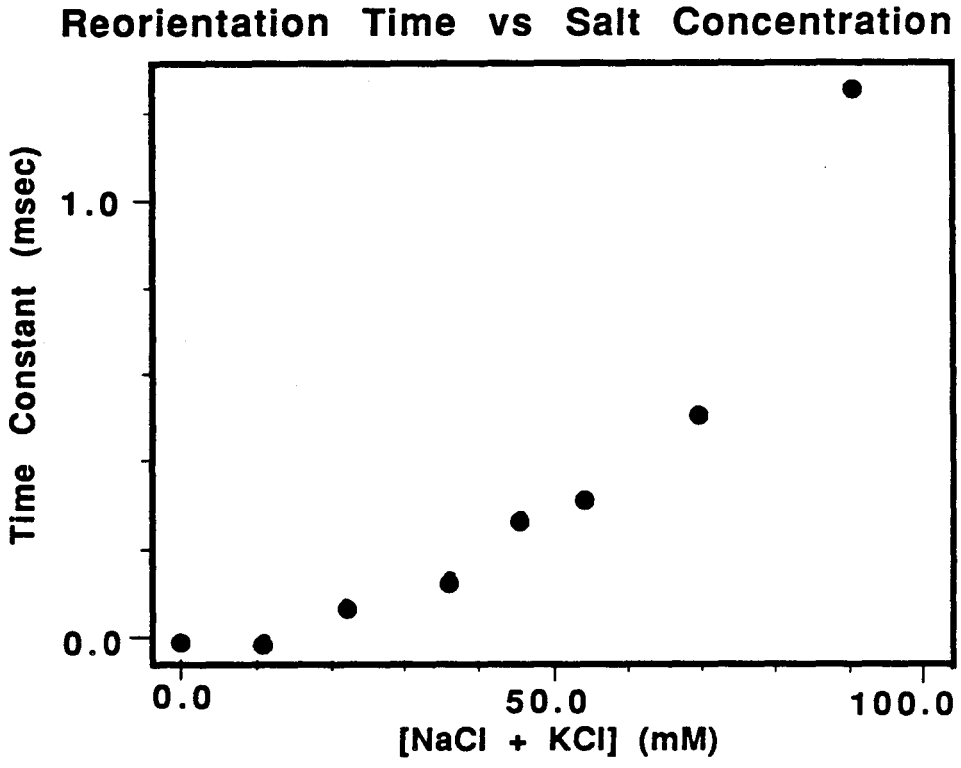

FIGURE 5-5: Best-fit relaxation times associated with the anisotropies shown in Fig. 4. The mMB point is not plotted because of its long (nominally infinite) relaxation time.

Both the initial anisotropy and the relaxation time are monotonically increasing functions of salt concentration. Comparison of the pFRAP data obtained from nuclei in physiological salt and in mEB shows that simple chelation of the Mg^{2+} converts a rotationally immobile sample into one with a correlation time of 1.2 milliseconds. In 11 mM monovalent salt, the chromatin is so mobile that the sample is completely depolarized before the bleach period has ended, i.e., $r_b(0) = 0$. These salt-induced changes in relaxation rate were reversible. Addition of monovalent or divalent cations to low salt nuclei resulted in the return of anisotropy.

Several interesting regions of transition can be identified in figures 4 and 5. Between 11 and 50 mM monovalent salt there is a steep increase in $r_b(0)$, accompanied by a gradual increase in τ. Apparently compaction is dramatically inhibiting the extent of rapidly

relaxing motion. From 60-100 mM monovalent salt $r_b(0)$ is essentially constant, but the time constant increases dramatically. Thus, as salt changes refine the structure of the 30 nm fibers the increase in rigidity is primarily manifest in the rate of decay of the slow large amplitude motions of chromatin. The initial anisotropy and time constant both increase markedly upon addition of Mg^{2+}, demonstrating that aggregation inhibits a broad temporal spectrum of chromatin motion.

(c) Diffusion of Chromatin in Sea Urchin Nuclei

We have compared the rotational mobility of chromatin fibers in sea urchin and mudpuppy nuclei at physiological salt concentrations (see Fig. 5-6). In both types of nuclei the chromatin is highly immobile; however the sea urchin samples exhibited about 25% less anisotropy than the mudpuppy samples. The best estimate for τ was 7 msec, showing that the chromatin of the more active nuclei reoriented a minimum of 6x faster than the chromatin from the inactive *Neclurus* cells.

We also attempted to study the salt dependence of chromatin dynamics in sea urchin nuclei. The mobility of sea urchin chromatin in nuclei again increased as the salt concentration was lowered. However, the sea urchin nuclei lysed when the salt concentration was decreased to about 50 mM, causing irreversible changes.

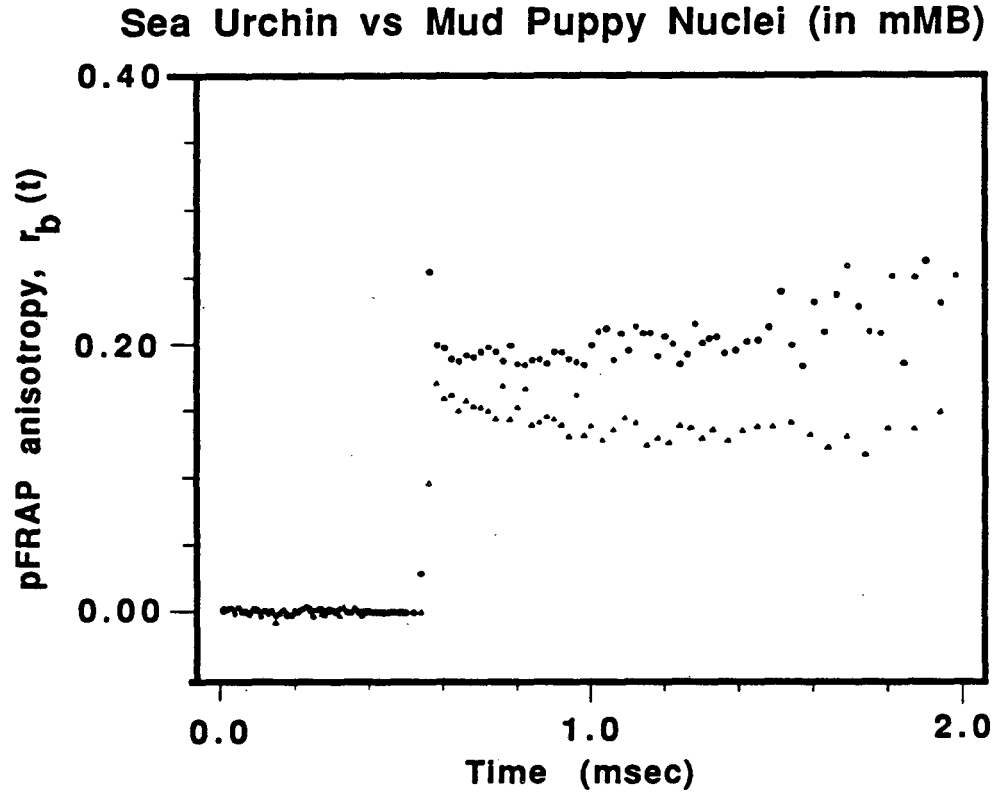

FIGURE 5-6: Comparison of the dynamics of sea urchin and mudpuppy nuclear chromatin in mMB. The initial value of the anisotropy and the time constant are both smaller in the sea urchin sample.

(d) *Diffusion of Digested Chromatin Fibers in Solution and Nuclei*

We have also measured the reorientational dynamics of nuclease digested chromatin fibers in solution and in nuclei. The anisotropy obtained from a 150 μg/ml solution of digested chromatin (M_w = 45 kbp.) in mEB is shown in Fig. 7. The initial anisotropy is 0.05 and $r_b(t)$ decays with a time constant of 100 μsec. Most of the digested fibers were not solubilized but remained in the nucleus. The nuclear-bound fragments have a slightly larger weight distribution (M_w = 53 kbp.) than those released into solution. The nuclear-bound fibers were much more immobile ($r_b(0)$ 0.14; r ≈ 2 msec) than their soluble analogues. Thus cleavage *per se* does not lead to increased mobility, but solubilization

does. Attachment of the insoluble chromatin to the nuclear matrix or the high concentration of the molecules left within the nucleus seems to be critical for immobilization.

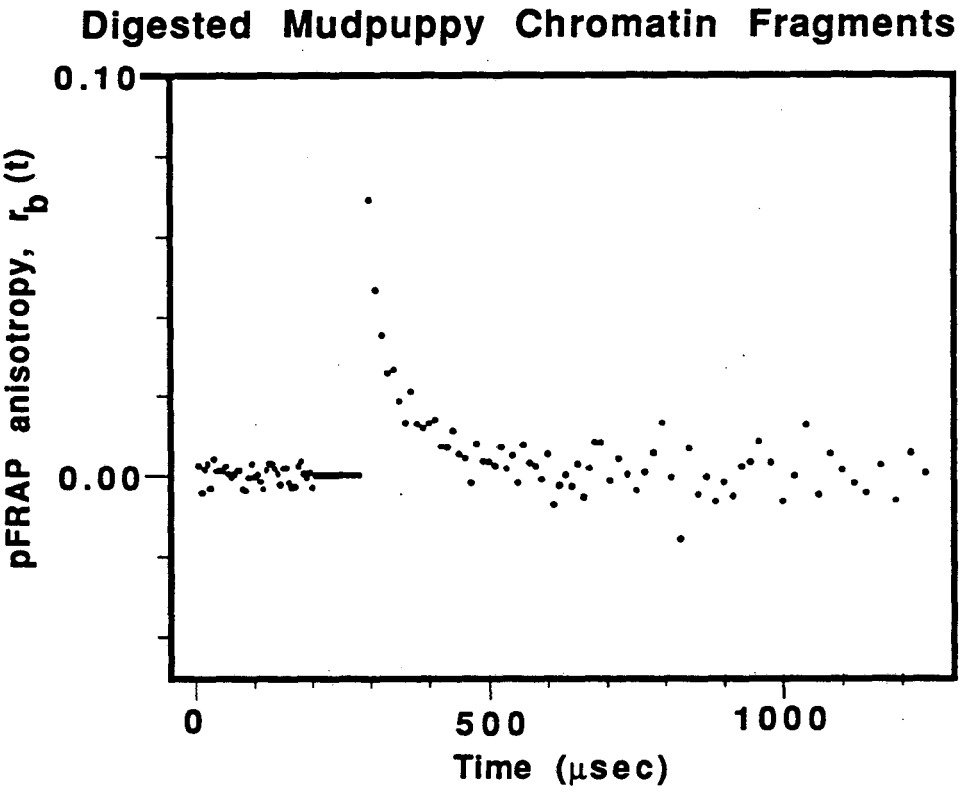

FIGURE 5-7: Anisotropy function obtained from digested mudpuppy chromatin fragments (150 μg/ml) in mEB. This sample contained chromatin fragments that were broadly distributed in molecular weight.

Discussion

(a) *Reorientation of Chromatin in Nuclei*

Because the focus here is on the dynamics of nuclear chromatin, we briefly discuss the spectrum of motions that chromatin is likely to exhibit and how this motion is manifest in a pFRAP experiment. Neither the static nor the dynamic flexibility of chromatin has been well studied. Previous measurements of dynamic flexibility have been limited to the

very rapidly (nanosecond) relaxing motions (Shindo *et al.*, 1980; Klevan *et al.*, 1979). Such studies have shown that the ethidium fluorophore wobbles when bound to DNA (Magde *et al.*, 1983) and that core and linker DNA twist on timescales shorter than approximately 100 ns (Wang *et al.*, 1982; Schurr and Schurr 1985; Ashikawa *et al.*, 1983; Hurley *et al.*, 1982; Hard *et al.*, 1988; Ashikawa *et al.*, 1985). These rapid components of the dynamics cause the initial value of the pFRAP anisotropy to be smaller than its static limiting value, 4/7.

Here we have extended previous studies of dynamic flexibility by systematically monitoring the μsec and msec internal motions of nuclear chromatin and by relating these slow dynamics to chromatin static structure. In this long time domain it is probable that independent rotations of internal segments and lateral deformations of chromatin give rise to the anisotropy decay. Other sources of μsec-msec reorientation certainly may exist; we cite the above two mechanisms explicitly as examples, because both have been demonstrated for naked DNA (Ding *et al.*, 1972; Schmitz and Schurr, 1973).

Another possible mechanism for motion, rigid body rotation of an entire nuclear chromosome, is unlikely to be the origin of the millisecond relaxation detected here. The calculated relaxation time for an entire mudpuppy chromosome containing $\geq 10^3$ megabase pairs lies far outside the time domain probed here. However, millisecond relaxation could represent independent rigid rotation of topologically independent units of chromatin. Paulson and Laemmli (1977) have estimated a domain to be 30-90 kbp. in size for HeLa tissue culture cells. Urodeles such as *Necturus* are estimated to have domains more than 10 times larger than those for human (HeLa) cells (MacGregor, 1980). If potential interactions with the nuclear matrix are neglected and a topological unit is assumed to fold back onto itself to form a freely diffusing rigid rod containing 500 kbp. (length about 2 μm; Williams *et al.*, 1986), the calculated long axis diffusion coefficient, $D_{\|}$, is 336 sec^{-1} (Broersma, 1960); $\tau_{\|}$ is of order $l/D_{\|}$ or 3 msec.

(b) *Salt Dependence of Chromatin Reorientation*

Salt-induced transitions of chromatin conformation and aggregation provide a model system with which to study the compaction and aggregation processes that occur during transcription, mitosis and replication. We have found that the internal dynamics of chromatin mirror the salt dependence of the internal structure and side-by-side aggregation of chromatin. Thus, we can study the cooperativity of the condensation of chromatin, the flexibility of the various conformers of chromatin, and the relative effectiveness of a given cation in producing condensation. The advantage of the pFRAP method is that dynamic measurements can be made when the chromatin is still present in the nucleus or, in principle, while in a living cell.

Studies of chromatin structure have shown that at physiological salt concentrations (high monovalent salt and in the presence of Mg^{2+}) chromatin exists as a compact 30 nm fiber and that these fibers are packed together side-by-side (aggregated). The pFRAP data reported here show that the motion of the linker region is very restricted under these conditions. (Our signal is expected to reflect primarily linker dynamics because it has been shown that ethidium binds preferentially to this region of chromatin if the level of dye labeling is kept low (Paoletti *et al.*, 1977; Erard *et al.*, 1979; Genest *et al.*, 1981). Specifically, we find that in physiological buffers the pFRAP anisotropy is constant and large (r_b= 0.2); this result indicates that the linker DNA is immobilized on time scales that range between 10 μsec and 2 msec. However, our data also show that fluorophores bound to aggregated fibers retain a substantial amount of localized mobility; these local, rapidly relaxing motions cause deviation of $r_b(0)$ from the rigid limit, 4/7. This "fast" depolarization seen in the pFRAP experiments is probably due to a combination of dye wobble and twisting motions. Such rapid relaxation is ubiquitious; even in immobilized (dry) DNA samples the initial anisotropy is only 0.2 (see Chpt 3).

Electron microscopy and X-ray studies have shown that when Mg^{2+} is removed the 30 nm fiber is intact but the chromatin is dispersed (see, *e.g.*, Thoma *et al.*, 1979; Langmore and Paulson, 1983). Under these conditions we see in the optical microscope that the chromatin becomes uniformly dispersed throughout the nucleus (Fig. 5-8). The initial pFRAP anisotropy decreases to 0.14 and $r_b(t)$ decays characteristically to zero in about 1 msec.

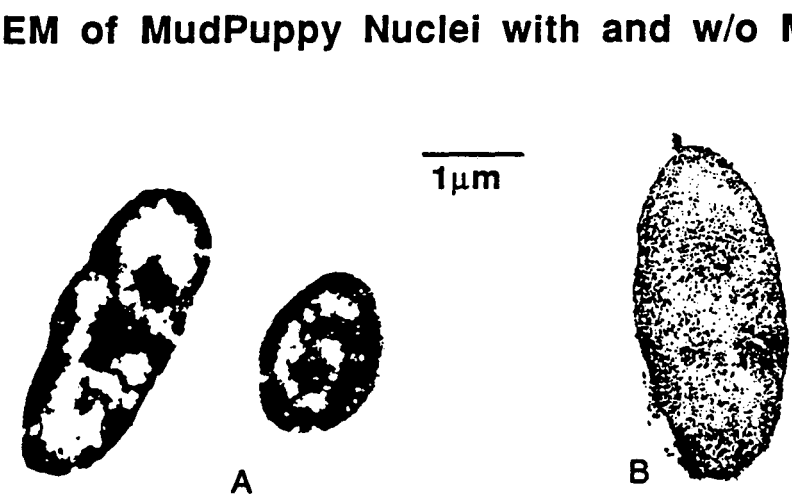

FIGURE 5-8: Electron Micrographs of mudpuppy nuclei in the presence of magnesium (A) and without magnesium (B). In both cases the 30nm fiber is intact (see figure 5-1), but the fibers are aggregated in the presence of magnesium and dispersed without it. The dispersion of the chromatin upon removal of magnesium can similarly be seen in the optical microscope, though of course with less magnification.

This millisecond relaxation may arise from slow lateral deformations of the 30 nm fiber that were suppressed when the chromatin was aggregated. Alternatively, as demonstrated in Section (a), this relaxation can also be attributed to a long axis rigid rod rotation of the topologically independent units that have been postulated to exist in nuclear chromatin (reviewed by Nelson *et al.*, 1986).

Upon dilution of the monovalent salt (and in the absence of Mg^{2+}) structural studies show that the compact 30 nm fiber opens to a "beads-on-a-string" (10 nm) conformation consisting of loosely packed nucleosome core particles connected by linker DNA. Upon reduction of monovalent salt concentration, the pFRAP initial anisotropy and the relaxation time monotonically decrease. Thus, as chromatin unfolds the extent of rapid internal reorientation increases, and the observable slow motions relax more rapidly. We attribute these changes to a gradual unfolding of the 30 nm conformer which leads to greater mobility of the linker DNA region. At the lowest salt concentration studied here, we find that the postbleach anisotropy has fallen to zero; thus in the low salt structure the linker DNA is relatively free to move. In fact, the low salt conformer is so flexible that its dynamics is too rapid to be measured by pFRAP.

For *in vitro* work it is important to identify the salt conditions that stabilize the physiologically relevant conformation of chromatin. Unfortunately, as Widom (1989) has noted, some experimental data suggest that there is a well-defined endpoint to the structural transitions of chromatin while other data suggest that no such endpoint exists. Here we have found that when measurements are made on intact nuclei, the pFRAP time constant, τ, continues to change as the salt concentration is varied between 11 and 90 mM monovalent salt. In contrast, our measurements of $r_b(0)$ as a function of salt concentration do show a semiplateau from 50 to 90 mM monovalent salt. Thus, the salt dependence of the *larger amplitude* internal dynamics of chromatin (the τ data) indicates that there is no sub-physiological endpoint to dynamic/structural change, while the salt dependence of the *smaller amplitude* internal motion (the $r_b(0)$ data) indicates that a sub-physiological endpoint may exist. To reconcile these two results we note that the salt-induced folding of chromatin might first damp the most rapid internal dynamics of the molecules and might damp the slower internal dynamics at higher salt concentrations. Overall, the pFRAP data indicate gradual structural change without a clearly delineated endpoint.

The pFRAP data both complement and confirm results obtained in a fluorescence depolarization (FD) study of the dynamics of ethidium bromide-stained linker DNA in nuclei (Ashikawa *et al.*, 1985). The FD experiments indicate that fast (nanosecond) motions (presumably twisting) are inhibited in intact 30 nm nuclear chromatin fibers. Our data show a similar supression of linker DNA dynamics upon 30 nm fiber formation, although, presumably we are seeing the same effect manifest by the slow motions of DNA.

Linear and saturation transfer EPR have also been used to examine the dynamics of nuclear chromatin and isolated chromatin fibers (Hurley *et al.*, 1982). It was found that a spin-labeled ethidium bromide intercalated in the linker region of chromatin fibers or nuclear chromatin is less mobile than a spin label intercalated into naked DNA. Hurley *et al.* report a 100 μsec rotational correlation time for nuclei in 5 mM $MgCl_2$, 20 mM Tris-HCl, 250 mM sucrose, but state that this figure may be too small because it is difficult to extract long-time dynamical data from computer simulations of EPR spectra. Because Hurley *et al.* have used a viscous buffer and different ionic conditions it is somewhat difficult to compare their result with ours.

(c) Correlation with Studies of Chromatin Structure

Electron microscopy has shown that all of the chromatin fibers are extensively unfolded below about 15 mM monovalent salt (Thoma *et al.*, 1979). Here we find that at 11 mM monovalent salt chromatin exists in a very flexible conformation characterized by zero postbleach anisotropy. Between 11 mM and 50 mM monovalent salt $r_b(0)$ increases rapidly and there is a gradual increase in τ. These data indicate that a substantial fraction of the chromatin is becoming less flexible, but the compaction is not yet complete. This observation is consistent with electron microscopy, which shows a disappearance of the "beads-on-a-string" structure and the formation of rather loose, disordered 30 nm fibers

(Thoma *et al.*, 1979). The sedimentation coefficient of chromatin also increases abruptly as the monovalent salt concentration approaches 50 mM (Butler and Thomas, 1980). From 50-90 mM monovalent salt the extent of rapid relaxation is nearly constant, while the time constant increases dramatically. Electron microscopy has shown a tightening of the structure in this salt range (Thoma *et al.*, 1979). When Mg^{2+} is added (at 90 mM monovalent salt) $r_b(0)$ and r increase quickly. It is in this ionic range that the chromosome fibers become less soluble *(i.e.*, aggregate) with few, if any, changes in internal structure (Langmore and Paulson, 1983). Thus it is reasonable to attribute the first pFRAP salt transition to packing of the nucleosomes, and the second transition to aggregation of the fibers.

(d) *Concentration Dependence of Chromatin Dynamics*

The dynamics of DNA in dilute solution has been the subject of extensive experimental study (for reviews see Hagerman, 1988; Shibata *et al.*, 1985; Frank-Kamenetski, 1981). However, in the nuclei of eukaryotic cells, in the nucleoli of prokaryotic cells and in bacterial phage heads, the concentration of chromatin/DNA is enormously high (Kellenberger, 1987; Livolant and Maestre, 1988); it is also, therefore, of interest to monitor the dynamics of nucleic acids in concentrated solution and to see if interparticle interactions modify the motions exhibited by these molecules *in vivo.*

Interaction-induced modification of the translational motion of nucleic acids is a moderately well-studied phenomenon (see among others Sorlie and Pecora, 1988 and Scalettar *et al.*, 1989, and refererences cited therein). However, the effects that interactions have on the reorientational motion of nucleic acids are much less well characterized. Rill *et al.* (1983) have conducted ^{31}P NMR and ^{13}C NMR studies of concentrated, liquid crystalline phases of short DNA molecules and have found that at critical DNA concentrations the local (nanosecond) motions of DNA that are monitored by

NMR are not present. For DNA of several hundred base pairs in length these critical concentrations are on the order of 100 mg/ml.

Interaction-dependent modification of the reorientational motion of DNA has also been detected, by Ashikawa *et al.* (1984), in the bacteriophage head. DNA in phage heads is believed to be ordered in a closely packed structure and, therefore, the phage is an in vivo system in which one might expect to see marked inhibition of the mobility of DNA. Ashikawa *et al.* have detected such inhibition of DNA mobility in wild type and mutant (DNA deficient) λ phage, and they have correlated dynamic changes with structural changes measured by X-ray scattering. On the timescales (<100 ns) accessible to an FD experiment the DNA in both phages was much less mobile than DNA in dilute solution. Moreover, the DNA in wild type phage was found to be more immobile than the DNA in the mutant (DNA deficient) phage. Thus, these data indicate that *in vivo* DNA concentrations are an important determinant of the dynamics of DNA.

Here we have also shown that at physiological salt (mMB) concentrations the (microsecond and millisecond) internal motions of chromatin are largely inhibited by intermolecular interactions (see Fig. 5-2). The extent to which nuclear chromatin is immobilized at physiological salt concentrations can perhaps best be appreciated by noting that the pFRAP anisotropy obtained from nuclear chromatin fibers in mMB is the same as is obtained from DNA that is immobilized by drying it down onto a quartz coverslip (see Chpt 3) We attribute the rotational immobilization of nuclear chromatin to fiber aggregation because magnesium, which immobilizes the chromatin (see Fig. 5-2, nuclei in mMB, compared to Fig. 5-3, nuclei in mmB), is believed to induce aggregation of chromatin — which we could see in the microscope — but not to alter its monomeric structure. The change in time constant should therefore reflect a local change in chromatin concentration rather than a structural change. We conclude that the observed increase in τ indicates that intermolecular aggregation suppresses intramolecular motion.

It is also worth noting that the 45 kbp. digested chromatin fibers are much more mobile when suspended in solution at low concentration (150 μg/ml) than when retained at high concentration in the nucleus. This effect may arise from concentration-induced damping of motion or interaction of the chromatin with the nuclear membrane.

(e) *Comparison of Digested Chromatin and Naked DNA*

We have also compared the microsecond reorientational motion of solubilized 30 nm chromatin fibers of relatively well-defined length (≈45 kbp.) to that of a 50 kbp. naked DNA from phage λ (data not shown). The concentration of DNA in both of the samples studied was 150 μg/ml. In such a relatively dilute solution, a sample of naked DNA exhibits essentially no anisotropy at the end of a 10 μsec bleaching pulse. In contrast the chromatin sample retains a small but significant anisotropy at the end of the bleach ($r_b(0)$=0.05); this anisotropy then decays with a time constant of about 100 μsec.

If the 45 kbp. fibers were to behave like rigid rods with a mass per unit length of 170 kDa/nm and a diameter of 30 nm (Williams and Langmore, submitted) their long axis and endover-end rotational diffusion coefficients would be 3300 sec^{-1} and 80 sec^{-1}, respectively. Thus, the 100 μsec decay time measured here is of the same order of magnitude as the long axis relaxation time of the digested fibers. The magnitude of $r_b(0)$ will primarily reflect internal motion of chromatin, rather than global reorientation. Internal motions are not expected to be significantly affected by interactions between chromatin molecules at concentrations as low as 150 μg/ml. Therefore, because samples containing 30 nm digested chromatin fibers retain more anisotropy at the end of the bleach than do solutions containing naked DNA, it is probable that compaction of DNA into the 30 nm fiber acts to suppress internal motions which would normally be manifest in naked DNA.

(f) *Comparison of Dynamics of Quiescent and Active Nuclei*

We have studied the dynamics of both sea urchin and mudpuppy chromatin because several lines of evidence suggest that chromatin in sea urchin is less condensed than in mudpuppy. For example, one can visually detect this difference under the optical microscope. Nuclease digestion experiments show that sea urchin embryo chromatin is much more susceptible to enzymatic attack by micrococcal nuclease than mudpuppy erythrocyte chromatin (Jan Fronk & John Langmore, unpublished results). Of course, embryonic sea urchin nuclei are transcriptionally active while mudpuppy nuclei are inactive.

Here we have also demonstrated that sea urchin chromatin is more mobile than mudpuppy chromatin at physiological salt concentrations. We find that the mudpuppy anisotropy is static and equal to 0.2. In contrast, the initial value of the sea urchin anisotropy is 0.15 and $r_b(t)$ decays slightly. These dynamic differences are certainly consistent with the underlying biological differences and may indeed be a direct consequence of the latter.

(g) *Comparison with Dynamics in Congested Gel Solutions*

Recently, pFRAP has also been used to study the reorientational motion of naked DNA molecules in agarose gels (Chapter 6 and Scalettar *et al.*, 1990). The gel experiments indicate that under moderately congested conditions the rapidly relaxing reorientational motions of naked DNA molecules are largely unperturbed. Specifically, it is found that in gels that are 5% agarose by weight, the initial anisotropy is <0.03, or about 1/5 that measured in the unaggregated nuclei solutions. Hence, gels do not damp out many of the smaller amplitude motions of naked DNA that lead to depolarization during the bleach pulse. The relative immobility of the chromatin samples studied here

seems to be a consequence of both the inherent rigidity of the chromatin fibers (Section b) and the concentration of fibers within the nucleus (Section d).

Conclusions

We have monitored chromatin reorientation in intact nuclei as a function of salt concentration and local chromatin concentration. It is found that nuclear chromatin becomes progressively more rigid as it undergoes a salt-induced conformational transition from an extended "beads-on-a-string" structure to a compact 30 nm fiber. The folding process proceeds gradually as the salt concentration is varied and does not appear to reach any well-defined subphysiological end point. Local increases in chromatin concentration, such as those that are induced by the side-by-side packing (aggregation) of chromatin, were found markedly to inhibit chromatin reorientation. Hence, the data presented here show that cellular chromatin, which is believed to exist primarily in the aggregated state, is highly immobile. We suggest that the immobilization is due to suppression of internal motion by high local concentration. In the future we hope to use the pFRAP technique to monitor chromatin dynamics directly in living cells and, thereby, to study the effects that mitosis and the binding of enzymes or drugs have on chromatin dynamics.

References

Ashikawa, I., Kinosita, K., Ikegama, A., Nishimura, Y., Tsuboi, M., Watanabe, K., Iso, K. & Nakano, T. (1983) *Biochemistry* 22, 6018-6026.

Ashikawa, I., Furuno, T., Kinosita, K., Ikegami, A., Takahashi, H. & Akutsu, H. (1984). *J. Biol. Chem.* 259, 8338-8344.

Ashikawa, I., Kinosita, K., Ikegami, A., Nishimura, Y. & Tsuboi, *M. (* 1985). *Biochemistry* 24,1291 -1297.

Bevington, P.R. (1969). *Data Reduction and Error Analysis in the Physical Sciences* pp. 237-239 McGraw-Hill Book Co., New York.

Broersma, S. (1960). J. *Chem. Phys.* 32, 1626-1631.

Butler, P.J.G. (1983). *CRC Crit. Rev. Biochem.* 15, 57-91.

Butler, P.J.G. & Thomas, J.O. (1980). J. *Mol. Biol.* 140, 505-529.

Ding, D., Rill, R. & Van Holde, K.E. (1972). *Biopolymers* 11, 2109-2124.

Erard, M., Das, G.C., de Murcia, G., Mazen, A., Pouyet, J., Champagne, M. & Duane, M. (1979). *Nucleic Acids Res. 6,* 3231-3252.

Felsenfeld, G. & McGhee, J.D. (1986). *Cell* 44, 375-377.

Finch, J.T. & Klug. A. (1976). *Proc. Natl. Acad. Sci. USA* 73, 1897-1901.

Frank-Kamenetskii, M.D. (1981). *Comments Mol. Cell. Biophys. 1,* 105-114.

Fulton, A.B. (1982). *Cell* 30, 345-347.

Genest, D., Sabeur, G., Wahl, P. & Auchet, J-C. (1981). *Biophys. Chem.* 13, 77-87.

Hagerman, P.J. (1988). *Ann. Rev. Biophy. Biophys. Chem.* 17, 265-286.

Hard, T., Nielson, P.E. & Norden, B. (1988). *Eur. Biophys.* J. *16,* 231-241.

Hurley, I., Osei-Gyimah, P., Archer, S., Scholes, P. & Lerman, L.S. (1982). *Biochemistry 21,* 4999-5009.

Kellenberger, E. (1987). *TIBS* 12, 105-107. Klevan, L., Armitage, I.M. & Crothers, D.M. (1979). *Nucleic Acids Res. 6,* 1607-1616.

Langmore, J.P. & Paulson, J.R. (1983). *J. Cell Biol. 96,* 1120-1131.

Livolant, F. & Maestre, M.F. (1988). *Biochemistry* 27, 3056-3068. MacGregor, H.C. (1980). *Heredity 44,* 3-35.

Magde, D., Elson, E.L., Webb, W.W. (1974) *Biopolymers* 13, 29-61.

Magde, D., Zapalla, M., Knox, W.H. & Nordlund, T.M. (1983). J. *Phys. Chem.* 87, 3286-3288.

McGhee, J.D., Rau, D.C., Charney, E. & Felsenfeld, G. (1980). *Cell* 22, 87-96.

McGhee, J.D., Nickol, J.M., Felsenfeld, G. & Rau, D.C. (1983). *Cell* 33, 831-841.

Nelson, W.G., Pienta, K.J., Barrack, E.R. & Coffey, D.S. (1986). *Ann. Rev. Biophys. Biophys. Chem.* 15, 457-475.

Olins, D.E. & Olins, A.L. (1972). J. *Cell Biol.* 53, 715-736.

Paoletti, J., Magee, B.B. & Magee, P.T. (1977). *Biochemistry 16,* 351-357.

Paulson, J.R. & Laemmli, J.K. (1977). *Cell* 12, 817-828.

Rill, R.L., Hilliard, P.R. Jr. & Levy, G.C. (1983). J. *Biol. Chem* 258, 250-256.

Rill, R.L. (1986). *Proc. Natl. Acad. Sci. USA* 83, 342-346.

Scalettar, B.A., Selvin, P.R., Axelrod, D., Hearst, J.E., & Klein, M.P. (1988). *Biophys. J.* 53, 215-226.

Scalettar, B.A., Hearst, J.E., & Klein, M.P. (1989). *Macromolecules* 22, 4550-4559.

Scalettar, B.A., Selvin, P.R., Axelrod, D., Klein, M.P. & Hearst, J.E. (1990) *Biochemistry* 29, 4790-4798.

Schmitz, K.S. & Schurr, J.M. (1973). *Biopolymers* 12, 1543-1564.

Schurr, R.L. & Schurr, J.M. (1985). *Biopolymers* 24, 1931-1940.

Selvin, P.R., Scalettar, B.A., Langmore, J.P., Axelrod, D., Klein, M.P.& Hearst, J.E., (1990) A Polarized Photobleaching Study of Chromatin Reorientation in Intact Nuclei. *J. Mol. Biol.* 214(4), 911-922.

Sen, D. & Crothers, D.M. (1986). *Biochemistry* 25, 1495-1503.

Shibata, J.H., Fujimoto, B.S. & Schurr, J.M. (1985). *Biopolymers* 24, 1909-1930.

Shindo, H., McGhee, J.D. & Cohen, J.S. (1980). *Biopolymers 19,* 523-537.

Smith, M.F., Athey, B.D., Williams, S.P. & Langmore, J.P. (1990). *J. Cell. Biol.* 110, 245-254.

Sorlie, S.S. & Pecora, R. (1988). *Macromolecules* 21, 1437-1449.

Suau, P., Bradbury, E.M. & Baldwin, J.P. (1979). *Eur. J. Biochem. 97,* 593-602.

Thoma, F., Koller, Th. & Klug, A. (1979). *J. Cell. Biol.* 83, 403-427.

Van Holde, K.E. (1989). *Chromatin* Springer-Verlag, New York.

Velez, M. & Axelrod, D. (1988). *Biophys. J.* 53, 575-591.

Wang, J., Hogan, M. & Austin, R.H. (1982). *Proc. Natl. Acad. Sci. 79,* 5896-5900.

Williams, S.P., Athey, B.D., Muglia, L.J., Schappe, R.S., Gough, A.H. & Langmore, J.P. (1986) *Biophys. J.* 49, 233-248.

Widom, J. (1986). *J. Mol. Biol.* 190, 411-424.

Widom, J. (1989). *Annu. Rev. Biophys. Biophys. Chem. 18,* 365-395.

Workman, J.L. & Langmore, J.P. (1985). *Biochemistry 24,* 4731-4738.

Chapter Six

DNA Reorientation in Agarose Gels

A pFRAP Study

Abstract:

Polarized fluorescence recovery after photobleaching (pFRAP) has been used to study the internal dynamics of relatively long DNA molecules embedded in gels ranging in concentration from 1%- 5% agarose. We find that the rapid, short wavelength motions of DNA are relatively unhindered, even in the highest gel concentrations, but that the gel matrix does dampen the larger amplitude, slower (micro- to millisecond) modes. Qualitatively, the results can be explained if one assumes that motions on the order of, and larger than, the gel pore size are damped out, and those motions smaller than the pore size are relatively unperturbed.

Introduction:

Gel electrophoresis is widely used to separate molecules of different sizes. Because of its importance, much experimental (reviewed by Cantor *et al.*, 1988) and theoretical (Deutsch, 1988; Lerman and Frisch, 1982; Lumpkin *et al.*, 1985; Noolandi *et al.*, 1989) work has been done to understand the separation mechanism. Many of the molecular details, however, remain uncharacterized, although in a general sense it is known that separatation is achieved because interactions between the gel matrix and the DNA impart a size dependence to the electrophoretic mobility (reviewed by Cantor *et al.*, 1988). In our

experiment, we examine the Brownian reorientation of DNA in agarose gels in the absence of an electric field.

Translation of DNA in gels has been studied by observing the motion of "bands," or large populations of DNA molecules. For constant (electric) field gel electrophoresis, it has been shown that the electrophoretic mobility of DNA generally increases with field strength and temperature, and generally decreases with molecular weight, gel concentration and ionic strength (Hervet and Bean, 1987). Studies of DNA migration in pulsed-field gels have shown similar effects (Mathew *et al.*, 1988).

Video microscopy, which permit visualization of individual long DNA molecules has revolutionized the understanding of DNA motion in gels in the last few years (Smith *et al.*, 1989; Schwartz and Koval, 1989; Houseal *et al.*, 1989). In the absence of an applied field, the large DNA's look like random coils, more or less immobilized by the gel matrix (Smith *et al.*, 1989, using 1.5% agarose). In the presence of an electric field, the DNA elongates and migrates in the direction of the field.

Video microscopy, however, has rather poor temporal resolution — on the order of 10 frames a section, or 100msec. Consequently, the technique cannot resolve many of the internal motions of DNA, which occur on the nanosecond to millisecond time scale, and are thought to be important in the separation achieved with modern electrophoretic methods, such as field inversion electrophoresis (Carle *et al.*, 1986; Noolandi *et al.*, 1989). While the internal modes of isolated DNA have been studied (see previous chapters), the dynamics can be greatly affected when the DNA is placed in a congested environment, such as a gel, or very concentrated DNA solutions (Rill *et al.*, 1983).

What is therefore needed is a technique capable of temporally resolving the internal modes of DNA in a gel. We present here such a study, using polarized fluorescence after recovery (pFRAP), which has 5msec resolution, and sufficient sensitivity to yield good

signal to noise with small amounts of DNA, even in the highly scattering environment of a gel. Because pFRAP is a fluorescence technique, the signal arises solely from the labelled DNA — the background agarose does not contribute. Chu *et al.*, (1989) has recently used a photobleaching technique to measure (translational) electrophoretic mobility of DNA in agarose gels.

Theory:

As discussed in Chapter 3 on triplet spectroscopy, the pFRAP technique uses a brief (a few microsecond) pulse of intense, polarized light to preferentially bleach those dye molecules with absorption dipole moments oriented roughly parallel to the polarization of the light. This polarized photobleaching produces an anisotropic distribution of unbleached fluorophores in the sample. The evolution back to an isotropic distribution, caused by rotational diffussion and rotation-independent chemical processes, is monitored with a weak probe beam, polarized either parallel or perpendicular to the polarization of the bleach pulse. The probe beam is sufficiently intense to excite fluorescence from the sample (the signal), but weak enough not to cause additional photobleaching.

Taking the ratio of fluorescence in the parallel and perpendicular modes isolates the rotational component of the recovery, in this case due to Brownian reorientation of the fluorophore/DNA complex. The ratio, R(t), is defined as the post-bleach fluorescence minus the pre-bleach fluorescence in the parallel mode, divided by the same quantity in the perpendicular mode.

$$R(t) = \Delta F_{\parallel}(t)/\Delta F_{\perp}(t)$$

where

$$\Delta F_{\parallel}(t) = F_o - F_{\parallel}(t) \qquad \Delta F_{\perp}(t) = F_o - F_{\perp}(t).$$

F_o is the pre-bleach fluorescence with just the probe beam on, and $F_i(t)$ is the post-bleach fluorescence in the relevant mode.

Qualitatively, the faster the Brownian rotational motion, the quicker the ratio approaches one. Reversible photobleaching does not contribute to the ratio, except in the second order effect to reduce the bleach depth at all times, which decreases the signal to noise.

Instead of a simple ratio, the anisotropy can be formed, in analogy with fluorescence depolarization experiments. The choice of the ratio or the anisotropy function is purely a matter of personal taste. We will use the anisotropy.

$$r_b = [\Delta F_{\parallel}(t) - \Delta F_{\perp}(t)]/[\Delta F_{\parallel}(t) + 2\Delta F_{\perp}(t)]$$

Velez and Axelrod (1988) have shown that the pFRAP technique provides an accurate measure of rotational relaxation rates in well-defined control samples of fluorescently labelled spherical beads.

Although a general and elegant theory can be written for the time evolution of the anisotropy (see chapter 3 and Velez and Axelrod, 1988) in terms of multiple diffusion constants, here we simplify the analysis by fitting the data to a single exponential decay with two adjustable parameters — the initial anisotropy and the time constant. This is clearly crude, but justified because the quality of data does not warrant multi-exponential fits and because no quantitative theory presently exists for the complex case of DNA dynamics.

The initial anisotropy gives an indication of the extent of rapid motions (<5usec) that take place during the bleach pulse. $r_b(0) = 4/7 = 0.57$ indicates the sample molecules are immobile during the pulse; $r_b(0) = 0$ indicates they have completely reoriented. If $r_b(0)$ lies between these two extrema, the molecules have undergone some restricted amplitude motion during the bleach.

Materials and Methods

Sample Preparation:

DNA: pBR322, primarily in closed circular form, and linear phage λ DNA and was obtained from Bethesda Research Laboratories. An 18 base pair oligomer, used as a control, was synthesized in our laboratory with a DNA synthesizer (Biosearch) and then purified on a standard polyacrylamide gel.

DNA was labelled with ethidium bromide (Sigma Chemicals) by combining appropriate amounts of stock DNA with an ethidium bromide solution and then allowing the dye to intercalate in the dark. Approximately one dye molecule was bound per 200 DNA base pairs when using phage λ or pBR322 DNA . On the average one dye was bound to each oligomer.

Gels: DNA gels were prepared as follows. Several milliliters of a concentrated low-melting-temperature (LMT) agarose (Sigma Chemicals, lot #115F-0666, $M_r = 0.08$) solution, buffered with 0.089 M Tris, 0.089 M Boric acid, 0.0032 M EDTA, pH = 8.3, were prepared by stirring and warming on a hot plate. Simultaneously, a solution of ethidium bromide-stained DNA was heated in a water bath on the hot plate. The volume of this DNA solution and the concentration of agarose in the gel were adjusted to ensure that when the two solutions were combined the agarose concentration (weight/volume) would have the final desired value; the final DNA concentration in all the samples was 80 μg/ml.

The gel and DNA were combined and gently mixed (not stirred) until the sample was homogenous — we chose LMT agarose because it solidified sufficiently slowly to permit thoroughly mixing of the DNA and agarose. Before beginning an experiment these gel/DNA mixtures were warmed (melted) and an aliquot was placed on a quartz coverslip and allowed to solidify in a nitrogen saturated glove bag (see below, deoxygenation). No degradation of DNA was detected even after several warming and cooling cycles.

Deoxygenation of DNA Samples: Samples were deoxygenated to increase the reversible recovery lifetime. Samples were manipulated in a nitrogen-saturated glove bag and buffers were deoxygenated by bubbling nitrogen or argon through them for approximately 15 minutes. Deoxygenated agarose samples were sandwiched between two quartz coverslips separated by a thin (approximately 100um) thick teflon spacer and held together in a custom made aluminum holder. All interfaces were coated with vaseline or vacuum grease, making the unit airtight.

pFRAP Apparatus and Experimental Methods:

The pFRAP apparatus has been described elsewhere (see Chapter 3 and Velez and Axelrod, 1988; Scalettar *et al.*, 1988, 1990). Since the first published description, the microscope stage has been automated with a microstepping motor and AT-compatible computer. After each round of bleach and probe, the stage is now horizontally translated about 3mm, approximately the beam diameter. Translation of the stage ensures that no point on the sample is exposed to bleaching light more than once.

For all the agarose experiments we used a 5μsec bleach pulse. The pre-and post-bleach fluorescence signals were recorded for 50 and 200 (5μsec) time points, respectively. The standard pre-bleach fluorescence photon count rate ranged between 50,000 and 100,000 counts/sec. The signal was averaged approximately 100,000 times (for several hours) to achieve good signal-to-noise.

The light intensity was adjusted to produce a 25% to 40% bleach in the sample; a larger bleach was avoided because $r_b(0)$ decreases when the bleach is deep (see chapter 3, Velez and Axelrod, 1988). The bleach was produced by a 15watt Coherent argon-ion laser running at 2 watts output power on the 514.5nm line. The beam was sometimes attenuated slightly, e.g. with an 0.2-0.4 O.D. filter. After passing through numerous pinholes and optical elements, approxiately 100mW of power actually impinges on the sample in the microscope. An epi-illumination 10x glycerine immersion objective with a numerical aperture of 0.5 was used to focus light onto the sample and collect fluorescence. Under such conditions, calculations show that negligible light-induced heating occurs in the sample (Chapter 3, Velez and Axelrod, 1988; Scalettar *et al.*, 1988).

Data Analysis: The pFRAP anisotropy function was computed from the either the raw pFRAP data, $F_{\parallel}(t)$ and $F_{\perp}(t)$, or data that were given a five point quadratic smooth (Savitzky and Golay, 1964). The anistropy function was fit to a single exponential. Curvefits were obtained using a modified version of the program Curfit (Bevington, 1969). This program uses all data points in obtaining the best-fit parameters, with the appropriate weight attached to each data point according to its statistical significance.

Results

Rotational Diffusion of Short Oligomers in Agarose Gels: The rotational diffusion of an 18 base pair oligomer in agarose was monitored with the pFRAP technique. This allows us to follow the reorientation of a small DNA molecule in a matrix. Figure 7-1a shows that the individual curves, $F_{\parallel}(t)$ and $F_{\perp}(t)$, obtained from a 5% agarose/oligomer sample are essentially indistiinguishable. The anisotropy computed from the data is shown in Figure 7.1b — it is flat and zero over the entire time regime examined.

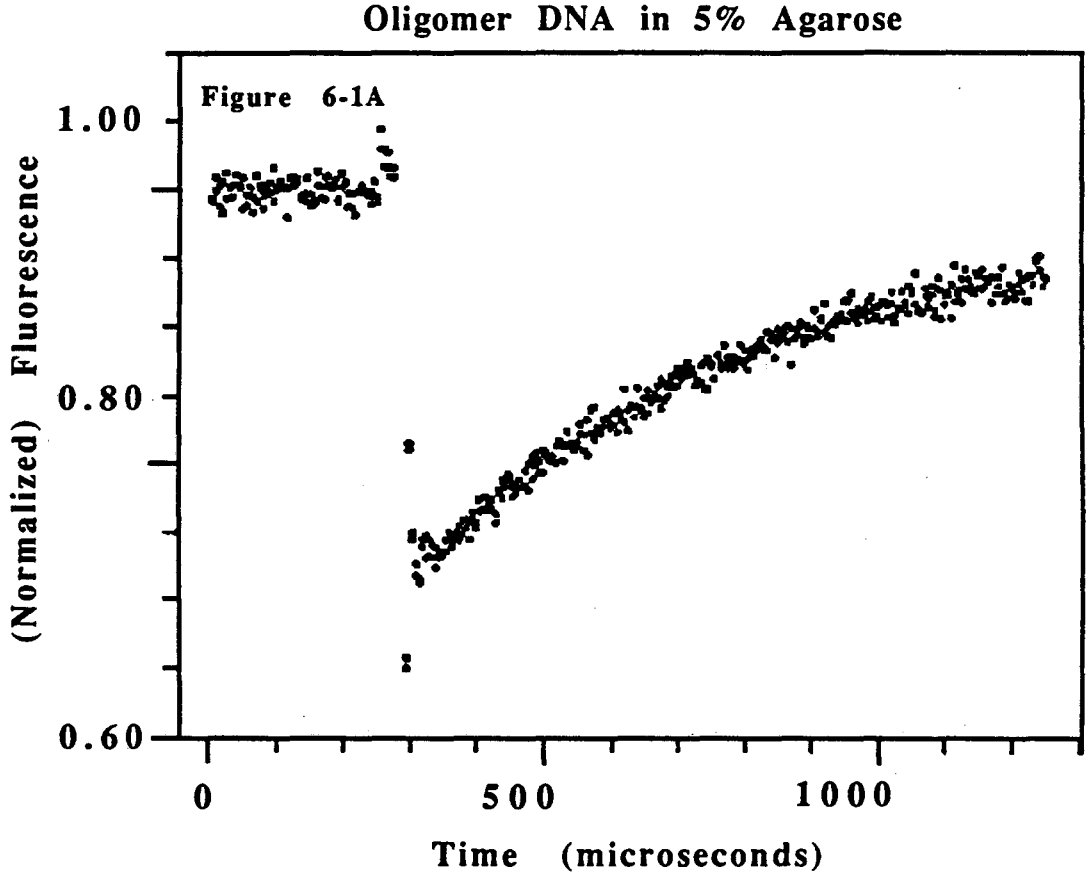
Oligomer DNA in 5% Agarose
Figure 6-1A
1.00
0.80
0.60
(Normalized) Fluorescence
0
500
1000
Time (microseconds)

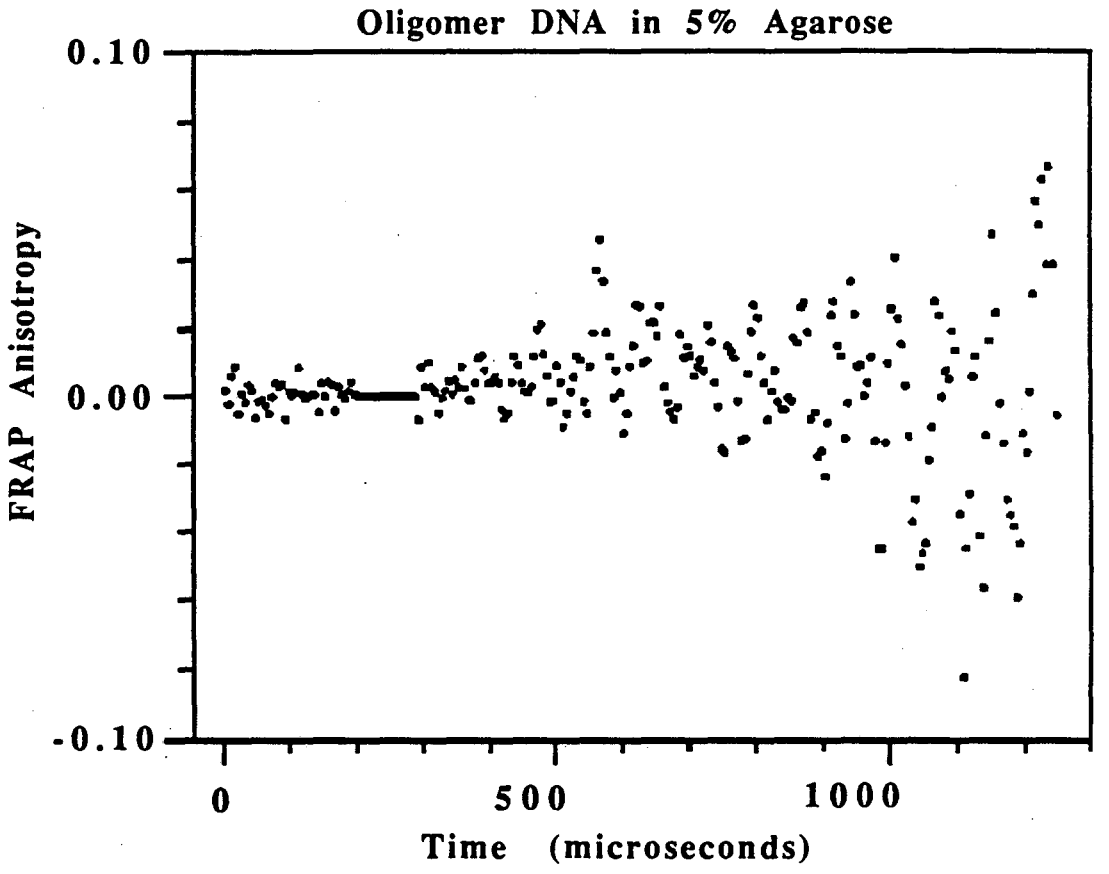

FIGURE 6-1: (A) Polarized photobleaching curves $F_{\parallel}(t)$ (closed circles) and $F_{\perp}(t)$ (open circles) obtained from an ethidium bromide stained oligomer embedded in a 5% agarose gel. The individual curves superimpose and, hence, the numerator, $\Delta F_{\parallel}(t) - \Delta F_{\perp}(t)$, of the anisotropy function, $r_b(t)$, is zero over the entire time regime examined (B).

Rotational Diffusion of pBR322 in Agarose Gels: This experiment examines the reorientational motion of a typical circular DNA plasmid in an agarose gel. The pFRAP data obtained from a sample consisting of the plasmid PBR 322 (≈4300 bp.) embedded in a 5% agarose gel are shown in Fig. 7-2a and b.

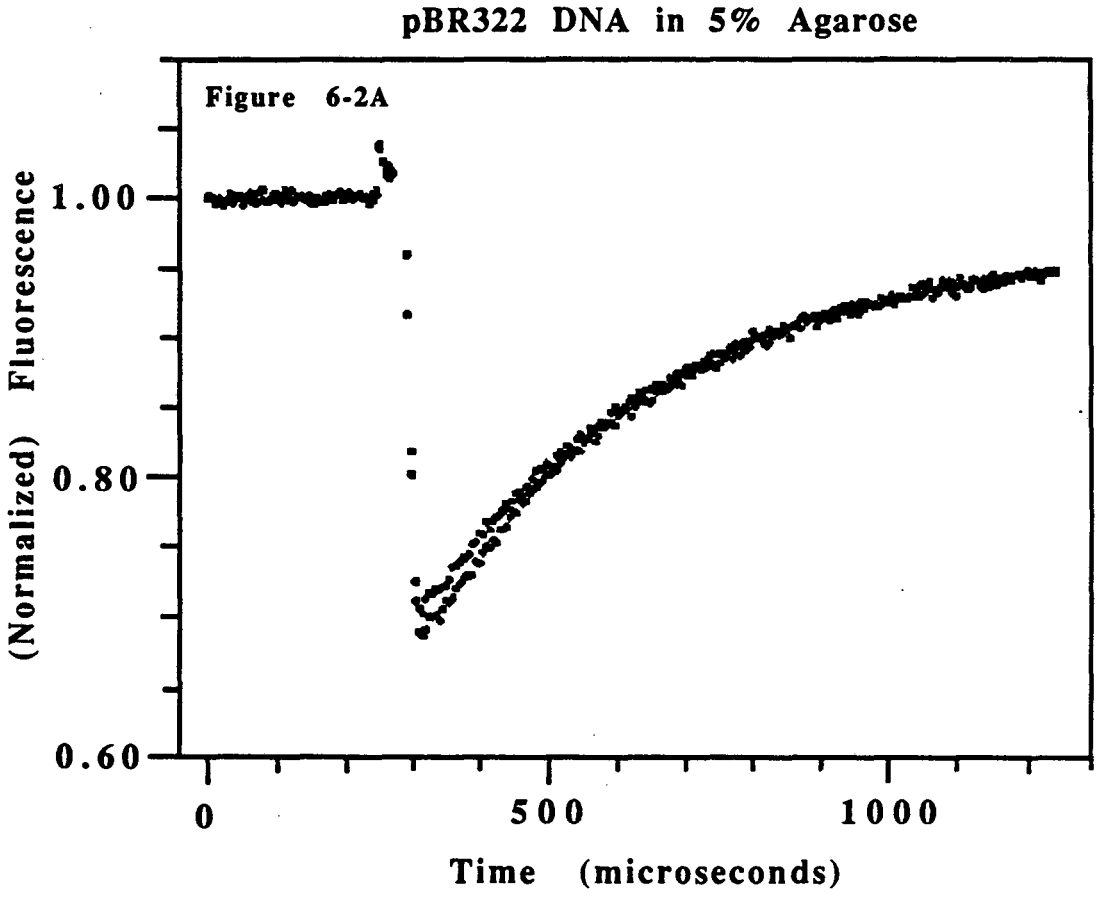
pBR322 DNA in 5% Agarose
Figure 6-2A
(Normalized) Fluorescence
1.00
0.80
0.60
0
500
1000
Time (microseconds)

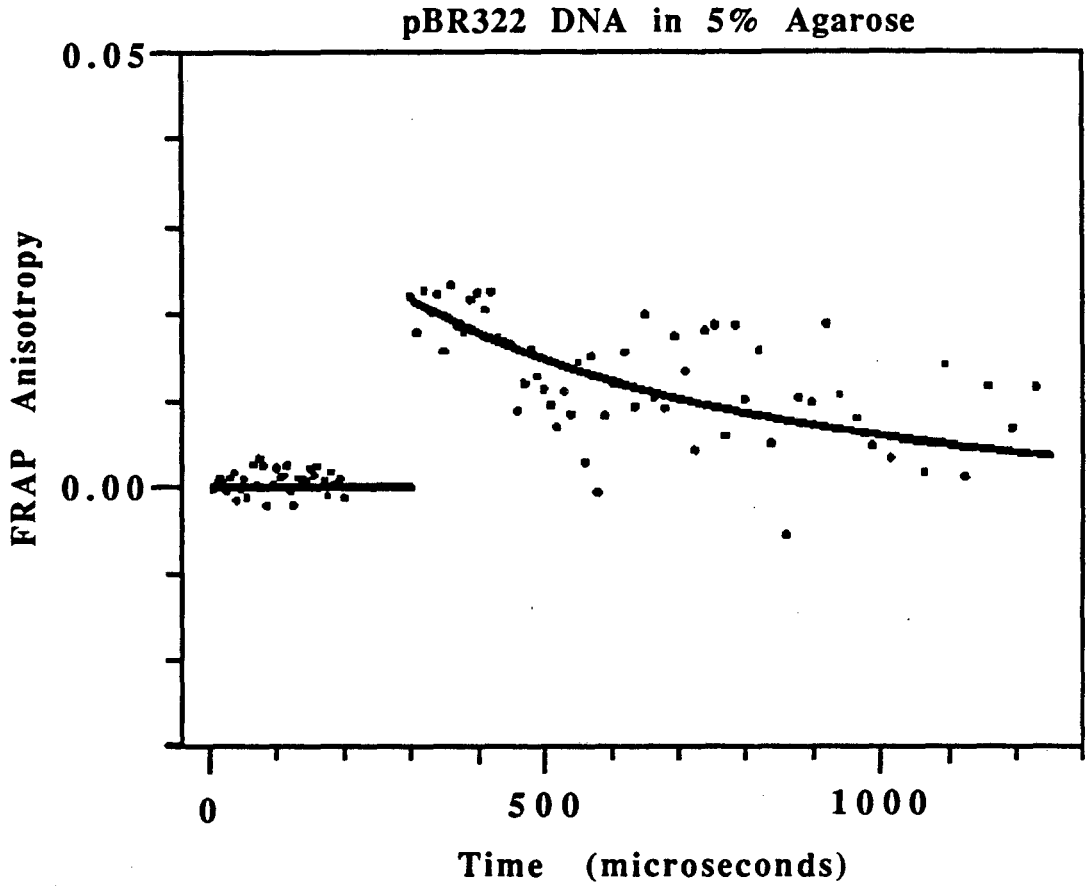

FIGURE 6-2: Parallel and perpendicular mode pFRAP curves (A) and associated anisotropy (B) obtained from a sample consisting of ethidium bromide stained pBR322 embedded in 5% agarose. In this gel sample the bleach is deeper in the parallel mode (lower curve) than in the perpendicular mode (upper curve). The initial anistropy is small and we therefore conclude that pBR322 undergoes a substantial amount of rapid, unresolved motion during the bleaching pulse. The temporal decay of $r_b(t)$ then allows us to monitor the evolution of the more slowly relaxing reorientational motions of the DNA. Note that although the data were collected at 5μsec sample intervals (bins), the anisotropy functions displayed in Figs. 6-2 and 6-3 were obtained by adding together neighboring bins (for the long time data points only); this procedure improves the signal-to-noise at long times, when there is little bleach left.

For pBR322, which is considerably larger than the oligomer, it is apparent that $F_{\parallel}(t)$ and $F_{\perp}(t)$ differ. In particular, it is seen that the depth of bleach is slightly deeper in the parallel mode than in the perpendicular; therefore, we conclude that, in this sample, the DNA molecules have not completely reoriented at the end of the 5μsec bleaching pulse. The anisotropy function $r_b(t)$ computed from the data shown in Fig. 6-2a is displayed in Fig. 6-2b. The magnitude of the initial anisotropy is small, ≈0.02; the best fit time constant is 540 μsec.

Rotational Diffusion of Phage λ DNA in Agarose Gels: We have studied the reorientational relaxation of phage λ DNA (50,000 bp) in agarose as a function of gel concentration. Dynamics in gels that were 1%, 2%, 3%, 4% and 5% by weight were monitored. These studies allowed us to follow the effects that interactions with gel matrices have on the various relaxation modes of relatively long linear DNA molecules.

The anisotropy obtained from a sample consisting of phage λ DNA in 5% agarose is shown in Fig. 6-3a. Two other anisotropy functions, corresponding to agarose concentrations of 3% and 1% are shown, for comparative purposes, in Figs. 6-3b and 6-3c.

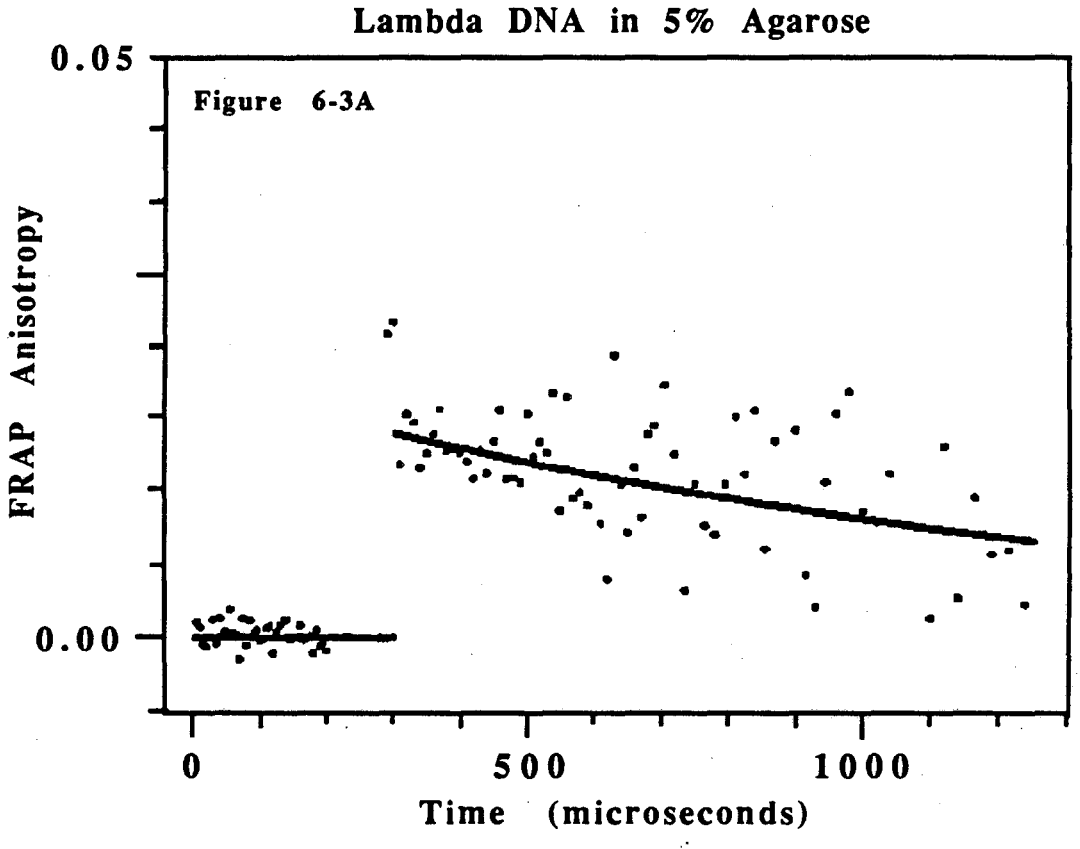
Lambda DNA in 5% Agarose
Figure 6-3A
0.05
0.00
FRAP Anisotropy
0
500
1000
Time (microseconds)

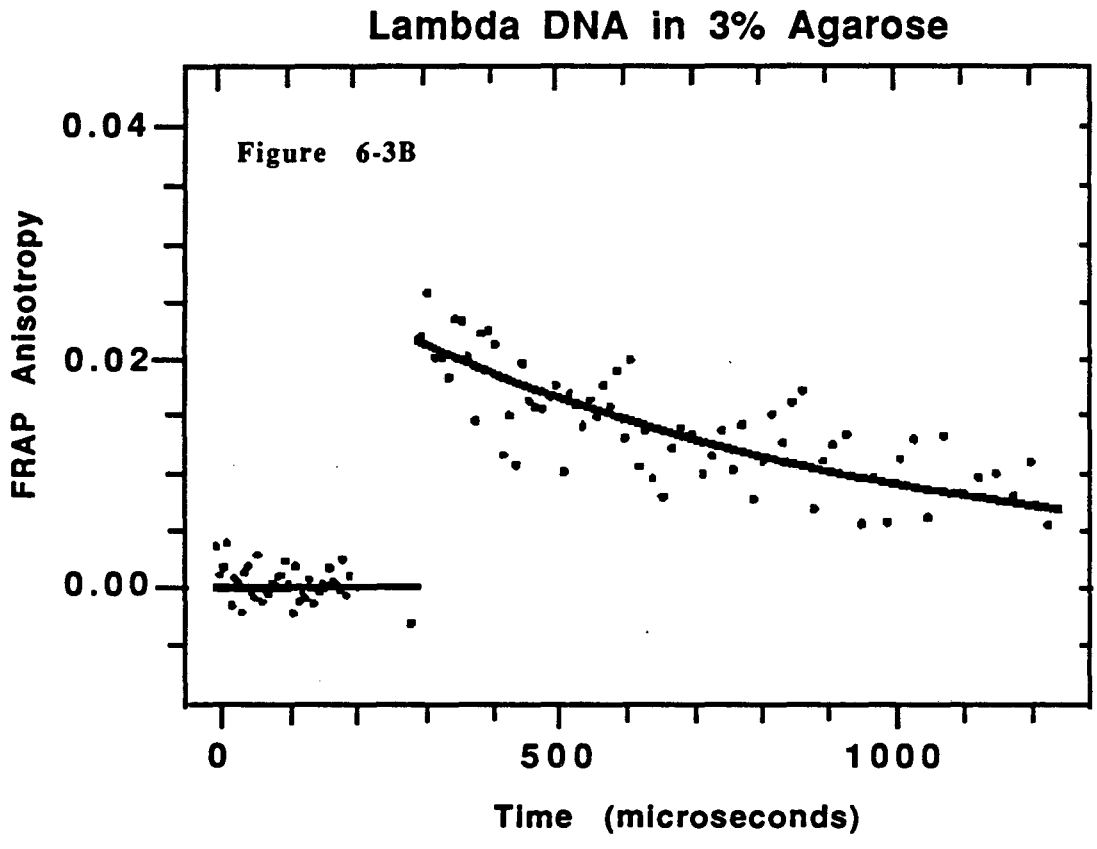
Lambda DNA in 3% Agarose
Figure 6-3B
FRAP Anisotropy
0.04
0.02
0.00
0
500
1000
Time (microseconds)

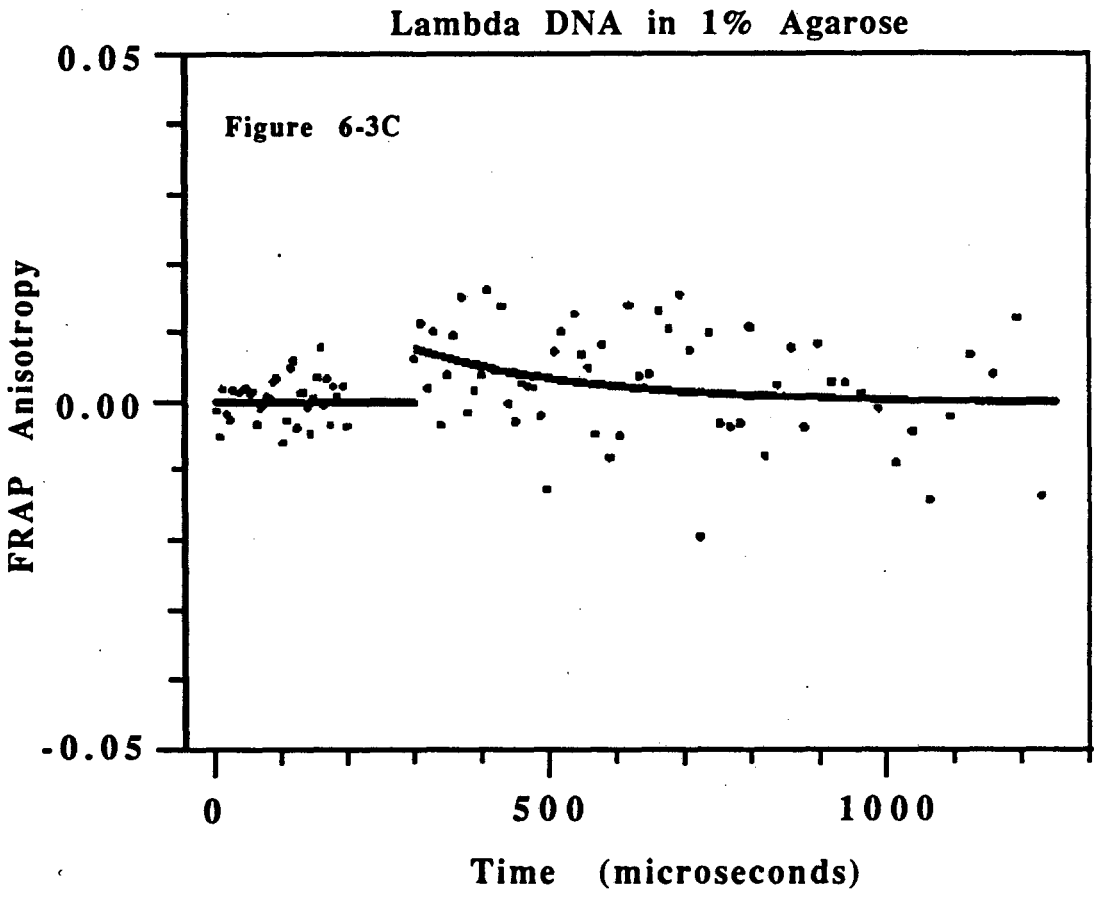

FIGURE 6-3: Anisotropy functions obtained from samples consisting of phage λ DNA embedded in 5%, 3% and 1% agarose. The DNA in the most dilute gel (C) exhibited very little anisotropy ($r_b(0) \approx 0.01$) at the end of the bleaching pulse; in contrast both the 5% (A) and 3% (B) agarose/DNA samples yielded signficantly higher values for $r_b(0)$ (≈ 0.03 and ≈ 0.02, respectively). Visual inspection of the data shows that the temporal decay of residual anisotropy was more rapid in the 3% gel than in the most dense gel.

The best fit time constants and initial anisotropies obtained from all five samples are summarized in Figs. 6-4 and 6-5. It is seen that both the time constant and $r_b(0)$ increase systematically as the agarose concentration is changed.

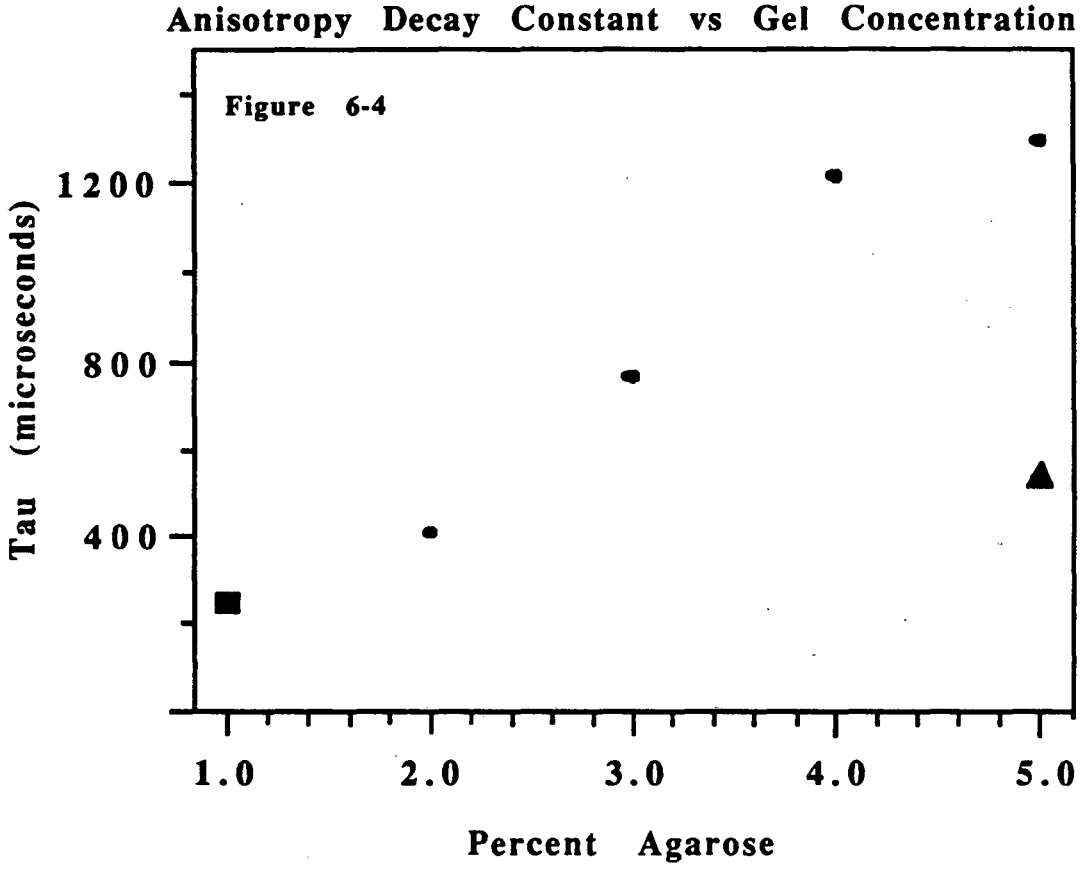

FIGURE 6-4: Best-fit time constants obtained from the five phage Lambda DNA samples (square and closed circles) and the pBR322 sample (triangle). The phage Lambda DNA time constant increases monotonically with agarose concentration. The pBR322 time constant is somewhat smaller than its Lambda DNA analogue. Note that each of the phage lambda DNA and pBR322 experiments was repeated at least once and that reproducibility was quite good. The symbol for the 1% agarose data point (square) is different than the other agarose points because the fitting parameters could not be determined very precisely.

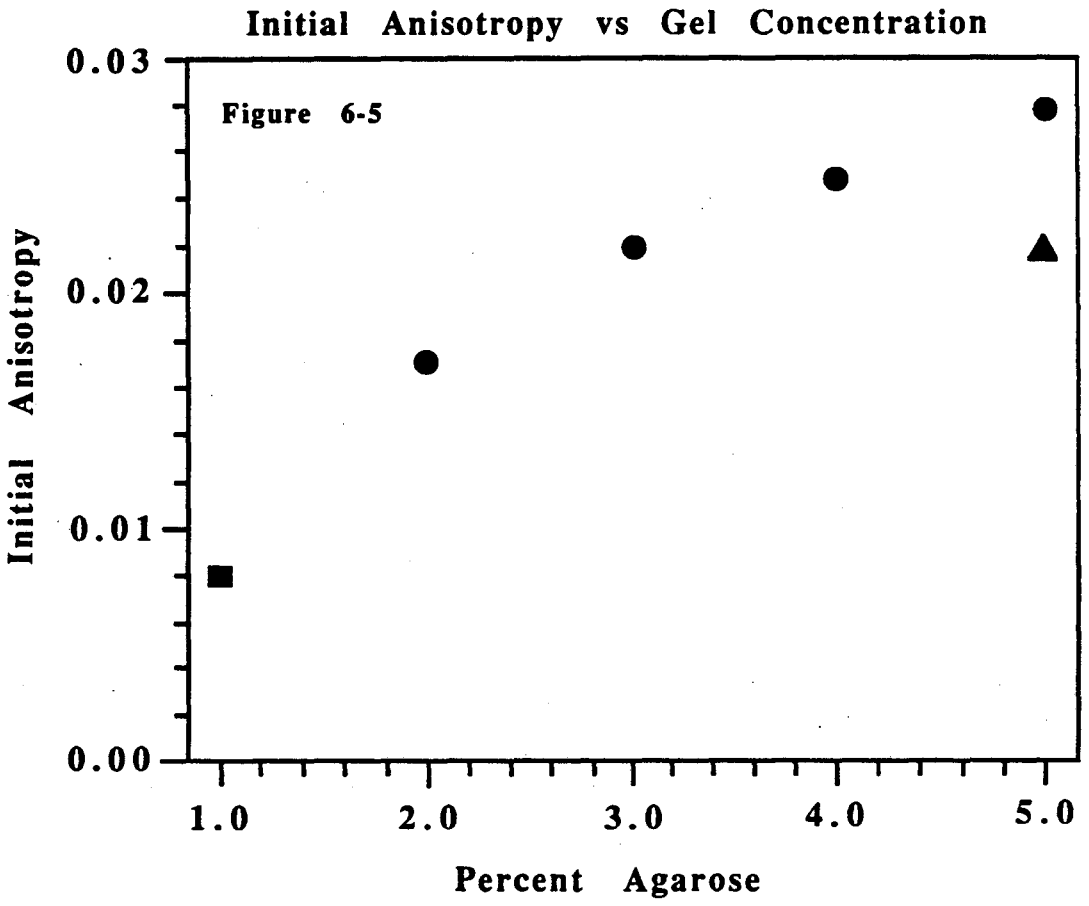

FIGURE 6-5: Best-fit initial anisotropies obtained from the five Lambda DNA samples and the pBR322 sample. For the Lambda DNA gels the initial anisotropy increases with agarose concentration. Symbols are defined in Fig. 6-4.

Discussion

Rotational Diffusion of Short DNA Fragments in Agarose gels: The agarose gels studied here are composed predominantly of buffer. Therefore, over small distance scales, a DNA molecule should be interacting primarily with an aqueous solution, and the forces that act on it will largely be Brownian in origin. Indeed, if the effective pore size of the gel is much larger than the dimensions of the DNA, it seems likely that the rotational motion

exhibited by the DNA will not differ much from that of an identical molecule which is tumbling unimpeded in solution under the influence of Brownian torques.

Stellwagen (1985) has conducted a systematic study of the Brownian rotational diffusion of DNA restriction fragments (622-2936 bp. in length) in agarose gels using the transient electric birefringence technique (see also Wijmenga & Maxwell, (1986) for related work). The birefringence data do indeed indicate that the longest detected relaxation mode is unperturbed by the presence of a gel if the median gel pore diameter exceeds the hydrodynamic length of the DNA; however, interactions with the matrix markedly slow this relaxation mode if the median pore diameter is smaller than the hydrodynamic length.

The oligomer/agarose sample studied here has properties which would lead us to expect it to approach the freely tumbling limit. An 18 base pair oligomer is effectively a rigid rod with a length of ≈61Å. Moreover, the pore sizes of agarose gels that are a few percent by weight LMT agarose range between 250 and 1000 Å (Griess *et al.*, 1989; Serwer, 1983). Hence our oligomer is indeed much smaller than are the pores of the gel.

One can easily calculate, from the Broersma formulae (Broersma, 1960), the long-axis and end-over-end rotational diffusion coefficients for a rigid rod of 61Å in length. The values obtained are 3×10^7 sec^{-1} and 2×10^6 sec^{-1}, respectively. The associated long axis and end-over-end relaxation times are on the order of a few tens and a few hundreds of nanoseconds, respectively. These correlation times are so short that unless interactions between the oligomer and the matrix had markedly impeded the rotational motion of the 18mer, the pFRAP anisotropy obtained at the end of a 5 μsec bleaching pulse should be zero. This is indeed what we have observed.

This oligomer experiment thus serves as a control on our λ DNA and pBR322 work; in particular, it serves as a test for instrumentally introduced anisotropy in the data. The

oligomer result demonstrates, for example, that the intensities of the bleaching light in the parallel and perpendicular modes are the same. If these two intensities were not essentially equal, a rapidly tumbling (on the microsecond time scale) molecule would yield a static, nonzero, anisotropy.

Reorientation of pBR322 and Phage λ DNA in Agarose Gels: Longer DNA molecules, like phage λ DNA, are semi-flexible macromolecules that undergo, in dilute solution, both twisting and bending motions, rotations of internal segments and entropically driven coil deformations (see Chpt 4, Shibata *et al.*, 1985; Langowski *et al.*, 1985; Hagerman, 1988). It would, therefore, be very useful to know how the pFRAP anisotropy evolves in time if reorientational relaxation in the system has its origins in twisting and bending dynamics. Unfortunately, in this case, the analysis of the time dependence of the angular quantities that contribute to common spectroscopic signals has proven to be a formidible theoretical problem. For example, although twisting and coil motions have been successfully incorporated into the description of many types of time resolved experiments, bending dynamics has been analyzed only within the confines of approximate theories (Shibata *et al.*, 1985; Barkley & Zimm, 1979).

In discussing our results for the longer DNA's we thus do not attempt to present a rigorous theoretical analysis of the pFRAP data. We have opted, instead, to describe semi-quantitatively the approximate amplitudes and timescales associated with some of the more rapidly (twisting) and slowly (coil) relaxing motions exhibited by long DNA molecules and, then, to discuss how these motions may be affected by interactions with gel matrices. It should also be mentioned, in this context, that some of the gel-induced effects that we have detected may arise when DNA molecules become entangled on the agarose (Smith *et al.*, 1989). In the analysis that follows we will, nevertheless, focus primarily on molecules that are interacting transiently with the matrix.

We have seen that samples consisting of relatively large DNA molecules, embedded in concentrated agarose gels, exhibit anisotropy (unlike the oligomer sample discussed above, and unlike a dilute solution of phage λ or pBR322 DNA). It is, however, important to note that the magnitude of the anisotropy that remains in our PBR and λ DNA gels, at the end of the bleach, is quite small. Therefore, we conclude that DNA molecules embedded in gels undergo substantial amount of reorientational motion on timescales shorter than 5 μsec.

This conclusion is in contrasted to the observations made by Smith *et al.* (1989) when they used video techniques to monitor the Brownian dynamics of phage λ DNA in gels. At the level of resolution that is achieved with video cameras λ DNA appears to be immobile in a gel. In fact, however, the DNA is apparently free to undergo many small scale reorientational motions, even in very congested gels.

Indeed, we would expect the nanosecond twisting of DNA to be largely unhindered. These nanosecond twisting motions are fluctuations in local twist that do not (coherently) add up to a net twist for the entire molecule (see Chpt 4) – consequently, they do not require a (significant) change in conformation or writhe of the molecule. As a result, the matrix is not expected to interfere with these localized modes. The same should be true for local bending modes. And indeed, the small initial anisotropy in all the DNA/Agarose pFRAP data indicate that much motion is occuring on a time scale less than 5 μsec.

If we consider just the twist, and use the results of Allison *et al.*, (1982) for the mean squared twist angle of a subunit (labeled j) in the middle of the DNA, $\langle\theta_j(t)^2\rangle$, as a function of time, we can calculate the expected anisotropy at the end of a 5μsec bleach.

$$\langle\theta_j(t)^2\rangle = 2k_BT(t/\pi\alpha\gamma)^{1/2}$$

Here t is time, $\alpha = 3.8 \times 10^{-12}$ dyn-cm is the twisting rigidity, $\gamma = 6.15 \times 10^{-23}$ dyn-cm is the friction factor for rotation of a DNA subunit about its z axis, k_B is Boltzman's constant, and T = 293°K is the temperature.(The relatively high value of the twisting rigidity, as compared to the results in chapter 4 and other workers, is because of the different friction factor used by Schurr and co-workers.) At the end of a 5μsec bleaching pulse $\langle\theta_j(t)^2\rangle^{1/2} = 148°$. Hence there will be a large amount of depolarization due to twisting after 5μsec. The experimental results of chapter 4 for isolated DNA also indicate there is much depolarization of an unperturbed molecule after 5μsec. The small initial anisotropy is therefore consistent with, and can likely be explained by unperturbed twisting motions.

Why is the initial pFRAP anisotropy nonzero? First, twisting alone does not cause the fluorophore to sweep out 2π solid angle. Consequently, there is still some polarization left even after unperturbed twisting is complete. This however, cannot completely account for the non-zero anisotropy of DNA in agarose: If phage λ or pBR322 DNA is suspended in solution at 80 mg/ml, rb(0) is zero (data not shown). In this case, bending modes contributes further to depolarization, bring the anistropy to zero.

Hence for long molecules of DNA in an agarose gel, we assume that interactions with the matrix inhibit motions which would normally cause comparable dilute DNA solutions to depolarize during the bleaching pulse. It is intuitively reasonable to assume that a lateral/transverse internal motion with an amplitude on the order of the gel pore size might be retarded by interactions with the agarose.

Which internal DNA motions are likely to lead to interactions with the gel and thereby be damped out, leading to a non-zero initial anisotropy?

Transverse displacements of the DNA helix axis are frequently described in terms of a set of normal coordinate motions. For example, equations that are often used to describe

the transverse internal dynamics of DNA (Rouse, 1953; Zimm, 1956; Harris & Hearst, 1966; Aragon & Pecora, 1985) yield normal mode solutions that give simple sinusoidal relationships between transverse displacement and contour length along the DNA. The Langevin relaxation time, τ_m, (which is related, but generally not equal, to spectroscopic relaxation times (Langowski *et al.*, 1985)), and the associated mean squared fluctuation amplitude, $<\delta_m^2>$ of a given mode m, can be calculated, within the confines of certain models, from the formulae (Fujime, 1971; Berne & Pecora, 1976)

$$\tau_m = 2R_g^2/[\pi^2 m^2 D_o]$$

and

$$<\delta_m^2> = NR_g^2/[6\pi^2 m^2].$$

Here R_g and D_o are, respectively, the radius of gyration and translational diffusion coefficient of a DNA molecule composed of N+1 subunits. If the relaxation time and mean squared amplitude expressions are evaluated using parameters appropriate for a molecule like phage λ DNA it is found that

$$\tau_m = 50/m^2 \text{ msec}$$

and

$$\langle \delta_m^2 \rangle^{1/2} = 3000/m \text{ Å}.$$

As previously noted, the pore sizes of 1% to 4% LMT agarose gels lie in the 250-1,000 Å range (Serwer, 1983; Greiss *et al.*, 1989). The normal mode analysis thus leads us to conclude that in, for example, a 4% LMT agarose gel, coil deformations associated with mode numbers 1-12 are likely to lead to interaction between a molecule like phage λ DNA and the agarose. Note that this calculation will probably underestimate the number of interacting modes because pore sizes represent the largest effective spacing between agarose strands. Normal modes 1-12 would, in noninteracting systems, relax components of the pFRAP anisotropy on timescales that are longer than about 100 μsec. However, in regions of the gel in which the interstrand spacing is half the pore size, the highest order interacting modes would relax components of the pFRAP anisotropy on timescales of a few tens of microseconds. Thus, this rough argument leads us to conclude that anisotropy retention in a gel on the microsecond time scale could arise from gel-induced inhibition of lateral deformations of DNA molecules.

In addition, the results of the ground-state depletion experiment of isolated DNA presented in chapter 4, and the light scattering and dichroism experiments of other (Schmitz and Schurr,1973; Ding *et al.*, 1972) indicate that there is an approximately 10μsec reorientational relaxation, most likely due to end-over-end tumbling of persistence, or statistical, length segments of long DNAs. Since the persistence length of DNA is about 550Å (the statistical length being twice this) one would expect such a motions to be inhibited in gels whose pore sizes range between 250 and 1000Å.

Inhibition of these motions would contribute to the non-zero anisotropy seen in our agarose experiments.

Relationship to Electrophoretic Phenomena: Several recent computer simulations of DNA migration under the influence of a pulsed field (Deutsch, 1988; Noolandi *et al.*, 1989) suggest that interactions between gel matrices and the internal modes of DNA are a critical determinant of pulsed electrophoretic separatory processes. For example, Noolandi *et al.* have been able to show that when internal motions of DNA are incorporated into simulations of mobility during field inversion gel electrophoresis (FIGE), the FIGE mobility has a minimum value at a certain pulse duration; this dramatic phenomenon has also been observed experimentally (Carle *et al.*, 1986).

Our experimental data indicate that the internal motions of DNA which relax in the microsecond and millisecond time domain do indeed interact significantly with gels whose concentration is >1%. Moreover, it is likely that the interaction-induced effects detected here reflect interactions between transverse displacements of DNA and the embedding matrix.

A further, though speculative, correlation between our results and pulsed field gel mobilities: The initial value of the pFRAP anisotropy increases rapidly when the LMT agarose concentration is increased from 1% to 2%; in this same concentration regime pulsed-field gel electrophoretic mobilities measured in standard agarose (which differs somewhat in pore size from LMT agarose (Serwer, 1983; Greiss *et al.*, 1989)) begin to decrease rather dramatically (Mathews *et al.*, 1988). It possible that these two phenomena are related to one another; one might imagine, for example, that the same molecular interactions that hinder internal motions of DNA in a 2% agarose gel also fundamentally influence translational mobility in such a gel.

References

Allison, S.A., Shibata, J., Wilcoxon, J., & Schurr, J.M. (1982) *Biopolymers 21,* 729-762.

Aragon, S.R., & Pecora, R. (1985) *Macromolecules 18,* 1868-1875.

Atherton, S.J., & Beaumont, P.C. (1986) *Photochem. Photobiol. 44,* 103-105.

Atherton, S.J., & Beaumont, P.C. (1987) J. *Phys. Chem. 91,* 3993-3997.

Axelrod, D., Koppel, D.E., Schlessinger, J.S., & Webb, W.W. (1976) *Biophys.* J. 16, 1055-1069.

Barkely, M.D., & Zimm, B.H. (1979) J. *Chem. Phys. 15,* 2991-3007.

Berkoff, B., Hogan, M., Legrange, J., & Austin, R. (1986) *Biopolymers 25,* 307-316.

Berne, B.J., & Pecora, R. (1976) *Dynamic Light Scattering.* pp 182-188, John Wiley & Sons, Inc., New York.

Bevington, P.R. (1969) *Data Reduction and Error Analysis in the Physical Sciences* pp 237-239, McGraw-Hill Book Co., New York.

Broersma, S. (1960) J. *Chem. Phys. 32,* 1626-1631.

Cantor, C.R., Smith, C.L., & Mathew, M.K. (1988) Ann. *Rev. Biophys. Chem. 17,* 287304.

Cantor, C.R., & Schimmel, P.R. (1980) *Biophysical Chemistry II* pp 437, W.H. Freeman & Co., San Fransisco.

Carle, G.F., Frank, M., & Olson, M.V. (1986) *Science 232,* 65-68.

Chu, B., Wang, Z., & Wu, C. (1989) *Biopolymers 28,* 1491-1494.

Deutsch, J.M. (1988) *Science 240,* 922-924.

Ding, D., Rill, R.L., & Van Holde, K.E. (1972) *Biopolymers 11,* 2109-2124.

Fujime, S. (1971) *J. Phys. Soc. Japan 31* 1805-1808.

Griess, G.A., Moreno, E.T., Easom, R.A., & Serwer, P. (1989) *Biopolymers 28,* 1475-1484.

Hagerman, P.J. (1988) *Ann. Rev. Biophys. Biophys. Chem. 17,* 265-286.

Harris, R.A., & Hearst, J.E. (1966) *J. Chem. Phys. 44,* 2595-2602.

Hervet, H., & Bean, C.P. (1987) *Biopolymers 26,* 727-742.

Hogan, M., Wang, J., Austin, R.A., Monitto, C.L., & Hershkowitz, S. (1982) *Proc. Natl. Acad. Sci. 79,* 3518-3522.

Houseal, T.W., Bustamante, C., Stump, R.F., & Maestre, M.F. (1989) *Biophys. J. 56,* 507-516.

Johnson, P., & Garland, P.B. (1982) *Biochem. J. 203,* 313-321.

Jovin, T.M., Bartholdi, M., Vaz, W.L.C., & Austin, R.H. (1981) *Ann. N.Y. Acad. Sci. 366,* 176-196.

Langowski, J., Fujimoto, B.S., Wemmer, D.E., Benight, A.S., Drobny, G., Shibata, J.H., & Schurr, J.M. (1985) *Biopolymers 24,* 1023-1056.

Lerman, L.S., & Frisch, H.L. (1982) *Biopolymers 21,* 995-997.

Lumpkin, O.J., Dejardin, P., & Zimm, B.H. (1985) *Biopolymers 24,* 1573-1593.

Magde, D., Elson, E.L., & Webb, W.W. (1974) *Biopolymers 13,* 29-61.

Mathew, M.K., Smith, C.L., & Cantor, C.R. (1988) *Biochemistry 27,* 9204-9210 and companion papers.

Noolandi, J., Slater, G.W., Lim, H.A., & Viovy, J.L. (1989) *Science 243,* 1456-1457.

Rill, R.L., Hilliard, P.R. Jr., & Levy, G.C. (1983) *J. Biol. Chem 258,* 250-256.

Rouse, P.E. (1953) *J. Chem. Phys. 21,* 1272-1280.

Savitzky, A., & Golay J.E. (1964) *Anal. Chem 36,* 1627-1639.

Scalettar, B.A., Selvin, P.R., Axelrod, D., Hearst, J.E., & Klein, M.P. (1988) *Biophys. J. 53,* 215-226.

Scalettar, B.A., Selvin, P.R., Axelrod, D., Klein, M.P. & Hearst, J.E.(1990) *Biochemistry 29,* 4790-4798.

Schmitz, K.S., & Schurr, J.M. (1973) *Biopolymers 12,* 1543-1564.

Schwartz, D.C., & Koval, M. (1989) *Nature 338,* 520-522.

Serwer, P. (1983) *Electrophoresis 4,* 375-382.

Shibata, J.H., Fujimoto, B.S., & Schurr, J.M. (1985) *Biopolymers 24,* 1909-1930.

Smith, S.B., Aldridge, P.K., & Callis, J.B. (1989) *Science 243,* 203-206.

Stellwagen, N.C. (1985) *J. Biomol. Struct. Dynam. 3,* 299-314.

Velez, M., & Axelrod, D. (1988) *Biophys. J. 53,* 575-591.

Wijmenga, S.S., & Maxwell, A. (1986) *Biopolymers 25,* 2172-2186.

Yoshida, T.M., & Barisas, B.G. (1986) *Biophys. J. 50,* 41-53.

Zimm, B.H. (1956) *J. Chem. Phys. 24,* 269-278.

Chapter Seven

EPR

Abstract:

The goal of the Electron Paramagnetic Resonance work is to develop a time-domain electron-electron double resonance spectrometer to measure the dynamics of spin-labeled DNA. A single frequency, saturation recovery spectrometer has been built, and a DNA-binding, paramagnetic spin-label has been synthesized by collaborators. Preliminary measurements have been made which show good signal to noise and relatively tight binding of the spin-label to the DNA. A second frequency is currently being added to the saturation recovery spectrometer, which will complete the ELDOR spectrometer.

Introduction:

EPR spectroscopy is sensitive to the dynamics of paramagnetic molecules. Spin labeling, in which a paramagnetic label is attached to a molecule of interest, has been utilized to study the structure and dynamics of biomolecules in numerous experiments (Berliner 1976,79; Likhtenshtein, 1974).

All EPR techniques that utilize a spin-label to measure dynamics rely on the fact that the resonant absorption frequency of a paramagnetic electron depends on the angle of the spin label with respect to an external magnetic field (Fig. 7-1). As the spin label rotates, it's absorption frequency (in a given magnetic field) changes. Most studies of spin-labeled DNA (Kamzalova, 1981) have used conventional (or linear) EPR, which is

capable of measuring rotational correlation times from 10^{-10} to 10^{-5} seconds. (Lee, 1988; McCalley, 1972).

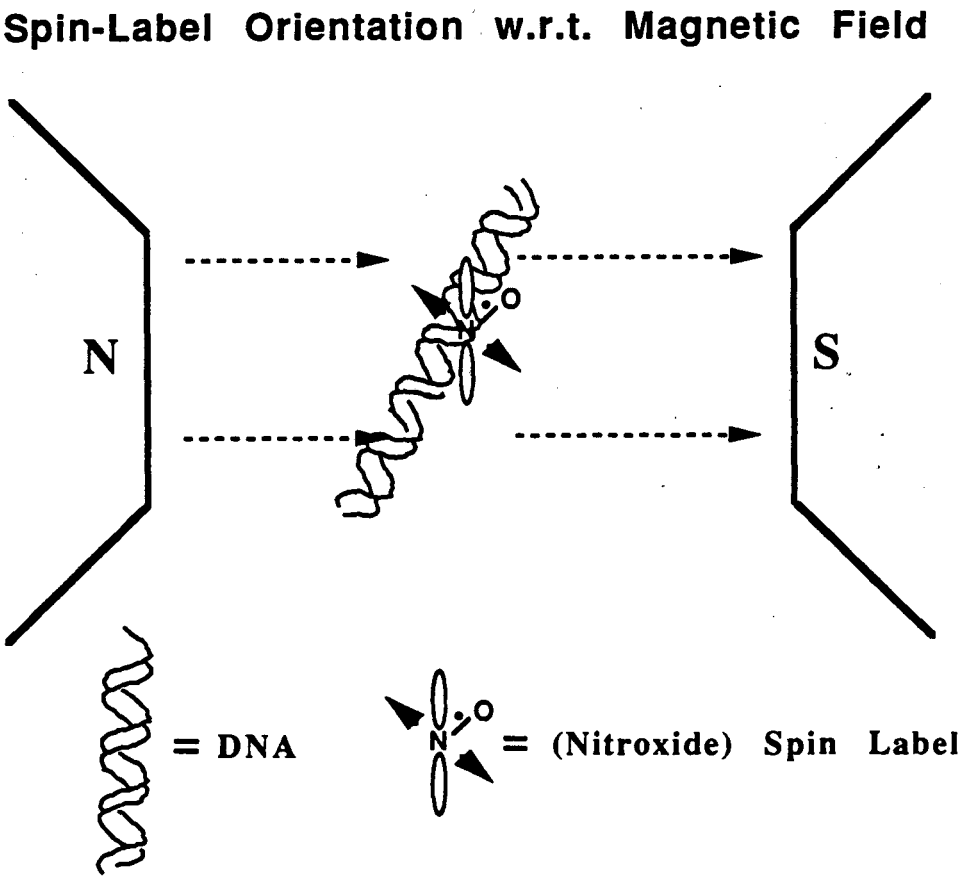

FIGURE 7-1: The spin-label is rigidly attached to DNA (or any macromolecule). As the DNA rotates, twists or bends, the spin-label will reorient with respect to the external magnetic field. This changes the frequency of absorption of the spin-label.

Passage saturation transfer (ST) spectroscopy, a non-linear EPR technique first introduced in 1972, extends the measurable correlation times to 10^{-3} seconds (Hyde, 1972, 1979). Non-linear EPR techniques rely on the fact that rotation will cause

saturation at one orientation (due to intense microwaves at the resonant frequency) to be transferred to a second orientation.

In the passage ST experiment, spectral shapes are a function of saturation transfer induced by both molecular rotation and an applied magnetic field modulation. Passage ST is experimentally simple, but information about molecular motion must be inferred by comparison with computer-generated (frequency domain) spectra (Thomas, 1978; and for a good qualitative explanation, see Hemminga, 1978). Passage ST studies of spin-labeled DNA have yielded rotational correlation times as long as 100 ns. Spin-labeled chromatin and nuclei have yielded even longer times (Robinson, 1980a,b; Hurley, 1982).

In 1974, Bruno and Freed proposed studying rotational motion by a different saturation transfer technique, continuous wave (i.e., steady state) Electron-Electron Double Resonance (CW-ELDOR) (Bruno, 1974). In the CW-ELDOR experiment, molecular reorientation is monitored by observing the transfer of saturation between two frequencies (corresponding to two orientations). The extent of saturation transfer between the two angular orientations as a function of time is then related to molecular rotation rates. ELDOR experiments are more easily interpreted than Passage experiments for two reasons: first, direct observation of the angular extent of saturation transfer is possible in ELDOR because two orientations are monitored, and second, ELDOR does not employ field modulation that can transfer saturation.

The angular resolution (i.e., the minimum angular difference through which saturation transfer can be detected) of ELDOR is determined by the ratio of the spin-packet width, $1/\gamma T_2$, to the angular dependence of the anisotropic hyperfine interaction, $dH_r/d\theta$. For ^{14}N nitroxide spin labels, angular resolution of approximately 10 degrees can be achieved

(Thomas, 1976). Significantly better resolution is possible using ^{15}N, deuterated nitroxide spin labels (Beth, 1981).

While CW spectroscopy (including CW-ELDOR) has the virtue of being relatively simple technically, it does not provide the temporal resolution of time-domain techniques. Time-domain techniques include 1) saturation-recovery, 2) electron spin-echo (ESE) studies of the transverse relaxation time, T_2 3) Fourier transform (FT) techniques, 4) pulsed ELDOR with a magnetic step between the pump pulse and the observation, and 5) pulsed ELDOR techniques using two microwave sources. In saturation-recovery, the EPR line is saturated at a single frequency and its recovery is monitored at that same frequency. This recovery is a function of both spin lattice relaxation, which is largely independent of rotation, and of rotation-induced saturation transfer. Fajer *et al.* has applied the technique to measure rotational motion of spin-labeled hemoglobin (Fajer, 1986). Because saturation recovery only monitors one frequency, corresponding to one angle, it has the drawback that it provides no direct information about the angular extent of saturation transfer. Saturation away from that one angle can be measured, but nothing more. ESE studies of T_2 also have this drawback, as well as not being sensitive to the slower motions accessible by saturation-transfer techniques (Millhauser, 1984; Stillman 1980; Madden, 1980). The other time-domain techniques overcome these limitations. However, FT-EPR studies of nitroxides (the paramagnetic moiety used in the overwhelming majority of spin-label studies) are technically quite demanding and have, therefore, only recently been exploited (Gorcester, 1989). For our purposes, the main drawback of FT techniques is the low experimental repetition rate currently achievable (< 150 Hz; roughly 10kHz-50kHz is desirable), which makes the detection of low-level signals very difficult when extensive signal averaging is required, as it will be for our experiments. The fourth time-

domain technique, field-step ELDOR, has been limited by its slow (≥1 msec) response time due to the rise time of the magnetic field (Rengan, 1979; Hornak, 1983; Dzuba, 1984).

For these reasons the goal of the work here is the development of the fifth technique: two frequency pulsed ELDOR. The technique is well suited for studies of DNA dynamics, especially in highly congested systems that exist *in vivo* : it is capable of measuring reorientational relaxation in the biologically important microsecond time regime, has good angular resolution, is capable of detecting restricted motion likely to be occurring in concentrated systems, and has relatively straight-forward data interpretation. As an intermediate step, a saturation recovery spectrometer has been built, and recently, this has been transformed into a two-frequency pulsed ELDOR spectrometer.

Note that there is considerable conceptual similarity between the ELDOR technique and the previously used techniques, and in particular, to the photobleaching and transient absorption techniques. All three are "hole-burning" techniques, in which an anisotropic distribution is established by bleaching (saturating) reporter molecules that have a particular orientation with respect to the polarization of the bleach beam, whether that is a laser polarization or a microwave field polarization. The signal in all cases is due to a combination of rotation and intrinsic relaxation processes, both of which tend to decrease the anisotropy, by making the saturation isotropic in the case of rotation, and by removing the saturaiton, in the case of relaxation. In EPR the relaxation is called spin-lattice relaxation, and in optical spectroscopy it is called (fluorescent) lifetime, but they are conceptually the same.

Description of Pulsed ELDOR Technique

In two frequency pulsed ELDOR, an intense microwave pulse of frequency n_{pump} saturates spins at one orientation (q_0) at time t_0 (see Fig. 7-2). Rotation of the spin-labeled DNA then carries the saturation to other angles (e.g., q_1). The temporal evolution of this saturation transfer can be measured either with a CW non-saturating microwave frequency $\nu_{observe}$ ($\nu_{observe}$ not equal to ν_{pump}) or by spin echo detection. For clarity, we call the former method "transient ELDOR" and the latter method "spin-echo ELDOR." In transient ELDOR, data is collected until saturation disappears due to spin-lattice relaxation. The experiment is then repeated many times for signal averaging. Once adequate signal to noise is achieved, the observe frequency is shifted to monitor a new orientation (e.g., θ_2). The process is repeated until all orientations of interest are monitored.

Saturation Transfer: Measurement via ELDOR

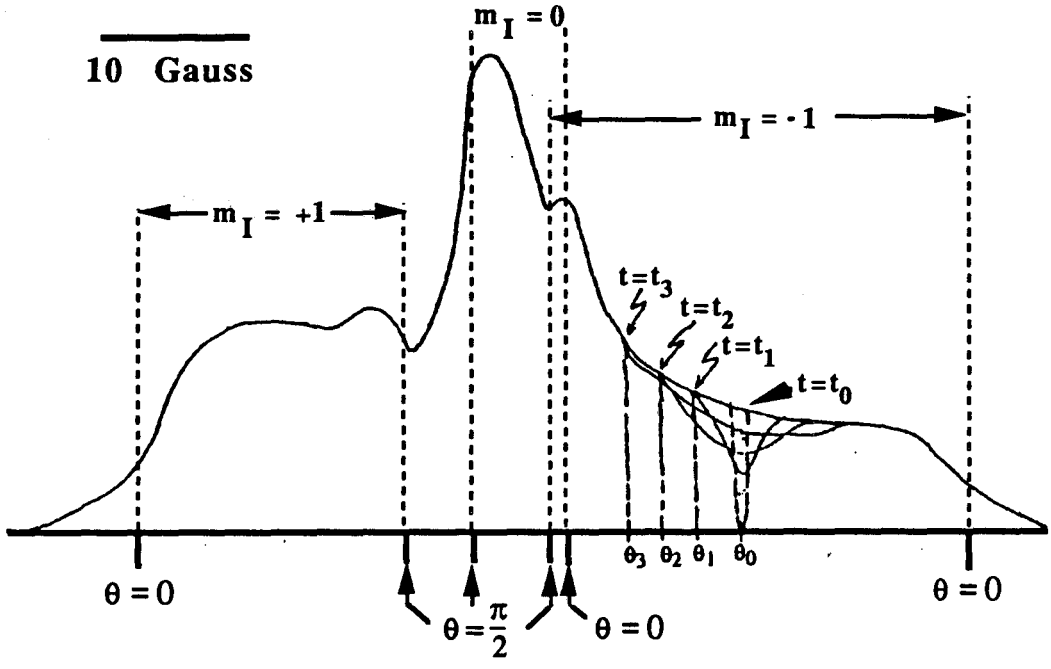

FIGURE 7-2: The EPR Spectrum consists of three nuclear manifolds for ^{14}N nitroxide spin label, identified here as m_i = -1,0,1. An intense microwave pulse saturates all spins at a given orientation (θ_0) at time t_o. Saturation is then transferred within one nuclear manifold to other angles as the spin-labelled DNA rotates. The saturation also disappears with a characteristic time T_1, the spin-lattice relaxation time, which is typically 5-15 microseconds. (Adopted from Thomas et al., 1976).

The experimental feasibility of the transient ELDOR technique for room temperature studies of nitroxides has been demonstrated (Hyde, 1984). Recent advances in microwave technology (namely the development of loop-gap resonators — see below) - and fast data acquisition electronics make studies on spin-labeled biological samples possible. For this reason work so far has been directed towards the transient ELDOR technique. However, in the future, the spin-echo ELDOR method (Hornak, 1983; Dzuba, 1984) will also be tried because of the similarity of the transient and spin-echo ELDOR machines. If spin-echoes can be formed, the spin-echo method may be able to detect lower levels of saturation than the transient method.

Construction of Time Domain EPR Spectrometer

We have constructed a saturation recovery (SR) spectrometer. Another graduate student, Nathan Hunt, has recently added a second frequency (as well as numerous other improvements) to make it into an ELDOR spectrometer.

Saturation Recovery / transient ELDOR Spectrometer

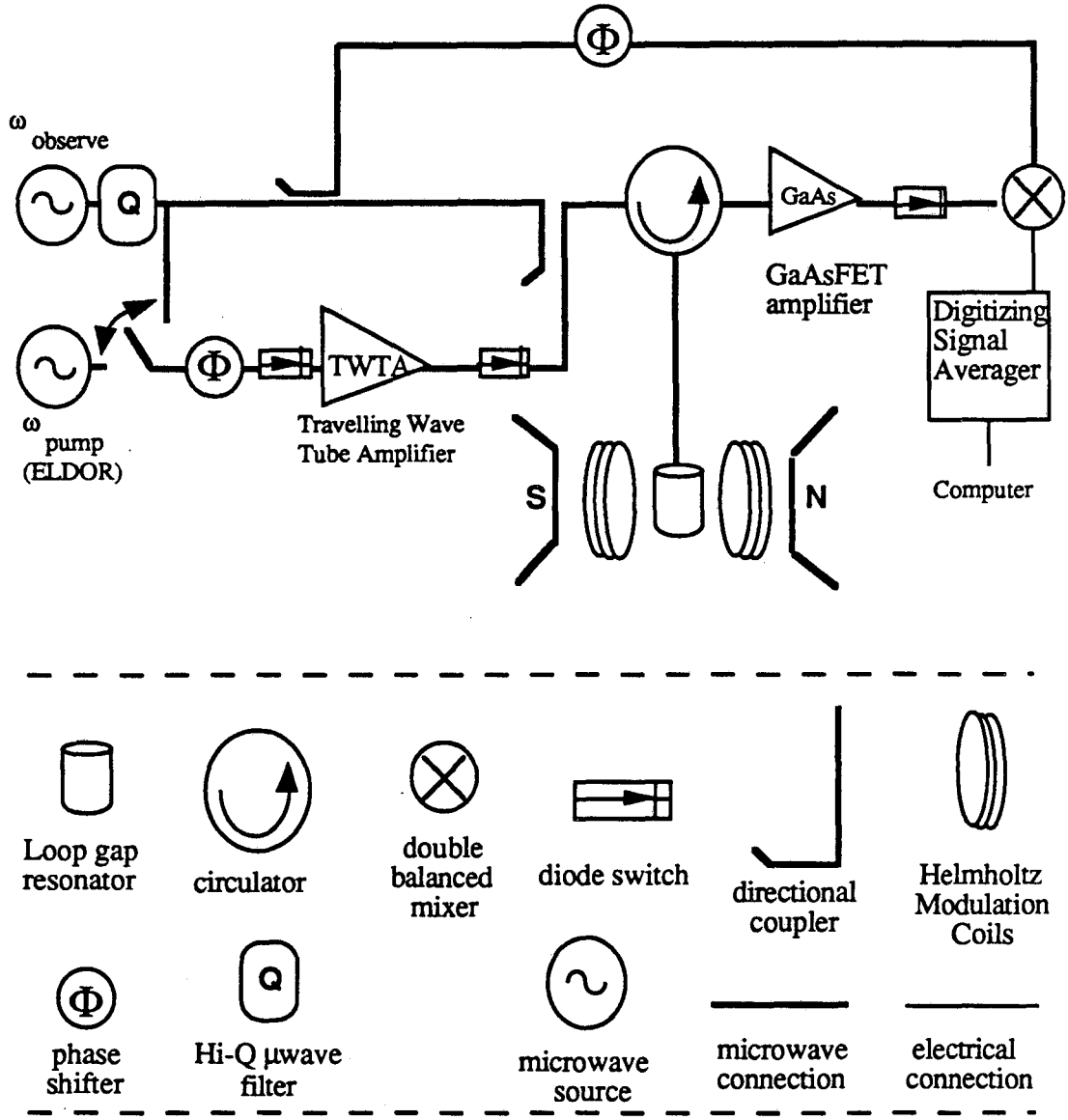

FIGURE 7-3: Spectrometer schematic for saturation recovery and transient ELDOR. In the SR mode, only one microwave source is used as both observe and pump frequencies. In the transient ELDOR mode, two separate frequency sources are used. The spectrometer is built from a base of a Varian E-3 CW-EPR spectrometer. For clarity of presentation, parts like isolators, attenuators, etc. are not shown.

An important element in both spectrometers is the microwave resonant cavity in which the sample is placed. The resonant cavity is a loop-gap resonator, first developed for EPR spectroscopy in 1982 (Froncisz, 1982). Loop-gap resonators are ideally suited for time-domain EPR studies on aqueous biological samples of limited quantity (such as our DNA samples). Briefly, loop-gap resonators have several advantages over conventional (TE_{102} or bimodal) cavities including: (1) improved signal to noise with small sample volumes, (2) faster time resolution and less dead time after the saturating pulse, (3) greater efficiency of conversion of microwave power to saturating pulse intensity, allowing greater saturation with smaller amplifiers, and (4) wider bandwidth, allowing convenient excitation of the sample by widely separated observe and pump frequencies.

We constructed a number of two-gap loop gap resonators, made of both metal and thermally-stable macor. We have settled on a two-loop one-gap commercially available loop-gap resonator (Fig. 7-4) made by Medical Advances Inc. (Milwaukee, WI). It is made of macor and is both thermally and mechanically stable, minimizing frequency and coupling drifts due to heating.

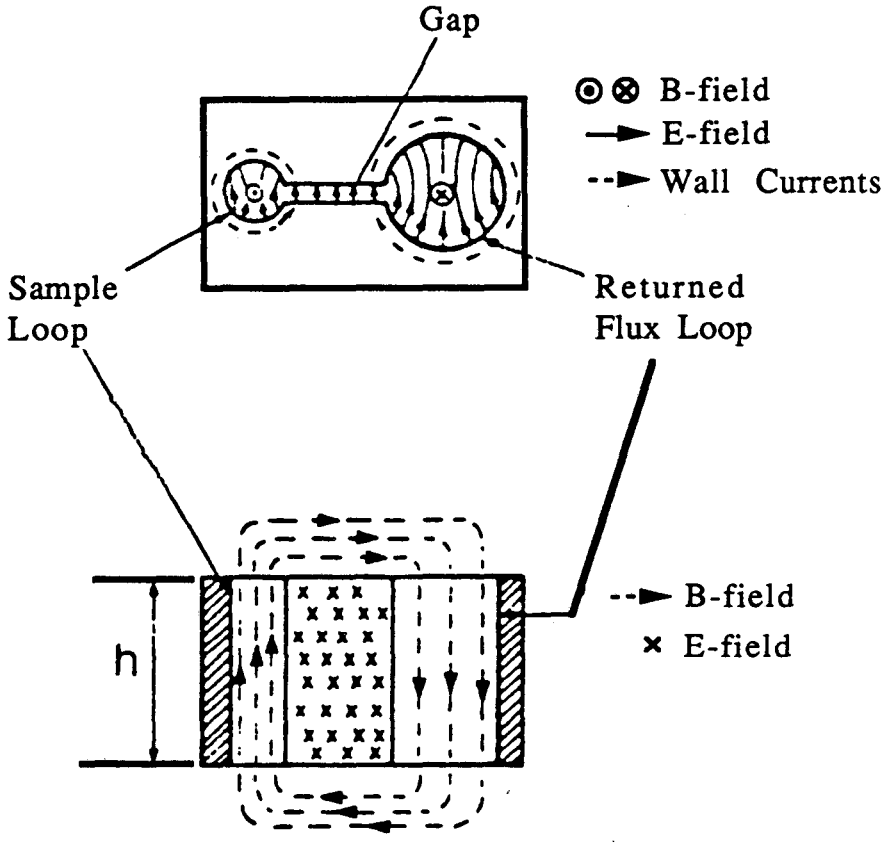

FIGURE 7-4: Commercially available two-loop, one-gap loop gap resonator. The sample is placed in the smaller loop to get very high microwave power to H-field conversion. The E-field is largely constrained to the gap region, allowing a large filling factor and the use of aqueous (and other dielectrics that absorb microwaves) with minimum loss in resonance Q. The resonant frequency is determined by the size of the gap (the "capacitor") and the loops (the "inductors").

The microwave pulses are formed by a series of Stanford Research System pulse generators driving fast (< 10nsec rise time) microwave switches (Hewlett Packard, Narda and General Microwave). The microwave sources for the pump and observe frequencies are two MITEQ frequency synthesizers which are stable to 1 kHz. (When using ^{15}N spin labels, one degree of rotation is approximately 1MHz in frequency.) A high Q-cavity (Q = 1000) filters out extraneous sub-harmonics. The pump frequency source is amplified by a 1 kW Travelling Wave Tube Amplifier (Applied System Engineering, Fort Worth, TX) and phase cycling (VMC, New Jersey phase shifter model DP629.25HS) of the pump channel is used to separate out the free-induction decay from the saturation recovery (Percival, 1975). To eliminate switching transients associated with the microwave pulses, we use 1GHz bandpass filters centered around 9.0GHz, SMA to waveguide DC-blocks, and LC filters placed at the switches power supply inputs to minimize current surges. Finally, low frequency square-wave field modulation (typically 10 to 30 Hz) is used to stabilize the baseline and reduce noise. All timing and pulse generation is run from a central clock (Metrabyte Corp.) embedded in an AST AT-compatible computer.

The first stage of detection is a low-noise GaAs FET microwave amplifier, protected from the hi-power pump pulse by a diode limiter. The noise figure of this amplifier determines the ultimate sensitivity of the instrument and is therefore critical. We have purchased a low noise amplifier with a noise figure of 2.3dB from MITEQ (AMF-4S-8596-23-L 8.5-9.6GHz). A double balanced mixer, biased with observe power then down-converts the microwave signal to video frequencies, where it is amplified by fast timing amplifiers (ORTEC 574 and 535). Data collection and signal averaging is carried out by a fast digitizer and signal averager (DSP Technology, Fremont CA, Model#2030S and 30nsec/pt 4101 averager capable of signal averaging at over 10,000 scans/sec at

30nsec/pt with 128 to1024 points per scan. (For 5nsec resolution, DSP sells the TRAQ H system). The data is then sent to an AST AT-compatible computer for graphics and data analysis.

Saturation recovery signals for a variety of samples have been detected, including polyacetylene, galvynoxyl, and nitroxide spin labels free in aqueous and organic solutions. Most importantly, we have also detected a saturation recovery signal from a nitroxide spin label embedded in a lipid bilayer (Fig. 7-5) (Hubbel, 1971). The lipid bilayer significantly slows the rotation rate of the nitroxide to greater than 10μsec, which is expected to simulate the environment a DNA-bound nitroxide, especially when the DNA is partially immobilized. The good signal to noise in Fig. 7-5 was achieved in less than a minute of data collection, indicating that the spectrometer has sufficient sensitivity to measure the weak signals from spin-labelled biological samples. The concentration of spins is probably an order of magnitude higher than is reasonable for the DNA. (In order to minimize perturbation to the DNA helix, attaching a minimum number of spin labels is desired. In order to avoid spin-spin interaction between nitroxides, an upper limit is about 1mM — 10^{15} spins in our 1.2μliter sample (Gorcester, 1989; Popp, 1982).

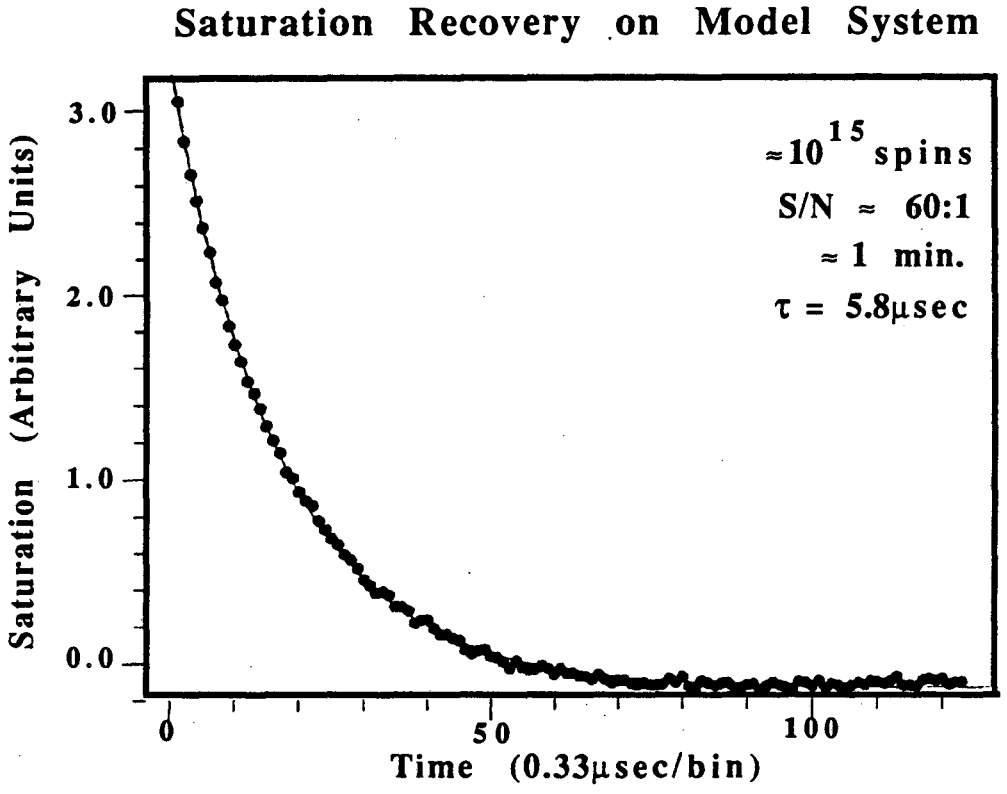

FIGURE 5: Saturation Recovery data from a slow-motion nitroxide radical. The particular system used is deoxygenated 0.5mM 5-doxylstearic acid (Molecular Probes, Eugene OR) in an aqueous suspension of 0.05M cholesterol:0.1M lecithin (Hubbel, 1971). Because tumbling is so slow, the decay constant is just the spin-lattice relaxation time. The good signal-to-noise achieved in the short period of time indicates that the spectrometer has sufficient sensitivity to measure spin-labelled biological molecules, which generally give weak signals because of their aqueous environment and limited number of spins.

To assure that the saturation recovery signal in Fig. 7-5 arises from the spins and not some systematic noise, we performed two control experiments. The first is just changing the magnetic field off resonance. As expected, the signal goes away. The second is measuring the recovery time (T_1) as a function of observe power. From the Bloch equations, the measured value of T_1 ($\equiv T_{1m}$) is:

$$\frac{1}{T_{1m}} = \frac{1 + \gamma^2 H_1^2 T_1 T_2}{T_1}$$

$\gamma^2 H_1^2 T_1 T_2$ is sometimes called the saturation factor. As the observe power increases, the rate of transitions stimulated by the observe power will start to become appreciable compared to the spin-lattice relaxation rate. Consequently, as the monitoring power increases, the *measured* spin-lattice relaxation time T_{1m} will decrease. This indeed is observed (Fig. 7-6), lending strong credence to the claim that the signal arises from the paramagnetic spins.

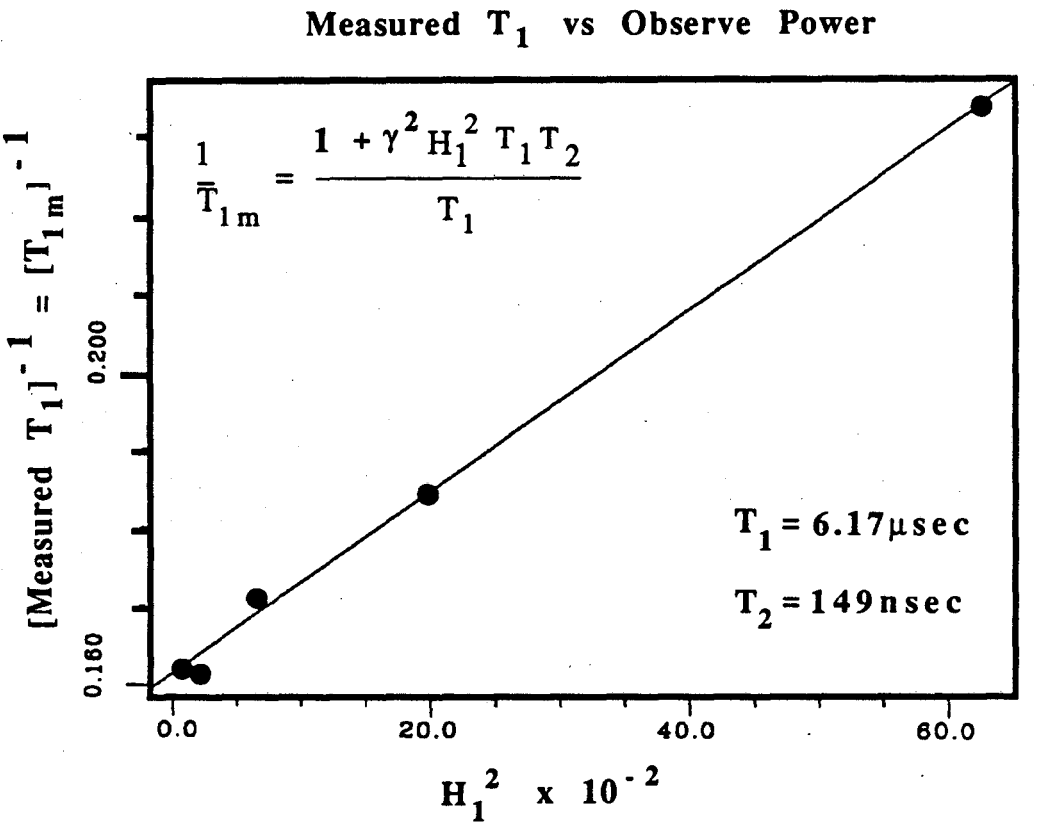

FIGURE 7-6: Effect of observe power on measured spin-lattice relaxation time. As the observe power increases, some saturation due to the observe beam will occur, giving an anomalously small measurement of T_1 (T_{1m}). The true values of both T_1 and T_2 can be extracted from the graph. Because the graph fits theory so well, it strongly indicates that the saturation recovery data in Fig. 7-5 is indeed from spins and not some artifact. H_1 is the microwave-probe magnetic field and g is the gryromagnetic ratio. H_1 is taken from measurements of Hubbel et al. (1987) who use the identical loop gap resonator.

Simulating Spectra

A critical element in measuring the dynamics of spin labels using EPR is the ability to establish the relationship between the resonant frequency of absorption and the angle of the spin label (see figures 7-1 and 7-2). While one can measure saturation transfer from frequency A to B, this does no good unless these frequencies can be related to angles and thus rotation.

Fortunately this relationship is well established for nitroxide spin labels. The frequency of absorption is determined by the **g** and **A** tensors (**g** is the usual g tensor — for an isolated electron it is a scalar with value ≈ 2.002; **A** is the hyperfine tensor) as well as the electron spin, **S**, nuclear spin **I**, and external magnetic field strength, **H**. These are well known for nitroxide spin-labels (Berliner, 1974,79). Typical values for **g** and **A** are: g_{xx}=2.0086, g_{yy}=2.0056, g_{zz}=2.0022; A_{xx}=10.18 $\cdot 10^4 cm^{-1}$, A_{yy}=10.01 $\cdot 10^4 cm^{-1}$, A_{zz}=47.17 $\cdot 10^4$ cm^{-1}, although they vary somewhat depending on the specific chemical composition of the carbon and hydrogen atoms surrounding the nitroxide. Givent hese values, the Hamiltonian can be written and from the Hamiltonian, the energy levels, and consequently the frequency of absorption corresponding to transitions between these levels, can be calculated. Computer simulations of the first derivative absorption for both ^{15}N and ^{14}N show good agreement with experimentally measured spectra (Fig. 7-7) indicating the frequency to angle correlation can be accurately established. (EPR spectra are usually plotted as first derivative of absorption with respect to the magnetic field because data is collected via lock-in detection — the external magnetic field is amplitude modulated slightly and the detector locks into this frequency — the signal is now proportional to the slope of the absorption line, which is just a first derivative.)

Frequency to Angles: Simulating Spectra

$$H = \beta \vec{H} \leftrightarrow \vec{g} \cdot \vec{S} + h \vec{S} \cdot \leftrightarrow \vec{A} \cdot \vec{I}$$

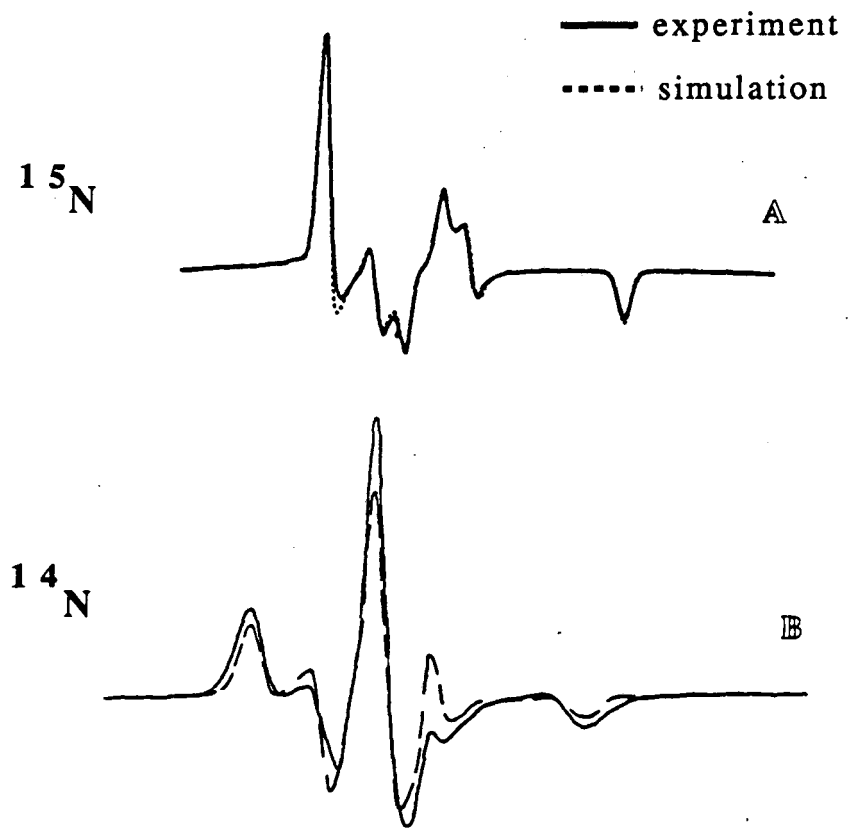

FIGURE 7-7: Simulations of first derivative absorption spectra for immobilized ^{15}N (A) and ^{14}N (B) nitroxide spin-labels. Figure A is from Beth et.al., 1981. Figure B was taken

on a E-3 Varian spectrometer and simulated using EPRSIM, a computer program available in the Calvin Lab.

Spin-Labelled Probes for DNA

In order for nitroxide spin-labels to be useful for measuring DNA dynamics, they must be rigidly attached to the DNA and in a way that does not significantly perturb the DNA helix. We are developing two approaches: one is to incorporate spin-labelled bases, a technique first introduced in 1978 (Bobst, 1978) and more recently extended by Spaltenstein (1988). Spaltenstein has synthesized a spin-labelled thymidine and site-specifically incorporated it into oligonucleotides using phosphoramidite technology with a commercially available DNA synthesizer (Fig. 7-8). These site-specifically labeled oligomers can be ligated to longer pieces of DNA (Hopkins, private communication). The spin-labelled thymidine has already been shown to be relatively non-perturbing (using melting studies) and rigidly attached to the DNA (by comparing the rotational correlation time of a dodecamer to free spin label) (Spaltenstein, 1988). We have constructed a spin-labeled deoxyadenosine (Fig. 7-8). (This work was done by chemistry graduate student Peter Spielmann and post-doc Dae Yoon Chi)

Spin-Labelled Bases

Modified Thymidine **Modified Adenosine**

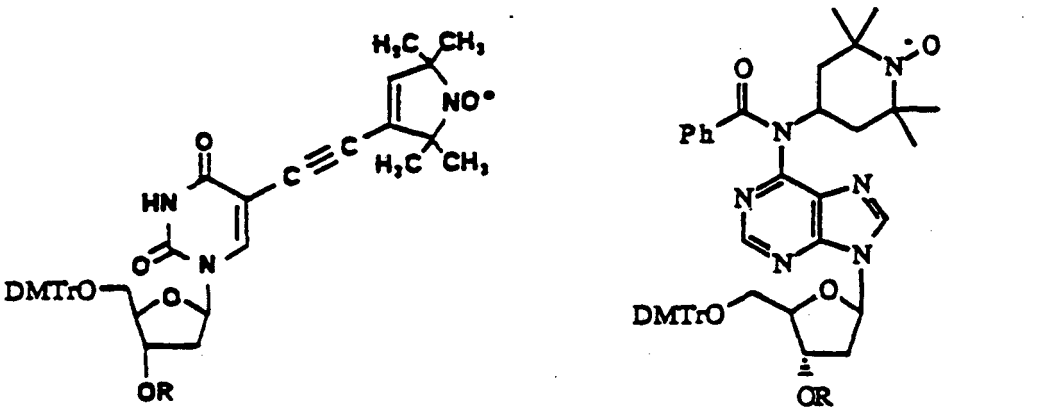

$$R = P[N(i\text{-}Pr)_2]OCH_2CH_2CN$$

FIGURE 7-8: Spin-Labelled DNA bases. The thymidine was synthesized and incorporated into DNA by Spaltenstein (1988).

The 6 position of deoxyadenosine, one of the hydrogen bonding groups that confers base-pairing specificity to DNA, was chosen for labelling. The nucleoside analogue that we have synthesized still allows this hydrogen bonding to take place. In addition, the 6 position places the spin label in the major groove of B-DNA. We hope to make use of the steric bulk of the DNA to hold the spin label rigidly in place, so that the independent motion of the nitroxide relative to the base to which it is attached is minimized. Synthesis of the protected, spin-labeled nucleoside was achieved by routine methods, starting from guanosine, and has been characterized by ^{1}H-NMR, mass spectrometry, and elemental

analysis. The nucleoside will be incorporated into several oligonucleotides using an automated DNA synthesizer (sequences I, II, and III, labelled at the starred sites). Both the spin-labeled thymidine and the spin-labeled adenosine can be incorporated into the same polymer. Oligomers II and III are designed to self-assemble into double stranded multimers of 16 and 12 base sequences respectively. These can then be ligated together using T4 DNA ligase into a single piece of double stranded DNA.

Sequence I: 5'-CGCGA*ATTCGCG

Sequence II: 5'-GCGCGCGCGA*ATTCGC

Sequence III: 5'-AGCTCGGTA*CCG

The second approach, which is currently further developed in our lab than the modified base approach, is to attach the spin-label to a psoralen and then photoreact the psoralen with DNA. Psoralens can either cross-link or form mono-adducts with DNA. Note that both the psoralen and spin-labeled bases are covalently attached to the DNA which eliminates problems with on/off kinetics. We have selected the 4' and 8 positions of psoralen for labeling. The stereo- and regio-chemistry of the psoralen crosslink show that the 4' of the psoralen is in the major groove, that the 8 position is in the minor groove of B-DNA and that these positions are readily functionalizable. We chose short linker arms between the spin label and the psoralen to let the steric bulk of the DNA restrict any independent motion of the spin label. Psoralen crosslinks introduce a perturbation into the normal B-DNA helix. The solution NMR structure of the AMT (4'-aminomethyl-4,5',8-trimethylpsoralen) crosslinked self-complementary DNA oligomer 5'GGGTACCC-3' has been determined and indicates that the DNA duplex is kinked into the major groove by 56 degrees (Tomic, 1987). This deformation should immobilize the spin label attached to the

4' position of the psoralen. We have synthesized two sets of compounds that have a nitroxide spin label attached to a psoralen via single bonds (Fig. 7-9). Compounds with R groups (1) and (2) are derivatives of AMT, and compounds with (2) and (3) are derivatives of 8-hydroxypsoralen. These compounds were synthesized in high yield by routine methods and have been fully characterized (1H-NMR, EPR, UV, MS, satisfactory elemental analysis). All six of the new psoralen derivatives show photoreactivity with double stranded DNA oligomers, and the spin label is stable to irradiation with long wavelength UV light. The psoralen spin-labelled with compound 2 has been used to crosslink the DNA octamer S'-GGGTACCC-3' at the central 5'-TpA site.

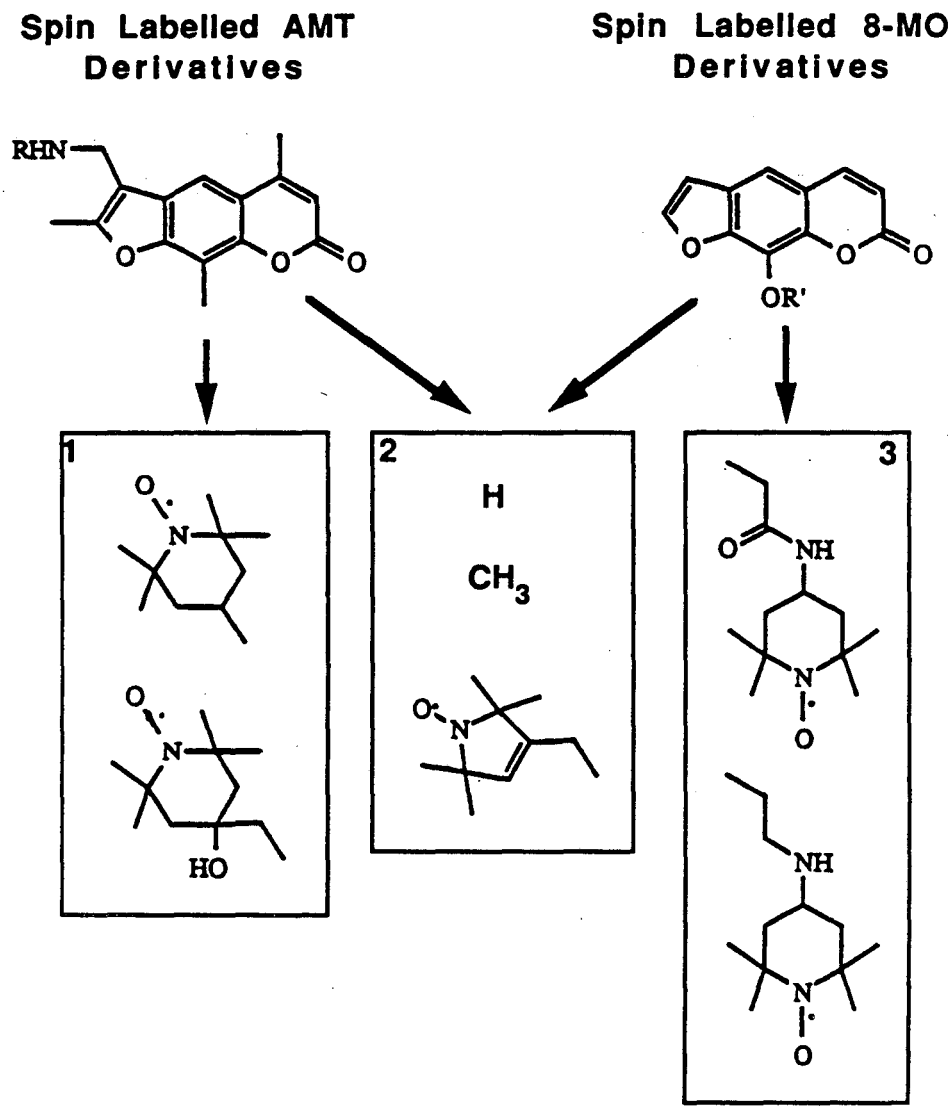

FIGURE 7-9: Spin-labelled psoralens. The compounds in the boxes are substitutions for the R groups. AMT derivatives have been made with groups 1 and 2; 8-MOP derivatives with groups 2 and 3.

In figure 7-10 we show that the spin-labelled psoralens can be attached in sufficient quantity for EPR studies. Furthermore, the graphs show that the spectra changes as the mobility of the macromolecule changes, indicating that the spin-label is rigidly bound, reporting the motion of the macromolecule. The free spin-label tumbles very rapidly, leading to a motionally narrowed CW-EPR spectrum (A). The spin-label attached to an octamer, which acts like a rigid rod of length 27.2 A and diameter 15-20A, leads to a spectra characteristic of anisotropic motion with a long time correlation time of 3nsec (B). And the spin-label attached to DNA frozen in solution leads to the characteristic powder pattern, indicative of immobilization.

Spin-Labelled Psoralen DNA: Tumbling Times

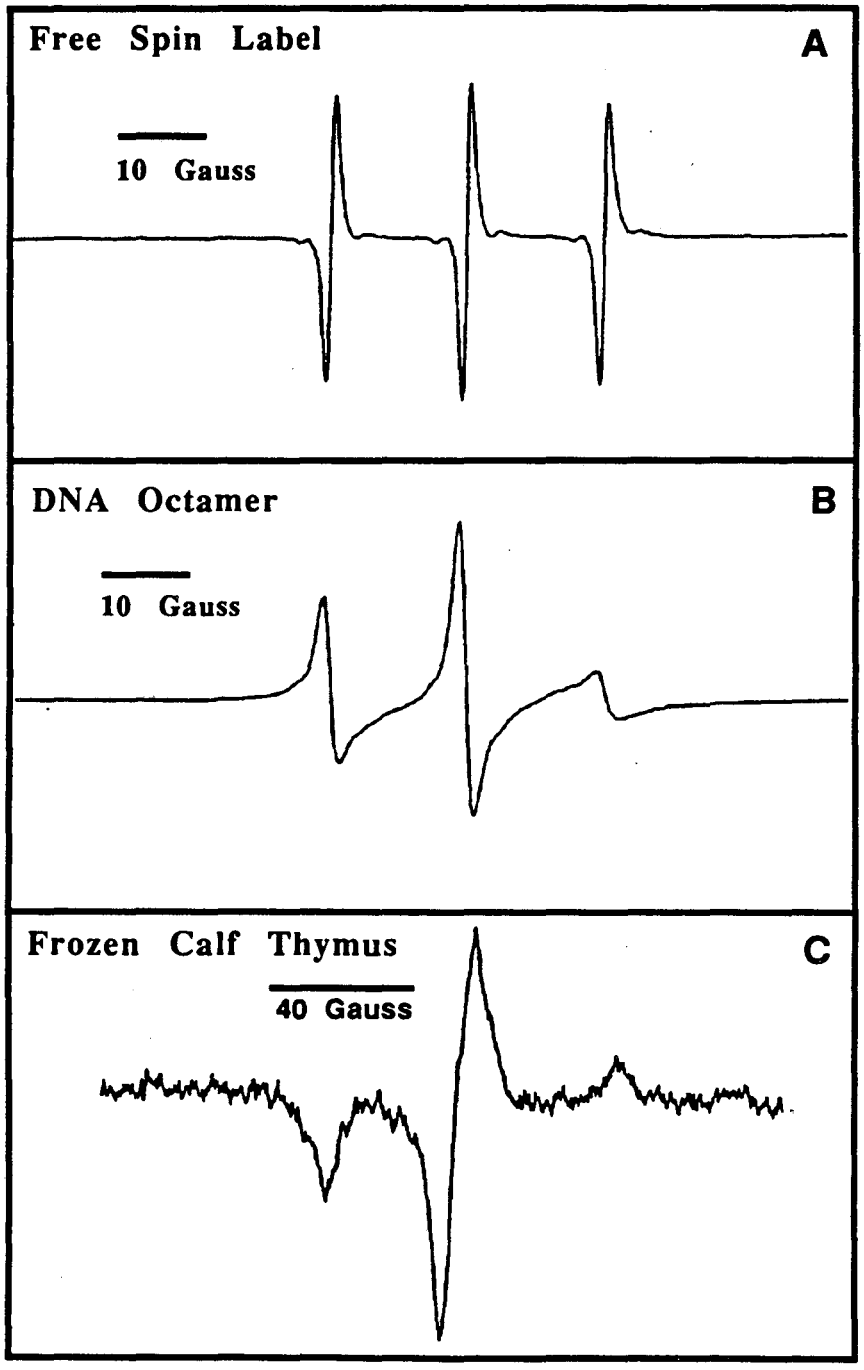

FIGURE 7-10 (see previous page): First Derivative Absorption spectra of psoralen-nitroxide spin-label (A) unattached, free in solution, (B) attached to a DNA octamer in solution and (C) attached to calf thymus DNA, frozen in solution. The free spin label spectrum is characteristic of a rapidly tumbling (τ_R 100psec) molecule; the octamer-bound spectrum is characteristic of anisotropic motion with a slow component of approximately 3nsec, in good agreement with simple hydrodynamic calculations for a DNA octamer; and the calf thymus-bound spectrum exhibits the characteristic "powder pattern of an immobilized spin label. All samples in water: Fig A and C at room temperature and Fig. C with gas from liquid nitrogen bath flowing through around sample. Note that Fig. C is plotted on a different scale — roughly twice that of A and B.

Angle between DNA Axis and Spin-Label

To distinguish between torsional and bending motions of the DNA, the relative orientation of the probe with respect to the DNA long axis must be measured. (If the label's p-orbital is parallel to the long axis, it will not report twisting motion of the DNA, but will be maximally sensitive to bending modes; if the p-orbital is perpendicular to the long axis, it will be sensitive to both types of motion.)

The angle between the spin label and the DNA can be measured if the DNA is oriented at a known angle with respect to the magnetic field. The shape of the EPR spectrum then shows the spin label's orientation with respect to the helix axis. Oriented nucleic acid fibers can be drawn from highly concentrated, viscous gells formed by alcohol precipitation of the DNA from an aqueous buffer. Hong and Piette successfully oriented spin-labeled DNA for EPR studies (Hong, 1976).

^{15}N-^{2}H Spin Labels

Utimately we hope to synthesize a ^{15}N-^{2}H nitroxide spin label for DNA. The ^{15}N nucleus is spin one-half, as opposed to the spin one ^{14}N nucleus. Consequently, the signal-to-noise is better for the ^{15}N because the signal is spread into only two, instead of three manifolds (Beth, 1981). Furthermore, because the ^{15}N nucleus is spin one-half, it does not have a nuclear quadrupole moment which can induce transitions between nuclear manifolds. This simplifies the data interpretation. By deuterating the molecule, the coupling of neighboring protons to the paramagnetic electron is eliminated, thereby increasing T_2. In our experiment, this means increased angular resolution. Finally, the two nuclear manifolds in the ^{15}N-^{2}H nitroxide powder spectrum are well separated (in

contrast to the ^{14}N spectrum — see Fig. 7-2), which means that the only mechanism which can transfer saturation within one manifold is rotation.

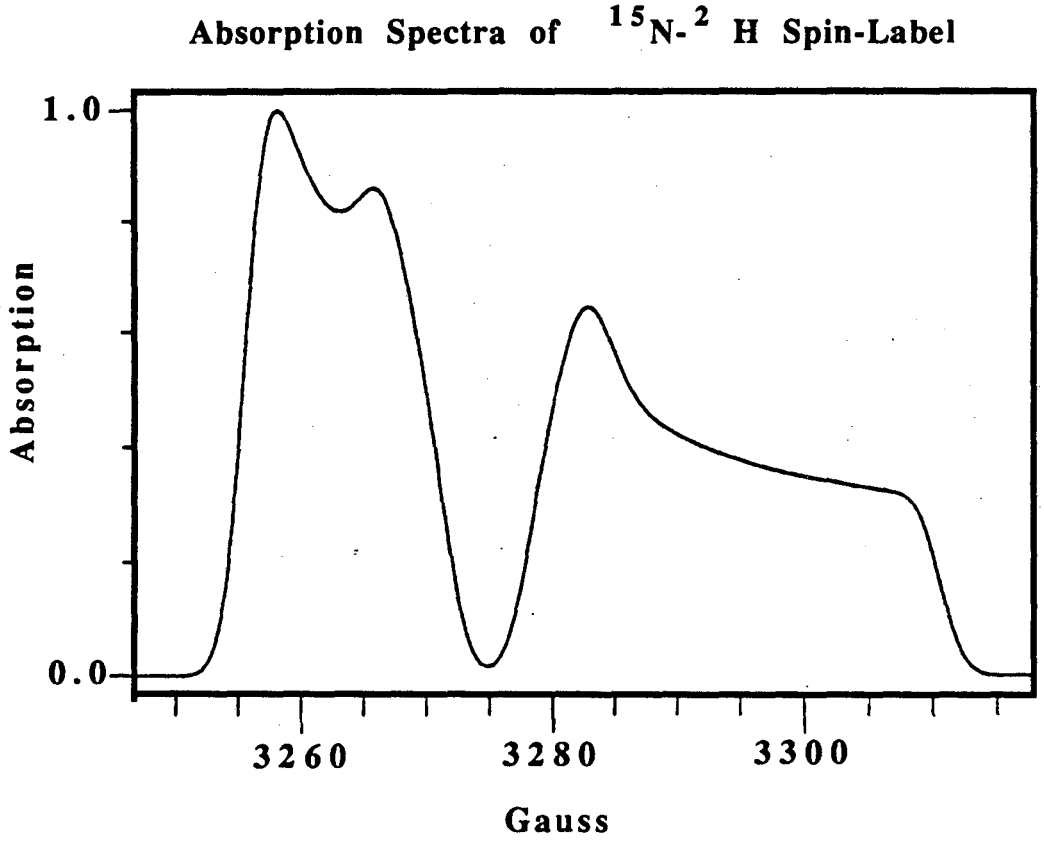

FIGURE 7-11: The absorption spectrum of a deuterated ^{15}N is split into two nuclear manifolds because ^{15}N is a spin one-half nucleus. They are also well separated, in part because of the long T_2 due to deuteration which eliminates super-hyperfine interactions from protons near the paramagnetic electron.

ELDOR Data Analysis

Data are most conveniently presented in the form shown in Fig. 7-2. Each contour on the figure represents the distribution of saturation at a given time after the pump pulse. The spread of saturation is converted into angular displacement using the well-known relationship between microwave frequency (or equivalently, magnetic field) and orientation of the spin label (see, e.g. Bruno, 1974).

The spread of saturation, however, yields only semi-quantitative information about the rotation of the spin-labeled DNA because the spread of saturation within one nuclear manifold (due to rotation) is complicated by saturation transfer to other nuclear manifolds, predominantly due to the Electron-Nuclear Dipole (END) mechanism. The rate of saturation transfer out of the manifold is a funcion of the molecule's rotational speed. This distorts the shape of the saturation transfer *within* one nuclear manifold. The magnitude of this effect will be measured by saturating one nuclear manifold and observing at a different manifold, and can then be accounted for in the data analysis.

Other complications include anisotropy of the g- and diffusion tensors, nuclear quadrupole terms (which can be eliminated by using ^{15}N), and proton hyperfine interactions (which can be reduced by deuterating the spin label). Freed developed a detailed theory which can incorporate these effects, and his treatment successfully describes the results of passage saturation transfer experiments (Freed, 1974). These calculations are lengthy. It is possible to obtain satisfactory results with a simpler analysis for ELDOR experiments (Percival, 1975; Huisjen, 1974).

Conclusion

The criteria for a successful experiment are the following:

- Saturation transfer is due to rotation
- Angle is correlated to microwave absorption frequency
- Spin-label accurately reports motion of DNA
    - Tightly Bound
    - Non-perturbing to DNA
- Sufficient sensitivity
    - Minimum number of detectable spins using non-saturating monitoring power levels

We have constructed a saturation recovery spectrometer, the precursor to a transient ELDOR spectrometer and shown, using a model system, that the spectrometer has sufficient sensitivity to measure the relatively small number of nitroxide spins in an aqueous environment that simulates the conditions of spin-labelled DNA. The saturation transfer (within one nuclear manifold) using nitroxides is due almost solely to rotation, especially if one uses ^{15}N-^{2}H nitroxide spin labels. Because the **g** and **A** tensors of nitroxide spin labels are accurately known, the absorption spectra can be accurately simulated by computer, thereby establishing the relationship between microwave absorption frequency and angle. Finally, CW-EPR spectra show that spin-labelled

psoralen can be firmly attached to DNA. Others have shown tight binding and non-perturbation of DNA structure using a spin-labelled DNA base.

References

Berliner L.J., ed. Spin Labeling Theory and Applications (Academic Press, New York) Vol. I (1976) and II (1979).

Beth A. H., S. D. Venkataramu, K. Balasubramanian, L. R. Dalton, B. H. Robinson, D. E. Pearson, C. R. Park and J. H. Park (1981) ^{15}N- and ^{2}H-subtituted Malemide Spin Labels: Improved Sensitivity and Resolution for Biological EPR Studies, *Proc. Nat. Acad. Sci. USA* 78 967.

Bobst A. M. and P. F. Torrence (1978) Incorporation of Spin Probes into Polynucleotides by Enzymatic Polymerization, *Polymer 19* , 115.

Bruno G. V. and J. H. Freed(1974) ESR Lineshapes and Saturation in the Slow Motional Region: ELDOR, *Chem. Phys. Lett. 25* 328.

Dzuba S. A., A G. Maryasov, K. M. Salikhov and Yu. D. Tsvetkov(1984) Superslow Rotations of Nitroxide Radicals Studied by Pulse EPR Spectroscopy, *J. Mag. Res. 58* .

Fajer P., D. D. Thomas, J. B. Feix and J. S. Hyde (1986) Measurement of Rotational Molecular Motion by Time-Resolved Saturation Transfer Electron Paramagnetic Resonance, *Biophy. J. 50* 1195.

Freed J. H. (1974) Theory of Saturation and Double Resonance in Electron Spin Resonance Spectra VI. Saturation Recovery, *J. Phys. Chem. 78* 1155.

Froncisz W. and J. S. Hyde(1982) The Loop-Gap Resonator: A New Microwave Lumped Circuit ESR Sample Structure, *J. Mag. Reg. 47,* 515.

Gorcester J. and J. Freed (1989) Two-dimensional Fourier Transform ESR Correlation Spectroscopy, *J. Chem. Phys.*

Hemminga M.A. (1979) Qualitative Explanation of Saturation Transfer ESR Effects Using the Concept of Hole-Burning, J. *Mag. Res. 33* , 215-218.

Hong S. and L.H. Piette (1976) Electron Spin Resonance Spin-Label Studies of Intercalation of Ethidium Bromide and Aromatic Amine Carcinogens in DNA, *Cancer Res. 36,* 1159.

Hornak J. P. and J. H. Freed (1983) ELDOR Spin Echoes and Slow Motions, *Chem. Phys. Lett. 101,* 115.

Hubbel W.L. and Harden M. McConnel (1971) Molecular Motion in Spin-Labeled Phospholipids and Membranes, *J. Am. Chem. Soc. 93:2,* 314.

Hubbel W.L., W. Froncisz and J.S. Hyde (1987) Coninuous and Stopped Flow EPR Spectrometer Based on a Loop Gap Resonator, *Rev. Sci. Instru. 58(10),* 1879.

Huisjen M. and J. S. Hyde (1974) A Pulsed EPR Spectrometer, *Rev. Sci. Instrum. 45,* 669.

Hurley I., P. Osei-Gyimeh, S. Archer, C. P. Scholes and L. S. Lerman (1982) Torsional Motion and Elasticity of the Deoxyribonucleic Acid Double Helix and Its Nucleosomal Complexes, *Biochemistry 21* 4999.

Hyde J. S. and L. R. Dalton (1972) Very Slowly Tumbling Spin Labels Adiabatic Rapid Passage, *Chem. Phys. Lett. 16,* 568.

Hyde J. S. and L. R. Dalton. Saturation Transfer Spectroscopy in Spin Labeling II (Berliner, L. J. ed.) pp. 1-70, Academic Press, New York (1979).

Hyde J. S., W. Froncisz, and C. Mottley (1984) Pulsed ELDOR Measurement of Nitrogen T_1 in Spin Labels, *Chem. Phys. Lett. 110,* 621.

Lee S. and D. P. Ames (1988) Experimental ESR Method for Investigating Slow-orientational Diffusion of Normal Nitroxides with ^{14}N (I=l), *J. Chem. Phys. 88* 4213.

Kamzalova S. G. and G. B. Postnikova. Spin-labelled Nucleic Acids, *Q. Rev. Biophys. 14*, 223 (1981)

Likhtenshtein G.I. Spin Labeling Methods in Molecular Biology (Nauka, Moscow, 1974)

Madden K., L. Kevan, P. D. Morse and R. N. Schwartz (1980). Electron Spin-Echo Studies of Nitroxide Spin Probes in Lipid Bilayers. Direct Measurement of Transverse Relaxation Times as a Sensitive Probe of Molecular Motion, *J. Phys. Chem. 84* , 2691.

McCalley R. C., E. J. Shimshick and H. M. McConnell (1972). The Effect of Slow Rotational Motion on Paramaenetic Resonance Spectra, *Chem. Phys. Lett. 13* , 115.

Millhauser G. L. and J. H. Freed (1984) Two-dimensional Electron Spin Echo Spectroscopy and Slow Motions, *J. Chem. Phys 81*, 37

Percival P. W. and J. S. Hyde (1975). Pulsed EPR Spectrometer, II, *Rev. Sci. Instrum. 46* 1522.

Popp C. A. and J. S. Hyde (1982) Electron-electron Doublc Resonance and Saturation-recovery Studies of Nitroxide Electron and Nuclear Spin-lattice Relaxation Time and Heisenberg Exchange Rates: Lateral Diffusion in Dimyristol Phosphatidylcholine, *Proc. Natl. Acad. Sci. USA 79* , 2559.

Rengan S. K., V. R. Bhagat, V. S. Sastry and B. Venkataraman (1979) . Magnetic Field-pulsed ELDOR Spectroscopy, *J. Mag. Res. 33* 227.

Robinson B. H., L.S. Lerman, H. L. Frisch, L. R. Dalton and C. Auer (1980a) Analysis of Doublt-Helix Motions with Spin-labeled Probes: Binding Geometry and the Limit of Torsional Elasticity, *J. Mol. Biol. 139*, 19.

Robinson B. H., G. Forgacs, L. R. Dalton, and H. L. Frisch (1980b) A Simple Model for Internal Motion of DNA Based upon EPR Studies in the Slow Motion Region, *J. Chem. Phys. 73*, 4688.

Spaltenstein A., B. H. Robinson and P. B. Hopkins (1988) A Rigid and Nonperturbing Probe for Duplex DNA Motion, *J. Am. Chem. Soc. 110,* 1299.

Stillman A. E., L. J. Schwartz and J. H. Freed (1980) Direct Determination of Rotational Correlation Time by Electron-Spin Echoes, *J. Chem. Phys. 73* , 3502.

Thomas D.D., L. R. Dalton and J. S. Hyde (1976) Rotational Diffusion Studied by Passage Saturation Transfer Electron Paramagnetic Resonance, *J. Chem. Phys. 65* 3006.

Thomas D.D. (1978) Large-Scale Rotational Motions of Proteins Detected by Electron Paramagnetic Resonance and Fluorescence, *Biophys. J., 24,* 439.

Tomic M., D.E. Wemmer and S-H Kim.(1987) Structure of a Psoralen Cross-linked DNA in Solution by Nuclear Magnetic Resonance, *Science 238* , 1722.

LAWRENCE BERKELEY LABORATORY
TECHNICAL INFORMATION DEPARTMENT
1 CYCLOTRON ROAD
BERKELEY, CALIFORNIA 94720